DISSERTATION

DESIGN OF BAFFLED HYDRAULIC JUMP STILLING BASINS FOR DAMS

Submitted by

Dana Wesley Moses

Department of Civil and Environmental Engineering

In partial fulfillment of the requirements

For the Degree of Doctor of Philosophy

Colorado State University

Fort Collins, Colorado

Spring 2025

Doctoral Committee:

Advisor: Christopher Thornton

Brian Crookston
Robert Ettema
Pierre Julien
Sara Rathburn

ABSTRACT

DESIGN OF BAFFLED HYDRAULIC JUMP STILLING BASINS FOR DAMS

The hydraulic jump has been studied and used as a primary means of energy dissipation for hydraulic structures for well over a century. By the 1920s and 1930s, baffled hydraulic jump stilling basins were in widespread use as energy dissipators for large dams. These hydraulic jump stilling basins often consisted of toe blocks, a negative step and/or toe curve; one or more rows of baffle blocks; and a solid or dentated end sill. By the 1950's standard design guidance was developed by multiple agencies and universities.

A comparison of the standard baffled hydraulic jump guidance illustrates a drastic difference in recommended stilling basin geometry with identical incoming flow conditions. For example, given the same incoming flow conditions, the height of baffle block determined for a U,S, Bureau of Reclamation standard design can be more than twice the block size for a standard outlet works stilling basin determined from US Army Corps of Engineers guidance. The use and/or geometry associated with chute blocks, number of rows of baffle blocks, length of basin, distance to baffle blocks, and end sill geometry have similar discrepancies.

The current research includes a thorough reviewer and evaluation of data used in the development of standard guidance and a systematic physical model evaluation, performing over 400 individual experiments of the most often utilized baffled stilling basin design configurations. These experiments include 15 stilling basin configurations, each being evaluated for six discharge conditions and six tailwater scenarios. In addition, the USACE

standard stilling basin configuration was evaluated for the general scour tendencies for discharges below and above the design discharge by means of mobile bed physical modeling.

A numbered list of significant findings associated with the current research are provided below.

1. The USACE (1992) stilling basin configuration is recommended for incoming Froude Numbers less than 4.5.
2. The Modified Type III stilling basin configuration is recommended for incoming Froude Numbers in the range of 4.5 to 8.
3. The stilling basin length and minimum required tailwater for the USACE (1992) and USBR (1984) can be expressed by unified equations developed herein.
4. A toe curve is not recommended for the hydraulic jump basin due to increase in length required and the decrease in jump stability.
5. Intermittent ramps associated with the tapered baffle block configuration are not recommended due to increase in downstream scour potential, decreased tailwater resilience, cost, general lack of observed cavitation damage in stilling basins, and unproven effectiveness in reducing cavitation damage.
6. Macro-scale turbulent structures exiting the stilling basin are the primary phenomenon controlling downstream scour potential. A maximum downstream attack angle of 15-degrees from horizontal was determined for the USACE (1992) stilling basin configuration for incoming Froude Numbers in the range of 3 to 5.

AKNOWLEDGEMENTS

I would like to express my deepest gratitude to the numerous people that have supported the work presented in the Dissertation.

First, to my advisor Dr. Chris Thornton and committee members, Dr. Pierre Julien, Dr. Rob Ettema, Dr. Brian Crookston, and Dr. Sara Rathburn, who have provided significant advice and support related to this research and other general topics related to hydraulic engineering and geoscience. In addition, Dr. George Annandale, Dr. Hank Falvey, Mr. Ed Rossillon, and Mr. Sal Todaro, who have provided tremendous insights and contributions to my personal understanding of this topic and many others over my professional career.

I also express gratitude to the US Army Corps of Engineers (USACE) for providing the required support and resources to execute the research contained herein. Without the support of Mr. Pat Morgan, Mr. Don Whitmore, Mr. Steve Townsley, Mr. Bryant Robbins, and Mr. Nate Snorteland of the USACE Dam Safety Program and Dr. Ty Wamsley, Dr. Gaurav Savant, Dr. Duncan Bryant, Mr. Keith Flowers, Mr. Jeremy Sharp, and Mr. Curtis Blades of the Engineering Research and Development Center, this work would not have been possible. In addition, Mr. Nick Koutsunis, Mr. Brian Hall, Mr. Mike Phillips, Mr. Matt Piazza, Mr. Curtis Miller, Mr. Jesse Brown, Mr. Dave Margo, Mr. Haden Smith, Mr. Sean Smith, Mr. Ethan Thompson, and Mr. Adam Wenck have all provided significant support and/or inspiration for the current research, along with numerous other friends and colleagues who are too numerous to list.

I also express extreme gratitude to the Department of Defense SMART scholarship program, which provided a significant portion of the funding to support the academic degree training.

Most of all, I would like to thank my friends and family that have supported me along the way. Especially my wife (Andrea) and my two sons (Jackson and Jameson). Without their support and sacrifice, none of this would be possible, worthwhile, or satisfying.

TABLE OF CONTENTS

ABSTRACT ii

AKNOWLEDGEMENTS iv

LIST OF TABLES xi

LIST OF FIGURES xiv

LIST OF EQUATIONS xxvii

LIST OF SYMBOLS xxx

1 INTRODUCTION 1

1.1 Structure of Dissertation 1

1.2 Overview of Hydraulic Jump Stilling Basins 2

1.3 Background and Significance 11

2 RESEARCH GOALS AND OBJECTIVES 17

2.1 Knowledge Gap 17

2.2 Research Goal and Objectives 23

3 LITERATURE REVIEW OF STILLING BASIN DESIGN AND EVALUATION (ABRIDGED) 25

3.1 Early History on Stilling Basins 25

3.2 Development of Current Standard Stilling Basins 28

3.2.1 Saint Anthony Falls Stilling Basin 28

3.2.2 USBR Stilling Basin 33

3.2.3 USACE Stilling Basin 38

3.3 Other Major Design Considerations 44

3.3.1 Downstream Scour and Erosion 44

3.3.2 Stilling Basin Wall Configuration 46

3.3.3 Wing/Tie-Back Walls 47

3.3.4 Exit Channel and Downstream Protection 49

3.3.5 Cavitation Damage 51

3.3.6 Abrasion/Ball Milling 73

3.3.7 Stilling Basin Hydraulic Loading 76

3.4 Physical Modeling Approaches 92

3.4.1 Model Similitude 92

3.4.2 Local Scour Estimation 98

3.5 Recent Advances 117

3.5.1 Tapered Blocks and Ramp Configuration 117

3.5.2 Baffled Roller Basin 118

4 EVALUATION OF PUBLISHED DATA 119

4.1 General 119

4.2 Stilling Basin Geometry 119

4.2.1 Critical Depth ... 119
4.2.2 Stilling Basin Length ... 122
4.2.3 Location of Baffle Block ... 126
4.2.4 Baffle Block Height ... 128
4.2.5 End Sill Height ... 129
4.3 Required Tailwater ... 131
4.4 Chute Slope ... 136
4.5 Mobile Bed Scour ... 137
4.5.1 SAF Basin ... 137
4.5.2 Keystone (USACE 1960) ... 139
4.6 Bluestone Dam Stilling Basin Evaluation ... 141
4.6.1 Overview ... 141
4.6.2 Hydraulic Jump Action ... 145
4.6.3 Hydrodynamic Forces ... 149
4.6.4 Stilling Basin Sidewalls and Deflector ... 157
4.6.5 Downstream Scour Behavior ... 165
5 PHYSICAL MODEL EVALUATION ... 170
5.1 Mobile Bed Evaluation ... 170
5.1.1 Methods ... 170

5.1.2 Results ... 173

5.2 Rigid Bed Evaluation ... 186

5.2.1 Methods ... 187

5.2.2 Results ... 217

6 CONCLUSIONS AND RECOMMENDATIONS ... 275

6.1 Summary of Significant Findings ... 275

6.2 Consolidation of Existing Guidance ... 276

6.2.1 General ... 276

6.2.2 Stilling Basin Length ... 278

6.2.3 Required Tailwater ... 280

6.2.4 Block Location and Height ... 284

6.2.5 End sill ... 285

6.2.6 Baffle Loads ... 286

6.3 Evaluation of Increased Hydrologic Loading ... 288

6.3.1 Tailwater Resiliency ... 288

6.3.2 Boil Height ... 291

6.3.3 Jump Angle ... 295

6.4 Baffle Shape ... 302

6.5 Intermittent Ramp ... 304

6.6 Modified Type III 306

6.7 Toe Curve 310

6.8 Cavitation and Abrasion 311

6.9 Local Scour Potential 313

6.9.1 General 313

6.9.2 Rigid Bed Experiments 314

6.9.3 Mobile Bed Experiments 317

6.10 Research Limitations and Future Study 319

7 REFERENCES 321

LIST OF ACRONYMS 333

LIST OF TABLES

Table 1. Free Jump Length on Horizontal Floor (Adapted from Elevatorski, 1959) 6

Table 2. Design Parameters for Baffled and Unbaffled Basins from Major Sources Found in Literature 20

Table 3. Model Flow Parameters for SAF Stilling Basin Experiments (Blaisdell, 1948) 29

Table 4. SAF Stilling Basin influence of various tailwater conditions 45

Table 5. Baffle Pier Drag Coefficient for use in Momentum Equation (USACE, 1965) 85

Table 6. Froude-Number Scale Relationships (Source: Expanded from Ettema et al., 2000) 98

Table 7. Critical Thresholds for Various Categories (NCHRP, 2019) 102

Table 8. SAF Stilling Basin influence of various tailwater conditions (Source: Blaisdell, 1948) .. 138

Table 9. Keystone Dam Model Evaluation Plans (Source: USACE, 1960) 140

Table 10. Keystone Dam Model (1960) Evaluation Scour Characteristics 141

Table 11. Initial and Optimized Baffle Block Geometry 147

Table 12. Bluestone Dynamic Baffle Forces (Modified from USACE, 2018) 152

Table 13. Comparison of Estimated and Observed Baffle Block Forces 153

Table 14. Sensitivity of Pressure Transducer Capture Rate for Bluestone Stilling Basin 1:65 Scale Model (USACE, 2018) 161

Table 15. Keystone Dam Model Froude Scale Similitude 171

Table 16. Keystone Dam Model Flow Parameters 172

Table 17. Keystone Dam Hydraulic Jump Action Data Summary 176

Table 18. Mobile Bed Scour Evolution, Design Discharge, Maintained Jump Action 184

Table 19. Mobile Bed Scour Evolution, Design Discharge, Lost Jump Action 185

Table 20. Parameters for Application within Typical Range of Model Scales 190

Table 21. Flow Conditions for the Evaluation of Various Stilling Basin Configurations............. 199

Table 22. Measurement Weir and Incoming Flow Conditions Discharge Estimate Summary ... 201

Table 23. Tailwater Depths used for High Froude Number Configurations 203

Table 24. Tailwater Ratios for High Froude Number Configurations 204

Table 25. Tailwater Depths used for Low Froude Number Configurations 204

Table 26. Tailwater Ratios for Low Froude Number Configurations 205

Table 27. Dimensions of High Froude Number Basin Configurations 211

Table 28. Comparison of Planned verse Calibrated Incoming Flow Conditions 214

Table 29. Comparison of High Fr_1 Stilling Basin Dimensions (used verse estimated with calibrated incoming flow parameters) 214

Table 30. Dimensions of Low Froude Number Basin Configurations 216

Table 31. Comparison of Planned verse Calibrated Incoming Flow Conditions 216

Table 32. Comparison of Dimensions Used verse those based on Updated Incoming Flow Conditions 217

Table 33. Observed TW_{req} as a Function of q_x / q_d for High Froude Number Configurations ... 229

Table 34. TW_{req} / d_2 as a Function of q_x / q_d for High Froude Number Configurations 230

Table 35. TW_{req} normalized to TW_{req} at q_d 231

Table 36. TW_{req} / d_c as a Function of q_x / q_d for High Froude Number Configurations............... 234

Table 37. TW_{req} / d_1 as a Function of q_x / q_d for High Froude Number Configurations 235

Table 38. Semi-Quantitative Near-Bed turbulence severity index 236

Table 39. Summary Table for Near-Bed Turbulence Severity Index for High Froude Configurations........ 238

Table 40. Observed Maximum Boil Heights for High Froude Configurations 242

Table 41. Minimum Observed Jump Angle for High Froude Configurations 252

Table 42. Required Tailwater Depth for Low Froude Number Configurations 264

Table 43. Ratio of Required Tailwater to Sequent Depth for Low Froude Number Configurations 265

Table 44. TW_{req} / d_c as a Function of q_x / q_d for Low Froude Number Configuration........ 266

Table 45. TW_{req} / d_1 as a Function of q_x / q_d for Low Froude Number Configurations........ 267

Table 46. Observed Maximum Boil Heights for Low Froude Configurations........ 269

Table 47. Minimum Observed Jump Angle for Low Froude Configurations 273

LIST OF FIGURES

Figure 1. Hydraulic Jump Sketch (Source: USBR, 1984) 3

Figure 2. Characteristics and Energy Dissipation provided by a Free Hydraulic Jump (Source: USBR, 1955) 5

Figure 3. Comparison of Flow Conditions for High and Low Relative Incoming Velocities (Riegle and Beebe, 1917) 5

Figure 4. Length of Jump in Terms of d_2 (Source: USBR, 1955) 7

Figure 5. Baffled Hydraulic Jump Stilling Basin Definition Sketch 8

Figure 6. Stilling Basin Baffle Shapes (Source: USBR, 1987) 9

Figure 7. Definition Sketch for Parameters to Determine Theoretical Velocity at the Base of Free Overflow Spillway 10

Figure 8. Empirical Adjustment Factors to Determine Actual Velocity at the Base of Free Overflow Spillway 11

Figure 9. Bluestone Dam Stilling Basin Modification Construction (Photo by Author) 12

Figure 10. Distribution of Dam Construction by Year and Continent (Source: Zhang et al.., 2018) 13

Figure 11. El Guapo Dam Failure (Source: Suarez and Suarez, 2016) 14

Figure 12. Risk Informed Approach to Inflow Design Floods (Source: Moses and Margo, 2023) 16

Figure 13. Demonstration of Inconsistency in Stilling Basin Guidance Related to Basin Length. 18

Figure 14. Demonstration of inconsistency in stilling basin guidance related to Baffle Height ... 18

Figure 15. Demonstration of inconsistency in stilling basin guidance related to Baffle Station .. 19

Figure 16. Demonstration of inconsistency in stilling basin guidance related to end sill height . 19

Figure 17. Gatun Dam Spillway Model-Prototype (Source: ICC, 1910; ICC 1919) 26

Figure 18. Illustration of Chute Geometry with (In RED) and without Toe Curve. 27

Figure 19. Profile of the SAF Stilling Basin (Source: USDA, 1959) 30

Figure 20. Effect of Floor Block Locations on Center-Line Bed and Water-Surface Profiles (Source: Blaisdell, 1948) 31

Figure 21. Proportions of the SAF Stilling Basin (Source: Blaisdell, 1948) 32

Figure 22. Proportions of USBR Type III Stilling Basin (USBR, 1954) 35

Figure 23. Baffle Block and End Sill Height Proportions of USBR Type III Stilling Basin (1984) 37

Figure 24. USBR Baffled Stilling Basin for Fr_1 from 2.5 to 4.5 (Source: USBR, 1978) 38

Figure 25. Standard USACE Stilling Basin Configuration (USACE, 1969) 41

Figure 26. Distance to and Height of Baffle Block for Standard USACE Stilling Basin (USACE, 1992) 43

Figure 27. Proportions of the SAF Stilling Basin (Source: Blaisdell, 1948) 45

Figure 28. Typical Scour Pattern of SAF Basins with Highly Erodible Bed Material (Source: Adapted from Rice and Kadavy, 1993) 48

Figure 29. Critical Velocity for Stone Stability (USACE, 1957) 50

Figure 30. Riprap Size and Extents Downstream of SAF Stilling Basin (Source: Rice and Kadavy, 1993) 51

Figure 31. Collapse of individual bubble near a boundary (Source: USBR, 1990) 52

Figure 32. Sonic Velocity of Air-Water Mixtures (Source: USBR, 1990) 54

Figure 33. Bluestone Dam Sluice Deflector Damage (Source: a) author, b) USACE, 1946) 56

Figure 34. Baffle Block Sidewall Pressure with Varied Froude Number and Block Location (USACE, 1970) 57

Figure 35. Relationship of Damage Intensity to Cavitation Index Ratio (Source: Rozanov and Kaveshnikov, 1973) 58

Figure 36. Super-cavitating Baffle Block Configurations (Source: Rozanov et al. 1971) 59

Figure 37. Cavitation Damage on Side of Yellowtail Afterbay Baffle Block (Source: ACI, 2008) .. 61

Figure 38. Spillway Flow Event of 1940 at Claytor Dam (Courtesy: AEP, 2024) 62

Figure 39. Cavitation Damage and Flow Characteristics of Claytor Baffles (Source: adapted from Thomas and Hopkins) 62

Figure 40. Bull Shoals Stilling Basin Damage (Source: USACE, 1958) 64

Figure 41. Porto Columbia Project Spillway Profile (Source: ICOLD 2015) 64

Figure 42. Porto Columbia Project Spillway Damage (Source: Pereira, 2021) 65

Figure 43. Section of Bonneville Dam Original Spillway (Source: Cochrane, 1959) 66

Figure 44. Original Construction Photographs of Bonneville Spillway (Source: USACE, 1935-1937) 66

Figure 45. Bonneville Spillway Flow Event Prior to Spillway Completion - June, 1936 (Source: USACE, 1935-1937) 67

Figure 46. Sediment Laden flow Abrasion Study Results (Source: USACE, 1943) 68

Figure 47. Bonneville Spillway Baffle Damage Observe in 1954 (Source: USACE, 1954) 69

Figure 48. Evidence of Potential Abrasion Damage at Bonneville Spillway (Source: USACE, 1954) 70

Figure 49. Spillway and Stilling Basin Configuration for Chief Joseph Dam (Modified from Gedney, 1961) 71

Figure 50. Damage Observed from Dive Inspection Survey 1957 (Adapted from Gedney, 1961) 72

Figure 51. General Recirculating Patterns that Result in Entrainment/Entrapment of Rock (Source: USBR, 2010) 74

Figure 52. Abrasion-Erosion of Dworshak Dam Stilling Basin Floor (Source: USACE, 1981) 75

Figure 53. Karnafuli Spillway Damage (Bowers and Toso, 1988) 76

Figure 54. Fluctuating Pressure on Chute and Stilling Basin (Source: Bowers and Toso, 1988)... 77

Figure 55. Variations in Jump Profile and Pressure Extremes (Bower and Toso, 1988) 78

Figure 56. Dynamic Pressure Coefficient for Stilling Basin (Source: Toso and Bower, 1988) 79

Figure 57. Uplift Force Coefficients (Source: Bellin and Fiorotto, 1995) 80

Figure 58. Water Surface and Pressure Profiles with Type III Stilling Basin (Source: USBR, 1984) 81

Figure 59. Experiments to Determine Dynamic Loads on Sidewalls (Source: USACE, 1988) 82

Figure 60. Resultant Force and Location from PI (USACE, 1988) 83

Figure 61. Velocity-Depth Relationship in the Streamwise Direction of a Free Hydraulic Jump (Source: USACE, 1992) 86

Figure 62. Baffle Drag Coefficient Definitions (USACE, 1970) 87

Figure 63. Typical Forced Jump Profile (USACE, 1970) 88

Figure 64. Drag Coefficient for Varied Block Height and Location (USACE, 1970) 89

Figure 65. Impacts of Baffle Height and Station on Force Ratio (USACE, 1970) 90

Figure 66. Impacts of Blockage Ratio and Location on Baffle Drag Coefficient (USACE, 1970).... 91

Figure 67. Scale Effects Impact on Hydraulic Jump Behavior (Source: Chanson and Gualtieri, 2008) 94

Figure 68. Flow Features Produced by Two-dimensional Flow with Uniform Approach (Source: Ettema et al. 2004) 95

Figure 69. Principle Mechanisms of Rock Fracturing (Bollaert, 2010) 99

Figure 70. Erosion Rates for Various Categories (NCHRP, 2019) 102

Figure 71. Annadale Erodibility Threshold (Annadale, 1995) 104

Figure 72. Geological Strength Index Chart (Hoek, 2006) 106

Figure 73. Discontinuity Adjustment Fator for Erosion for Horizontal Beds (Pells, 2017) 107

Figure 74. eGSI applied to Spillway Scour Case Histories (Pells, 2016) 108

Figure 75. Universal energy balance in the near-bed region (Source: Annandale, 2006b) 110

Figure 76. Experimental Data of Shields (1936) 112

Figure 77. Tilt-Flume for use in determining submerged angle of repose of bed material (Coarse Gravel Material) 114

Figure 78. Relationship of the P_{RMS} / τ_w as a function of Reynolds Number (Source: Farabee and Casserella, 1991) 116

Figure 79. Observed Cavitation in Vacuum Tank Experiments (USBR, 2009) 118

Figure 80. Re-evaluation of USBR (1955) Experimental Data Related to Free Jump Length 121

Figure 81. L_{SB} / d_2 as a Function of Fr_1 122

Figure 82. L_{SB} / d_c as a function of Fr_1 123

Figure 83. L_{SB} / d_1 as a function of Fr_1 123

Figure 84. Comparison of Existing Data/Guidance and Unified Equation for $LSBd1$ 125

Figure 85. Comparison of Existing Data/Guidance and Unified Equation expressed as $LSBd2$125

Figure 86. X_{B1} / d_2 as a function of Fr_1 126

Figure 87. X_{B1} / d_c as a function of Fr_1 127

Figure 88. X_{B1} / d_1 as a function of Fr_1 127

Figure 89. H_B / d_1 as a function of Fr_1 128

Figure 90. H_B / d_c as a function of Fr_1 129

Figure 91. H_B / d_2 as a function of Fr_1 129

Figure 92. H_{ES} / d_1 as a function of Fr_1 130

Figure 93. H_{ES} / d_c as a function of Fr_1 130

Figure 94. H_{ES} / d_2 as a function of Fr_1 131

Figure 95. Efficiency of Energy Dissipation of Hydraulic Jump with Reduced Tailwater 132

Figure 96. TW_{req} / d_2 as a function of Fr_1 133

Figure 97. TW_{req} / d_1 as a function of Fr_1 134

Figure 98. TW_{req} / d_c as a function of Fr_1 134

Figure 99. Comparison of Existing Data/Guidance and Unified Equation for $d'2d1$ 135

Figure 100. Comparison of Existing Data/Guidance and Unified Equation for $d'2d2$ 136

Figure 101. Stilling Basin Parameters by Chute Slope (Adapted from USACE 1969 and USBR 1955) 137

Figure 102. Proportions of the SAF Stilling Basin (Source: Blaisdell, 1948) 138

Figure 103. Evaluation of observed scour with decreasing tailwater below that required for hydraulic jump action (Adapted from Blaisdell, 1948) 139

Figure 104. Keystone Dam Model Study Typical Profile (Source: USACE, 1960) 140

Figure 105. Bluestone Dam General Overview Aerial (Source: Moses and Koutsunis, 2018).... 142

Figure 106 – Original Bluestone Dam Stilling Basin (Adapted from USACE, 1947) 143

Figure 107.Shooting Jet and Associated Impingement Related Scour (Source: George and Annandale, 2010) 144

Figure 108. Bluestone Dam Physical Models.. 146

Figure 109. Overly Forced Hydraulic Jump 147

Figure 110. Bluestone Dam General Model Asymmetric Jump Location................................. 148

Figure 111. Isometric views of Baffle Manifold System (USACE, 2018) 150

Figure 112. Location of Instrumented Baffle Block within Sectional Model (USACE, 2018) 151

Figure 113. Fabricated Baffle and Manifold (photos by author) 151

Figure 114. Observed Scaled Characteristic Woody Debris Impact (USACE, 2018) 155

Figure 115. Stainless Steel Face Plate and Reinforcement (Photos by Author) 155

Figure 116. Locations of side wall force observations (USACE, 2018) 156

Figure 117. Comparison of pressure transducer observations and water surface profiles (USACE, 2018) 156

Figure 118. Bluestone Stilling Basin 1:36 Scale Model for Evaluation of Sidewall Overtopping (USACE, 1937) 158

Figure 119. Bluestone Dam Right Sidewall Overtopping Observations (USACE, 2018; Author) 159

Figure 120. Comparison of Left Side Wall Overtopping Flow Behavior With and Without Deflector 160

Figure 121. Left Side Overtopping Pressure Transducer Locations (USACE, 2018; Author)....... 161

Figure 122. Right Side Wall Overtopping Unit Applied Stream Power Estimates (Bluestone, 2018) 162

Figure 123. Mobile Bed Experiments for Left Side Overtopping (USACE, 2018) 163

Figure 124. Surface Protection Configurations 164

Figure 125. Left-Side Wall Overtopping Experiments (Photos by author) 165

Figure 126. Construction Photos of Constructed Sidewall Modifications (Photos by Author) 165

Figure 127. Erodibility Index for Bluestone Dam Scour Estimates (Source: Humphries and Annadale, 2015) 166

Figure 128. Turbulence and Scour Behavior Downstream of Bluestone Second Stage Basin (overview) 167

Figure 129. Turbulence and Scour Behavior Downstream of Bluestone Second Stage Basin (Closeup) 168

Figure 130. Location of Pressure Transducers in Downstream Face of Second Stage Stilling Basin 169

Figure 131. Keystone Dam Overview (Adapted from USACE, 2012) 170

Figure 132. Keystone Dam Current Model Schematic 172

Figure 133. Keystone Dam Updated Required Tailwater Curve 173

Figure 134. Hydraulic Jump Action Maintained 174

Figure 135. Transitional Jump Action 174

Figure 136. Hydraulic Jump Action Lost 174

Figure 137. Jump Action Lost, Lower Unit Discharge (High Froude) 175

Figure 138. Jump Action Lost, Higher Unit Discharge (Low Froude) 175

Figure 139. Transient Nature of Baffle Block Separation 176

Figure 140. Comparison of Keystone Findings and Combined Required Tailwater/D2 Ratio Data from USBR and USACE 177

Figure 141. Comparison of Keystone Findings and Combined Required Tailwater/Critical Depth Ratio Data from USBR and USACE 178

Figure 142. Comparison of Keystone Findings and Combined Stilling Basin Length / Sequent Depth Ratio Data from USBR and USACE 178

Figure 143. Keystone Dam Stilling Basin Construction Photos 179

Figure 144. Graphical Illustration of Threshold Stream Power.. 180

Figure 145. Keystone Mobile Bed Material Proxy 181

Figure 146. Keystone Basin Mobile Bed Scour Patterns, geometric mean = 28mm (Adopted from USACE, 1960).. 182

Figure 147. Observational Methods of Submerged Angle of Repose 183

Figure 148. Mobile Bed Scour Evolution, Design Discharge, Maintained Jump Action 184

Figure 149. Mobile Bed Scour Evolution, Design Discharge, Lost Jump Action 185

Figure 150. Existing Stilling Basin, Design Discharge 186

Figure 151. Typical Ridge and Trough for Mobile Bed Downstream of Hydraulic Jump 186

Figure 152. Sectional Flume Configuration, Shown with High Fr_1 Crest 188

Figure 153. Video Recording Camera Locations 191

Figure 154. Typical Camera Views 191

Figure 155. Headwater Piezometer Board 192

Figure 156. Incoming Flow Instrumentation with High Crest 193

Figure 157. Incoming Flow Instrumentation with Low Crest 194

Figure 158. Instrumentation Carriage for Hydraulic Jump and Tailrace Observations 195

Figure 159. Tailwater Piezometer Configuration 196

Figure 160. Flow Measurement Weir Point Gauge Carriage System 197

Figure 161. Plot of Target, Avg. Est. from Incoming Flow Conditions, and Avg. Est. from Measurement Weir 201

Figure 162. Tailgate for Control of Stilling Basin Tailwater 202

Figure 163. Baffle Block Geometries 206

Figure 164. Baffle Magnetic Connection (left) and Intermittent Ramps (right) 206

Figure 165. Comparison of with and without Toe Curve 208

Figure 166. High Froude Number Stilling Basin Configurations 210

Figure 167. Low Froude Number Stilling Basin Configurations 215

Figure 168. Example of Determining Required Tailwater using Time Synchronized Cameras 219

Figure 169. High Froude Configurations, Before and After Loss of Hydraulic Jump Action, q_{60} 222

Figure 170. High Froude Configurations, Before and After Loss of Hydraulic Jump Action, q_D 224

Figure 171. High Froude Configurations, Before and After Loss of Hydraulic Jump Action, q_{160} 227

Figure 172. Dynamic and Unstable Transition Region for Configuration 3c, q_{160}, ... 228

Figure 173. Observed TW_{req} as a Function of q_x / q_d for High Froude Number Configurations 229

Figure 174. TW_{req} / d_2 as a Function of q_x / q_d for High Froude Number Configurations 230

Figure 175. TW_{req} normalized to TW_{req} at q_d 231

Figure 176. TW_{req} / d_c as a Function of q_x / q_d for High Froude Number Configurations 234

Figure 177. TW_{req} / d_1 as a Function of q_x / q_d for High Froude Number Configurations 235

Figure 178. Examples of Qualitative Turbulence Intensity 237

Figure 179. Graphical Matrix for Near-Bed Turbulence Severity Index for High Froude Configurations 239

Figure 180. Example of Boil Height Observation 240

Figure 181. Graphical Results for Stilling Basin Boil Height Ratio $Zmaxd2$ for High Froude Configurations 244

Figure 182. Typical Boil Height Observations for High Froude Number Configurations at q_{60} and tailwater scenario C. 245

Figure 183. Typical Boil Height Observations for High Froude Number Configurations at q_D and tailwater scenario A. 248

Figure 184. Example of Minimum Jump Angle Observation.. 249

Figure 185. Minimum Observed Jump Angle for High Froude Number Configurations 254

Figure 186. Comparison of Typical Jump Angles for Configuration 3a 255

Figure 187. Determination of Required Tailwater to Maintain the Hydraulic Jump Action for Low Froude Configurations 256

Figure 188. End sill tailwater control for USBR (1984) Configurations at q_{60} and q_{80} 257

Figure 189. Comparison of Configurations 11a, 12a, 13a, and 15a for q_D and end sill control ($d'/d_2 \sim 0.75$) 259

Figure 190. Configuration 14a Before and After Loss of Hydraulic Jump Action 261

Figure 191. Comparison of Configurations 15a and 16a at ~ 0.75 $d'2d2$. 263

Figure 192. Required Tailwater Depth for Low Froude Number Configuration......................... 264

Figure 193. TW_{req} / d_2 as a Function of q_x / q_d for Low Froude Number Configurations............ 265

Figure 194. TW_{req} / d_c as a Function of q_x / q_d for Low Froude Number Configurations 266

Figure 195. TW_{req} / d_1 as a Function of q_x / q_d for Low Froude Number Configurations 267

Figure 196. Graphical Results for Stilling Basin Boil Height Ratio $Zmaxd2$for Low Froude Configurations 270

Figure 197. Typical High Boil for Configuration 11a at q_{60} with Varied Tailwater 271

Figure 198. Example of Determination of Minimum Jump Angle for Low Fr_1 Experiments 272

Figure 199. Minimum Observed Jump Angle for Low Froude Number Configurations 274

Figure 200. Figure 84. Comparison of Existing Data/Guidance and Unified Equation for $LSBd1$ 279

Figure 201. Comparison of Existing Data/Guidance and Unified Equation expressed as $LSBd2$ 280

Figure 202.Required Tailwater Ratio ($TWreqd1$) for Low (~4) and High (~8) Fr_1 Configuration 289

Figure 203. Required Tailwater Ratio ($TWreqd2$) for Low (~4) and High (~8) Fr_1 Configuration 289

Figure 204. Required Tailwater Ratio ($TWreqd2$) for USACE (1992) Configurations as a Function of $qxqD$ 290

Figure 205. Dynamic and Unstable Transition Region for Configuration 3c, q_{160}, ... 291

Figure 206. Example of Minimum Jump Angle Observation Figure 184. Example of Minimum Jump Angle Observation 301

Figure 207. Standard and Modified Type III Baffled Stilling Basin 307

Figure 208. Tailwater Resiliency for Modified Type III Stilling Basin 307

Figure 209. Configuration 7c Turbulence Intensity 308

Figure 210. Boil Heights for Modified Type III Configuration 309

Figure 211. Minimum Jump Angle for Modified Type III Stilling Basin 309

LIST OF EQUATIONS

Equation 1. Momentum Equation for Hydraulic Jump. 3

Equation 2. Froude Number 3

Equation 3. Kinematic Flow Factor 4

Equation 4. Theoretical Velocity at Base of Free Overflow Spillway 9

Equation 5. Method to Estimate incoming Flow Conditions Based on Total Specific Head (USACE, 1987) 11

Equation 6. SAF Stilling Basin Length (USDA, 1959) 30

Equation 7. SAF Stilling Basin Required Tailwater (USDA, 1959) 33

Equation 8. Length of USACE Stilling Basin associated with Dam Spillways (USACE, 1992) 42

Equation 9. Stilling Basin Freeboard (USBR, 1987) 47

Equation 10. Minimum Length of Riprap Protection Downstream of SAF Stilling Basin (Source: Rice and Kadavy, 1993) 50

Equation 11. Minimum Median Stone Size for Protection Downstream of SAF Basin, placed at Elevation of Stilling Basin Floor (Source: Rice and Kadavy, 1993) 51

Equation 12. Minimum Median Stone Size for Protection Downstream of SAF Basin, placed at Elevation of End Sill (Source: Rice and Kadavy, 1993) 51

Equation 13. Cavitation Index 52

Equation 14. Dynamic Pressure Coefficient 78

Equation 15. Maximum Force Acting on Slab (modified from Bellin and Fiorotto, 1995) 80

Equation 16. Average Minimum Static plus Dynamic Force at the Toe of Hydraulic Jump 83

Equation 17. Momentum Equation for Hydraulic Jump, Including Baffle Forces (USACE, 1965) 84

Equation 18. Expression for Baffle Pressure (USACE, 1965) 84

Equation 19. Force acting on Baffle Face (Adapted from USBR, 1987) 91

Equation 20. Reynolds Number 93

Equation 21.Weber Number 96

Equation 22. Scale Ratio for Manning's "n" (Henderson, 1966) 97

Equation 23. Ultimate Scour Downstream of Stilling Basin from Novak (2007) 101

Equation 24. Annadale's Erodibility Index 103

Equation 25. Annadale's Scour Threshold for Low EI Materials 104

Equation 26. Annadale's Scour Threshold for High EI Materials 105

Equation 27. Power Similitude Relationship 109

Equation 28. Annandale's Relationship of Turbulent shear stress to Stream Power 109

Equation 29. Shields Particle Stability Criterion 111

Equation 30. Incipient Shear Stress Slope Adjustment Factor 113

Equation 31. Generalized Relationship between P_{RMS} and τ_w (Source: Humpries and Annandale, 2015) 116

Equation 32. Critical Depth for Rectangular Channel 120

Equation 33. Expression for change in pressure from hydraulic jump 120

Equation 34. Expression for change in momentum for hydraulic jump 120

Equation 35. Unified Equation for Stilling Basin Length 124

Equation 36. Unified Equation for Required Tailwater Depth 135

Equation 37. Physically Based Maximum Baffle Block Load 149

Equation 38. Expression for Required Tailwater for Configuration 14a 290

Equation 39. Expression for Required Tailwater for Configuration 4a 290

LIST OF SYMBOLS

Symbol	Description	Dimensions	units
A_B	area of baffle perpendicular to flow	L^2	ft^2
d_1 or y_1	Depth of flow entering stilling basin	L	ft
d'_2	Actual tailwater depth	L	ft
d_2 or y_2	sequent depth	L	ft
d_3	Depth over end sill	L	ft
d_c	critical depth	L	ft
$DS_{end\ sill}$	scour depth immediately downstream of end sill	L	ft
DS_{max}	maximum mobile bed scour downstream of stilling basin	L	ft
F_B	Force acting on baffle block	$M\ L\ T^{-2}$	lbf
Fr_1	incoming Froude number	-	-
h_{v1}	Incoming velocity head	L	ft
H_o	Reference specific energy head	L	ft
H_1	incoming total specific energy head	L	ft
H_2	Exiting total specific energy head	L	ft
H_B	height of baffle block	L	ft
H_{crest}	Total head on the spillway crest	L	ft
H_{ES}	height of end sill above stilling basin floor	L	ft
H_T	Total specific energy from reservoir to tailwater	L	ft
H_s	Height of spillway from the crest to the apron floor	L	ft
L	Characteristic flow length	L	ft
L_j	Length of Hydraulic Jump	L	ft

L_{SB}	Distance from Intersection of Chute and Horizontal Stilling Basin (PI if Toe Curve is Included) to End of Stilling Basin	L	ft
P_0	Reference pressure	$ML^{-1}T^{-2}$	Pa
P_v	Vapor pressure of water given specific temperature and ambient pressure	$ML^{-1}T^{-2}$	Pa
q	unit discharge	$L^2 T^{-1}$	$ft^2 s^{-1}$
q_D	Stilling basin design unit discharge (ft^3/s/ft or ft^2/s)	$L^2 T^{-1}$	$ft^2 s^{-1}$
q_T	Target unit discharge based on planned flow conditions	$L^2 T^{-1}$	$ft^2 s^{-1}$
q_W	Unit discharge based on downstream partially contracted rectangular sharp-crest weir	$L^2 T^{-1}$	$ft^2 s^{-1}$
q_x	percentage of design discharge (e.g. q_{60} is 60-percent of the design discharge)	-	-
Q	total discharge	$L^3 T^{-1}$	$ft^3 s^{-1}$
r	Distance between first and second row of baffles	L	ft
R_B	Ratio of blockage by a row of baffles $[W_B / (W_B + W_S)]$	-	-
R_m	Average minimum static plus dynamic unit force at the toe of the hydraulic jump	$M T^{-2}$	lbf/ft
S_{ES}	Exit slope of end sill	-	-
TW_{req}	Tailwater depth required to maintain hydraulic jump action	L	ft
U	Characteristic flow velocity	$L T^{-1}$	$ft s^{-1}$
V_0	Reference velocity	$L T^{-1}$	$ft s^{-1}$
V_1	Velocity entering stilling basin	$L T^{-1}$	$ft s^{-1}$
V_2	Velocity exiting stilling basin	$L T^{-1}$	$ft s^{-1}$
V_A	Empirically estimated velocity including spillway losses	$L T^{-1}$	$ft s^{-1}$
V_{baffle}	Velocity immediately upstream of baffle block (ft/s)	$L T^{-1}$	$ft s^{-1}$
$V_{end\ sill}$	Velocity immediately above end sill (ft/s)	$L T^{-1}$	$ft s^{-1}$
V_p	Average Velocity in upstream approach pool	$L T^{-1}$	$ft s^{-1}$
V_T	Theoretical velocity without spillway losses	$L T^{-1}$	$ft s^{-1}$
W_B	Width of front face of baffle blocks	L	ft

W_S	Width of space between baffle blocks	L	ft
W_T	Width of top of standard baffle block	L	ft
X_{B1}	Distance from Intersection of Chute and Horizontal Stilling Basin (PI if Toe Curve is Included) to First Row of Baffle Blocks	L	ft
X_{B2}	Distance from Intersection of Chute and Horizontal Stilling Basin (PI if Toe Curve is Included) to 2^{nd} Row of Baffles (if applicable)	L	ft
X_{B3}	Distance from Intersection of Chute and Horizontal Stilling Basin (PI if Toe Curve is Included) to 3^{rd} Row of Baffles (if applicable)	L	ft
Z_{fall}	Total fall distance from pool to stilling basin floor	L	ft
Z_{max}	maximum boil height	L	ft
Z_p	Stage or elevation of upstream pool	L	ft
Θ_{j-min}	Minimum angle of hydraulic jump action, as measured from the point of intersection of the d_1 and the horizontal stilling basin floor	Degree	Degree
Θ_{scour}	downstream characteristic scour angle measured, as measured from horizontal immediately downstream of the vertical face of the end sill	Degree	Degree
λ_1	Incoming kinetic-flow factor	-	-
μ_*	Shear velocity	$L\ T^{-1}$	$ft\ s^{-1}$
ρ	Density of water	$M\ L^3$	$m^3\ s^{-1}$
Π	Total stream power	$M\ L^2\ T^{-3}$	W
Π_c	Threshold unit stream power	$M\ L\ T^{-3}$	$W\ m^{-2}$
Π_r	Froude scale stream power ratio	-	-
Π_U	Unit stream power per area	$M\ L\ T^{-3}$	$W\ m^{-2}$
Π_{UD}	Unit stream power dissipated per area	$M\ L\ T^{-3}$	$W\ m^{-2}$
τ	Shear Stress	$M\ L^{-1}\ T^{-1}$	Pa
$\bar{\tau}_b$	Average bed shear stress	$M\ L^{-1}\ T^{-1}$	Pa
τ_{crit}	Critical shear stress for incipient sediment motion	$M\ L^{-1}\ T^{-1}$	Pa
τ_{Re}	Reynolds Stress	$M\ L^{-1}\ T^{-1}$	Pa

T_{wall}	Wall shear stress	$M\ L^{-1}\ T^{-1}$	Pa
ρ	Mass density	$M\ L^{-3}$	lb ft^{-3}
γ	Unit weight of water	$M\ L^{-2}\ T^{-1}$	lbf ft^{-3}

1 INTRODUCTION

This dissertation describes the background, relevant literature, purpose, objectives, research methods, results, and conclusions to fulfill the research requirements of the Degree of Doctor of Philosophy for the Department of Civil and Environmental Engineering within the Colorado State University.

1.1 Structure of Dissertation

Section 1 introduces the phenomenon of the hydraulic jump, provides an overview of the fundamental principles, describes its use as an energy dissipator and terminal structure for dams and other hydraulic structures, and establishes the overall context for the need for the research described herein.

Section 2 identifies the inconsistencies and gaps associated with the current state-of-the - practice for the design of baffled hydraulic jump stilling basins and details the goals and objectives of the current research.

Section 3 provides a broad description of the relevant literature and state-of-practice related to the use of the hydraulic jump.

Section 4 provides a re-evaluation of existing published data related to the use of baffled hydraulic jump stilling basins for dams and other hydraulic structures. This includes collecting and compiling the data that was utilized for the various standardized design guidance. This data is combined and evaluated collectively to assess trends and inconsistencies. This section also describes the recent efforts that were conducted for the evaluation of the stilling basins at Bluestone Dam.

Section 5 describes the current research efforts associated with physical modeling. Mobile bed experiments were conducted for the standard USACE stilling basin, along with rigid bed experiments for a systematic evaluation of the performance of the standard USACE (1992) and USBR (1984) baffled stilling basins, and variations thereof.

Section 6 summarizes the findings based on the combination of experimental data from current research, re-evaluation of previously published data, and interrogation of relevant facts related to other considerations for the use of the baffled hydraulic jump stilling basin, such as cavitation damage potential, the use of a toe curve, and dynamic forces on baffle blocks.

Section 7 provides a comprehensive citation of literature and correspondence utilized for this dissertation.

1.2 Overview of Hydraulic Jump Stilling Basins

The hydraulic jump has been used as a primary means of energy dissipation for spillways, outlets, barrages, diversion works, and culverts for well over a century (Riegel and Beebe, 1917; Freeman, 1929; Schoklitsch, 1937; Elevatorski, 1957). A classical description of the basic mechanics of the hydraulic jump are illustrated in Figure 1.

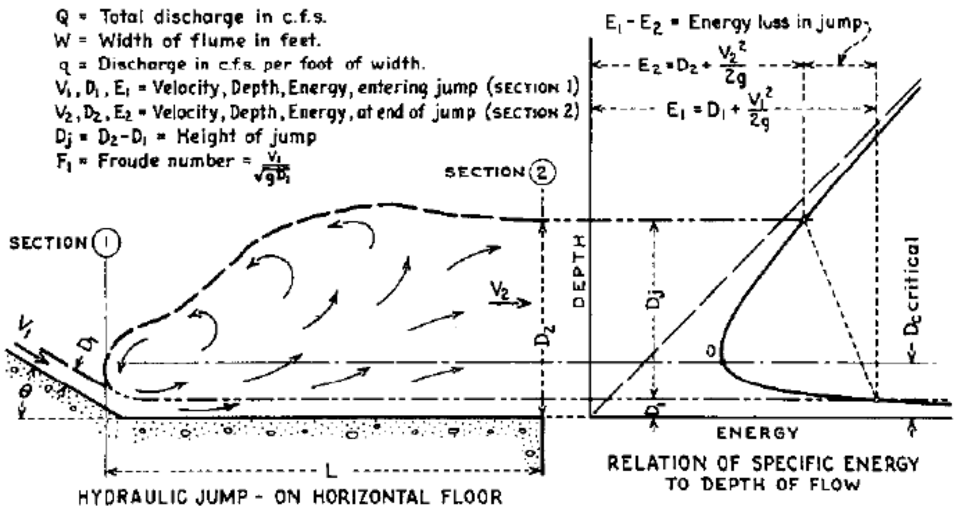

Figure 1. Hydraulic Jump Sketch (Source: USBR, 1984)

The most common form of the momentum equation applied to the prediction of the hydraulic jump is the Belanger equation (Chanson, 2009) and is shown in Equation 1.

Equation 1. Momentum Equation for Hydraulic Jump.

$$\frac{d_2}{d_1} = \frac{1}{2}\left(\sqrt{1 + 8{Fr_1}^2} - 1\right)$$

Where, d_1 is the approach depth, d_2 is the sequent (or conjugate) depth, and Fr_1 is the incoming Froude number. The Froude number is defined by Equation 2.

Equation 2. Froude Number

$$Fr = \frac{U}{\sqrt{gL}}$$

Where U is a characteristic velocity (typically taken as depth averaged velocity), L is a characteristic length (taken as incoming flow depth), and g is a gravitational constant. When referring to the incoming Froude number into a hydraulic jump stilling basin, the expressions Fr_1, v_1, and d_1 are typically used.

Prior to the use of the Fr_1 , the kinetic flow factor λ_1 was often used and is expressed as the square of the Fr_1 (Blaisdell, 1948; Elevatorski, 1957), as shown in Equation 3.

Equation 3. Kinematic Flow Factor

$$\lambda_1 = \frac{{v_1}^2}{gd_1} = {Fr_1}^2$$

It has been found experimentally by numerous researchers that the characteristics and the amount of energy dissipation provide by a free hydraulic jump is dependent on the incoming Fr_1 or λ_1 (Riegel and Beebe, 1917; Stanley, 1934; USBR, 1939; Blaisdell, 1948; USBR, 1954; USACE, 1970). The characteristics of the hydraulic jump are described by USBR (1955) as providing a practical range of the use of the hydraulic jump for energy dissipation. It was determined that the most effective hydraulic jump energy dissipators have Fr_1 in the range of 4.5 to 10. Below Fr_1 of 4.5, the hydraulic jump is weak and provides for low energy dissipation. Above an Fr_1 of 10 the jump is an effective energy dissipator, although the jump is highly dynamic and may not be the most economical choice in most situations. The general flow characteristics (a) and amount of energy dissipated (b) of a free hydraulic jump as a function of Fr_1 are shown in Figure 2. Chow (1959) states that hydraulic jumps in the range of 2.5 to 4.5 are oscillatory and not used if possible.

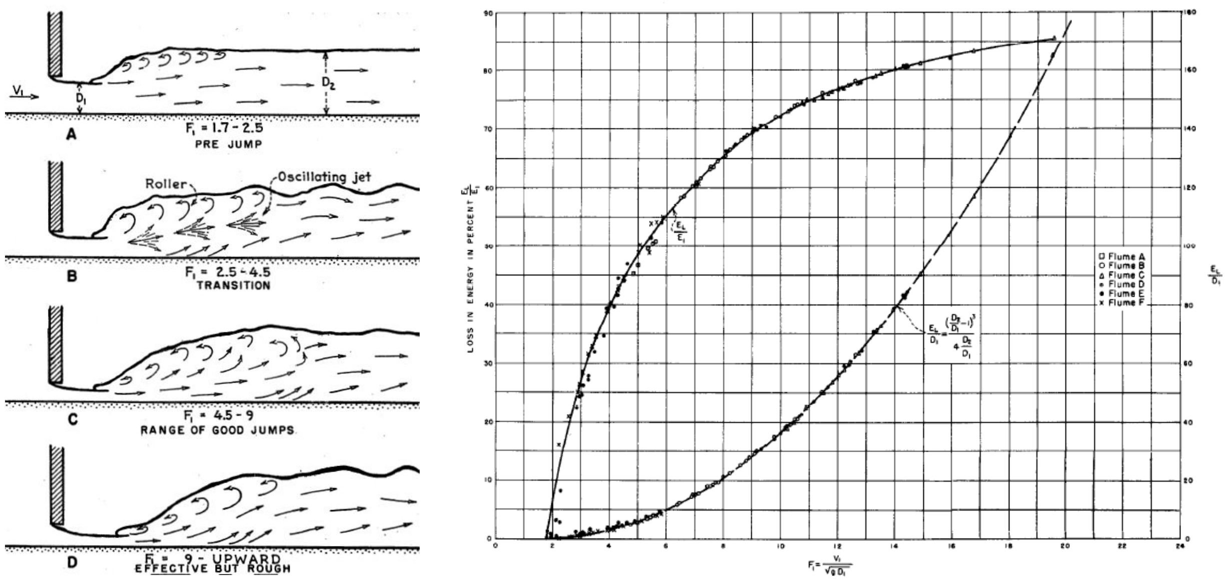

a) Characteristics of Jump

b) Energy Dissipated in free jump

Figure 2. Characteristics and Energy Dissipation provided by a Free Hydraulic Jump (Source: USBR, 1955)

Prior to the use of Fr_1 to explain the characteristics of the hydraulic jump, the ratio of the incoming velocity head to the incoming flow depth was utilized by many researchers as summarized by Riegle and Beebe (1917). An illustration of the strength of the hydraulic jump as a function of the velocity head (H_1) to incoming flow depth (d_1) is shown in Figure 3; with equivalent Froude numbers annotated.

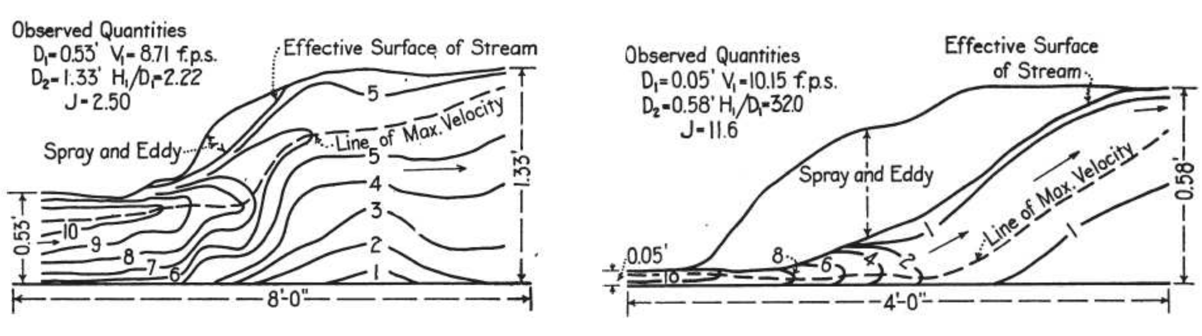

a) Fr_1 approximately 2

b) Fr_1 approximately 8

Figure 3. Comparison of Flow Conditions for High and Low Relative Incoming Velocities (Riegle and Beebe, 1917)

The dimensionless length of the hydraulic jump roller has been characterized by Wang and Chanson (2015) to have a linear relationship to the Fr_1 for values between 1.5 to 8.5. Elevatorski (1959) provides a summary of the various expressions of the hydraulic jump length, as shown in Table 1.

Table 1. Free Jump Length on Horizontal Floor (Adapted from Elevatorski, 1959)

Investigator	Year Published	Proposed Formula
Ludin	None given	$L_j = y_2\left(4.5 - \frac{v_1}{v_2}\right)$
Safranez	1927	$L_j = approx.\ 5.2\, y_2$
Bakhmeteff and Matezke	1932-1933	$L_j = 5\,(y_2 - y_1)$
Knapp	1932	$L_j = \left(62.5\frac{y_1}{H_1} + 11.3\right)[\frac{(v_1 - v_2)^2}{2g} - (H_1 - H_2)]$
Smetana	1934	$L_j = approx.\ 6\, y_2$
Kinney	1935	$L_j = 6.02\,(y_2 - y_1)$
Douma	None Given	$L_j = 3\, y_2$
Posey	1941	$L_j = 4.5\ to\ 7\,(y_2 - y_1)$
Wu	1949	$L_j = 10\,(y_2 - y_1)Fr^{-0.16}$
Woycicki	1934	$L_j = (y_2 - y_1)(8 - 0.05\frac{y_2}{y_1})$
Ivanchenko	None Given	$L_j = 10.6\,{\lambda_1}^{-0.185}(y_2 - y_1)$
Einwachter	1933	$L_j = \left(15.2 - 0.241\frac{y_2}{y_1}\right)[\left(\frac{y_2}{y_1} - 1\right) - \frac{{v_1}^2\left(\frac{y_2}{y_1} - 1\right)}{g\left(\frac{y_2}{y_1}\right)^2}]$
Chertoussov	1935	$L_j = 10.3\,(Fr - 1)^{0.81}$
Page	1935	$L_j = 5.6\, y_2$
Reigel and Beebe	1917	$L_j = approx. 5\,(y_2 - y_1)$

A frequently cited work on determining the length of a free jump was performed by the USBR (1955). The study utilized multiple experimental flumes and a total of 125 tests with discharges ranging from 1- to 28- $\frac{\mathrm{ft}^3}{\mathrm{s}}$ to establish the relationship. The length of the jump was normalized to the d_2 as shown in Figure 4.

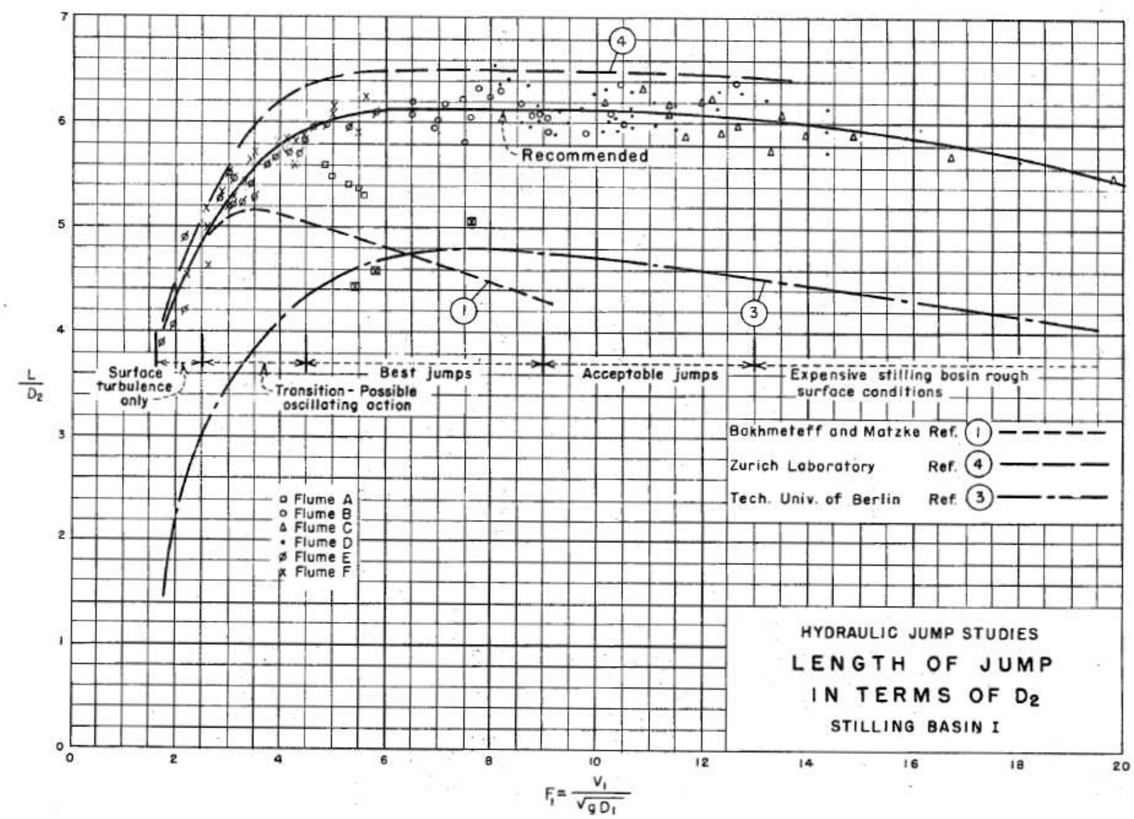

Figure 4. Length of Jump in Terms of d_2 (Source: USBR, 1955)

Often the hydraulic jump stilling basin incorporates appurtenant features to aid in energy dissipation to reduce the erosive capacity of the flow exiting the hydraulic jump. The incorporation of these features helps initiate the hydraulic jump via the momentum transferred to them, often denoting them as “forced” hydraulic jumps. The appurtenant features typically consist of chute blocks or negative step, one or multiple rows of baffle blocks, and a dentated or solid end sill. Stilling basins with erodible downstream channels often have additional downstream scour mitigation features (e.g. armor stone on invert and/or banks, concrete lining, flexible mattress).

Blaisdell (1948) concisely describes the function of the individual appurtenances as follows:

1) Chute blocks: provide additional depth at the entrance to the jump, break up the solid incoming jet into a series of smaller jets, and create turbulence for effective energy dissipation;
2) Baffle blocks: transfer momentum to the basin and create additional turbulence for energy dissipation; and
3) End sill: acts to deflect the bottom currents upward and away from the streambed, thereby minimizing downstream erosion near the structure.

The major features of the baffled hydraulic jump stilling basin are illustrated in Figure 5.

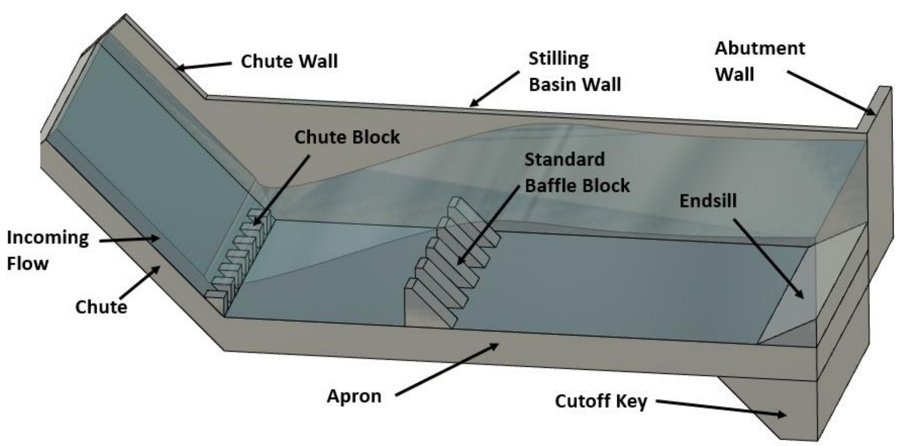

Figure 5. Baffled Hydraulic Jump Stilling Basin Definition Sketch

There have been numerous baffle shapes studied and utilized for stilling basins; most were used prior to the development of standard guidance. These include square, rectangle, recurve, stepped, and pyramid shapes as illustrated in Figure 6; with the most common shape being "f" (or standard). The use of many other shapes has been abandoned because of their fragility to hydrodynamic forces, economy, and propensity for cavitation damage. It is worth noting that baffle shape "d" has been used on many low Fr_1 stilling basins associated with high unit discharge and run-of-river dams.

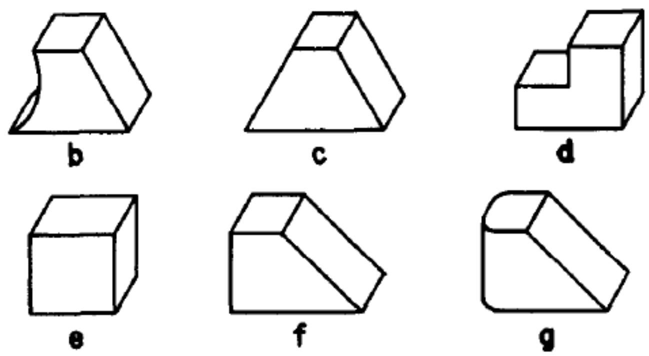

Figure 6. Stilling Basin Baffle Shapes (Source: USBR, 1987)

The determination of the incoming flow conditions for design of the hydraulic jump stilling basin is achieved by computing the incoming flow depth and velocity at the toe of the spillway or outlet, often using empirical relationships of losses associated with the crest and chute itself. The influence of piers and other features that may impact the uniformity of flow are often omitted and evaluated during physical or numerical verification modeling. USBR (1984) provides an empirical formula to determine the incoming flow conditions based on a ratio of the actual velocity to the theoretical velocity for high head dams. The equation and definition sketch are provided in Equation 4 and Figure 7; respectively.

Equation 4. Theoretical Velocity at Base of Free Overflow Spillway

$$V_T = \sqrt{2g(Z_{fall} - \frac{H_{crest}}{2})}$$

Where V_T is the theoretical velocity, Z_{fall} is the total fall height, and H_{crest} is the total head on the crest. It is worth noting that this equation does not account for the theoretical total specific head available at the base of the spillway; and is therefore an empirical baseline to apply the adjustment factors for spillway losses.

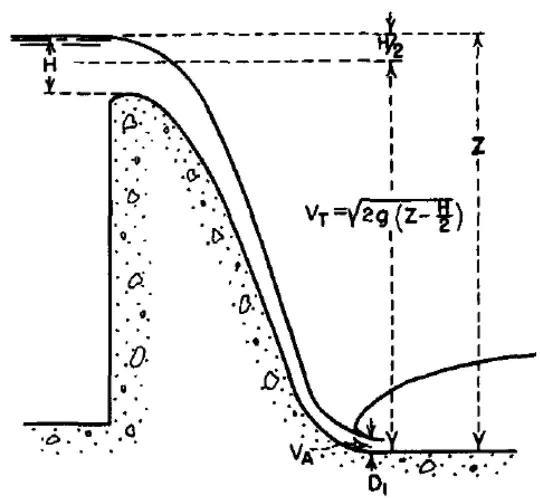

Figure 7. Definition Sketch for Parameters to Determine Theoretical Velocity at the Base of Free Overflow Spillway

The actual velocity is determined by applying the adjustment factor presented in Figure 8 to account for losses on the chute. As can be seen, the equation results in no adjustment factor for large overflows on short spillways.

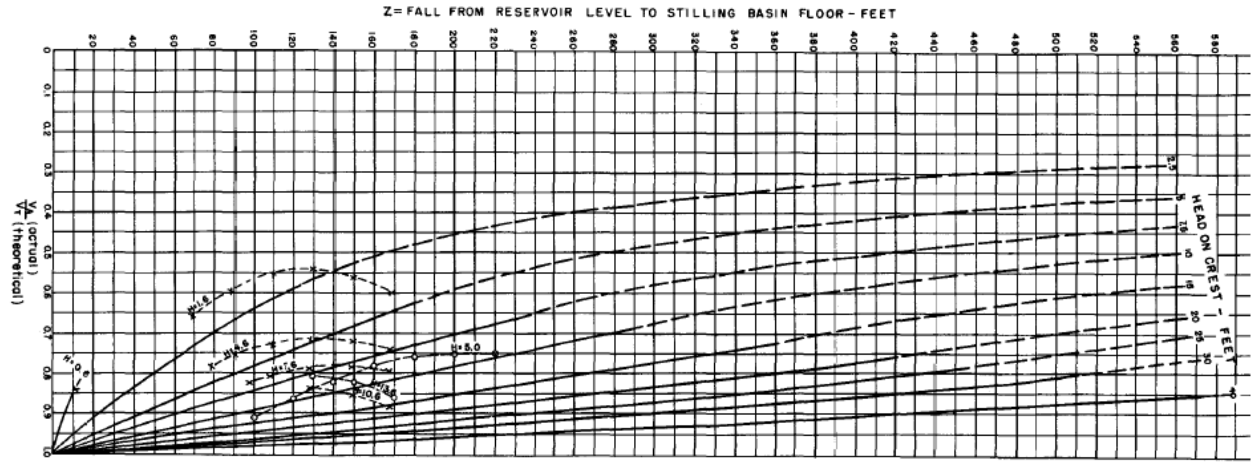

Figure 8. Empirical Adjustment Factors to Determine Actual Velocity at the Base of Free Overflow Spillway

USACE (1987) provides a method for estimating incoming flow conditions to a stilling basin for short spillways assuming the total energy head from the pool to the tailwater; and is solved through trial and error. The expression is shown in Equation 5.

Equation 5. Method to Estimate incoming Flow Conditions Based on Total Specific Head (USACE, 1987)

$$Z_P + \frac{{V_p}^2}{2g} = \frac{{V_1}^2}{2g} + d_1$$

Where Z_p is the depth in the pool above the datum and V_p is the depth averaged velocity in the pool above the control weir.

1.3 Background and Significance

The American Society of Civil Engineers (ASCE) Infrastructure Report Card states that there are over 91,000 dams in the United States, of which, 15,600 dams are listed as high-hazard-potential (ASCE, 2021). The Infrastructure Report Card also states that the average age of these dams is 57 years old; and by the year 2030, seven of 10 dams will be over 50-years old. It is estimated that the rehabilitation of these dams is approximately $94-Billion USD.

The USACE's current rehabilitation of Bluestone Dam's baffled hydraulic jump stilling basin will have a total cost exceeding $600 million USD by completion, in addition to a recently completed auxiliary spillway which had a cost of approximately $100-million USD. Recent construction status of the basin modification is shown in Figure 9, with the completed auxiliary stilling basin shown to the left. In addition to current construction activities, there are several additional baffled hydraulic jump basins within the USACE dam portfolio that will require modification at a planned cost of approximately $3-billion USD.

Figure 9. Bluestone Dam Stilling Basin Modification Construction (Photo by Author)

Many dams within the United States, and throughout the world, were constructed prior to modern methods of estimating extreme floods. This has resulted in inadequate spillway capacity being a common deficiency of dams, including thousands of dams in North America (FEMA, 2014).

The rate of construction of new hydropower dams has increased in the last decade as it is a primary energy source for 28 emerging and developing countries (IEA, 2020). The rate of hydropower dam constructed is expected to increase in Asia Pacific, Africa, and the Middle East due to increased energy demands and significant investment from the Chinese government.

Zhang et al. (2018) developed a geospatial database of dams from various sources and demonstrated that, although there is relatively little new dam development in North America and Europe, new dam development is high in South America and Oceania, as illustrated in Figure 10.

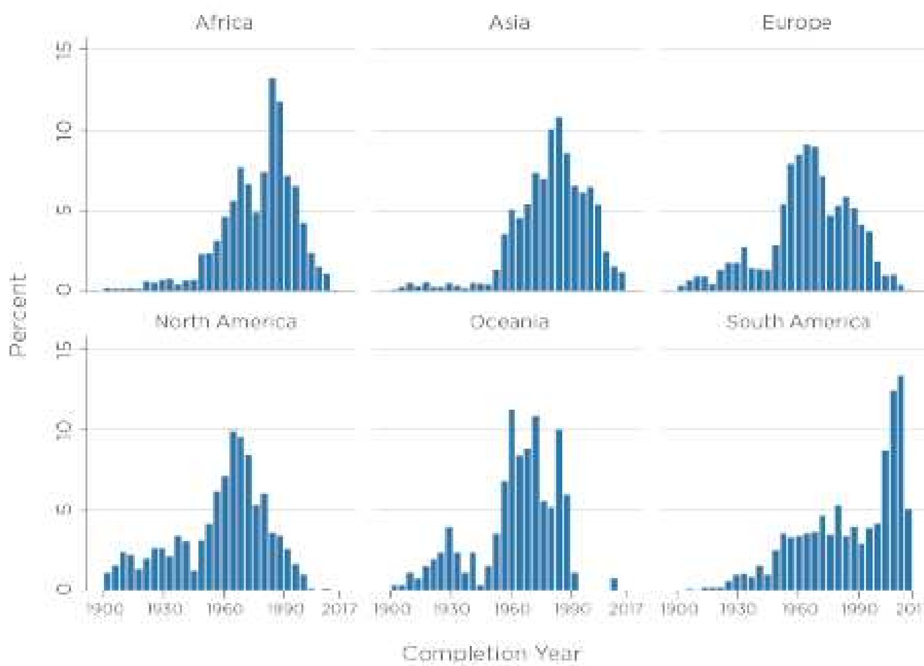

Figure 10. Distribution of Dam Construction by Year and Continent (Source: Zhang et al.., 2018)

Many inflow design floods were developed by transposing the largest flood within the region or the use of early estimates of maximum precipitation depth and intensity (Weather Bureau, 1952). The Federal Energy Regulatory Commission (FERC) states that the Probable Maximum Flood (PMF) has been utilized for inflow design of high hazard for more than 70-years (FERC, 2001). The PMF is defined by FERC as *"the flood that may be expected from the most severe combination of critical meteorological and hydrologic conditions that are reasonably possible in the drainage basin under study"*.

The critical meteorological conditions for the PMF are defined by the Probable Maximum Precipitation (PMP) for high hazard dams (USACE, 1991). The Probable Maximum Precipitation is defined by the World Meteorological Organization as "…the theoretical maximum precipitation for a given duration under modern meteorological conditions" (WMO, 2009). In many cases, these estimates have resulted in significant increases in hydrologic loading to spillways and stilling basins for large dams (Moses et al., 2015; Moses and Koutsunis, 2018).

An example of a hydraulic jump stilling basin's design capacity being exceeded and subsequent loss of the hydraulic jump action is illustrated by the El Guapo Dam spillway. The insufficient capacity of the chute walls resulted in a catastrophic failure in December 1999 (USACE, 2022). After the breach of the dam, the replacement spillway design was increased from the original discharge capacity of $101\frac{\mathrm{m}^3}{\mathrm{s}}$ to a capacity of $2{,}700\ \frac{\mathrm{m}^3}{\mathrm{s}}$, representing an increase by a factor of 27 (Suarez and Suarez, 2016). The breach progression is shown in Figure 11.

a) Before Breach *b) During breach* *c) After breach*

Figure 11. El Guapo Dam Failure (Source: Suarez and Suarez, 2016)

Costa (1985) performed a survey of the approximately 200 significant failures of dams throughout the world; of these, the primary failure mechanism was overtopping, representing 34-percent of the failures. Regan (2009) attributed the overall percentage of dam failures related to hydrologic deficiencies to 49-percent of all failure mechanisms. As new dams are constructed and existing dams undergo major spillway capacity upgrades to meet modern design criteria and risk guidelines, many stilling basins require upgrades to prevent failure from extreme floods.

Nonstationary climate trends and associated increased variability in extremes may also impact requirements for spillway capacity upgrades. Probable Maximum Precipitation (PMP) analyses are typically performed assuming stationary climate variables and typically do not account for the potential for increasing intensities resulting from climate trends. The peak moisture content has increased in time for many areas, and it is estimated that the PMP values could increase 10-percent every few decades (FEMA, 2013). The National Research Council (2024) has stated that there is no compelling evidence that an upper bound for precipitation intensity exists. This suggests that any inflow design based on upper estimates of precipitation depths could be exceeded with future understanding of extreme precipitation; and highlights the need for resilient hydraulic structures.

Considering the uncertainties associated with flood loading, a risk informed approach has been increasingly utilized to make prudent decisions related to extreme flood loading (Moses and Margo, 2023). An illustration of the major considerations in determining the inflow design flood loading is provided in Figure 12.

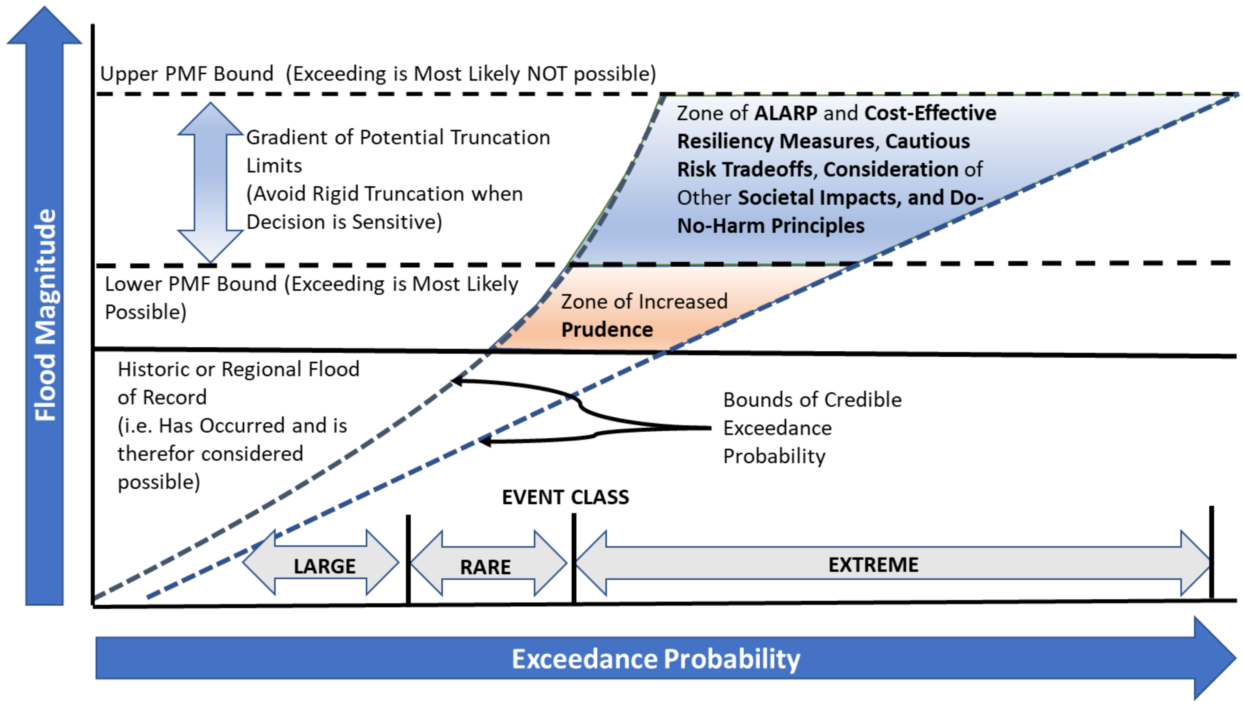

Figure 12. Risk Informed Approach to Inflow Design Floods (Source: Moses and Margo, 2023)

The baffled hydraulic jump stilling basin is the primary means of energy dissipation for low head dams and is often used for medium and high head dam applications (ICOLD, 2015). There will be increasing demands for spillway and stilling basin capacity upgrades due to increasing potential for extreme floods, remediation of aging infrastructure, increasing demands for water storage and hydropower, and significant new dam development in several regions of the world. The research described herein is performed to improve the efficiency and safety of both new stilling basin designs and the evaluation and modification of existing infrastructure.

2 RESEARCH GOALS AND OBJECTIVES

2.1 Knowledge Gap

There are three primary referenced sources for generalized baffled hydraulic jump stilling basin design guidance for spillways in the US, and throughout much of the world (Saint Anthony's Falls (SAF), USBR Type III, and USACE EM1603). This guidance has been adopted and reproduced in many engineering texts and adopted by various organizations for technical guidance and specifications for energy dissipators.

The standard design guidance is derived from separate and moderately independent series of physical hydraulic model experiments of baffled hydraulic jump stilling basins. The derivation of the SAF and USBR basins were the result of systematic physical model experimentation to determine typical basin geometries; while that of the USACE was derived from trends of specific project experimentation, thought to have reached near optimization of hydraulic performance for each project design.

Although the specifics of the experimental approaches were different, the basic experimental philosophy and primary goal of developing a generalized baffled hydraulic jump stilling basin geometry for use across a wide range of incoming flow conditions was the same. Surprisingly, the resulting published guidance for baffled hydraulic jump stilling basin geometry is drastically different. Figure 13 thru Figure 16 illustrate the inconsistency in basin parameters assuming a fixed incoming flow depth (d_1) of 4-feet and varied Froude numbers. Table 2 summarizes the published design guidance found in various literature and design guides.

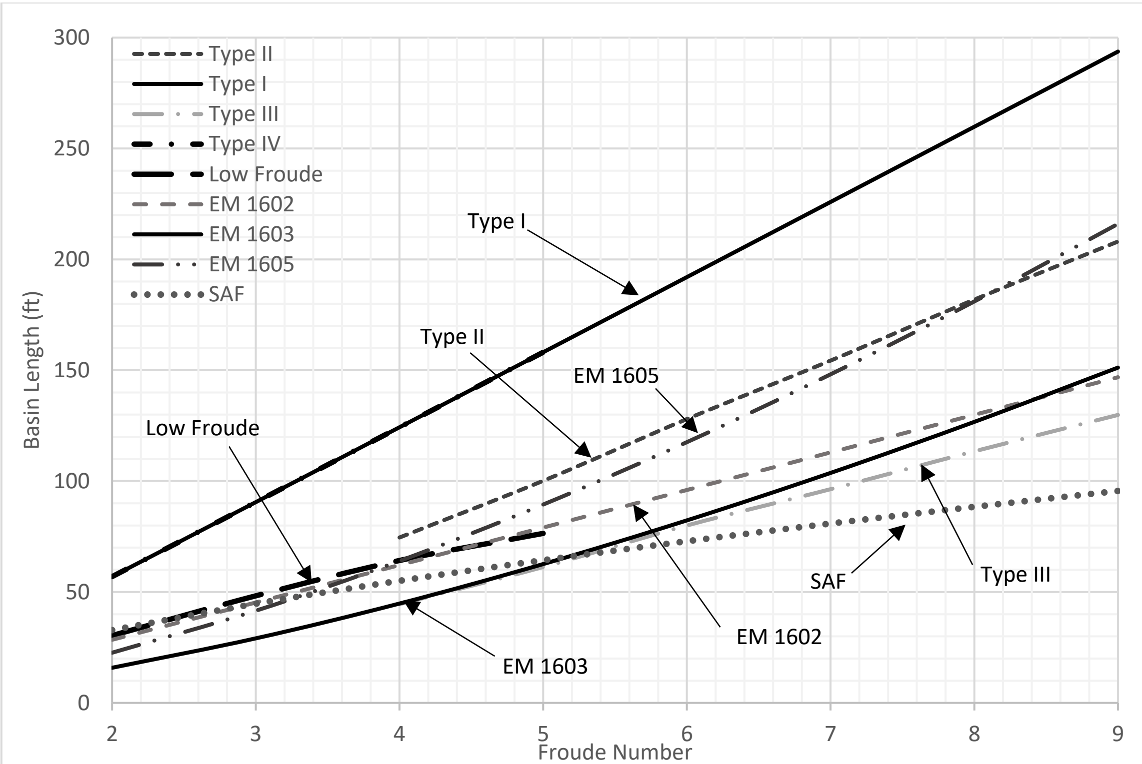

Figure 13. Demonstration of Inconsistency in Stilling Basin Guidance Related to Basin Length

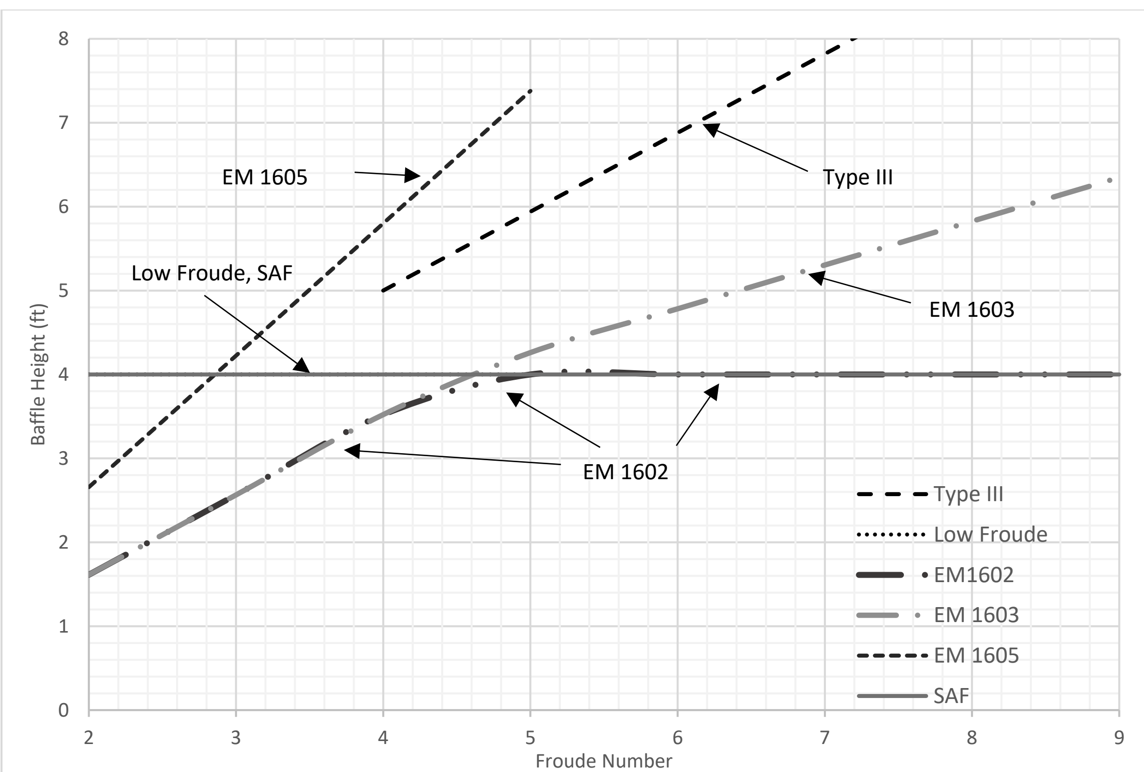

Figure 14. Demonstration of inconsistency in stilling basin guidance related to Baffle Height

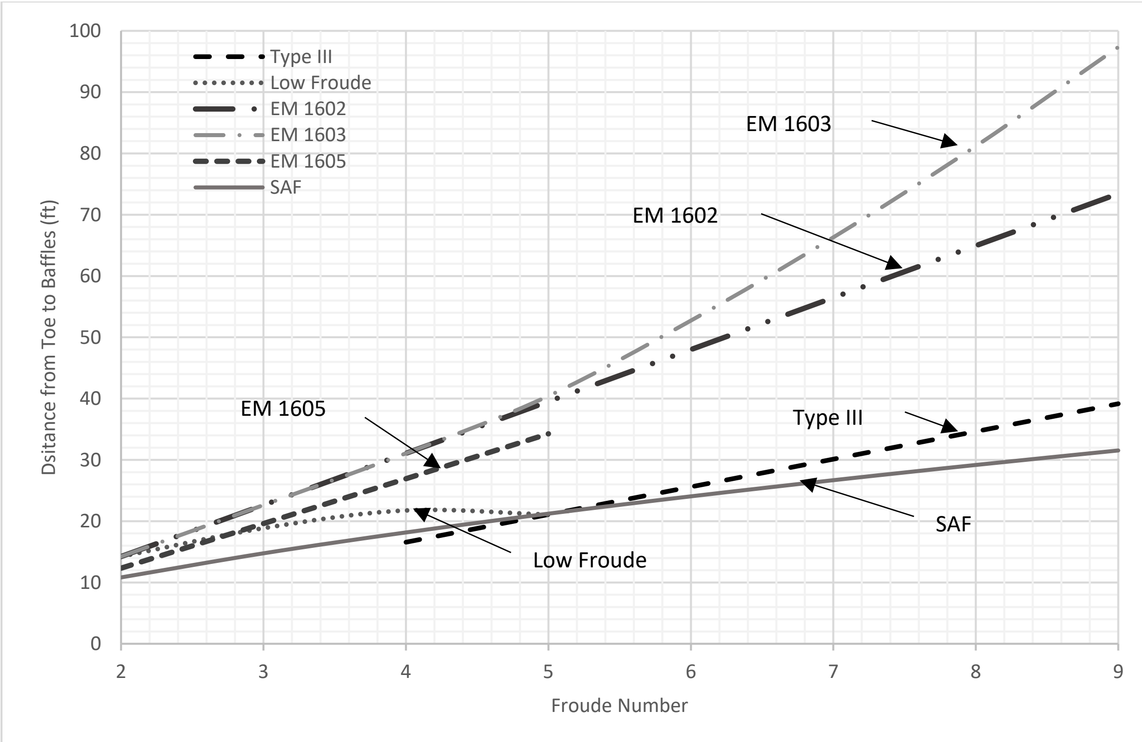

Figure 15. Demonstration of inconsistency in stilling basin guidance related to Baffle Station

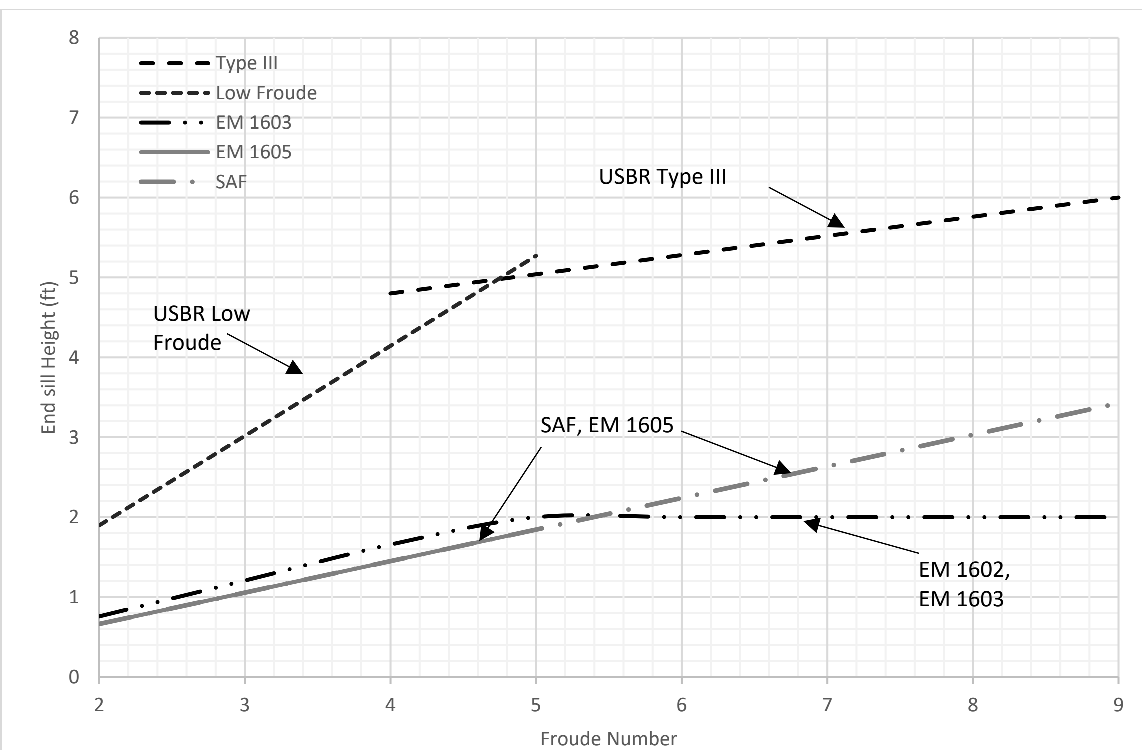

Figure 16. Demonstration of inconsistency in stilling basin guidance related to end sill height

Table 2. Design Parameters for Baffled and Unbaffled Basins from Major Sources Found in Literature

Item	USBR					USACE Baffled Basin			SAF
	Type I	Type II	Type III	Type IV	Low Froude	EM 1603	EM 1602	[1]EM 1605	
Basin Length	~ 6 d_2	3.6 to 4.4 d_2	2.2 to 2.6 d_2	~ 6 d_2	[2]2.5 to 3.2 d_2	[3]$K*d_1*Fr_1^{1.5}$	[4]2.5 to 5 d_2	$2*d1*Fr_1^{1.5}$	$d_2*4.5/Fr_1^{0.38}$
Chute Block Height	N/A	1.0 d_1	1.0 d_1	2.0 d_1	1.0 d_1	N/A	N/A	N/A	1.0 d_1
Chute Block Width	N/A	1.0 d_1	1.0 d_1	0.75 d_1	0.7 d_1	N/A	N/A	N/A	0.75 d_1
Chute Block Space	N/A	1.0 d_1	1.0 d_1	1.9 d_1	0.7 d_1	N/A	N/A	N/A	0.75 d_1
Baffle Height	N/A	N/A	1.4 d_1 to 3d_1	N/A	1.0 d_1	[5]0.17 d_2 to 1.6 d_1	Less of d_1 or 0.17 d_2	0.25 d_2	1.0 d_1
Baffle Width	N/A	N/A	0.75 Height	N/A	0.7 d_1	~ Height	~ Height	Not Given	[6]0.75 d_1
Baffle Space	N/A	N/A	0.75 Height	N/A	0.7 d_1	~ Height	~ Height	Not Given	0.75 d_1
Baffle Location	N/A	N/A	0.8 d_2	N/A	~ 0.8 to 1.5 d_2	[7]1.5 to 2 d_2	[8]1.5 d_2	1.3 d_2	0.33 * L_B
Second Row[9]	N/A					If Erodible Downstream Channel			N/A
End Sill Type	N/A	Dentated	Solid	Solid	Dentated	[10]Solid			Solid
End Sill Height	N/A	0.2 d_2	1.3 to 1.8 d_1	1.3 to 1.8 d_1	0.2 d_2	Less of 0.5 d_1 or 0.08 d_2	0.5 Baffle Height	0.15 d_2	0.07 d_2
End Sill Out Slope	N/A	[11]Vertical	1V to 2H	1V to 2H	[12]Vertical	1V to 1H	1V to 1H	1V to 5H	Vertical
Min TW	*1.0 d_2*				1.05 d_2	0.85 d_2			1.0 $d_1*Fr_1^{0.45}$

[1] Values provided are for gates full open
[2] The basin length extends past the end sill, with a horizontal apron being the termination of the apron.
[3] K is a factor that is a function of basin geometry, and ranges from 1.4 to 2
[4] 3 d_2 recommended for low erodibility, 2.5 d_2 for non-erodible channels, 3.5- to 4d_2 for high erodibility or Froude Numbers above 12, 3.5- to 4 d_2 for basins with no baffles.
[5] Height is 0.17 d_2 for Froude numbers under 4.5, then a factor of d_1 ranging from 1 to 1.9 for Froude numbers from 4.5 to 9
[6] The width of the baffles can vary to accommodate a flared basin, a blockage of 40 to 55 percent should be used.
[7] Located 1.5 d_2 for Froude numbers below 4.5, to 2 d_2 for Froude Number of 9
[8] For velocities under 60 ft/s with Fr 3.5 to 6.0, father back for higher velocities
[9] Second Row location is 0.5 d_2 for EM 1602 and EM 1605, location of 2.5 Baffle Heights for EM 1603
[10] Not specified; but USACE projects suggest intended to be solid.
[11] Vertical Upstream face and 1V to 2H out-slope in dentate
[12] Vertical upstream face and 1V to 2H out-slope in dentate, the upstream face of the end sill ranging from 1.5 to 2.9

The standard design guidance does not consider downstream channel erodibility, with the exception of the USACE (1987) recommending a second row of baffle blocks for erodible channels, although the term erodible is not described. This results in not being able to differentiate between a baffled hydraulic jump stilling basin founded on virtually non-erodible massive high strength rock verses one founded on highly erodible fine non-cohesive alluvium. This may result in the adoption of either an inefficient or ineffective design for the extremes of these two erodibility categories. Although there is a relatively large body-of-knowledge related to turbulence distribution in free hydraulic jumps, there is limited literature related to forced hydraulic jumps that occur in baffled hydraulic jump basins (Islam et al., 2007) as well as when the hydraulic jump action is lost within the basin.

There is also no systematic evaluation of performance of standard design guidance when the unit discharge is increased beyond the design value. Considering the consistent trend in increasing inflow design floods due to changing understanding of extreme precipitation, climate change, and increase water storage and hydropower demands this has been, and will continue to be, of primary interest to designers and infrastructure owners.

The recent development of a tapered block design and intermittent ramp (USBR, 2009; USBR, 2012; Moses and Koutsunis, 2018) has demonstrated potential applicability of baffled hydraulic jump stilling basins beyond the previous design criteria related to incoming velocity and required tailwater. A robust and systematic comparison of the tapered baffle block geometry to that of the standard baffle block design has not yet been performed, leaving one unable to determine the suitability and applicability of this block design in comparison to the standard block. In addition, the individual contribution to the reduction in required tailwater of the tapered block design and the intermittent ramps between the blocks is not known.

The combination of the recent findings of Ettema et al. (2019) related to the optimum baffle location for steep chutes and the unreconciled contradiction of the toe curves impact on baffled hydraulic jump basin performance, suggests that the influence of the steepness of the approach condition is not well known. This is important when considering the basin geometry for steep chutes and/or the influence of implementing a toe curve to align the streamwise flow in the horizontal direction.

The major inconsistencies and knowledge gaps described herein are often encountered in engineering practice, resulting in the somewhat arbitrary selection of a specific guidance, or the costly customization of an individual geometry through physical and/or numerical hydraulic modeling. This potentially results in sub-optimum design and modifications to existing infrastructure for increased capacity or to remediate maintenance issues and/or dam safety risks.

In addition to the development of design guidance for new and modified structures, established guidance is also used to evaluate the performance of existing structures to determine if modification is required. The assessment of the performance and associated vulnerabilities is dependent on the ability for the baffled hydraulic jump to maintain the jump action on the apron itself and/or prevent downstream erosion and undermining and/or scour and undermining of sidewalls or adjacent embankment materials. There is a general lack of knowledge related to the characteristics of the hydraulic jump and associated scour potential and boil heights for the standard basin geometries when incoming unit discharge exceeds that of which it was designed. Two examples of the need for specific project model investigations required to evaluate the performance and vulnerabilities of baffled hydraulic jump stilling basins subjected to increased unit discharge, are subsequently described.

2.2 Research Goal and Objectives

The primary goal of the research described herein is to provide additional information to facilitate the evaluation of standard baffle stilling basin design configurations under varied flow conditions, including resilience to increased unit discharge.

The objectives of the proposed research are related to the knowledge gaps previously described and to rectifying the differences in basin geometries across published design guidance and newer emerging trends. These objectives include the following:

1. Consolidate standard guidance on hydraulic jump stilling basins, where applicable,
2. Evaluate unit discharges less/greater than the design discharge (i.e. resilience to increased hydrologic loading or operational requirements),
3. Determine the influence of baffle block shape (e.g. standard or tapered),
4. Determine the influence of intermittent ramps for the tapered block configuration,
5. Evaluate a modified Type III configuration,
6. Determine the influence of spillway toe curves on steep chutes,
7. Describe the state-of-knowledge associated with baffled stilling basin cavitation and abrasion damage potential, and

8. Describe the general scour behavior downstream of standard baffled stilling basins.

3 LITERATURE REVIEW OF STILLING BASIN DESIGN AND EVALUATION (ABRIDGED)

3.1 Early History on Stilling Basins

The subject of the hydraulic jump has been observed for centuries as an intriguing natural phenomenon, but it was not until the early 1800's that the experiments of Bidone in 1819 and the theoretical analysis of Belanger in 1828 provided a solid foundation for predicting the occurrence and characteristics of the hydraulic jump. Belanger developed an early form of the momentum equation that is used in practically every method of stilling basin design today. Experimental validation of the basic momentum principle has been performed by numerous researchers since that time; but the applied experiments of the Miami River Conservancy District are noteworthy since they were in direct relationship of the development of baffled stilling basins for several large dams planned in the 1910's (Riegle and Beebe, 1917).

The first baffled stilling basin found in the literature review is that of the Gatun Dam Spillway associated with the Panama Canal. This project was completed in 1914 (Riegel, 1917), and is cited by USACE (1970) as the earliest use of "devices" [baffles] in a hydraulic jump stilling basin. The arced spillway utilizes a staggered row of tapered blocks that were verified with a 1:32 scale model in 1910 (ICC, 1910). The project experienced a significant flow event in 1914 (ICC, 1914). The model physical model and early flow event are shown in Figure 17.

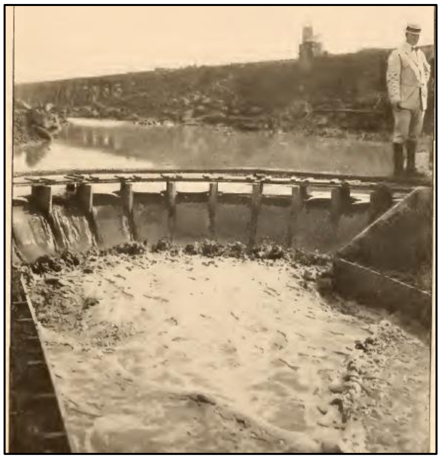

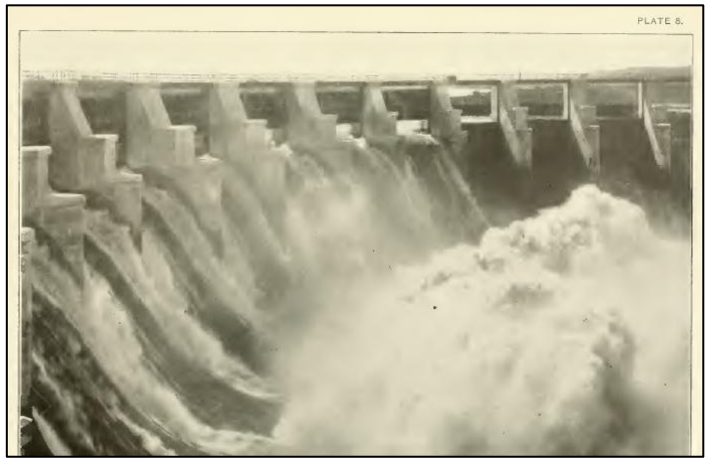

a) 1:32 scale model of Spillway

b) Spillway flow event of 1914

Figure 17. Gatun Dam Spillway Model-Prototype (Source: ICC, 1910; ICC 1919)

The spillway has been in operation for 110 years, including discharges exceeding the original design specifications. Outside some damage and removal of two baffles related to associated spray impacts to the powerhouse, the structure has performed well (Bal et al., 2020).

The Miami River Conservancy District was specifically charged with developing an effective and efficient energy dissipator for flood control projects planned after the devastating flood of 1913. The scope of the research was to develop basins that were satisfactory for a range of discharges from 9,000- to 50,000- $\frac{\mathrm{ft}^3}{\mathrm{s}}$ and with incoming velocities up to 60 $\frac{\mathrm{ft}}{\mathrm{s}}$. As with many engineers and researchers at the time, they determined that energy dissipation by means of “internal friction” (i.e. hydraulic jump) was the most effective method to apply to hydraulic structures.

At the same time, there were many similar developments going on throughout Europe in relation to developing, and often remediating, stilling basins. A rather complete compilation was developed by John Freeman (1929); who summarized the hydraulic laboratory practice at the time. One of the most consistent findings of Freeman was that deflecting the high velocity flows away from the downstream channel floor with the implementation of an end sill was of upmost importance. Many researchers were developing their own end sill through experiments to remediate structures in their respective regions. One particularly effective development was the dentated end sill by professor Rehbock of the Hydraulic Laboratory of Karlsruhe in the 1920s.

The Hydraulic Laboratory at Stockholm found that the shape of the spillway toe was significant when developing arrangements for the Chenderoh Power Plant, India. It was found that “It is evident that for a dam with a straight sloping face, the jump will be more certain to occur than with a bucket that discharges the water in a direction more horizontal.” (Freeman, 1929). .   An example of a standard baffled stilling basin with a toe curve and a straight line of intersection including chute blocks is illustrated in Figure 18.

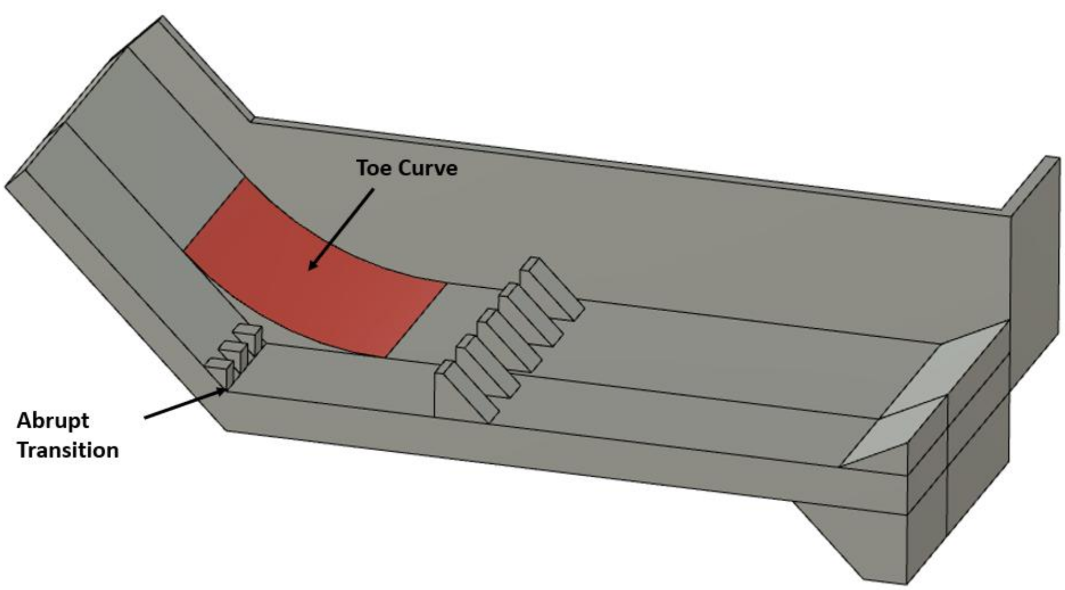

Figure 18. Illustration of Chute Geometry with (In RED) and without Toe Curve.

In addition to the baffled hydraulic jump stilling basin, hydraulic jump stilling basins with sloping aprons were used rather extensively in the first part of the 20th century. Solid and slotted bucket terminal structures were also widely used for sites with sufficient or excessive tailwater, whereas a bottom roller develops as opposed to a surface roller. These structures are not a focus of the current research and will not be discussed further.

3.2 Development of Current Standard Stilling Basins

In the first part of the 20th century, the design of stilling basins was a highly experimental procedure with a general lack of standard and verified design procedures. Various organizations had rules-of-thumb and there were several published design procedures (e.g. Schoklistch Basin), however many stilling basin designs and modifications were treated as a novel problem with much duplication and costly experimentation. In the 1940's and 1950's several important systematic evaluations of baffled hydraulic jump stilling basin design and performance were conducted by the US Soil Conservation Service, the US Bureau of Reclamation, and the US Army Corps of Engineers.

3.2.1 Saint Anthony Falls Stilling Basin

The Saint Anthony Falls (SAF) stilling basin was developed at the request of the United States Soil Conservation Service (SCS) in 1941. The SCS observed that most structures at the time were developed through individual model studies and that the SCS needed a standard stilling basin for smaller structures, in which individual physical model studies were not economically justified (USDA, 1959). The researchers tested several existing configurations at the St Anthony Falls Hydraulic Laboratory of the University of Minnesota. The research initiated with evaluation of previously published configurations, including the Schoklitsch stilling basin, and ultimately selected the rectangular hydraulic jump basin configuration currently being used by the USBR, as described by Warnock (USBR, 1939). This stilling basin consisted of chute blocks, baffle blocks, and an end sill.

The testing of the previous design suggested that the dimensions could be reduced from the initial configuration, leading to a series of 274 experiments using three flumes of various sizes to refine and standardize the stilling basin. The majority of these studies were conducted in a half-sectional model with a mobile bed comprised of commercial concrete sand (Blaisdell, 1948). The simulations were performed at constant flow rates until the downstream mobile sand bend had reached equilibrium. The flow conditions for the experiments are summarized by Blaisdell (1948) and shown in Table 3, the parameter "F" is the kinetic flow-factor λ_1.

Table 3. Model Flow Parameters for SAF Stilling Basin Experiments (Blaisdell, 1948)

Series	No. of tests	Q (ft³/sec)		V_1 (ft/sec)		d_1 (ft)		d_2 (ft)		F		$R \times 10^{-3}$	
		From	To	From	To	From	To	From	To	From	To	From	To
Culvert outlet...	100	0.09	0.4	2.9	12	0.04	0.17	0.17	0.8	3	57	12.7	54
Flume outlet....	108	0.04	0.8	2.8	22	0.05	0.15	0.13	1.8	5	200	14.2	237
Turbine room...	66	0.40	21	9.7	44	0.03	1.27	0.49	5.5	7	288	40.6	2,100
Total...........	274	0.04	21	2.8	44	0.03	1.27	0.13	5.5	3	288	12.7	2,100

The experiments iteratively and sequentially determined the optimum basin length, chute block dimensions, baffle dimensions and location, end sill dimensions, and wing wall configuration that resulted in minimum scour in the downstream mobile sand bed.

3.2.1.1 Basin Configuration

A profile view of the SAF stilling basin is provided in Figure 19, with the jump length being longer than the stilling basin length. The ultimate configuration of the chute blocks, baffle blocks, and end sill are discussed below.

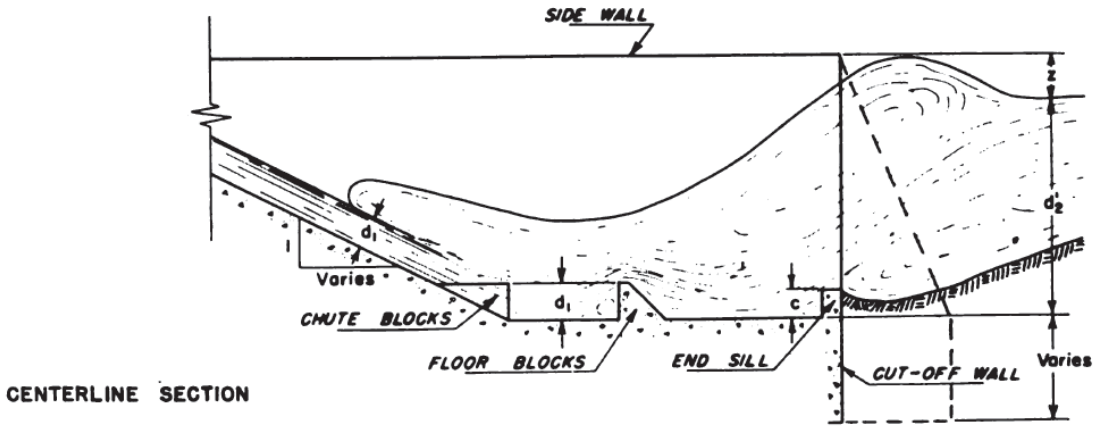

Figure 19. Profile of the SAF Stilling Basin (Source: USDA, 1959)

The length of the stilling basin is expressed by USDA (1959) as a function of the Froude number and normalized to the sequent depth, as shown in Equation 6.

Equation 6. SAF Stilling Basin Length (USDA, 1959)

$$\frac{L_{SB}}{d_2} = \frac{4.5}{{\lambda_1}^{0.38}} \ or \ \frac{4.5}{{Fr_1}^{0.76}}$$

Where L_{SB} is the length of stilling basin. Multiple configurations of chute blocks were evaluated in plan and section. Heights ranging from 0.75 d_1 to 1.75 d_1 were evaluated and ultimately a height of d_1 and a width of 0.75 d_1 was found to be optimum. The configuration of the chute and floor blocks was evaluated for the condition where the baffle blocks are aligned with the space in the chute blocks and one in which the spaces are aligned. It was observed that a "bad whirl" developed along the sidewall and downstream channel that caused considerable bed and bank erosion; therefore, it is recommended that the baffle blocks be aligned within the spaces of the chute blocks.

The distance to the baffle blocks were evaluated and it was found that both the location of $L_{SB}/3.2$ and $L_{SB}/2$ had nearly identical scour patterns, although $L_{SB}/2$ had a higher observed boil within the basin and therefore the remaining experiments were conducted using the distance of $L_{SB}/3$. The performance of the various configurations was judged semi-quantitatively based on the downstream scour-hole dimensions. Baffle heights of 1.5 d_1, 1.0 d_1, and 0.75 d_1 were evaluated with an incoming Fr_1 of 5.3 of with a height of d_1 exhibiting the least downstream scour and boil height.

An example of the experiments conducted to determine the optimum location of the baffle blocks is illustrated in Figure 20.

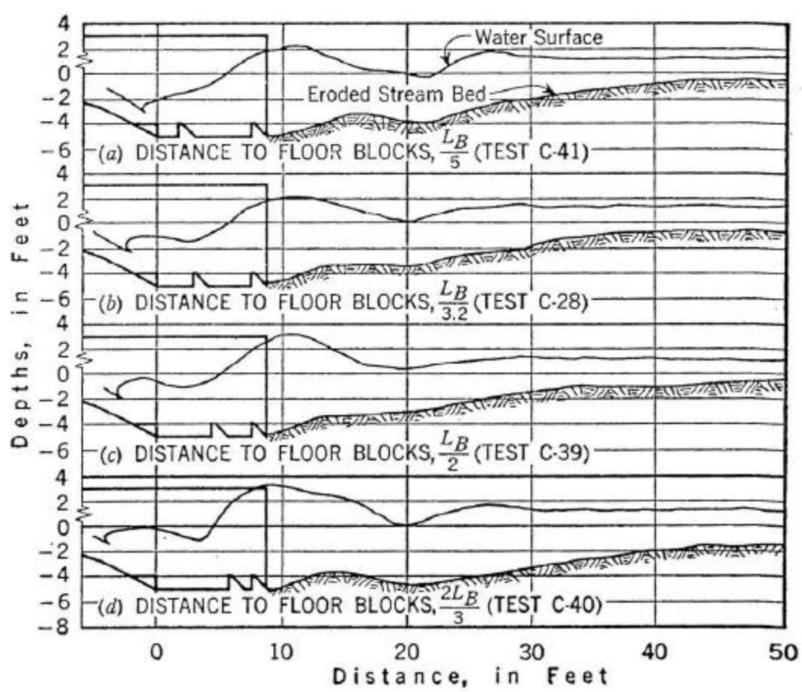

Figure 20. Effect of Floor Block Locations on Center-Line Bed and Water-Surface Profiles (Source: Blaisdell, 1948)

It was found that when the baffle block-out area was increased to 67-percent, the blocks behaved similarly to a continuous sill; resulting in the development of a significant boil and associated wall overtopping (Blaisdell, 1948). Based on this, the recommendation is made that the block-out ratio (R_B) for a single row of baffles to be between 40- and 55-percent of the basin width. A summary of the SAF basin proportions is shown in Figure 21.

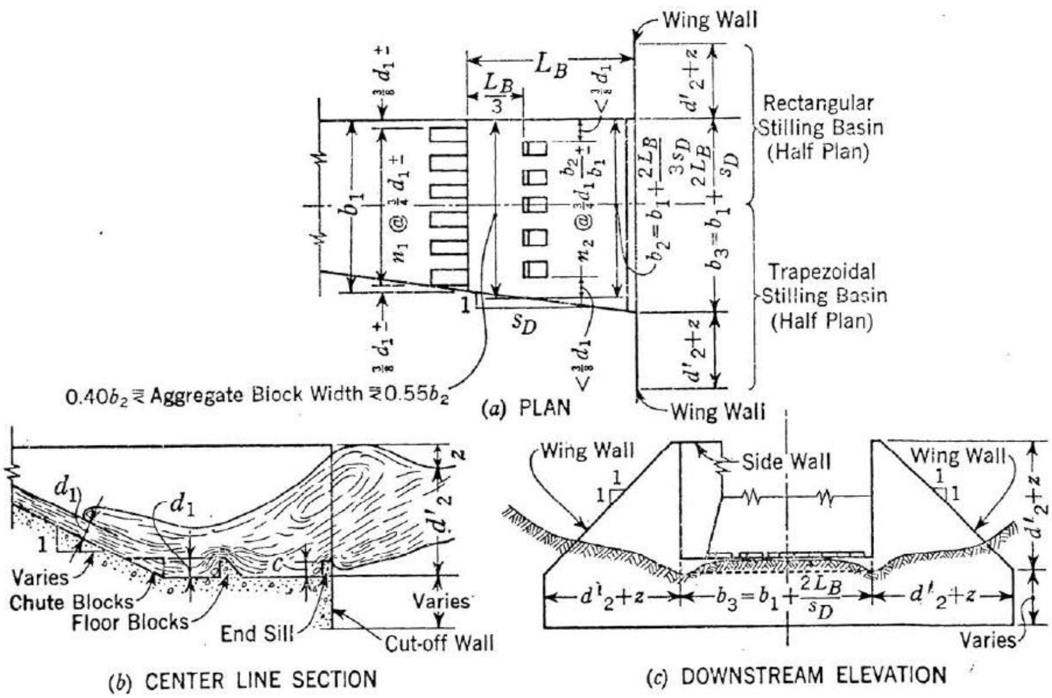

Figure 21. Proportions of the SAF Stilling Basin (Source: Blaisdell, 1948)

Many of the experiments to develop the standard basin were associated with a ratio of tailwater to sequent depth ($\frac{d'_2}{d_2}$) of approximately 0.85. It was determined that the lower tailwater provided good energy dissipation and economy related to stilling basin excavation depths, although it was found that tailwater could be reduced to a tailwater ratio of 0.76 d'_2/d_2 before the hydraulic jump action was lost. USDA (1959) adopted a required tailwater equation relating a ratio of the $\frac{d'_2}{d_2}$ to the kinetic flow factor, as shown in Equation 7.

Equation 7. SAF Stilling Basin Required Tailwater (USDA, 1959)

$$\frac{TW_{req}}{d_1} = 1.4{\lambda_1}^{0.45}$$

Where TW_{req} is the minimum required tailwater to maintain the hydraulic jump action.

3.2.2 USBR Stilling Basin

The baffled stilling basin currently used by the USBR is referred to as the Type III and was developed in the 1950's as a result of general research into various types of energy dissipators in 1952. The purpose of these investigations can be obtained through a quote from USBR (1955).

"Although the Bureau of Reclamation has design and constructed hundreds of stilling basins and energy dissipation devices in conjunction with spillways, outlet works, and canal structures, it has been necessary to make model studies on individual structures to be assured that these will operate as anticipated."

The experiments were conducted in four overflow flumes of various sizes and slopes ranging from 1 vertical to 0.7 to 2 horizontal. The Fr_1 ranged from 5.3 to 14.4 and the incoming velocities ranged from 10.5- to 23- $\frac{\text{ft}}{\text{s}}$. It is noteworthy that photos of the flumes provided in published documents suggest there were gradual toe-curves provided for the steeper sloped flumes. All flume experiments for baffled basins were conducted with rigid beds and performance was determined by observations related to jump length, jump stability, and exit flow conditions. It was determined that due to model scale effects, shorter jump lengths were observed at smaller scale due to "…out-of-scale frictional resistance on the floor and side walls". It is worth noting that the shorter jump length in the smaller flume may have also been associated with air-water phenomenon and the loss of the advection diffusion layer, which is discussed in Section 3.4.1.

It is stated that when developing the standardized baffled hydraulic jump stilling basins for the intermediate Froude number range, the SAF stilling basin was utilized as a starting point; but was deemed not conservative for use for larger structures that were the primary focus of the USBR at the time. Unlike the many of the stilling basins that the USACE was constructing during the 1940's and 1950's, the USBR Type III stilling basin adopted the incorporation of chute blocks from the SAF's basin.

The hydraulic jump length was the primary observational parameter for optimizing the baffled hydraulic jump basin geometry. Because this is a subjective term, there was a strict definition placed on its measurement and was taken as the greater length of a) the surface roller, or b) the high-velocity floor jet. To minimize observation bias, the same observers were utilized across experiments. The use of the floor jet as a length parameter implicitly includes consideration for downstream channel scour potential; but since the experiments were performed on a rigid bed, it does not allow for optimization of the appurtenance features explicitly for downstream scour potential. In addition, it does allow for the consideration of the solid-fluid interactions of the scoured bed as it relates to the jump length and behavior of the high velocity floor jet.

The USBR experiments concluded that the use of a toe curve did not have a perceivable impact on the stilling basin performance, although no description of the supporting experiments or data is included. This statement is in contradiction to that of previous literature (e.g. Freeman, 1929).

3.2.2.1 Basin Configuration

The USBR baffled stilling basin standard proportions are illustrated in Figure 22.

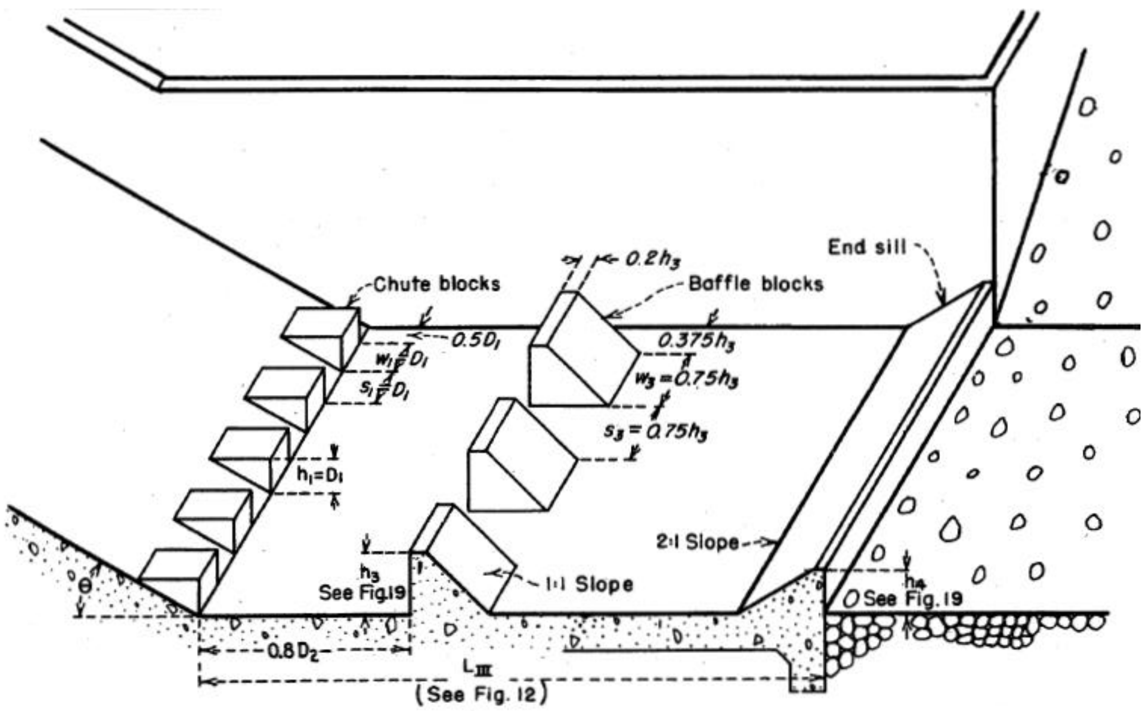

Figure 22. Proportions of USBR Type III Stilling Basin (USBR, 1954)

The chute blocks dimensions and configuration for the Type III basin were adopted from the Type II basin, which does not contain baffle blocks. The width, height, and spacing of the blocks is equal to the d_1. Unlike the observation of Blaisdell (1948), that the baffle blocks should be aligned at the spaces of the chute blocks, USBR (1984) states that "it is not necessary to stagger the baffle piers with the chute blocks as it is often difficult to avoid construction joints and there is little to be gained from a hydraulic standpoint". This finding may be a result of the experiments being conducted with a rigid bed and therefore the increased bed and bank erosion observed by Blasidell (1948) was not evident.

The USBR (1955) evaluated multiple block shapes as illustrated in Figure 6. Although there is not detailed data available for these tests, it is stated that block type “c” (pyramid) and “d” (positive step) were not effective at any height. It is also stated that the rounded blocks illustrated in Type “g” were significantly less effective than those types having a perpendicular face with sharp edges (Type “e” and “f”).

The block shape was found to have a rectangular face perpendicular to flow with a width to height ratio of 3/4ths (or slenderness ratio of 4/3rds). It is recommended that the blockage ratio is 0.5 and that the most effective location is that of 0.8 d_2 downstream from the chute blocks. The height of the baffle blocks and end sill increases with the Fr_1, as shown in Figure 22. The end sill has an exit slope of 2 horizontal to 1 vertical. The experiments found that the required tailwater was approximately 0.85 d_2, although it is recommended that the Type III basin be designed for 1.0 d_2. The dimensions of the baffle block and end sill normalized to d_1 as a function of Froude number is shown Figure 23.

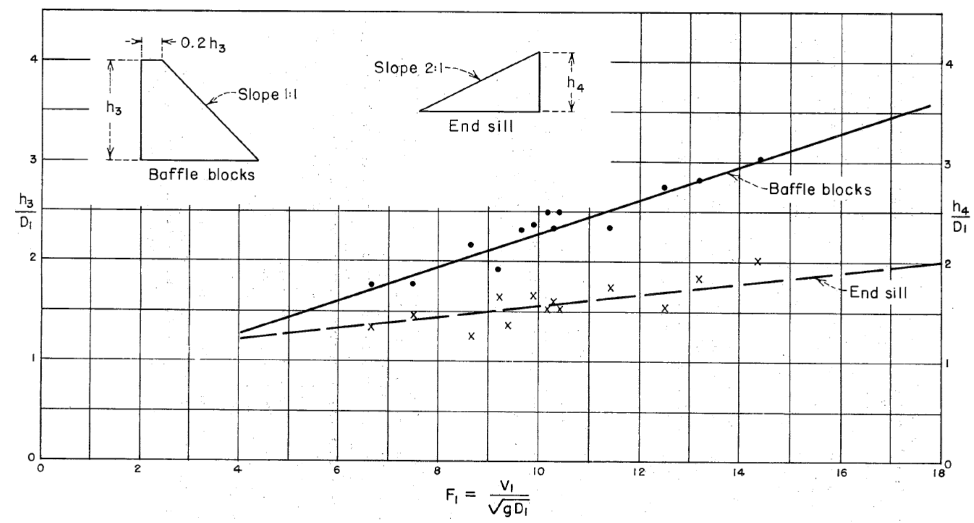

Figure 23. Baffle Block and End Sill Height Proportions of USBR Type III Stilling Basin (1984)

Additional experiments were conducted by USBR (1978) to evaluate a baffled stilling basin configuration for Fr_1 below 4.5. This evaluation determined that a baffled basin was recommended for lower Fr_1 instead of the previously recommended unbaffled Type IV stilling basin. The stilling basin features and dimensions are similar to that of Type III, consisting of chute blocks, a single row of baffle blocks, and a dentated end sill as shown in Figure 24.

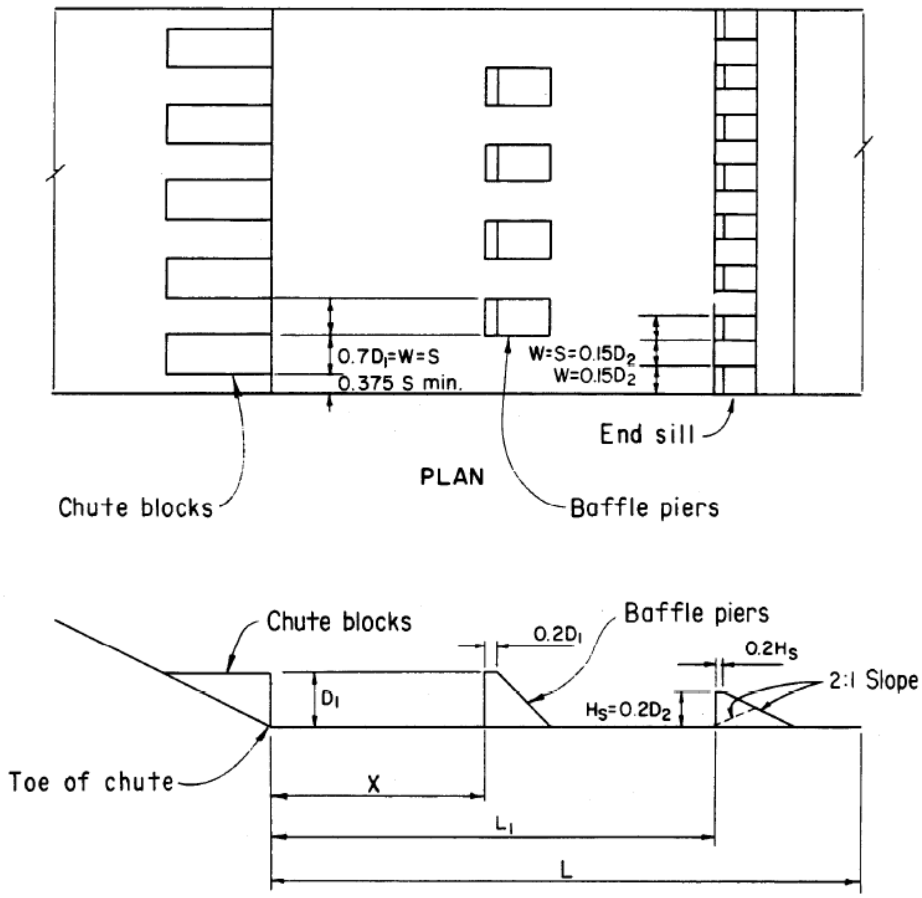

Figure 24. USBR Baffled Stilling Basin for Fr_1 from 2.5 to 4.5 (Source: USBR, 1978)

3.2.3 USACE Stilling Basin

The USACE developed many large navigation structures in the early 1900's, as well as constructing many large flood risk management dams starting in the 1930's. The stilling basin configuration for most of these structures was developed starting with rules-of-thumb and observations of performance from existing dams. It was common practice to develop designs through extensive physical model testing to determine the optimum stilling basin configuration considering site constraints, downstream erodibility, and a range of operating conditions.

The USACE has developed separate design guidance for baffled stilling basins that are described in three individual Engineering Manuals (EM). EM 1110-2-1603 is intended for open channel spillways applications and associated baffled hydraulic jump stilling basins (USACE, 1992). EM 1110-2-1602 describes stilling basins for use with reservoir bottom outlet works (USACE, 1980). EM 1110-2-1605 describes stilling basins for low head navigation dams (USACE, 1987). The baffled stilling basin for spillways will be the primary focus and subsequently described. This stilling basin is often referred to as “EM 1603” stilling basin.

The standard configuration includes one or two rows of baffle blocks and an end sill. It is noted that a second row of baffles is to be used if the downstream channel is “erodible”; but does not define this term. USACE (1980) states that the second row of baffles should be included if the tailwater is below a ratio of 0.9 of sequent depth. Unlike the USBR and SAF basins, the standard basin does not include chute blocks at the base of the chute. Although many stilling basins designed in the 1930’s and 1940’s by the USACE do have large negative steps at the chute entrance and multiple outlet works basins incorporated chute blocks to minimize the establishment of horizontal eddies in the basin associated with lateral expansions.

Based on the description included in a summary work related to trends in the design of baffled basins (USACE, 1969), the primary means of developing the general USACE guidance was through evaluation of trends and rules-of-thumb utilized by the staff at the Waterways Experiment Station (WES). The design guidance for baffled basin within the USACE is based on the prevailing configurations that were developed and evaluated at WES over the preceding decades. This approach assumes that the individual project designs were optimized for the given spillway, flow conditions, and channel geometry and erodibility.

USACE (1969) evaluated 28 USACE project specific experiments on baffled hydraulic jump stilling basins. The experiments/designs were conducted between 1947 and 1968 were catalogued based on the design flow conditions (e.g. incoming Froude number, velocity, and depth) and basin configuration (length, block location, block type/height, sill type/height). Approximately half of the stilling basins evaluated were in the 2.5 to 4.5 Fr_1 range, which is inconsistent with the argument that jumps in this range are oscillatory and should not be used if possible (Chow, 1959).

Most of the structures were associated with gravity overflow spillways and therefore most of the chute slopes were greater than 45-degrees. The mean unit discharge of the projects was 500 cfs/ft with a mean incoming velocity of 85 ft/s. The primary objective of most of the experimentation was to control the hydraulic jump and minimize downstream scour; therefore, evaluations were made with a mobile bed. An average of 12 configurations were evaluated for each of the 28 projects.

The guidance provided in USACE (1992) states that the maximum design conditions may have the ratio of actual tailwater to sequent depth ($\frac{d'_2}{d_2}$) not less than 0.85; with the recommendation that if optimum energy dissipation is required the basin should provide for the full sequent depth.

It is believed that the guidance for outlet works (USACE, 1979; USACE, 1980) is derived from several specific model studies and rules of thumb developed from the principal investigators of those studies. Unlike many baffled hydraulic jump stilling basins for overflow spillways, outlet works basins can often be submerged below tailwater with a low angle chute approach. This can result in weaker hydraulic jumps and eddies the entrain downstream material.

The guidance for navigation dams that typically have lower head and Fr_1 is believed to be derived by regression of at least 11 specific projects and general rules of thumb (USACE, 1987). Of the 11 projects specifically listed as references for guidance development, the mean Fr_1 was 3.4 with a maximum of 4.4.

There was at least one systematic evaluation of baffled basin performance performed by Basco (USACE, 1970) where many baffle configurations were evaluated to find the optimal baffled basin. It is believed that some of this information and lessons learned in subsequent model studies were incorporated into the current published guidance from the USACE (1992).

3.2.3.1 Basin Configuration

As previously mentioned, the standard USACE stilling basin does not include chute blocks and typically has two rows of baffle blocks with the second row aligned in the gaps of the first row, as shown in Figure 25.

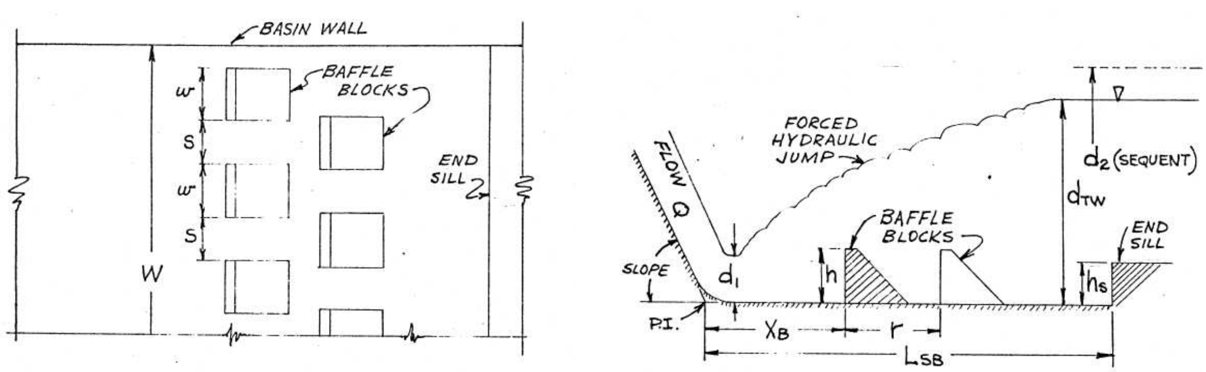

a) Plan *b) Profile*

Figure 25. Standard USACE Stilling Basin Configuration (USACE, 1969)

The stilling basin length is measured from the point of intersection of the toe curve to the end sill and is recommended as a function of the d_1 and the Fr_1 as shown in Equation 8. It is stated that this equation is valid for Fr_1 ranging from 2 to 20.

Equation 8. Length of USACE Stilling Basin associated with Dam Spillways (USACE, 1992)

$$L_{SB} = Kd_1 Fr_1^{\ 1.5}$$

K is a coefficient based on the configuration of the baffles and end sill and ranges from 1.4 to 2.0. The values for K recommended by USACE (1992) are:

- *K = 1.4*: Stilling basins with a vertical, stepped, or sloping end sill and one or two rows of baffles [implied is that these are stilling basins associated with dams and not run-of-river navigation structures];
- *K = 1.7*: Stilling basins with a vertical, stepped, or sloping end sill only; and
- *K = 2.0*: Stilling basin for low head broad crest weir navigation dam spillways with one or two rows of baffles and a sloping end sill (guidance included from USACE, 1987).

The shape of the baffles is similar to that of the USBR (1984) and USDA (1959) in that they are rectangular with a perpendicular face and sloping back. Many USACE stilling basins do have positive stepped, chamfered, or rounded baffle blocks that were evaluated with physical model experiments. USACE (1972) details the spillway and stilling basins of numerous USACE gated structures completed at the time. The majority of the low head navigation dams along the Ohio and Mississippi River have a block shape with positive steps (i.e. type “d” from Figure 6). USACE (1992) allows for a 6-inch chamfer on the baffle block edges to minimize chipping; but does not recommend the streamlined baffles (e.g. cavitation free) similar to those developed for Bluestone Dam (USACE, 1948).

The horizontal distance to the first row of baffles is constant at a ratio of 1.5 d_2 below a Fr_1 of 4 and increases with Fr_1 above that as shown in Figure 26 (a). When a second row of baffles are used, they should be placed 2.5 times the height of baffle downstream from the face of the first row.

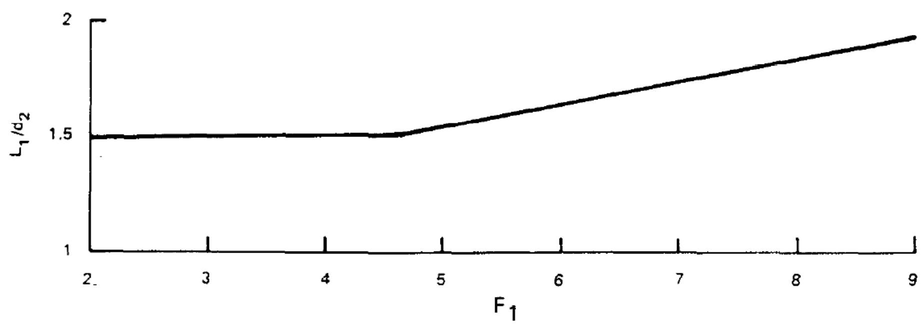

a) Distance to 1st Row of Baffle Blocks

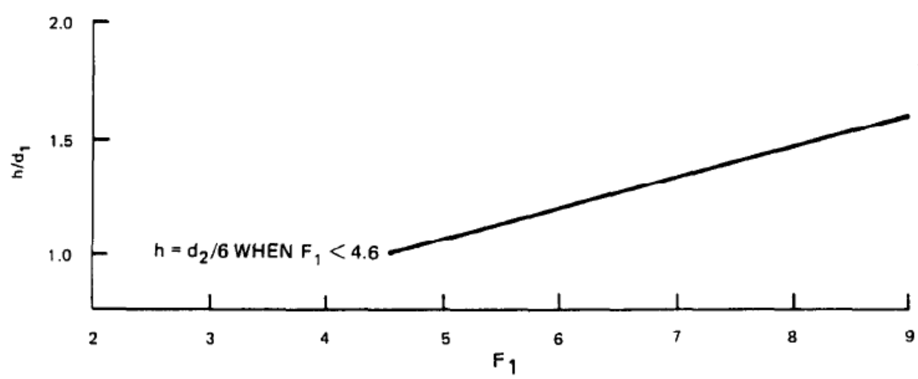

b) Height of Baffle Block

Figure 26. Distance to and Height of Baffle Block for Standard USACE Stilling Basin (USACE, 1992)

It is recommended by USACE (1992) that the end sill be a height based on the minimum of: a) $\frac{d_1}{2}$ or b) $\frac{d_2}{12}$. The recommended shape is sloping at a 1-horizontal to 1-vertcal to minimize the trapping of debris; although many stilling basins have utilized a vertical sill. It is stated that the shape does not affect the performance.

3.3 Other Major Design Considerations

3.3.1 Downstream Scour and Erosion

Downstream scour and erosion have been frequently encountered downstream of baffled hydraulic jump stilling basins, especially when founded on highly erodible foundations such as alluvium in sand bed river systems. It is noted by Hite (USACE, 1999) that many of the navigation dam baffled hydraulic jump stilling basins constructed prior to the 1960's were developed via experiments related to balanced flow conditions and uniform gate openings, and nearly all of them have experienced significant scour exceeding that observed in the model experiments related to unbalanced gate operations.

Localized downstream scour was a primary evaluation criterion for the development of the SAF stilling basin (Blaisdell, 1948) and many of the project specific model studies utilized in development of the standard USACE stilling basins (USACE, 1999; USACE, 1969; USACE, 1965).

Blaisdell (1948) evaluated the effects of varied tailwater on downstream scour potential for a Fr_1 of 5.4. The experiments evaluate the scour characteristics and average boil heights for various ratio of actual tailwater to sequent depth. It is worth noting that it was reported that no scour was observed for increased tailwater above that of sequent depth. There is also minimal scour related to a decrease in the tailwater ratio above 0.84. It is noted that for the initial loss of hydraulic jump action at a relative tailwater ratio of 0.69, no increase in the scour was observed immediately downstream of the end sill, although the total volume of material downstream "increased significantly". An illustration of the centerline profile and flow conditions is shown in Figure 27 and detailed in Table 4.

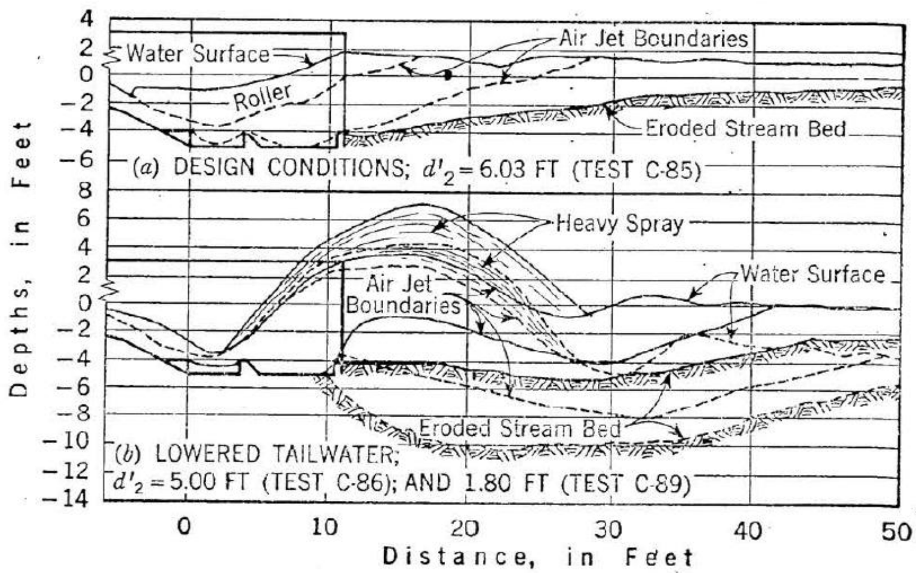

Figure 27. Proportions of the SAF Stilling Basin (Source: Blaisdell, 1948)

Table 4. SAF Stilling Basin influence of various tailwater conditions

Test No.	Flow, Q (ft^3/sec)	d'_2 (ft)	$\frac{d'_2}{d_2}$	Scour[a]	z_a (ft)	$\frac{z_a}{d_2}$
C92	277	11.49	1.60	−4.0	1.8	0.11
C91	274	9.56	1.33	−4.0	0.8	0.11
C90	277	8.54	1.19	−4.0	1.1	0.15
C83	286	7.71	1.07	−4.0	1.2	0.17
C84	280	7.08	0.98	−4.0	1.0	0.14
C85	272	6.03	0.84	−4.1	0.8	0.11
C86	280	5.00	0.69	−5.0	7.0[b]	0.97
C87	280	3.80	0.53	−7.0	7.1[b]	0.99
C88	277	2.77	0.38	−8.5	7.4[b]	1.03
C89	275	1.80	0.25	−10.1	7.9[b]	1.10
C98	284	−0.40	−0.06	−13.0	10.5[b]	1:46

[a] Elevation of maximum depth of scour, in feet, on the channel center line near the end of the stilling basin.
[b] Surface roller on hydraulic jump washed out of stilling basin.

3.3.2 Stilling Basin Wall Configuration

It is typical practice to configure spillway stilling basin walls to the height of the maximum tailwater elevation to eliminate the potential for return flow. Return flow can create dynamic conditions within the basin that affect performance, such as drowning the jump, excessive turbulence, and increasing localized scour downstream of the basin (USACE, 1990). Walls should be kept near vertical. Batters as small as 4V to 1H can result in downstream eddies (USACE, 1997). USACE (1965) states that "generally, in design, sidewall heights may be reduced moderate amounts, but hydraulic model studies are required to determine the maximum possible reduction in wall heights".

Blaisdell (1948) notes that there is an increase in scour downstream of the basin if recirculation flows into the basin due to inadequate sidewall height resulting from the increase in localized unit discharge and the decreased effectiveness of the end sill to deflect the high velocity floor jet upwards. There is also potential for wall overtopping resulting from the boil within the basin and these flows eroding material outside of the wall. Blaisdell (1948) found that the ratio of the maximum boil height (z_m) to the sequent depth is independent of Fr_1 and that the maximum ratio observed is 0.31, therefore recommending a freeboard height value equal to one-third d_2 is required to minimize flow over the sidewalls. It is also stated that for Fr_1 above 4.5, the maximum boil occurs downstream of the basin. Blaisdell (1948) also observed that placement of blocks too close to the sidewall would result in increased boil height, and recommended a 0.375 d_1 minimum offset from the stilling basin side wall. The USBR (1984) adopted a value of 0.375 the baffle block height. The USACE (1992) recommends a minimum offset of 0.5 the width of the baffle block.

The outer baffle blocks for the 178-feet high Conchas Dam were attached to the sidewall. An inspection after the basin experienced a significant prolonged flow event showed no signs of damage to the stilling basin, with the exception of downstream of the baffle block where there was wear on the downstream face of the baffle block, adjacent wall, and floor. The erosion of the concrete was attributed to a "dead" spot that formed along the two outer baffle blocks at the connection with the sidewall (Berryhill, 1957). There is no discussion related to the cause of the erosion (e.g. abrasion, cavitation, weak materials).

USBR (1987) recommends that the empirical relationship in Equation 9 is satisfactory for most basins to determine side wall heights so that walls are not overtopped by surges, splash and spray, and wave action set up by turbulence of the jump.

Equation 9. Stilling Basin Freeboard (USBR, 1987)

$$H_{SB\ freeboard} = 0.1(v_1 + d_2)$$

Where $H_{SB\ freeboard}$ is the freeboard height in feet, v_1 is in $\frac{\text{ft}}{\text{s}}$, and d_2 is in feet.

3.3.3 Wing/Tie-Back Walls

The flow exiting the stilling basin can have high erosive capacity; especially in the vicinity of the sidewall where the high velocity flows interact with the still water outside the downstream exit. If the stilling basin terminates in the vicinity of an erodible foundation, side slope, or earthen embankment; it is often necessary to provide a wing wall or tie-back wall to protect the toe of the side-slope to erosion. USACE (1980) states that wing walls are usually required if the invert of the downstream exit channel is 0.3 d_2 wider than the stilling basin.

USACE (1965) states that a 90-degree wall can suppress the formation of a side roller, with a 45-degree, or a rounded endwall being more optimal for suppressing the side roller. USACE (1992) states that free standing sidewalls without wing walls are preferred to reduce the reflection of downstream waves and associated scour and erosion of the downstream banks.

USDA (1959) states that a perpendicular wall approximately the length of half the stilling basin wall height can be used to decrease downstream scour along the side wall profile and that a 45-degree wall provides the best results. Additionally, the 45-degree wall can be tapered from the maximum wall height to the invert elevation at a 1 horizontal to 1 vertical slope.

The impact of the expansion of the SAF standard basin is shown in Figure 28, as described by Rice and Kadavy (1993) for an incoming Fr_1 of 6.5 using highly erodible bed material. As shown the additional hydraulic attack is likely at the sidewalls due to increase turbulence production with the flow expansion and associated eddies.

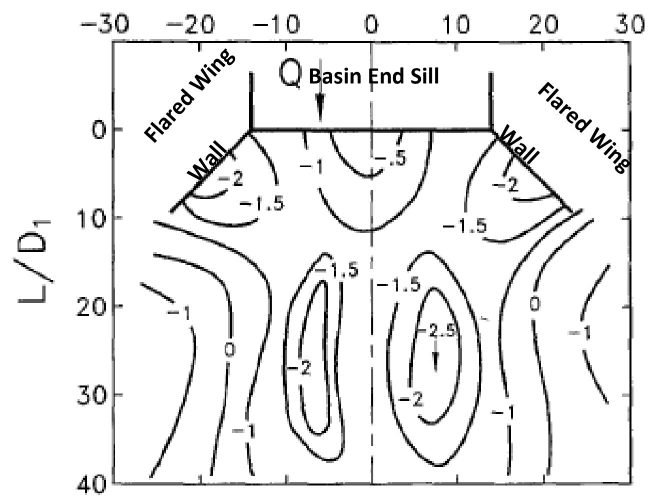

Figure 28. Typical Scour Pattern of SAF Basins with Highly Erodible Bed Material (Source: Adapted from Rice and Kadavy, 1993)

3.3.4 Exit Channel and Downstream Protection

USACE (1965) recommends that the downstream channel bottom width should be offset at a distance of 0.15 d_2 or a minimum of 5-feet and that any channel protection be located 0.25 to 0.5 times the maximum particle diameter below the top of the end sill. If the exit channel is required to be sloped upwards to the natural river channel, the slope is not steeper than 10 horizontal to 1 vertical to minimize the potential for material to be deposited into the basin from downstream, resulting in the potential for damage due to abrasion. USBR (1980) states that the wave and surge heights should be evaluated in relation to their potential to cause bank erosion downstream of stilling basins.

USACE (1957) utilizes the approach developed by Isbash (1932) to relate particle stability to average velocity, specific weight of the stone, and the turbulence intensity (e.g. low and high) that has often been used as a first estimation of required stone armor size on inverts downstream of stilling basins; as shown in Figure 29.

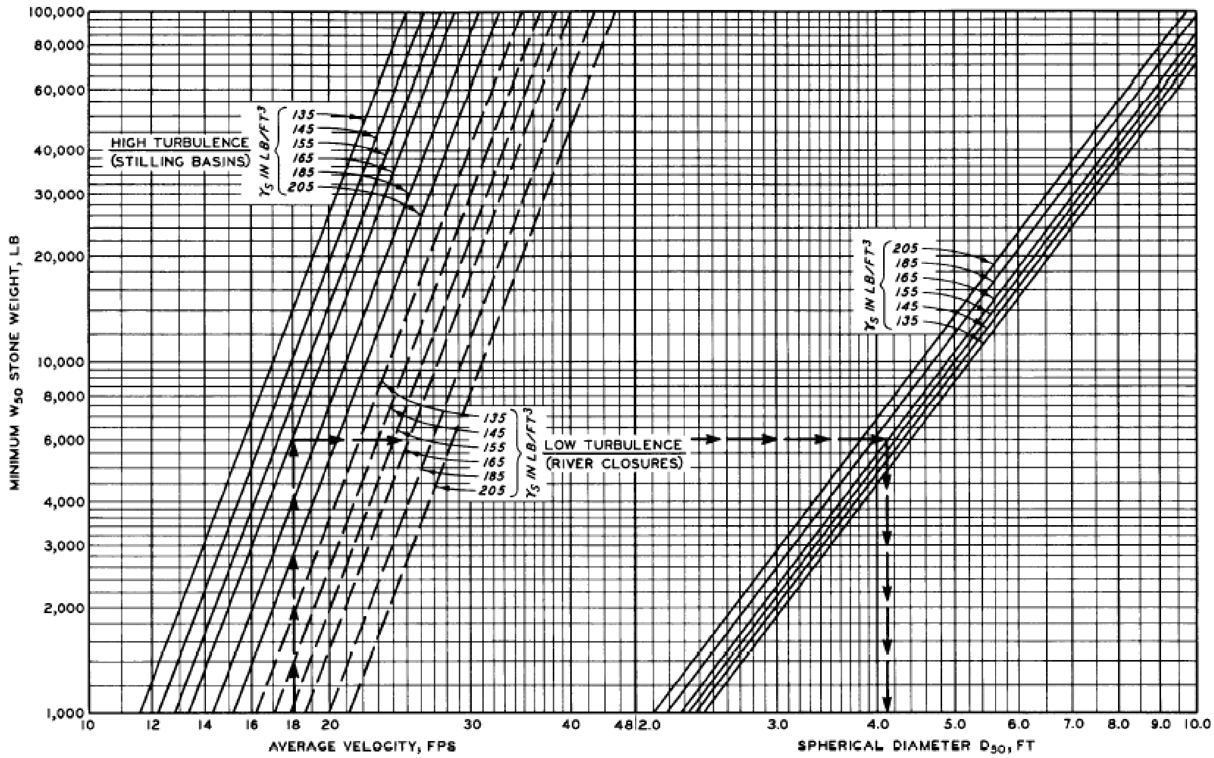

Figure 29. Critical Velocity for Stone Stability (USACE, 1957)

Rice and Kadavy (1993) utilized a comprehensive mobile bed physical Froude scale model to evaluate riprap protection downstream of the SAF stilling basin. A relationship to the d_1 was developed to estimate the stable median stone size and length of scour as a function of Fr_1. It was determined that the length of protection can be estimated with Equation 10.

Equation 10. Minimum Length of Riprap Protection Downstream of SAF Stilling Basin (Source: Rice and Kadavy, 1993)

$$\frac{L_s}{d_1} = 4.5Fr_1$$

Where L_s is the length of downstream riprap protection. Similarly, the median stone size is estimated for the apron elevation at the elevation of the stilling basin floor and the elevation of the end sill in; in Equation 11 and Equation 12, respectively.

Equation 11. Minimum Median Stone Size for Protection Downstream of SAF Basin, placed at Elevation of Stilling Basin Floor (Source: Rice and Kadavy, 1993)

$$\frac{D_{50}}{d_1} > \left(\frac{Fr_1 + 2.2}{10.2}\right)^2$$

Where D_{50} is the median stone size.

Equation 12. Minimum Median Stone Size for Protection Downstream of SAF Basin, placed at Elevation of End Sill (Source: Rice and Kadavy, 1993)

$$\frac{D_{50}}{d_1} > \left(\frac{Fr_1 + 4.0}{10.2}\right)^{3.33}$$

It is demonstrated that the stable median stones size increase if the elevation of the riprap apron is increased to that of the end sill. The relationship of the median stone size (a) and the length of RipRap apron (b) is illustrated in Figure 30.

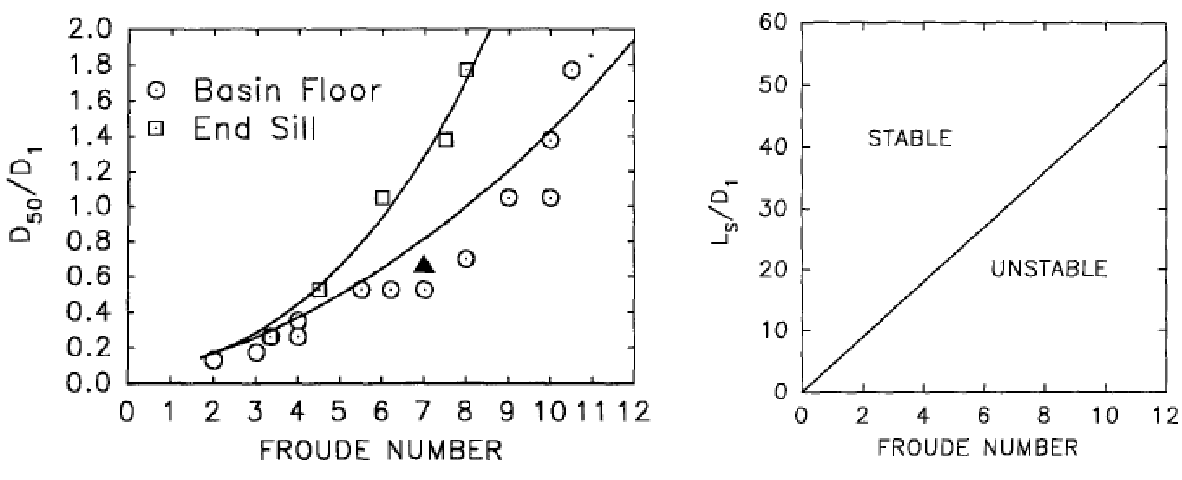

a) Riprap Size Required for Stability

b) Minimum Length of Riprap

Figure 30. Riprap Size and Extents Downstream of SAF Stilling Basin (Source: Rice and Kadavy, 1993)

3.3.5 Cavitation Damage

3.3.5.1 General

Damage associated with cavitation has been a critical concern for hydraulic structures for over a century. Cavitation is the formation of a gas and water vapor mixture due to localized low pressures that are below the vapor pressure of water. The collapse of these vapor pockets in the vicinity of high pressures along the boundary of a spillway or stilling basin can propagate a shockwave that can produce small pits in the material associated with the dynamic force of the collapse. The process of vapor bubble collapse and the associated shockwave is shown in Figure 31.

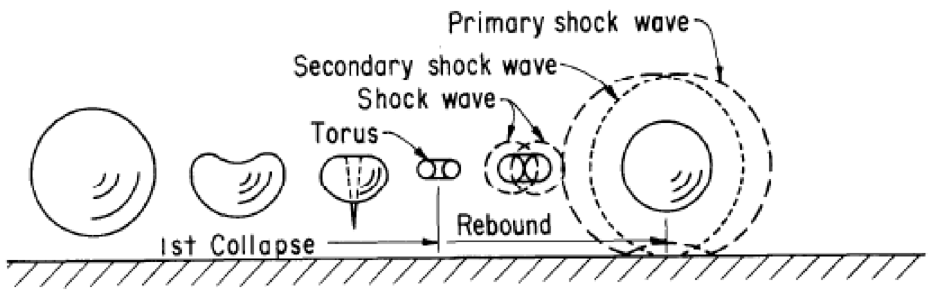

Figure 31. Collapse of individual bubble near a boundary (Source: USBR, 1990)

The potential for development of cavitation is often expressed by a version of the Euler number, defined as the cavitation index (USACE 1992, USBR 1990). The cavitation index is expressed mathematically by Equation 13, with lower values presenting more severe cavitation damage potential.

Equation 13. Cavitation Index

$$\sigma = \frac{P_0 - P_v}{\rho \frac{{V_0}^2}{2}} \; or \; \frac{H_0 - H_v}{\frac{{V_0}^2}{2g}}$$

Where ρ is the density of water, P_0 or H_0 are the Reference Pressure, V_0 is the reference velocity, P_v or H_v are the vapor pressure of water at ambient conditions, and σ is the cavitation index. Generally, values below 0.2 are considered flow conditions for significant concern for cavitation damage in spillways (USBR, 1990). The presence of large protrusions into flow such as chute blocks and baffle blocks may experience cavitation damage at a higher value than experienced for spillway chutes with relatively small protrusions or other surface anomalies that can promote the formation of cavitation.

Cavitation damage can often be identified by its impact on the surface texture. The texture associated with cavitation damage will often be highly irregular and rough, unlike the smooth texture created by erosion due to abrasion. Also, the damage is likely to be symmetrically in occurrence and located immediately downstream of a surface anomaly that forms the cavitation. The damage can often result in a positive feedback loop of damage, whereas the damage surface results in additional protrusion and subsequent damage farther downstream.

The air concentration of the gas/water mixture is found to be very important in the prevention of cavitation damage. This is because the presence of air in the mixture changes the sonic velocity of the mixture, thereby reducing the dynamic force applied to the material comprising the spillway. The sonic velocity properties of the air-water mixture are illustrated in Figure 32.

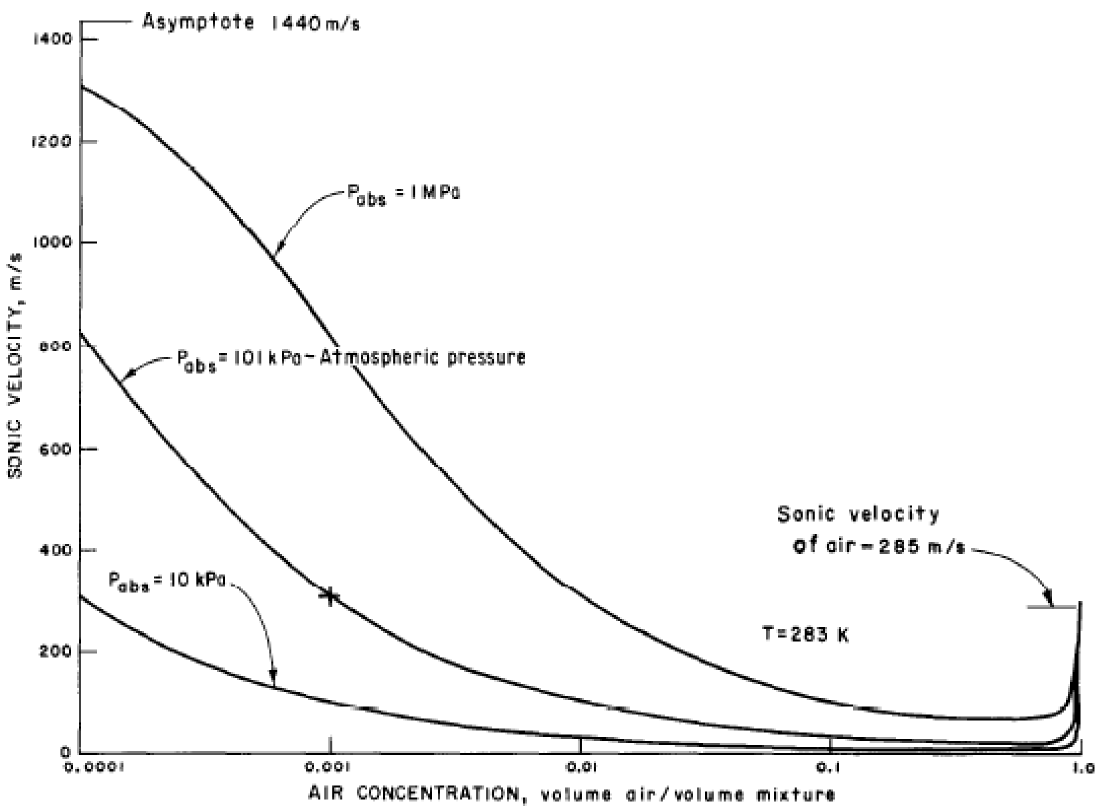

Figure 32. Sonic Velocity of Air-Water Mixtures (Source: USBR, 1990)

The phenomenon of the hydraulic jump includes significant aeration and mixing which also likely plays a role in the development of cavitation damage within hydraulic jump stilling basins. Chanson (2015) demonstrates that there can be a 10- to 30-percent decrease from the incoming depth average velocity to the maximum local velocity within ten times the incoming flow depth. Stonjnic (2020) found that the bottom air concentration exceeded 5-percent for the location of $0.1 < L_j < 0.5$ and this area is "…expected to be exempted from cavitation damage…".

There are multiple examples associated with cavitation damage immediately downstream of control gates where low cavitation index values exist due to low pressure and high velocity, as well as minimal aeration of flow (USBR, 1990). Another common location to experience cavitation damage is near the bottom of a spillway chute in the vicinity of a change in direction such as a bend (e.g. Hoover Dam, Glen Canyon Dam) or a trajectory bucket (e.g. Tarbela Dam, Shahid Abbaspour HPP, Guri Dam) which are detailed throughout the literature (Ripken and Dahlin, 1972;USBR, 1990; ACI, 2008; USACE, 1990; Pereira, 2020).

Another common location for cavitation damage is associated with the deflector systems for combined spillway and sluiceways associated with concrete gravity dams. Thomas and Hopkins described that this damage has been observed for at Tygart Dam (West Virginia) and was a focus for the development of the design for Bluestone Dam (West Virginia). The USACE (1946) evaluated multiple deflector designs based on the effectiveness of the energy dissipation as the jet spreads into the stilling pool, along with the potential to develop low pressures within the deflector and portal walls. The configuration with the highest average pressures (all positive) was selected and constructed. The sluiceways have been in operation for 77 years with significant damage occurring at a particular location on either side of the deflector baffles. The 1-inch thick steel lining has been destroyed in nearly the same location for all 16 sluice deflectors. An illustration of the damage (a) and a schematic of the deflector geometry and piezometer locations (b) are shown in Figure 33. Similar damage has been noted at Pine Flat Dam and Fort Gibson Dam.

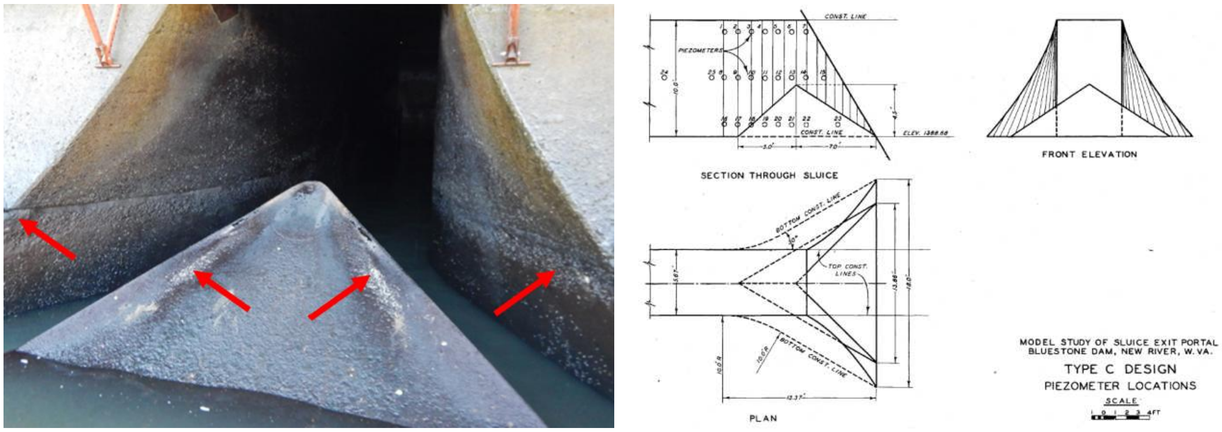

a) Observed Damage to Deflector and Sluice Portal

b) Illustration of Deflector and Piezometer tap locations

Figure 33. Bluestone Dam Sluice Deflector Damage (Source: a) author, b) USACE, 1946)

3.3.5.2 Physical Model Testing

Laboratory investigations have been conducted to evaluate pressures on the surface of baffle blocks (USACE, 1970). In addition, multiple laboratory investigations have evaluated the cavitation potential in vacuum tank experiments where sub-atmospheric pressures are used to reproduce the cavitation processes to the laboratory scale. May (1987) provides a thorough literature review of laboratory experiments conducted related to the evaluation of incipient cavitation for chute and baffle blocks.

USACE (1970) evaluate the side pressures on standard and tee shaped blocks to make relative comparisons of the cavitation potential associated with various ratios of heights and baffle locations. It was found that the pressure increased with increasing streamwise distance of baffle placement, as shown in Figure 34. It was also determined that the tee shaped blocks (with side taper and a flat top) had higher observed side pressures than that of the standard shape block.

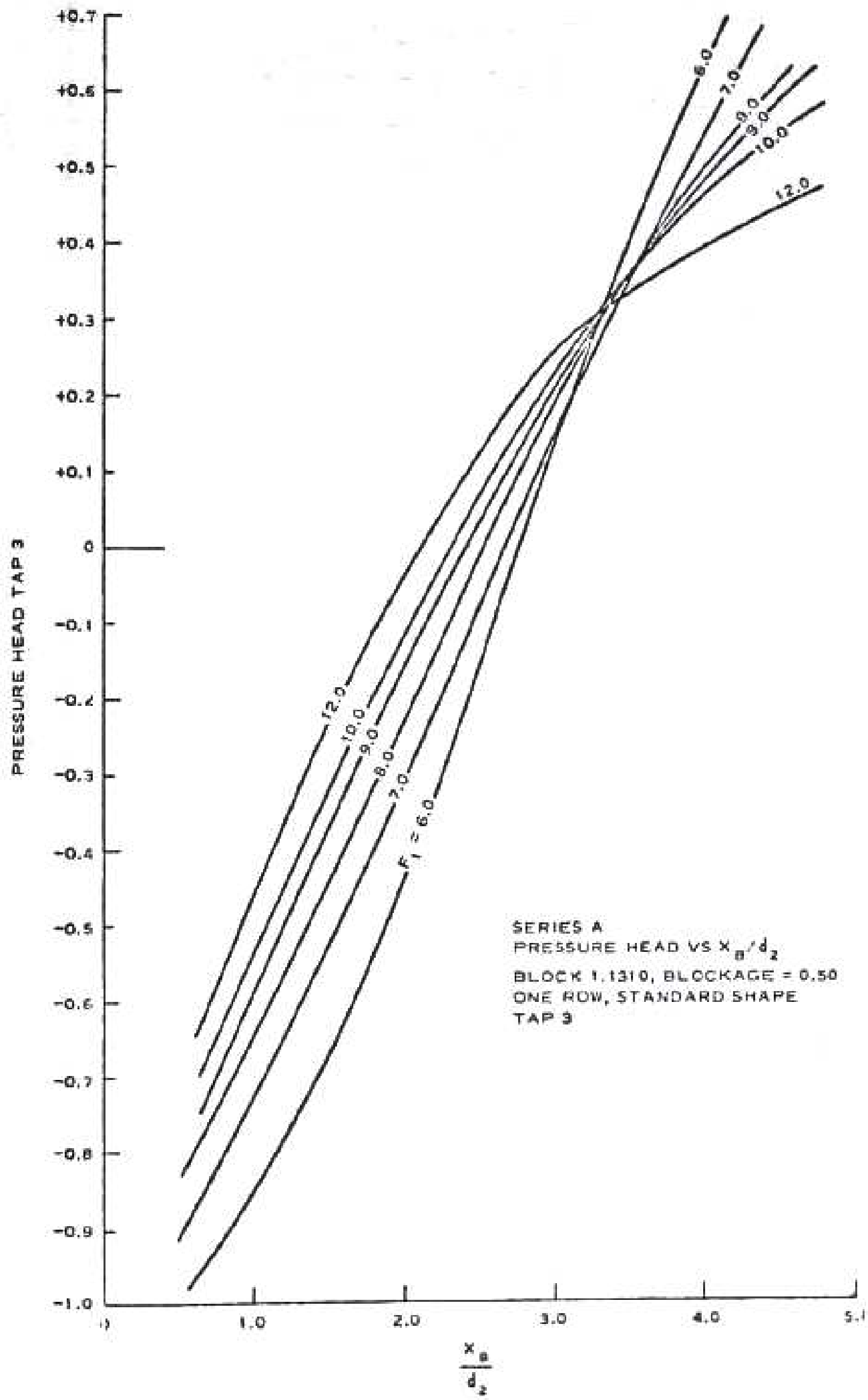

Figure 34. Baffle Block Sidewall Pressure with Varied Froude Number and Block Location (USACE, 1970)

Rozanov and Kaveshnikov (1973) evaluated 12 different baffle shapes in a vacuum chamber to evaluate if particular shapes were more susceptible to damage. The experiments used flow velocities of 5 to 10 m/s and concrete that was proportioned to be more susceptible to cavitation damage than typical concrete found in prototype structures; but not susceptible to damage without the cavitation phenomenon. It was found that the submergence of the hydraulic jump could increase the cavitation damage potential by a factor of 1.7 to 2.45. It was also found that by introducing air upstream of the block region producing a concentration of 1.25 to 1.5-percent, cavitation damage was reduced by a factor of 1.5 to 2; while a concentration of 6- to 7-percent fully eliminated cavitation damage for the conditions evaluated. The erosion rates and location of damage by the ration of the cavitation index "K" to the cavitation index threshold for incipient damage "K_{cl}" are shown in Figure 35 for a reference flow velocity of 8.1 m/s. It is worth noting that the pyramid block type exhibits the highest damage intensity for both the block and the floor. Also, the tapered block with intermittent ramps has similar observed floor erosion rates as square blocks.

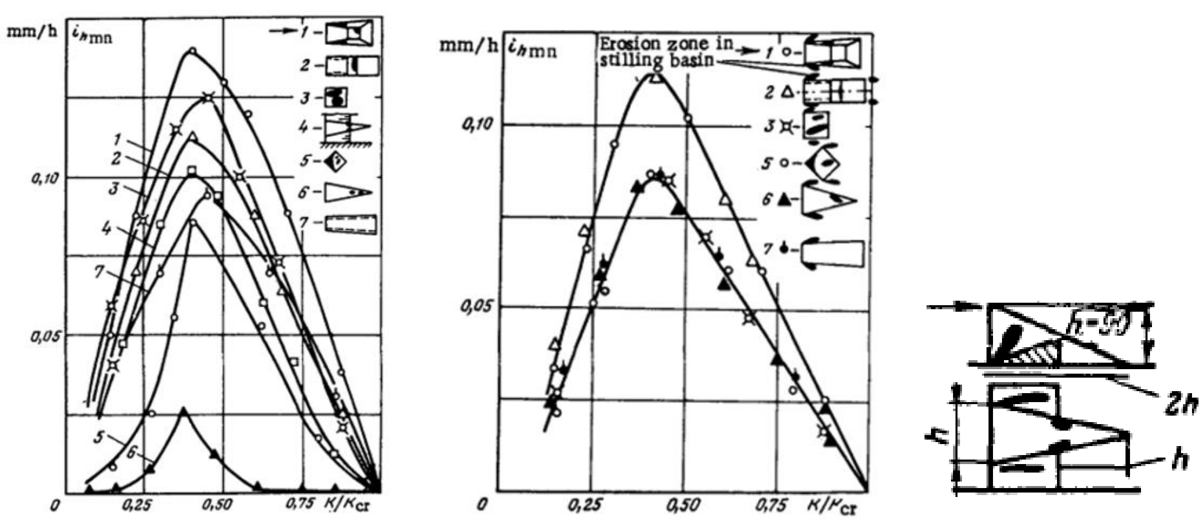

a) *damage to Baffle Blocks* *b)* damage to basin floor *c)* damage locations

Figure 35. Relationship of Damage Intensity to Cavitation Index Ratio (Source: Rozanov and Kaveshnikov, 1973)

Rozanov et al. (1971) determined that flow conditions in the range of super-cavitation occurs at approximately a cavitation index range of 0.3. In this range the cavitation forms a jet from it's source that has the potential to reattach to the surface creating significant damage intensity to hydraulic structures. If the jet can be redirected into the flow field as to not contact the boundary, then the cavitation can disperse and collapse within the flow field. Elements of hydraulic structures that use features to deflect the cavitation jet away from the boundary are thereby defined as super-cavitating elements. Potential modifications to a baffle block that redirects the cavitation jet into the flow field are illustrated in Figure 36. It is worth noting that there is no face perpendicular to the flow for any of the three configurations, making it's use as an appurtenant feature for a hydraulic jump stilling basin questionable.

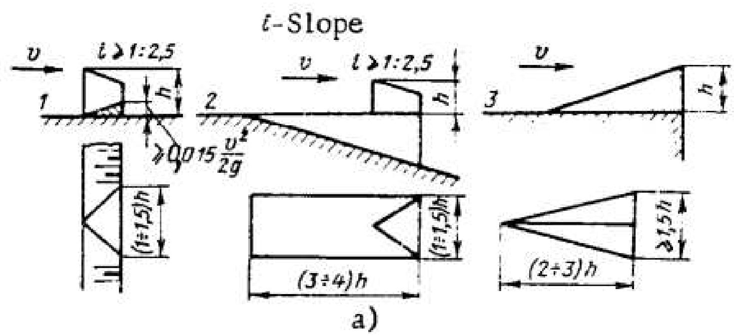

Figure 36. Super-cavitating Baffle Block Configurations (Source: Rozanov et al. 1971)

3.3.5.3 Observed Stilling Basin Damage

3.3.5.3.1 General

ICOLD (1987) states that the deflector blocks are very exposed to cavitation erosion since they are in an area of high velocity. Multiple authors have tied the potential for cavitation damage to a threshold incoming velocity at which special caution should be applied above this value (USBR, 1987; Thomas, 1942). USACE (1992) does not place thresholds for use of baffle blocks based on cavitation concerns; but states that “the baffle blocks at Chief Joseph Dam have experienced significant cavitation damage”.

The use of chute blocks at the toe of baffled stilling basins is less common in current time because of the cavitation damage potential. The chute blocks are located at a location of highest velocity and in a location that has not been aerated. Significant cavitation damage is reported to have occurred to the Porto Colombia HHP project in Brazil (Pereira, 2020). The damage occurred along the sides of the chute blocks and on the floor immediately downstream of the blocks.

There are fewer cases found in practice and literature associated with cavitation damage to stilling basins. It is also possible that damage associated with abrasion or ball milling has been attributed to cavitation. ACI (1999) developed a compendium of concrete erosion damage case histories in the US and Canada and identified two such case histories within stilling basins. One of these is at the Yellowtail main dam, whereas the damage occurred in the chute and the energy dissipator is a flip bucket (i.e. not a stilling hydraulic jump basin). The other is the Yellowtail Afterbay Dam.

The Yellow Tail afterbay stilling basin is a 33 feet high concrete gravity diversion dam with observed damage to the baffle blocks and floor. ACI (1999) states that there was abrasion damage to the dentates and floor of the sluiceways; although the damage to the side of the baffle blocks and floor adjacent were eroded by cavitation. The damage along the side of the baffle block is shown in Figure 37.

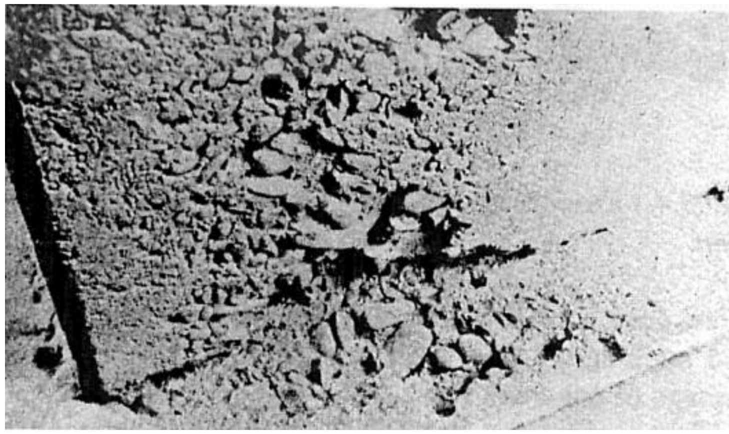

Figure 37. Cavitation Damage on Side of Yellowtail Afterbay Baffle Block (Source: ACI, 2008)

The damage was repaired with bonded concrete, epoxy-bonded concrete, and epoxy-bonded epoxy mortar and after 23 years of operation, it was noted that there was no additional damage outside minor spalls.

The Claytor Lake Spillway baffles are referenced by USACE, 1948 as the reason that there needed to be the development of "cavitation-free" baffle piers and justified additional investigations into the pressures on the side and back of standard block shapes. Soon after construction, the project was subject to the record flood of 1940 which was approximately the spillway design flood. The spillway consists of baffle piers immediately upstream of the end sill with a recurved face. The project operation during the 1940 flood (a) and the newly constructed baffle and end sill (b) are shown in Figure 38.

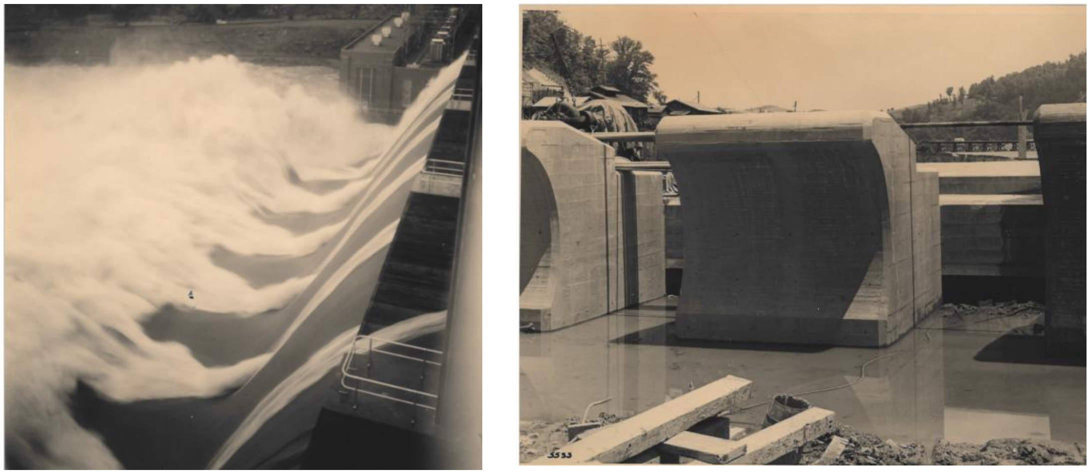

a) *Aerial View of Spillway* b) *Newly Constructed Baffle Block*

Figure 38. Spillway Flow Event of 1940 at Claytor Dam (Courtesy: AEP, 2024)

Observations after the flood event demonstrated minor pitting along the side of the baffle block (a) which match the locations of reattachment of cavitation flashes in the vacuum tank experiments (b) are shown in Figure 39.

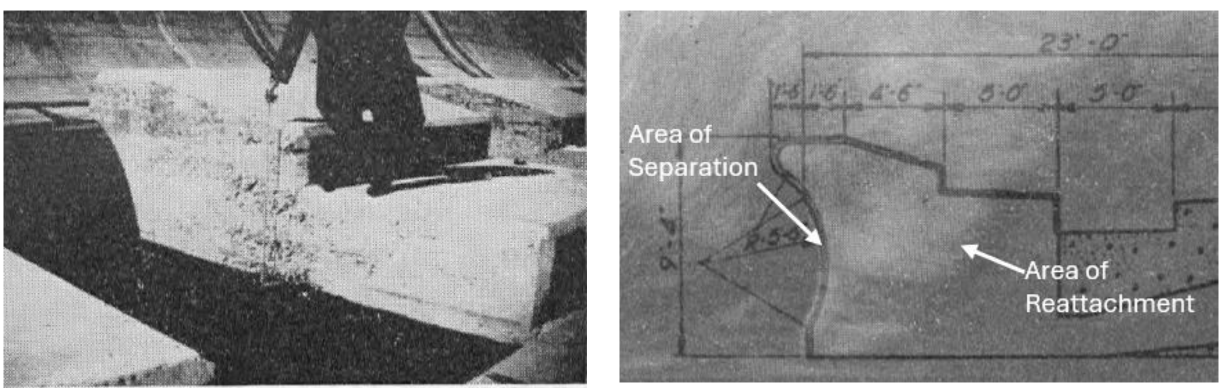

a) *Minor Pitting on the Side of Baffle Pier* b) *Model Flow Behavior in Vacuum-Tank*

Figure 39. Cavitation Damage and Flow Characteristics of Claytor Baffles (Source: adapted from Thomas and Hopkins)

The owner of the Claytor Dam was contacted related to the damage and noted that there are no official records of damage from the 1940 event or additional repairs required since (AEP, 2024).

Inozemtsev (1969) reported that damage had cavitation damage had repeatedly occurred on the front face of pyramid shaped baffles at V.I. Lenin Volga HHP in the Soviet Union. The accounts state that the most severe damage occurred in the center of the middle spillway span, where "one deflecting baffle and 13 dissipation baffles of the first row were severely damaged". The erosion patterns are also described as impacting the sides of the first row of baffles with characteristics of cavitation damage described in USBR (1990) and location of damage observed at Bonneville. The depths of side-wall erosion on the deflector and dissipation baffles are reported to range from 10 to 60 cm. exposing the reinforcement steel with additional concrete erosion on the interior of the reinforcement. There was also reported widespread minor damage to the face of the second row of dissipating baffles that consisted of a smooth erosion pattern that is more characteristic of abrasion damage. The erosion was reported to occur 0.5 to 1 m above the floor with an erosion depth of 2 to 5 cm. The texture was reported to be smooth with no large aggregate removed.

The Bull Shoals Dam stilling basin had experienced significant concrete erosion after approximately one year of operation under conditions of sluice flow only. The stilling basin consisted of four positive steps with a rounded edge. In some areas the damage was extensive and resulted in over 3 feet of concrete erosion depth (USACE, 1958). The damage was associated with both initial cavitation damage in the vicinity of the positive step along with subsequent abrasion/ball milling. The overall spillway and stilling basin profile (a) and damage characteristics (b) are shown in Figure 40.

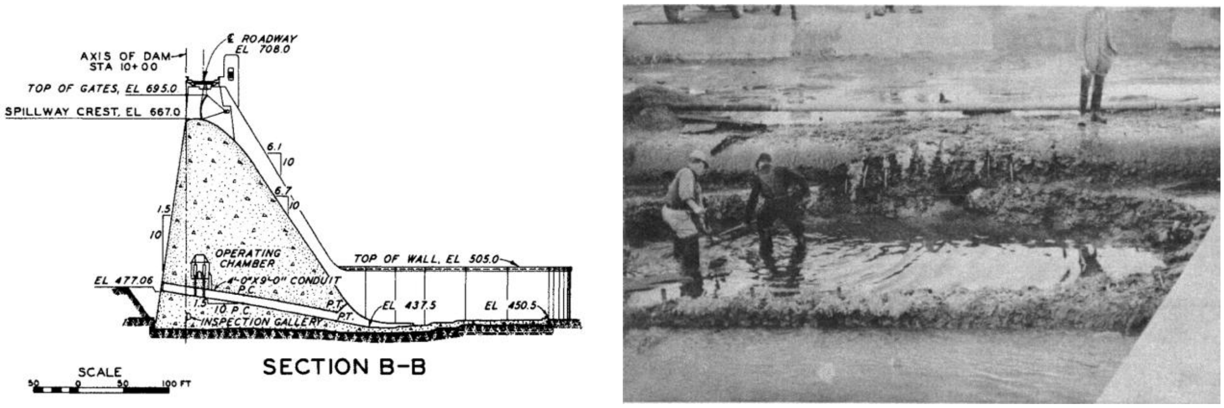

a) Typical Spillway and Stilling Basin Profile *b) Damage to Positive Steps and Floor*

Figure 40. Bull Shoals Stilling Basin Damage (Source: USACE, 1958)

The Porto Colombia Project (Brazil) had experienced significant damage on the floor immediately downstream of the chute blocks after 10 years of operation. The project consists of a gated ogee crest section, gated sluiceways, a 3 horizontal to 1 vertical chute, chute blocks, and a dentated end sill as shown in Figure 41.

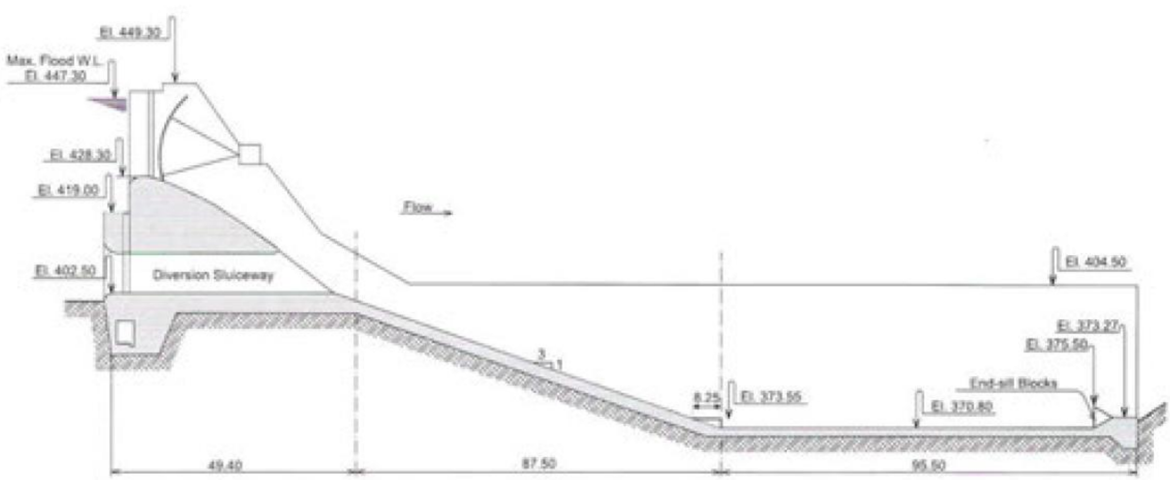

Figure 41. Porto Columbia Project Spillway Profile (Source: ICOLD 2015)

It was also noted that much less severe damage was noted on the dentates of the end sill. The damage has been contributed to cavitation (Pereira, 2021; ICOLD, 2015); although the location of the damage downstream of the end sill also coincides with a location that would be expected for abrasion damage and the damage. The typical damage observed is shown for the chute blocks(a) and end sill dentate (b) in Figure 42.

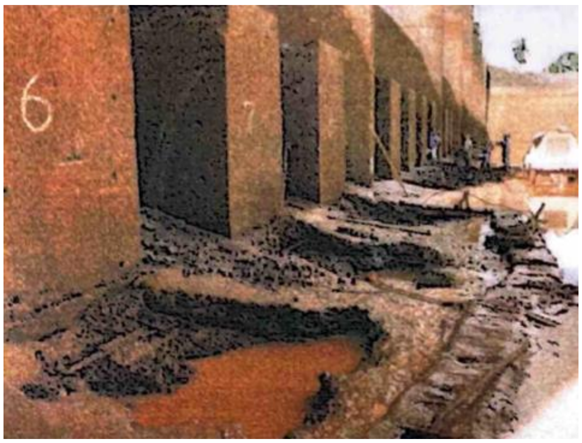

a) Chute Blocks

b) Dentated End sill

Figure 42. Porto Columbia Project Spillway Damage (Source: Pereira, 2021)

3.3.5.3.2 Bonneville Dam

The Bonneville Dam is frequently referred to as a case where significant cavitation damage has been observed on the blocks and floor adjacent to the blocks (Berryhill, 1957; Thomas and Hopkins; Inozemtsev, 1969; USACE, 1970). USACE (1970) states that “it was not until such damage was actually discovered on the baffle blocks at Bonneville Dam that hydraulic engineers became truly concerned with the problem”. Considering the significance of this case history in literature and that it is often referenced as the strong rationale for concern associated with cavitation damage to baffle piers, it was deemed prudent to provide more detailed treatment herein.

The Bonneville Dam is located along the Columbia River along the border of Oregon and Washington and was completed in 1936. The typical dam section is shown below in Figure 43. The spillway operates between a total head of approximately 64-feet at low flow conditions to 32-feet at normal high water (Cochrane, 1959). The original construction of a portion of the spillway and stilling basin is shown in Figure 44.

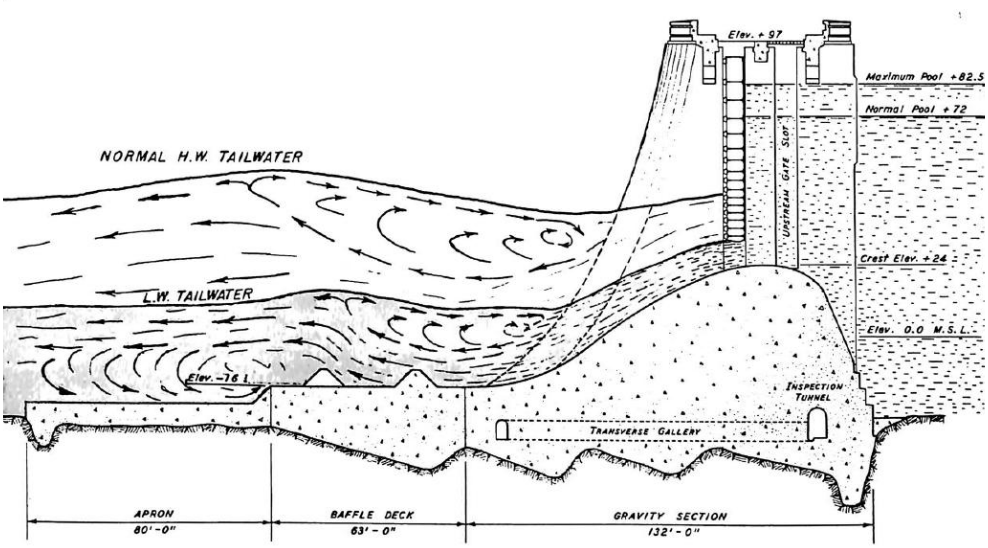

Figure 43. Section of Bonneville Dam Original Spillway (Source: Cochrane, 1959)

c) *Formed*/Completed Baffles

d) *Baffle Reinforcement*

Figure 44. Original Construction Photographs of Bonneville Spillway (Source: USACE, 1935-1937)

Although cavitation had been later commonly attributed as the principal cause of the damage, the USACE (1937) published a report related to defective concrete surfaces in the stilling basin, including the piers, baffles, and floor. The first indication of poor concrete quality noted was that the concrete was "wearing away in a path habitually used by workmen". It was noted in 1937 that significant scour (up to 8-inches on vertical faces of the baffles) had occurred across the south half of the dam at the piers and floor while the river was diverted through the partially constructed spillway. The diversion of approximately 200,000 $\frac{ft^3}{s}$ through the South half of the spillway is shown in Figure 45.

a) Aerial view of River Diversion into South Half of Spillway

b) Flow conditions on stilling basin

Figure 45. Bonneville Spillway Flow Event Prior to Spillway Completion - June, 1936 (Source: USACE, 1935-1937)

It was also observed through the winter of 1937 that concrete surfaces exposed to the period January 06, 1937 thru February 01, 1937 had suffered significant damage due to freezing conditions and certain areas had been destroyed to a depth of 1 ½ inches (USACE, 1937). Several potential sources for defective concrete were noted, including poor mixing of Portland cement/pozzolan and cold weather placement. Ultimately damaged surfaces were repaired with a Gunite covering.

A study was completed by the USACE (1943) related to the potential for silt laden flows to have been a major contributing factor to the erosion of the concrete surfaces at Bonneville. The study performed petrographic analysis of the materials in the fine sediments present at Bonneville Dam and concluded that they had a Mohs hardness of 7 in contrast to the cores taken of the concrete cylinders of the Ogee crest exhibited a Mohs hardness of 3; demonstrating the potential for abrasion. Additionally, experiments were conducted to evaluate the erosive potential of a sediment laden jet impacting concrete test samples. The impact of the sediment laden jets resulted in the removal of the cement/pozzolan binder and fine aggregate, leaving exposed coarse aggregates. This is illustrated for Pozzolan Cement (a) and Standard Cement (b) for specimens exposed to a high velocity jet for a duration of 10 days in Figure 46.

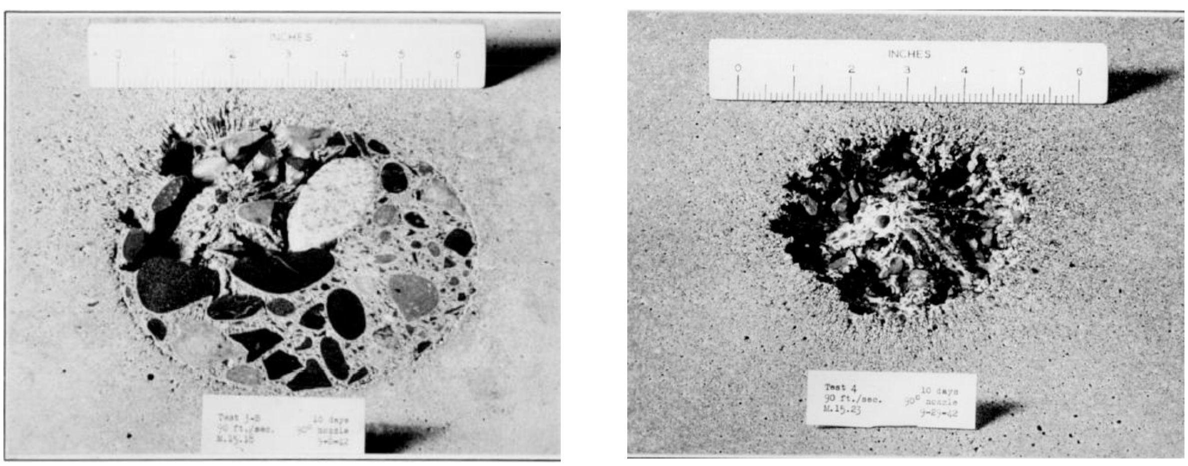

a) Pozzolan Cement *b) Standard Cement*

Figure 46. Sediment Laden flow Abrasion Study Results (Source: USACE, 1943)

The South half of the stilling basin was dewatered again in 1955, after 17 years of operation. A thorough inspection of the spillway and stilling basin performed, noting extensive concrete erosion to the toe curve (i.e. bucket), baffle piers, and floor (USACE, 1955). This study concluded that the majority of the damage to the spillway piers was a result of diversion during construction, although the damage to the floor and baffle piers was the result of cavitation phenomenon.

The damage to the baffles and floor was rather extensive. As shown in Figure 47, there was significant erosion observed on the floor downstream of the baffles (a) and along the vertical surface of the baffle piers themselves (b).

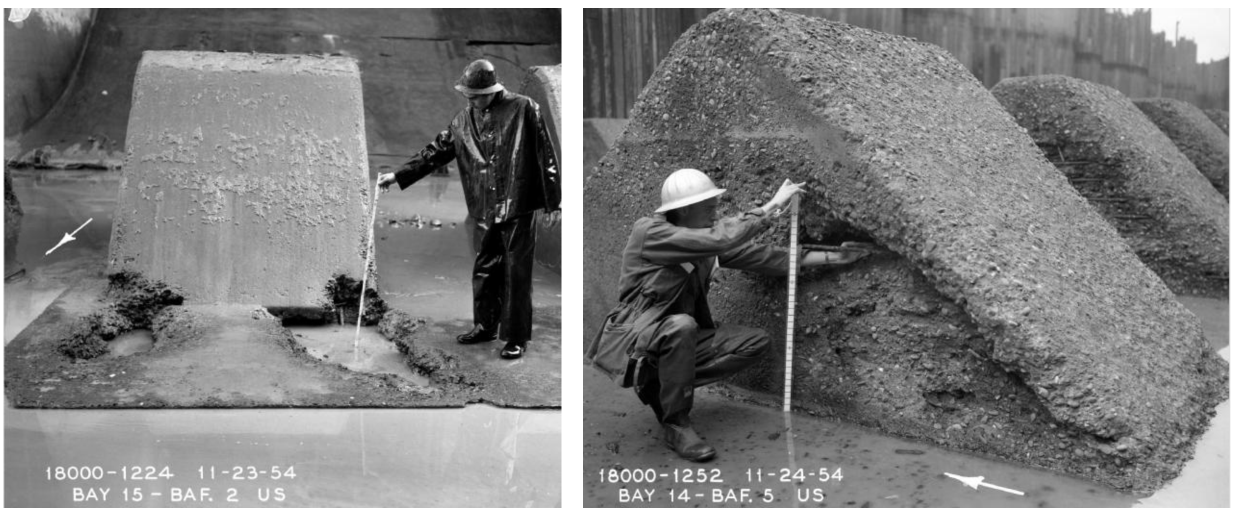

a) Pothole downstream of Baffle Edge *b) Erosion on Baffle Side and Face*

Figure 47. Bonneville Spillway Baffle Damage Observe in 1954 (Source: USACE, 1954)

It is noteworthy that the USACE (1955) report does not make mention of the defective concrete surfaces, the observed damage due to diversion flows on the spillway during construction, nor the sediment laden abrasion tests performed previously. Figure 48 illustrates the significant entrapped material on the downstream edge of the baffle block (a), the smooth erosion indicative of abrasion damage and reinforcement bent by debris (b), and a tool entrapped in a pothole just downstream of a construction joint (c); all suggesting that the damage to the floor is potentially associated with ball milling and abrasion of sediment laden flows.

a) Dowsntream View of Baffle Pier Prior to Cleanup   *b) Eroded Concrete Surface and Bent Reinforcing Bars*   *c) Tool for Abrasion Damage*

Figure 48. Evidence of Potential Abrasion Damage at Bonneville Spillway (Source: USACE, 1954)

It is stated that "Other than one extensive area of the Gunited surface of pier 15 that was lost, the repairs to the piers have not been affected noticeable by flows during the 17 years."; potentially providing evidence that the significant erosion of concrete surfaces is more associated with the low quality of the material and/or diversion during construction, as opposed to the significance of the cavitation damage potential.

Multiple repairs have been implemented including modification to the baffle shape based on physical modeling data to reduce the magnitude of negative pressures and even steel plating. The operation of the gates was also limited based on recommendations for uniform gate openings to reduce cavitation potential (Cochrane, 1959).

Thomas and Hopkins state that "All the scour…cannot be attributed to cavitation on the basis of the model tests. Some may be due to material carried by the water over the spillway or dragged onto the apron from the stream bed by eddies when certain methods of operation are used".

3.3.5.3.3 Chief Joseph Dam

As stated previously, USACE (1992) references Chief Joseph Dam as a case history of "…significant cavitation damage" on baffle blocks. Chief Joeseph Dam is located on the Columbia River, upstream of the Bonneville Dam. The spillway fall height from normal pool to stilling basin floor is 203-feet and the baffled hydraulic jump stilling basin is 167-feet in length and 915-feet in width. The stilling basin has a single row of baffle blocks and a stepped end sill; as shown in Figure 49.

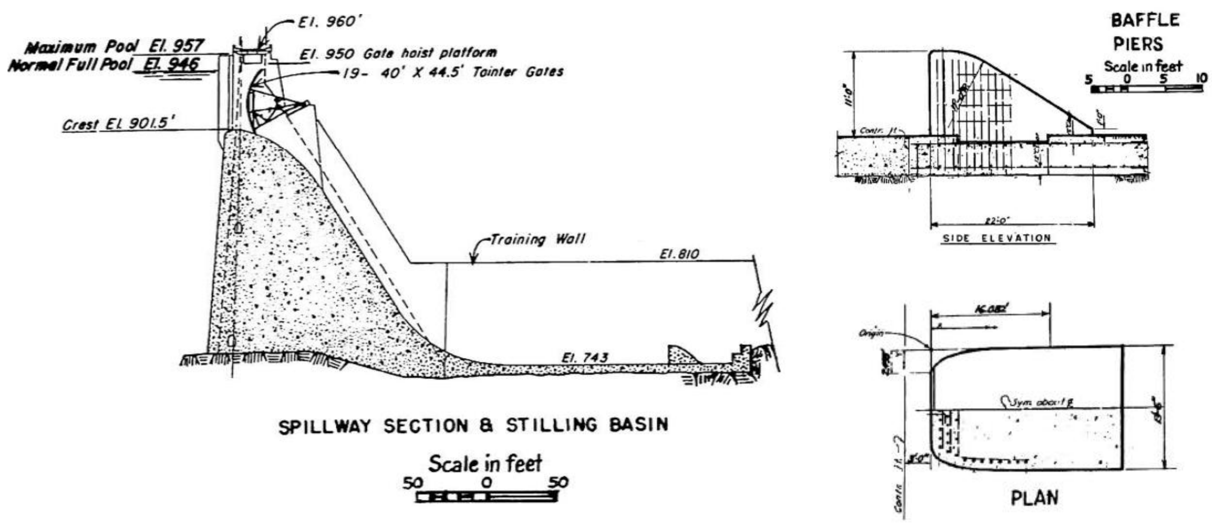

a) Spillway Section *b) Baffle Block*

Figure 49. Spillway and Stilling Basin Configuration for Chief Joseph Dam (Modified from Gedney, 1961)

The baffle piers were placed significantly downstream to reduce the negative pressure on the baffle blocks themselves to reduce the potential for cavitation damage. In addition, the rounded "cavitation free baffle block" shape was utilized (similar to that developed for Bluestone Dam).

Gedney (1961) provides a rather detailed accounting of the spillway use and related damage observed from first diversion of water into the stilling basin in 1952 until 1960. The spillway was utilized continuously from a period of 1955 thru 1957 during construction of the powerhouse and associated facilities. A dive inspection conducted in 1957 reveal widespread damage to the floor, baffle blocks, and end sill. It was noted that frequently the large 6-in aggregate was exposed and the concrete around it was eroded. It was noted that there were numerous pieces of aggregate that had been rounded and reduced in size, along with lose broken pieces of 1 ½ inch square reinforcement steel. Approximately half the baffles were reported to have some damage. It was observed that of the 43-total baffle blocks, 20 showed erosion 6-in or less. 16 of the remaining blocks showed erosion greater than 12-inch in depth. The majority of the damage “occurred principally on the lower front face and sides with generally accompanying damage to adjacent slab areas”. Four baffles suffered the largest extent on the downstream tail of the baffle. An illustration of the damaged areas and extents is shown in Figure 50

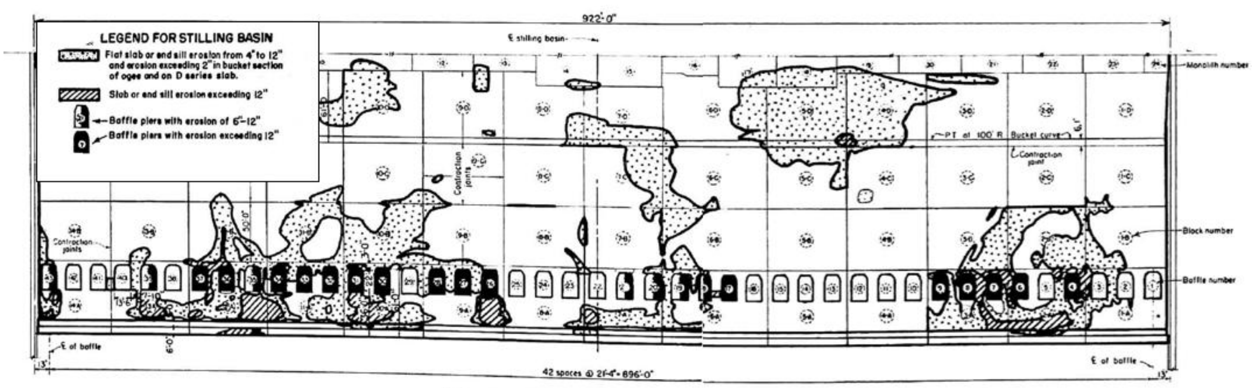

Figure 50. Damage Observed from Dive Inspection Survey 1957 (Adapted from Gedney, 1961)

An additional survey was completed in 1960, following two moderate spillway flood events in 1958 and 1959. It was observed that the erosion had continued principally in the areas that had experienced previous damage. It was noted that the areas that were in relatively good shape, did not suffer significant damage in the time between surveys. The survey also found that a portion of the vertical reinforcement bars exposed by the erosion, had been bent in the upstream direction. It is believed that this was a result of rock debris being recirculated in the upstream direction by the eddies that were created by the unbalanced flow conditions during the diversion flows.

It was determined by Gedney (1961) that the principal cause of the concrete erosion was abrasion by rock entrapped during the construction period that was used as armor stone for the cellular coffer dam that segmented the spillway during construction diversion scenarios.

3.3.6 Abrasion/Ball Milling

The turbulence in the hydraulic jump can use those materials more durable than concrete as tools for abrasion (i.e. ball milling) resulting in significant damage (USACE, 2022). The process of entraining downstream RipRap (a) and flow pattern after implementing a flow deflector (b) is shown in Figure 51.

a) Problematic Flow Pattern Entraining Materials

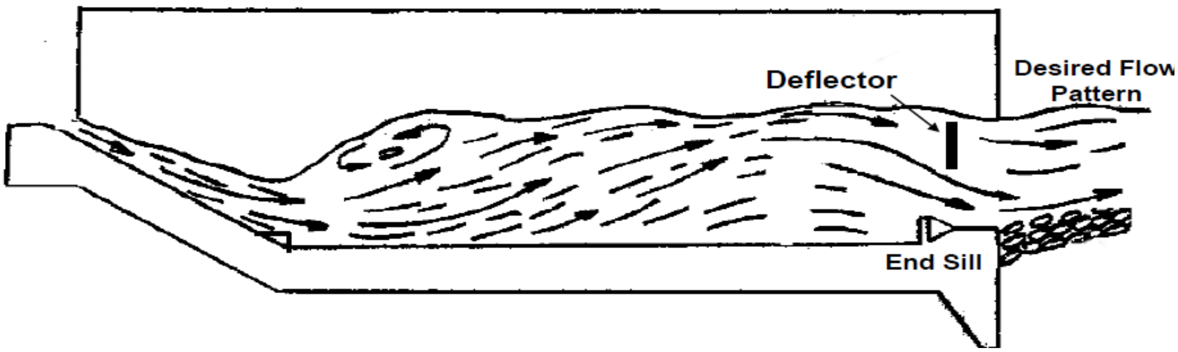

b) Desired Flow Pattern Flushing Materials

Figure 51. General Recirculating Patterns that Result in Entrainment/Entrapment of Rock (Source: USBR, 2010)

ICOLD (2015) identifies that ball milling associated with hydraulic jump stilling basins is a "rather common problem". The USBR (2019) developed an inventory of 89 baffled and unbaffled hydraulic jump stilling basins for outlets and combined outlets/spillways that do not have flow deflecting devices to assist the passage of debris and minimize entrainment of debris from downstream. Of the 89 basins in the inventory, 83 percent had documented rocks or sediment in the basin, and abrasion damage reported in 64-percent of the basins. The USACE conducted a survey of stilling basins within it's inventory and determined that 52 structures had experienced damage due to concrete abrasion-erosion (USACE, 1981). This damage ranged from inches to greater than 10-feet. This resulted in expensive remediation and reconfiguration of the stilling basins. The severe damage because of entrained rock ball milling the stilling basin apron at Dowarshak Dam is shown in Figure 52.

The Marimbondo Spillway (Brazil) provides a case history whereas the asymmetric operation of the spillway gates resulted in a large-scale horizontal eddy that moved downstream material into the basin creating conditions for significant damage to concrete and reinforcement (ICOLD, 2015). USBR (2019) states that many cases of entrainment of material from downstream results when the actual tailwater is higher than that needed to maintain the hydraulic jump action, resulting in the floor jet rising and creating a reverse roller in which downstream materials are moved into the basin.

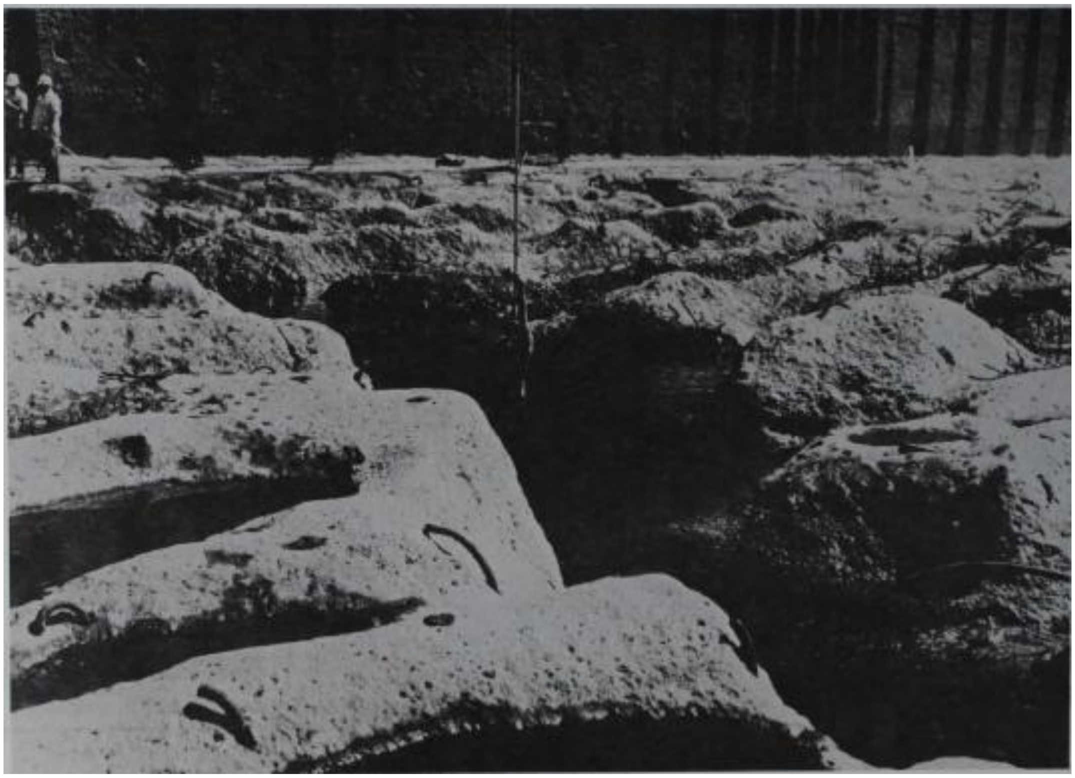

Figure 52. Abrasion-Erosion of Dworshak Dam Stilling Basin Floor (Source: USACE, 1981)

In addition to both vertical reverse rollers and horizontal eddy formation, vandalism in the form of launching adjacent rip rap into stilling basin pools has been attributed to numerous accounts of abrasion tools within stilling basins. Despite fences and signage, the USBR (1978) reports that this is still a large contributor of abrasion tools found within stilling basins within it's portfolio.

3.3.7 Stilling Basin Hydraulic Loading

The internal (failure within an element) and external (failure of the element itself) stability of the features within the hydraulic jump stilling basin are critical to reliability of the structure. Hydraulic structures are subject to both vibration (micro-scale) and large pulsations (macro-scale) that can affect various aspects of spillways and stilling basins.

3.3.7.1 Stilling Basin Apron

The dynamic fluctuations within hydraulic jump stilling basins can be extreme. A significant case history is the damage that was observed at the Karnafuli Hydroelectric Dam Spillway, Bangladesh in June 1961. A significant portion of the lower spillway chute was destroyed after an event that was approximately 20-percent of the design flood; as illustrated in Figure 53 by Bowers and Toso (1988).

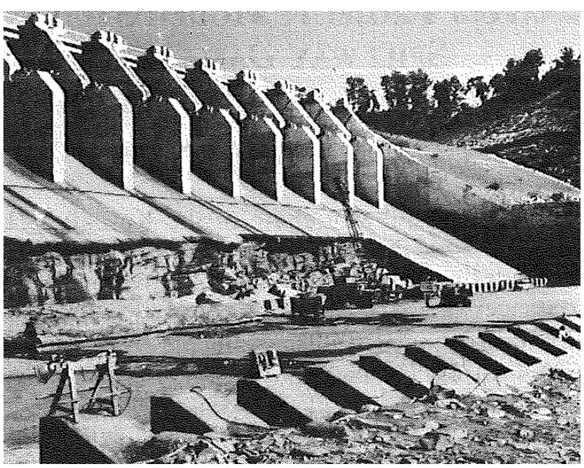

a) Severe damage to spillway

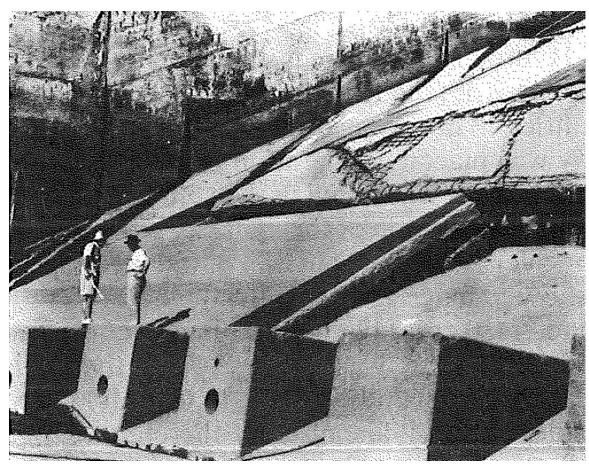

b) Chute block and drain

Figure 53. Karnafuli Spillway Damage (Bowers and Toso, 1988)

After significant forensics and physical model investigations, it was concluded that the damage was due to the dynamic pressure fluctuations occurring on the lower chute and upper stilling basin; whereas the chute block drains enabled the transmission of instantaneous high pressures underneath the slab at the same time that low pressures were occurring over the slabs creating instability and failure of the slabs. An illustration of the results of the forensic physical model that measured the instantaneous distribution of pressures is shown in Figure 54.

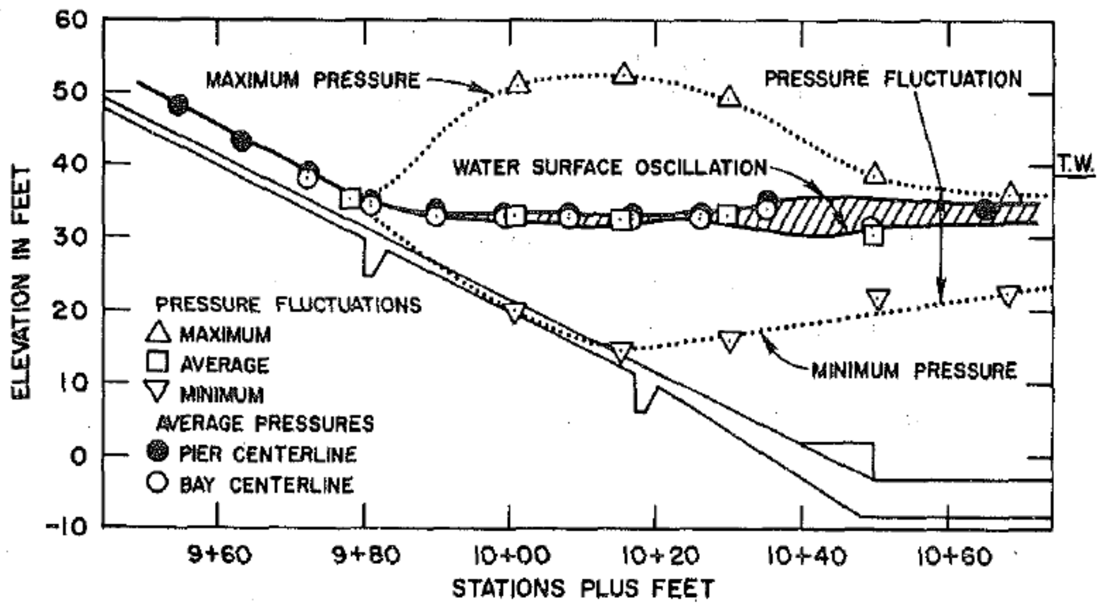

Figure 54. Fluctuating Pressure on Chute and Stilling Basin (Source: Bowers and Toso, 1988)

It was believed that the position of the tailwater may have contributed to the conditions resulting in slab failure. It was typical design practice to exit foundation drains on the downstream face of chute and baffle blocks because this is generally location of low pressure due to the wake that forms as flow separates off the face. The position of the lower chute in relation to the tailwater forced the jump onto the lower chute and allowed the positive pressure fluctuations to charge the drainage system and foundation. The position of the jump and the locations of the maximum and minimum pressures are illustrated in Figure 55.

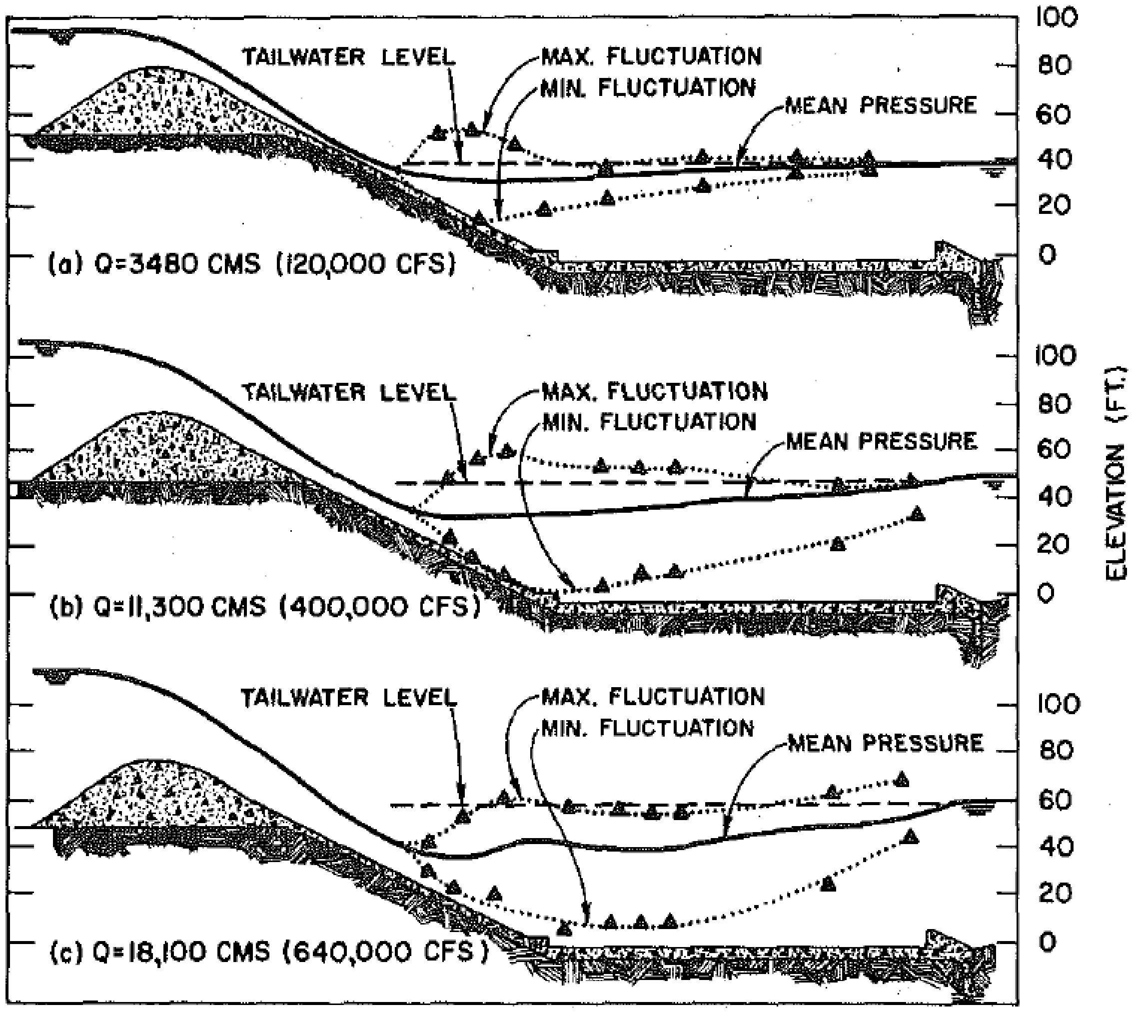

Figure 55. Variations in Jump Profile and Pressure Extremes (Bower and Toso, 1988)

Utilizing data from the forensics investigation of the Karnafuli Dam, Toso and Bower (1988) developed relationships for a dynamic pressure coefficient C_p that represents the maximum deviation from the mean pressure. This coefficient is expressed in Equation 14.

Equation 14. Dynamic Pressure Coefficient

$$C_p = \frac{\Delta P}{\frac{\alpha {V_1}^2}{2g}}$$

The values of the dynamic pressure coefficient by relative distance for a 30-degree chute with an Fr_1 of 5.1, for a Type II and Type III (USBR, 1984) stilling basin are shown in Figure 56.

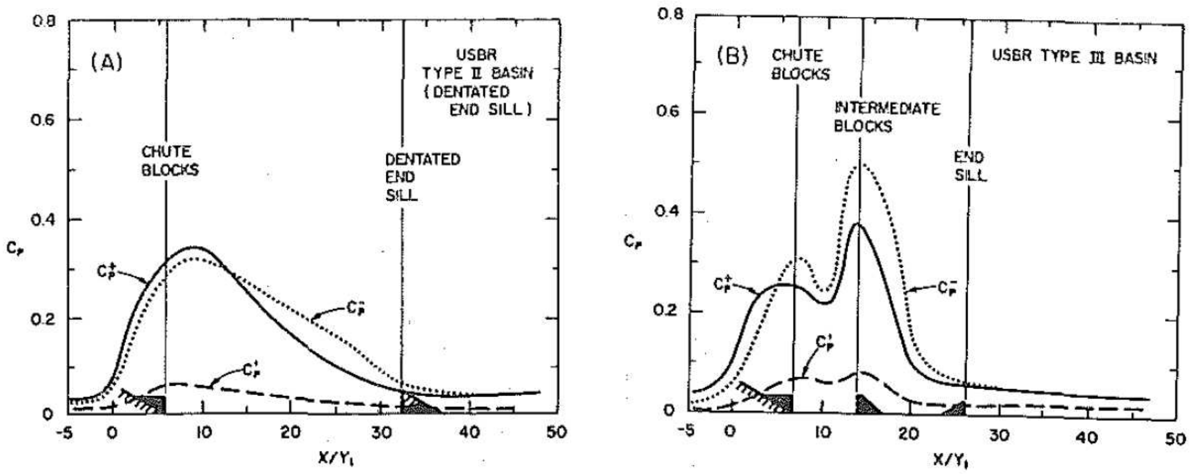

a) Type II Stilling Basin *b) Type III Stilling Basin*

Figure 56. Dynamic Pressure Coefficient for Stilling Basin (Source: Toso and Bower, 1988)

Fiorotto and Rinaldo (1992) performed additional experiments to investigate the spatial distribution of the extreme pressure fluctuations described by Toso and Bowers (1988) by evaluating force on stilling basin slabs of various length and width ratios into flow. They determined that the primary direction of the propagation of the fluctuating pressure was in the streamwise direction and that minimum damping would be expected related to the pressures propagating underneath the slabs. Toso and Bowers (1988) determined noted a value of the characteristic length scale to be 8-times d_1 in the streamwise direction and 13-times the d_1 in the cross-stream direction. Bellin and Fiorotto (1995) performed experiments with unseals slabs and measured direct force from the resultant of the pressure fluctuations. It was determined that the slab dimensions in the streamwise (l_x) and cross-stream (l_y) in relation to the characteristic length of the pressure fluctuations can be used to determine the magnitude of the total uplift force on the slab. This is in the form of an uplift coefficient Ω, and the expression is shown in Equation 15.

Equation 15. Maximum Force Acting on Slab (modified from Bellin and Fiorotto, 1995)

$$F'_{max} = \Omega \frac{{v_1}^2}{2g} \gamma l_x l_y$$

Where F'_{max} is the maximum fluctuating force. The values for the uplift coefficient various Fr_1,l_x, and l_y are shown in Figure 57.

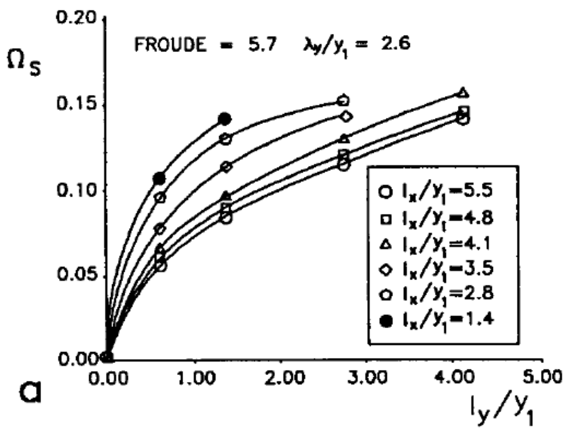

a) Fr_1 =5.7

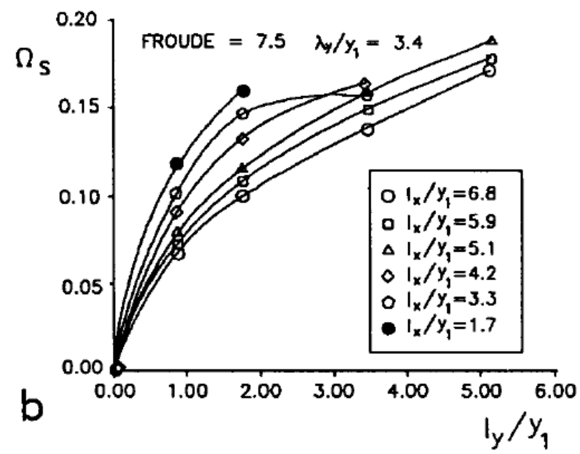

b) Fr_1 = 7.5

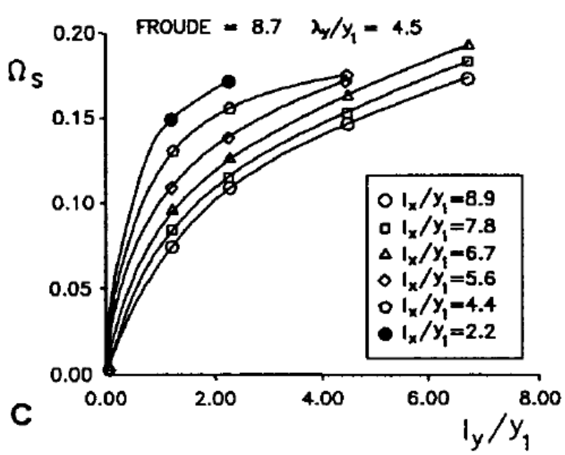

c) Fr_1 =8.7

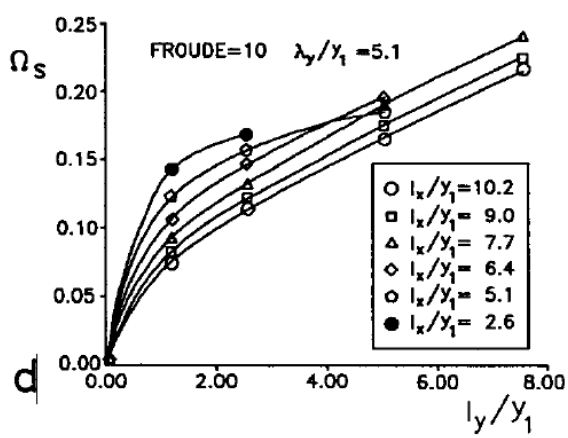

d) Fr_1 = 10

Figure 57. Uplift Force Coefficients (Source: Bellin and Fiorotto, 1995)

Based on the verification tests of the USBR (1955); the recommendation for uplift in USBR (1984) is to utilize two horizontal profile lines for the water surface and pressure profile within the Type III stilling basin. The pressure upstream of the baffles (stations from 0- to 0.8-d_2) will be half of the actual tailwater 0.5 d'_2.; this is shown in Figure 58 with the dashed lines representing d'_2 above and below d_2.

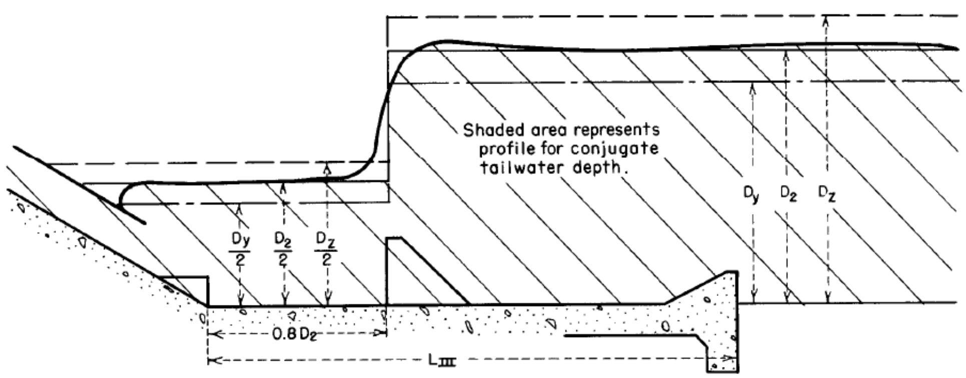

Figure 58. Water Surface and Pressure Profiles with Type III Stilling Basin (Source: USBR, 1984)

The approach of using static loading has been widely used for evaluating critical loading conditions, with many designers assuming that the minimum resisting force is the d_1 throughout the stilling basin for conservatism.

3.3.7.2 Side Walls

The failure of several stilling basin splitter walls has been attributed to dynamic pulsations within the stilling basin. Case histories of this phenomenon include Texarkana Dam and Bhakra Dams (USACE, 1965). Given the high magnitude of the dynamic pressure fluctuations within the stilling basin, splitter and side walls should be designed to accommodate these loads.

ICOLD (1987) states that in the worst case, the half-amplitude of the macro-scale turbulent fluctuations is close to 40-percent of the incoming velocity head and the root mean square of 10- to 12-percent. With the dominating pulsation having frequencies between 0 and 10 Hertz. This is much lower value than the value of 170-percent that was determined by Toso and Bower (1988).

The USACE (1992) recommends an empirical relationship be used based on an experimental study conducted by USACE (1988); whereas direct force measurements were obtained for a hydraulic jump downstream of a standard ogee crest spillway with piers without baffles or end sill. A photograph of the test facility (a) and a definition sketch (b) are included in Figure 59.

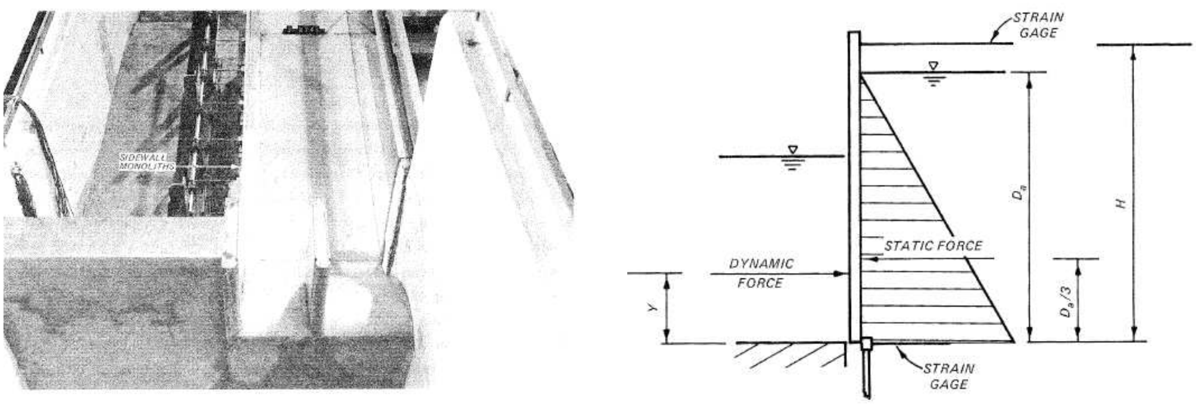

a) Photograph of test facility *b) Definition Sketch of apparatus*

Figure 59. Experiments to Determine Dynamic Loads on Sidewalls (Source: USACE, 1988)

The tests were performed with Fr_1 ranging from 2.7 to 8.7 and resulted in an empirical relationship to determine the average minimum static plus dynamic unit force at the toe of the jump (R_m) as a function of the spillway height (H_S), q, v_1, Fr_1. This relationship is shown in Equation 16.

Equation 16. Average Minimum Static plus Dynamic Force at the Toe of Hydraulic Jump

$$R_m = 3.75 H_S^{-1.05} \rho v_1 q Fr_1^{-1.42}$$

Once the R_m is computed, the average, minimum, and maximum unit force can be computed along the basin using the nomograph based on experimental data, as shown in Figure 60.

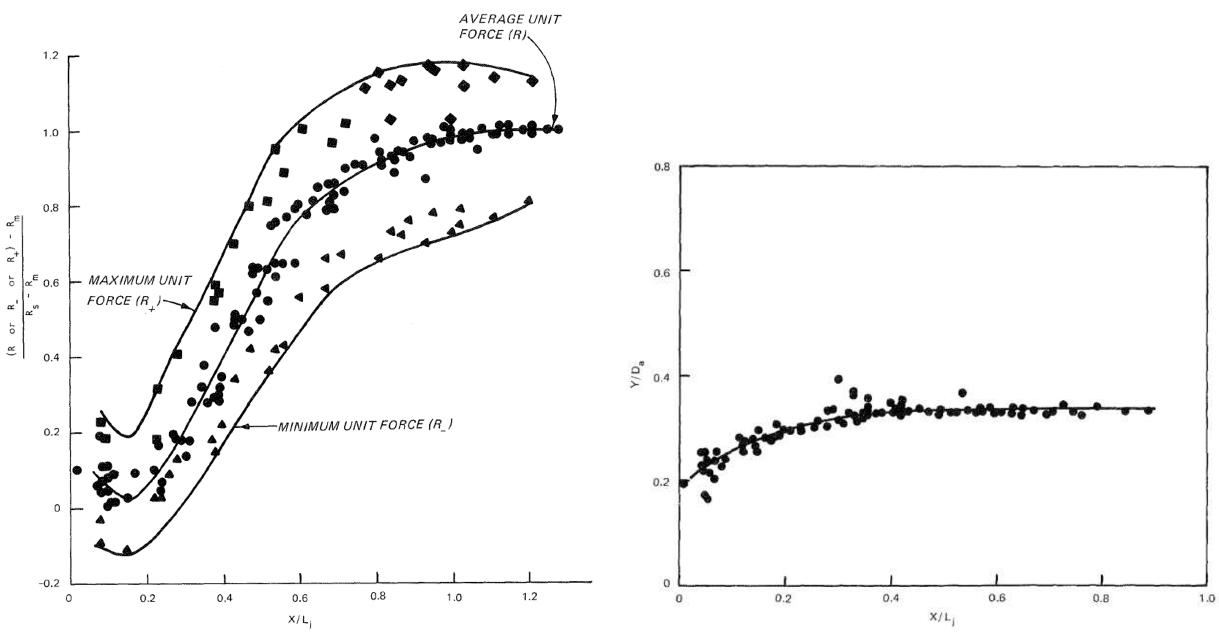

a) Variation in Resultant Force from PI *b) Variation in Resultant Location from PI*

Figure 60. Resultant Force and Location from PI (USACE, 1988)

An alternate approach has also been to utilize the dynamic surges observed in water surface fluctuations to estimate the dynamic side wall loads; whereas the static loading from the highest surge condition represents a reasonable design load, when incorporating appropriate load factors (USACE, 2018).

3.3.7.3 Baffle Blocks

The USACE (1965) prescribed that the forces on the baffle blocks can be determined by means of conservation of momentum and applying a drag coefficient to the baffle blocks, as shown in Equation 17; whereas the resulting baffle pressure is expressed in Equation 18

Equation 17. Momentum Equation for Hydraulic Jump, Including Baffle Forces (USACE, 1965)

$$\gamma\left(\frac{q^2}{gd_1}-\frac{q^2}{gd_1}\right)=\gamma\left(\frac{{d_2}^2}{2}-\frac{{d_1}^2}{2}\right)+C_D\rho\frac{V^2}{2}\frac{A}{W}+\gamma h(d_2+\frac{h}{2})$$

Where C_D is the baffle drag coefficient, A is the area of the baffle, and W is the width of the baffle.

Equation 18. Expression for Baffle Pressure (USACE, 1965)

$$P_B = C_D\rho\frac{V^2}{2}$$

Where P_B is the baffle pressure. Drag coefficient values associated with Equation 17 are provided in Table 5.

Table 5. Baffle Pier Drag Coefficient for use in Momentum Equation (USACE, 1965)

BAFFLE PIER DRAG COEFFICIENTS

Pier Type	Pier Spacing W_s/W_p	Row Spacing W_R/W_p	Drag Coeff. C_D	From Reference
Cavitation free (1 row)†	Unknown	----	0.68	47
Cavitation free (1 row)‡	Unknown	----	0.59	47
Cavitation free (2 rows)‡	0.592	0.428	0.40	45
Stepped (1 row)‡	0.917	----	0.70	45
Cube (single)†	----	----	1.33	48
Cube (single)†	----	----	1.50	49
Rectangular (single with $\frac{\text{width}}{\text{length}} = 0.4$)	----	----	1.0	50

† Pier in uniform flow.
‡ Pier at toe of hydraulic jump.

USACE (1992) states that the following drag coefficient values are reasonable:

1) $C_D = 0.6$ for a single row of baffles, and

2) $C_D = 0.4$ for a double row.

The velocity within a free jump spatially varies with relationship to the downstream direction, as shown in Figure 61.

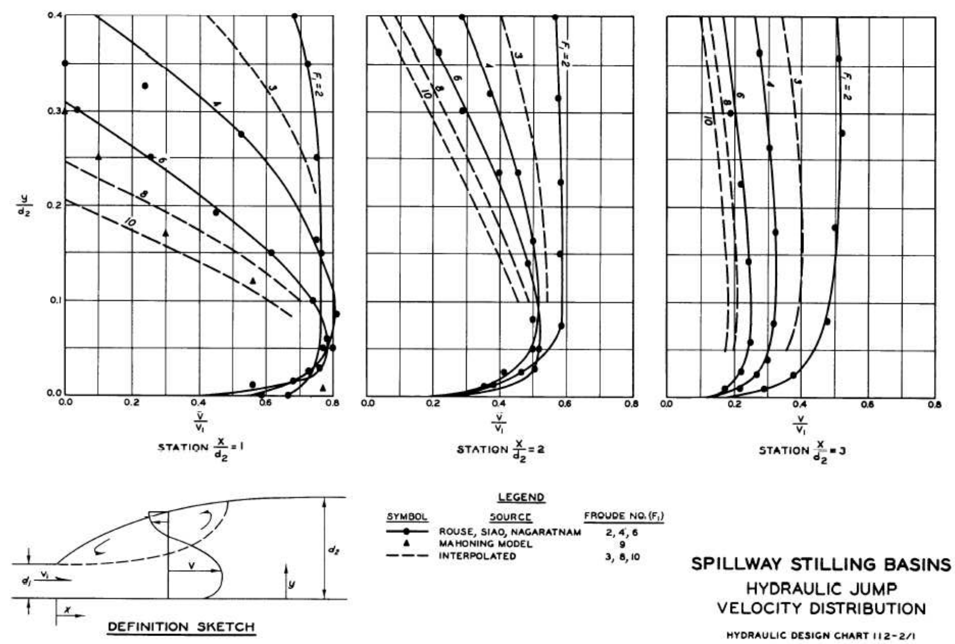

Figure 61. Velocity-Depth Relationship in the Streamwise Direction of a Free Hydraulic Jump (Source: USACE, 1992)

Similarly, USACE (1970) establishes a baffle block force ratio to determine the amount of momentum change resulting from the baffle force as opposed to the hydraulic jump. A schematic of the forces acting within the baffle stilling basin are shown in Figure 62.

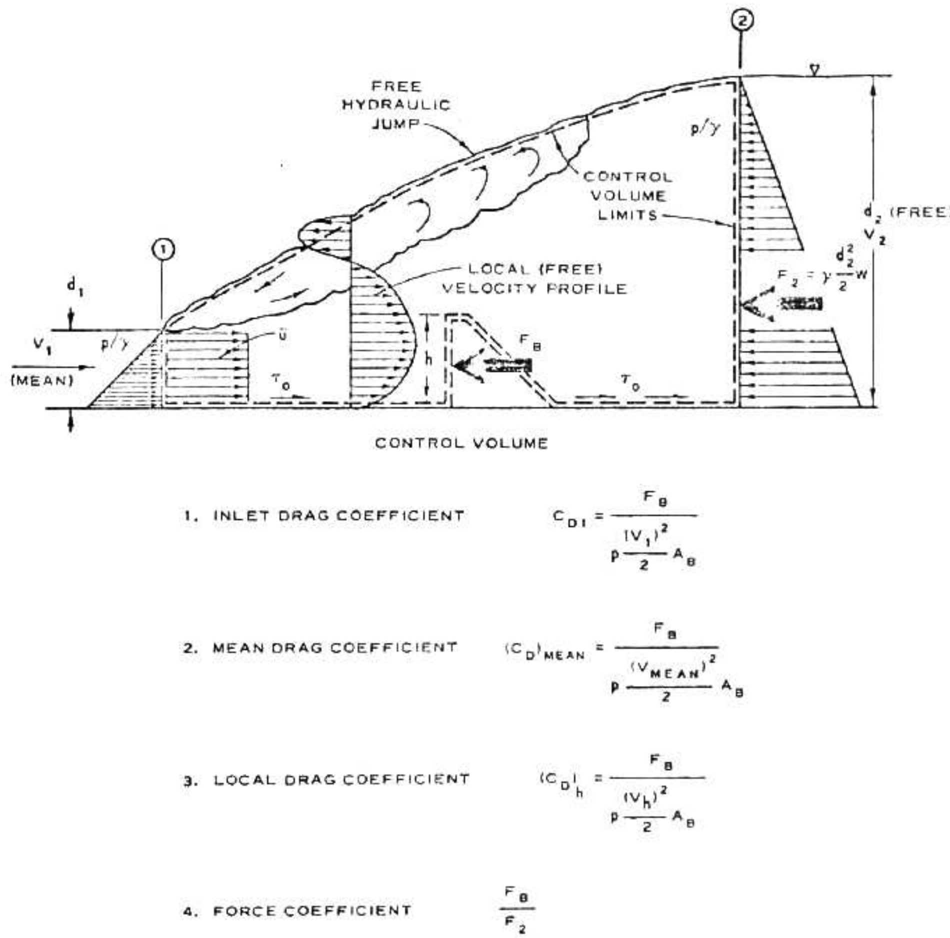

Figure 62. Baffle Drag Coefficient Definitions (USACE, 1970)

USACE (1970) found that the drag on the baffles was a function of the Fr_1, $\frac{X_B}{d_2}$, $\frac{H_B}{d_1}$, $\frac{W_B}{H_B}$, $\frac{W_S}{H_B}$, and shape of block. The experiments were conducted by setting the tailwater so that a forced hydraulic jump occurred, as shown in Figure 63. The forces acting on the baffles were determined from a single block and fool floor drag force dynamometer.

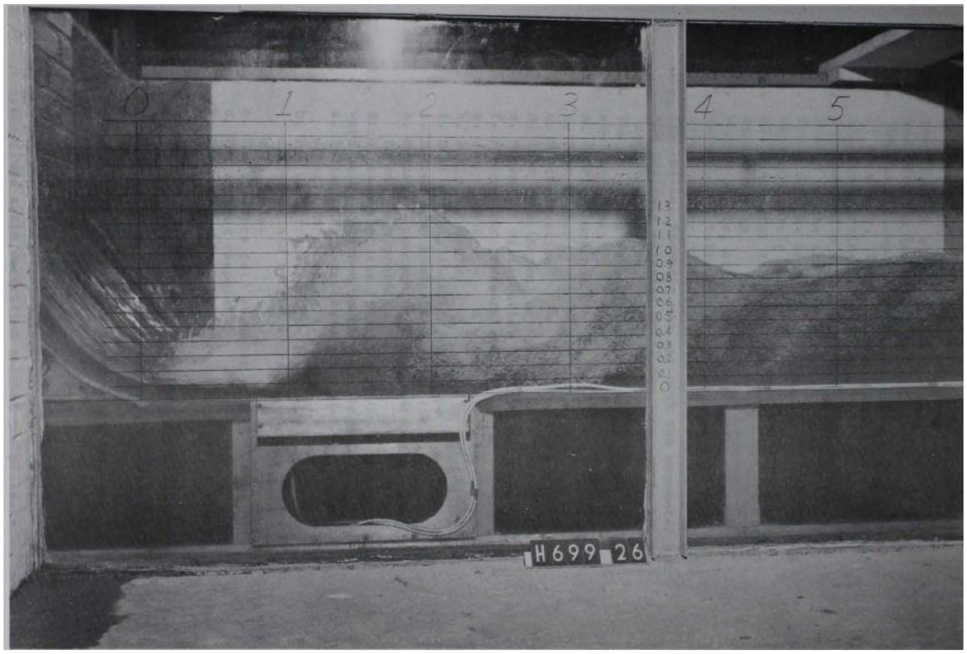

Figure 63. Typical Forced Jump Profile (USACE, 1970)

It was found that the drag coefficient increased with the increasing height of the baffle block and as the distance to the baffles decreased. This relationship is shown for a Fr_1 of 4 (a) and 8 (b) in Figure 64.

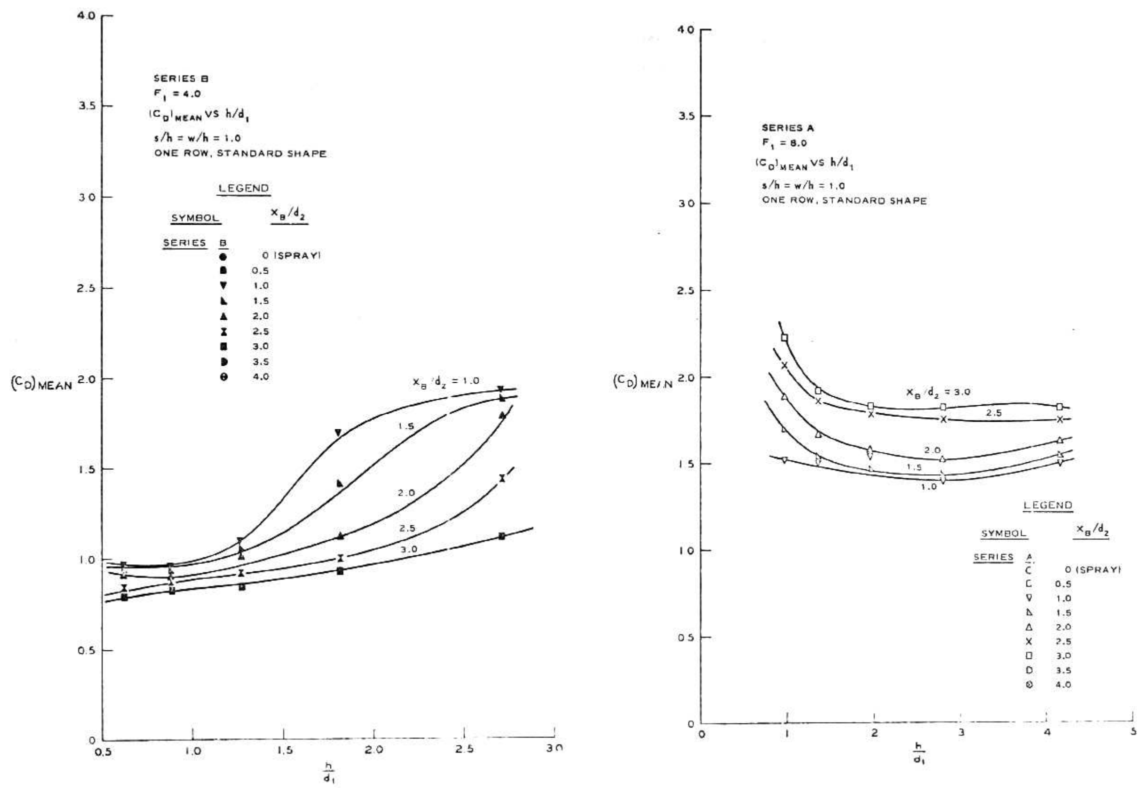

a) Incoming Froude number = 4.0 *b) Incoming Froude number = 8.0*

Figure 64. Drag Coefficient for Varied Block Height and Location (USACE, 1970)

Based on these experiments, it was determined by USACE (1970) that a more appropriate express the force on the blocks (F_B) as a ratio of the free jump hydrostatic pressure force at d_2 (F_2). The relationship of the force ratio ($\frac{F_B}{F_2}$) for a blockage ratio of 0.5, a standard block shape, a $\frac{W_B}{H_B}$ ratio of 1.0 for varied baffle block height ratios and block locations is shown for a Fr_1 of 4 (a) and 8 (b) in Figure 65.

.

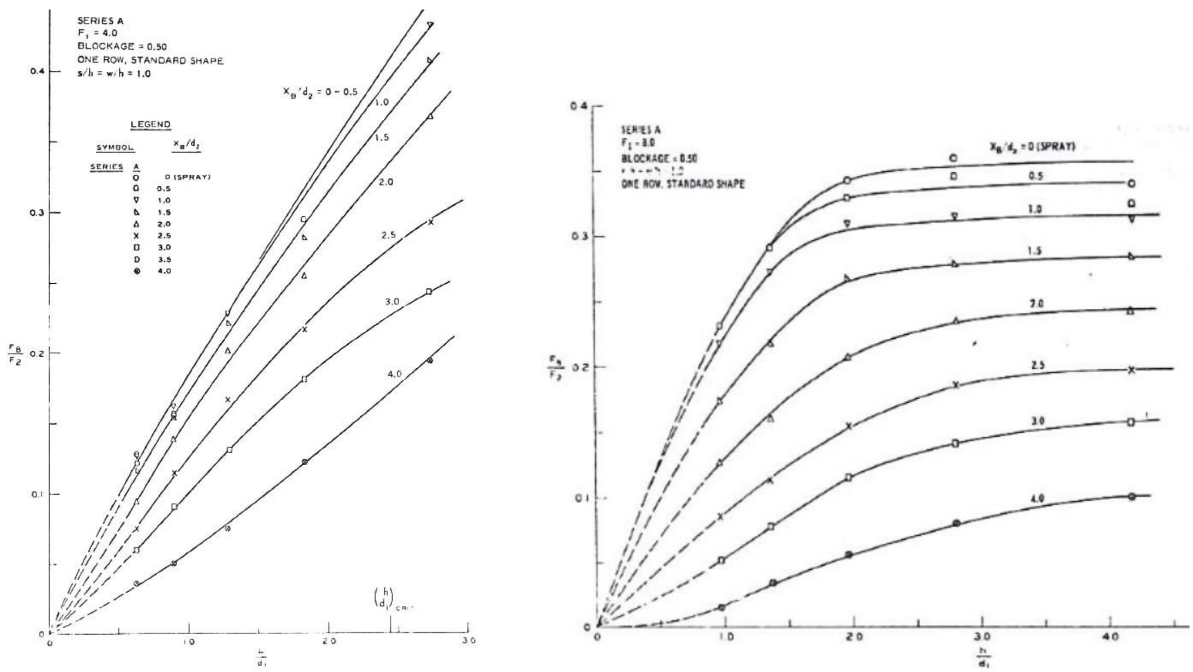

a) Incoming Froude number = 4.0 *b) Incoming Froude number = 8.0*

Figure 65. Impacts of Baffle Height and Station on Force Ratio (USACE, 1970)

The relationship of the force ratio ($\frac{F_B}{F_2}$) for a standard block shape, a $\frac{W_B}{H_B}$ ratio of 1.0 for varied blockage ratios and block locations is shown for a Fr_1 of 4 (a) and 8 (b) in Figure 66. The zone marked with roman numerals represent zones of qualitative jump performance, with Zone III being "good" performance.

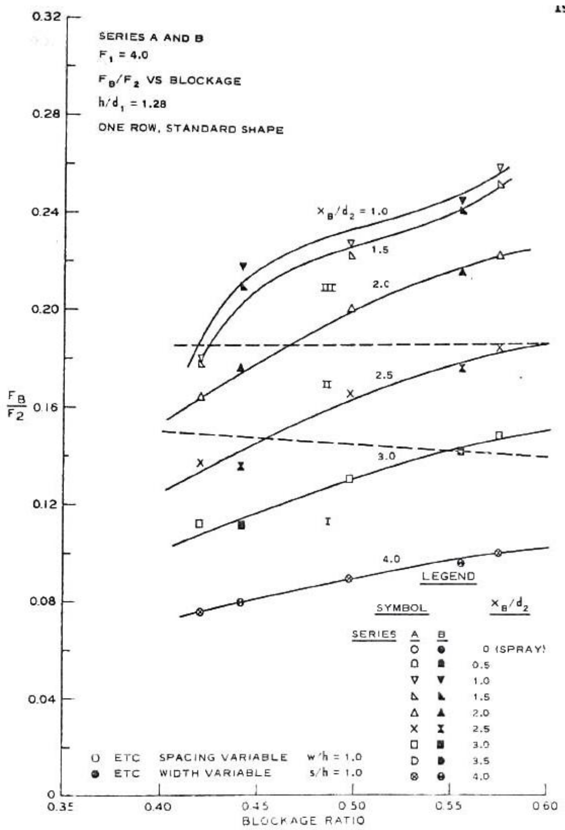

a) Incoming Froude number = 4.0

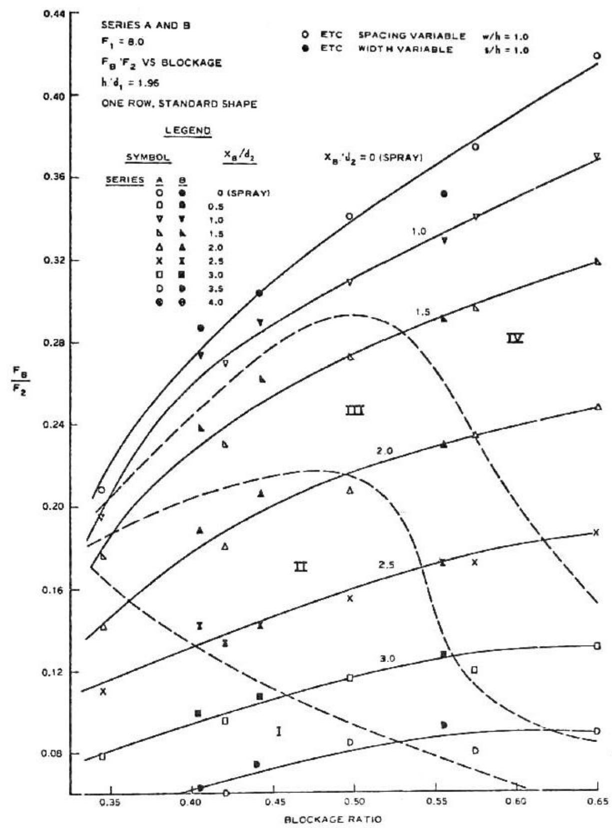

b) Incoming Froude number = 8.0

Figure 66. Impacts of Blockage Ratio and Location on Baffle Drag Coefficient (USACE, 1970)

The USBR (1987) has derived a theoretical relationship whereas the dynamic force will approximate that of a jet impinging upon a plane normal to the direction of flow, in other words that the incoming velocity is fully stagnated against the face of the baffles; this es acting on the baffle blocks have been prescribed in USBR (1987) by Equation 19. There is no explanation provided for the factor of 2 placed on the stagnation force, although it may be to account for the hydrodynamic concentrations and negative pressures on the top and back of the baffle block.

Equation 19. Force acting on Baffle Face (Adapted from USBR, 1987)

$$F_B = 2\gamma A_B(d_1 + h_{v1})$$

Where F_B is the force acting on the baffle block. It is worth noting that none of the methods described above estimate the lateral forces in the cross-stream direction. Nakato (2000) determined experimentally from a 1:28 Froude Scale model of the Pit 6 Dam Stilling Basin that the lateral (cross-stream) forces could be in excess of the force in the streamwise direction.

3.4 Physical Modeling Approaches

3.4.1 Model Similitude

The basis for the standard stilling basin design criteria currently available and the additional experiments described herein are obtained by means of undistorted Froude scale physical modeling. Froude scale modeling is often preferred for modeling of highly turbulent hydraulic phenomenon, such as the hydraulic jump, because the energy dissipation is mainly related to the turbulent shear stress and not the boundary frictional resistance (Heller, 2011).

Julien (2018) describes three primary considerations when developing physical described in additional detail in subsequent sections, paraphrased as:

1. The scale should be adequate to obtain reasonably accurate measurements,
2. The scale will be bound by the reasonable capacity of the research facility,
3. The boundary conditions must be reasonably represented.

The physical modeling is intended to develop dimensionless parameters that explain the behavior and performance of the evaluated geometries that can then be scaled to typical prototype dimensions without significant impacts related to scale.

Important dimensionless relationships to describe the similitude for open channel flow are the Froude Number, the Reynolds Number, and the Weber Number. The physical modeling experiments adhere to standards-of-practice associated with Froude scale similitude associated with these primary dimensionless relationships, as described below.

The Froude number is a basic relationship for explaining open channel flow conditions and is typically strictly adhered to for physical scale modeling of hydraulic structures (i.e. the model and the prototype have identical Froude Numbers). The Froude Number represents the ratio of initial forces to gravitational forces and is previously shown in Equation 2. Because gravity will be the same in the model and the prototype; the Froude number becomes the ratio of the velocity to the square root of the length ratio.

The Reynolds Number is the dimensionless ratio of the inertial forces to the kinematic viscosity and generally represents the measure of turbulence in the flow field caused by viscous forces. Strict adherence to Reynolds similitude is generally not feasible, although strict adherence is generally not required. If the flow in the model is sufficiently turbulent, the effects of viscosity can generally be ignored. For free-surface flows, a target model Reynolds number of 10,000 or greater is desired to minimize scale effects due to viscosity (Ettema et al., 2000; USBR, 1980). The Reynolds number is expressed in Equation 20.

Equation 20. Reynolds Number

$$R_e = \frac{UL}{\nu}$$

Where R_e is the Reynolds Number, U is a characteristic velocity (typically depth averaged), L is a characteristic length (depth of flow). It is noteworthy that because the product of UL is equal to the unit discharge, the depth averaged Reynolds number at any point in a sectional flume is identical. USACE (1970) states that drag coefficients have been determined to be nearly identical above a R_e of 10,000, in relation to scale effects associated with baffles and other bluff bodies in flow.

Chanson and Gualtieri (2008) found through relative scale experiments that there can be significant scale effects that result from the loss of the advective diffusion layer above the shear layer within the hydraulic jump. Figure 67 illustrates the comparison of two jets of identical Fr_1 and Re 27,000 (a) and 71,000 (b).

a) Re = 27,000 *b) Re = 71,000*

Figure 67. Scale Effects Impact on Hydraulic Jump Behavior (Source: Chanson and Gualtieri, 2008)

The advective diffusion layer is responsible for much of the air-entrainment. The experiments noted that below a Reynolds number of 25,000, there was no defined advective diffusion layer observed and a significant reduction in measured air-concentration.

The Reynolds number also influences the frequency and intensity of turbulent eddies being shed. Ettema et al. (2006) found that the frequency of vortex shedding for cylindrical piers was inversely proportional to the pier diameter and that both the frequency and vorticity of cortex shedding increased with decreasing pier diameter. This finding resulted in adjustment factors to reduce the scour depth determined by Froude scale model experiments by a ratio of the experiment diameter to the prototype diameter. Ettema et al. (2004) demonstrated that the streamwise length of the separation region created by lateral dikes perpendicular stream-wise direction was impacted significantly at very small scales. The general flow characteristics resulting from a perpendicular wall in the flow field with uniform approach flow is shown in Figure 68.   This is an important consideration provided that the separation streamline and the length of reattachment is a significant characteristic of associated scour downstream of an end sill.

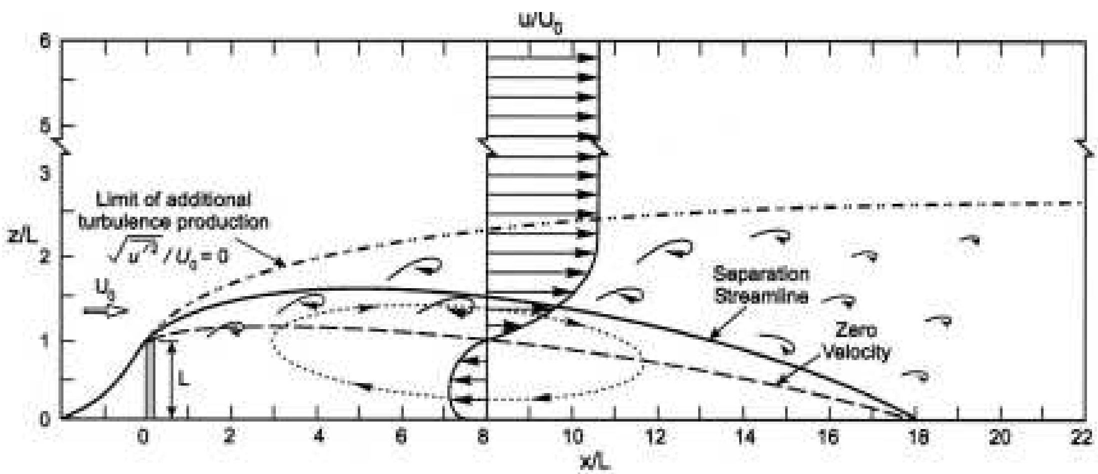

Figure 68. Flow Features Produced by Two-dimensional Flow with Uniform Approach (Source: Ettema et al. 2004)

In addition, the effects of surface tension play an important role on the forces acting on bed particles (e.g. lift and drag); therefore the Reynolds number is also an important indicator on particle similitude. Henderson (1966) states that if the model particle Reynolds number is greater than 1000 the drag coefficient on the particle will be the same in the model and the prototype. For the computation of the particle Reynolds number, U is expressed as the shear velocity and L expressed as the mean particle diameter.

The Weber number represents the ratio of the inertial forces to surface tension and generally represents those processes that are influenced by surface tension. In the case of this study, surface tension most notably influences shallow flow depths (e.g. depth over the weir) and air-entrainment processes (e.g. air-concentrations within the hydraulic jump). Published values (Ettema et al., 2000; Hager, 2021) suggest that the effects of surface tension on overfall crests and spillways can generally be ignored for discharge computations above a Weber number of 100. The Weber Number is expressed mathematically in Equation 21.

Equation 21.Weber Number

$$W_e = \frac{\rho L U^2}{\sigma}$$

Where W_e is the Weber Number and σ is the surface tension of water.

There are also various reported values for the minimum depth over an Ogee spillway crest to minimize the scale effect errors related to viscosity and surface tension. Hager (2021) reports that a flow depth of approximately 2 inch-model (50 mm) is used as a target to minimize scale effects on discharge over the crest related to discharge rating over the crest.

The surface tension is of critical importance for the process of air-entrainment. The stilling basin is characterized by a rapid increase in depth, turbulence production, recirculation, and air-entrainment along and above the shear layers of flow in the jump. In addition, the separation, expansion, air-entrainment, and decay of shooting jets can be affected by scale effects related to surface tension. Although experimental data suggest that the air-entrainment process likely occurs based on the relatively high Reynolds Number, there are still may be scale effects related to spray and jet expansion and decay.

Henderson (1966) describes a relationship for friction scaling whereas dynamic similitude is adhered to if the roughness scales are maintained at the 1/6th power as expressed for the Mannings "n" in Equation 22.

Equation 22. Scale Ratio for Manning's "n" (Henderson, 1966)

$$n_r = L_r^{\frac{1}{6}}$$

Where n_r is the scale ratio for Manning's "n", and L_r is the length ratio. This relationship demonstrates that the roughness ratios are not typically adhered to, even when smooth model materials are used (e.g. glass or acrylic). Although the USBR (1948) states that with scale ratios of 1:30 to 1:60 the effects of distorted friction in the model are small in comparison to the inertial effects and the results are transferable with few reservations. USBR (1980) states that models for medium sized spillways should have a minimum length scale ratio not exceeding 1:60.

When applying data derived from Froude-Number similitude scale physical models, the relationships contained in Table 6 can be used to estimate parameters for protype conditions.

Table 6. Froude-Number Scale Relationships (Source: Expanded from Ettema et al., 2000)

Variable	Relationship	Scale
length	$L = length$	$L_r = X_r = Y_r$
time	$t = \frac{length}{velocity}$	$t_r = L_r^{\frac{1}{2}}$
velocity	$U = \frac{length}{time}$	$U_r = L_r^{\frac{1}{2}}$
area	$a = length * length$	$a_r = L_r^{2}$
discharge	$Q = velocity * area$	$Q_r = U_r a_r = L_r^{\frac{5}{2}}$
unit discharge	$q = \frac{discharge}{length}$	$q_r = \frac{U_r a_r}{L_r} = L_r^{\frac{3}{2}}$
force	$F = mass * acceleration$	$F_r = \rho_r L_r^{2} L_r = \rho_r L_r^{3}$
pressure	$p = \sigma = \frac{force}{area}$	$p_r = \sigma_r = \frac{\rho_r L_r^{2} L_r}{L_r^{2}} = L_r$
power	$P = pressure * time$	$P_r = \frac{\rho_r L_r^{2} L_r}{L_r^{2}} L_r^{\frac{1}{2}} = L_r^{\frac{3}{2}}$

3.4.2 Local Scour Estimation

3.4.2.1 Basic Phenomenon

The basic process of local scour consists of a hydraulic related force mobilizing materials and transporting them away whereas additional materials can be mobilized. This can be described in categories related to the type of hydraulic attack mechanism, detachment/initial motion, and particle breakup and transport.

The vast majority of stilling basins are located on either stiff soil or rock materials; therefore the focus of the local scour described herein will be associated with cohesive materials. Bollaert

(2010) provides a graphical representation of major categories of mobilization phenomenon for rock, as illustrated in Figure 69.

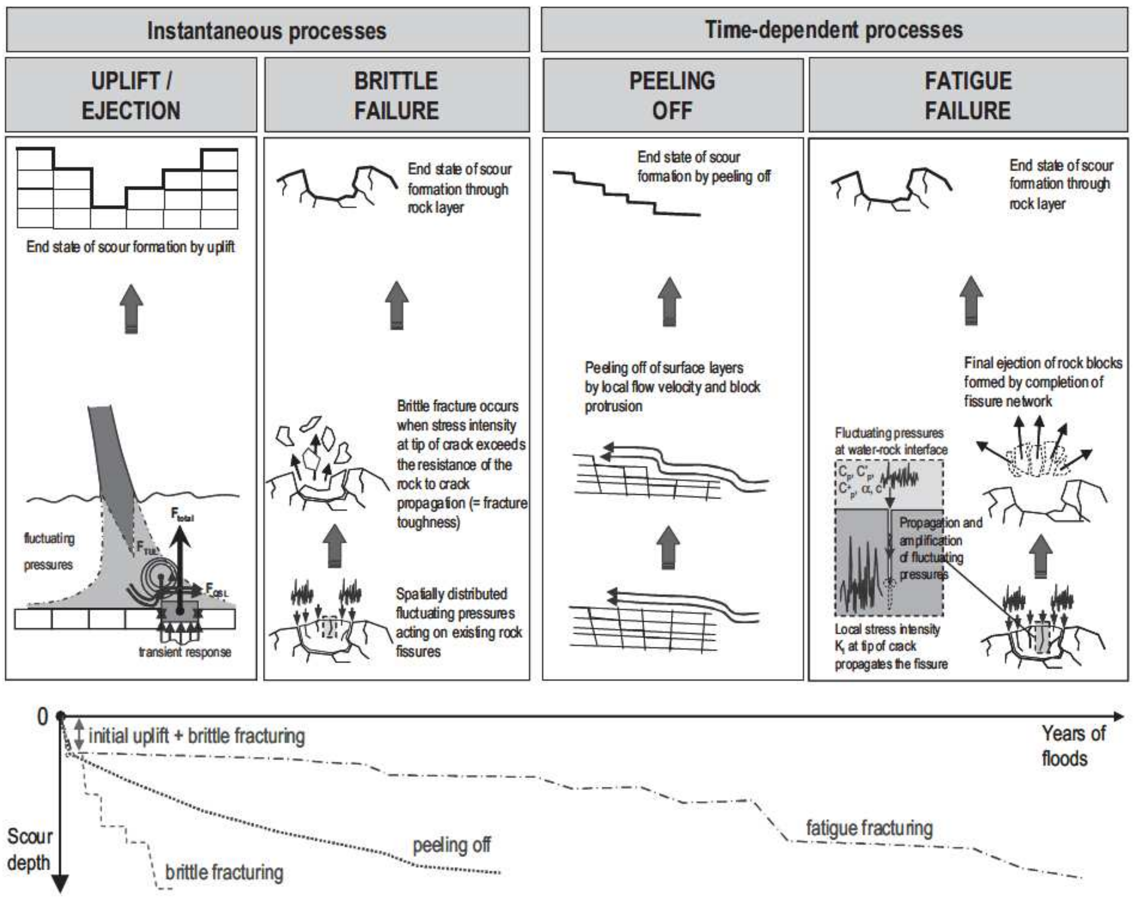

Figure 69. Principle Mechanisms of Rock Fracturing (Bollaert, 2010)

3.4.2.2 Mobile Bed and Qualitative Scour Estimation

The evaluation and design of hydraulic jump stilling basins is often focused on the primary function of reducing or eliminating the potential for hydraulic structure instability associated with progressive erosion of the foundation of hydraulic structures. For this reason, the evaluation of the downstream scour potential is of upmost importance. It is standard practice to represent the scour process for energy dissipators with a granular material, even in cases where the erodible material is a cohesive soil or a rock mass. The most common materials used are Sand and Coal for mobile bed modeling (USACE, 1978), although in the high turbulent areas downstream of stilling basins, the use of coal is not typical or required for design considerations.

The typical duration for the evaluation of stilling basin scour is that sufficient to provide a meaningful estimation of ultimate proto-type scour tendencies. It is typical that the duration of experimentation is performed until quasi-equilibrium is reached, whereas the general patterns are not changing. This interval has no fixed duration and has no relation to the time scale factors related to Froude similitude (USBR, 1948). USBR (1980) states that when models “when operated for a period of time sufficient to produce a stable bed, will indicate erosion tendencies and patterns in the prototype.”

Blaisdell (1942) compared the scour evaluation of a baffled hydraulic jump stilling basin at 1:4- and 1:12- Froude Scale, as well as at prototype scale. It is noted that all three scour hole geometries were comparable, although the bed material of the prototype is not described. It is stated that the scour resulting in the 1:4- and 1:12- Froude Scale models are “nearly identical” utilizing the same sand bed materials; even though the velocity, shear stress, and stream power would be significantly more in the larger model.

3.4.2.3 Semi-Empirical Scour Estimation Methods

Most applied scour estimation techniques are semi-empirical relationships between a hydraulic index value (e.g. velocity, shear stress, or stream power) and a geomechanical index (e.g. clay fraction, in situ moisture, block size, joint condition, unconfined compressive strength, joint orientation to flow). In general, these relationships are derived by estimating or measuring a hydraulic index and then observing the material behavior in a laboratory or field setting, whereas an empirical relationship can be estimated.

3.4.2.3.1 Ultimate Scour Equations

The use of empirical ultimate scour equations has been used widespread for flip buckets, grade control structures, and other cases related to free fall jets; although the literature related to baffle hydraulic jump stilling basins is limited. Novak et al. (2007) describes a modified version of the Veronese equation to estimate the ultimate scour downstream of a stilling basin based on the H_T, q, d_{90}, d'_2; as shown in Equation 23.

Equation 23. Ultimate Scour Downstream of Stilling Basin from Novak (2007)

$$y_S = 0.55(6{H_T}^{0.25}q^{0.5}\frac{{d'_2}^{\frac{1}{3}}}{d_{90}} - d'_2)$$

Where y_S is the depth of scour below the riverbed in meters, H_T is the total hydraulic head in meters, D_{90} is the 90-percent grain size in millimeter, d'_2 is the tailwater depth in meter, and q is the unit discharge in $\frac{\mathrm{m}^2}{\mathrm{s}}$.

3.4.2.3.2 Velocity/Stress Models

The use of velocity and computed shear stress have long been used for evaluation of incipient scour related to channels and surface erosion. These methods typically evaluate a “critical” value of velocity or shear stress required to mobilize material based on material properties. Above the critical hydraulic index value, a rate may be applied to the “excess” to develop time-dependent relationships of scour.

The National Cooperative Highway Research Program (2019) illustrates material erodibility categories to both velocity and shear stress, as illustrated in Figure 70 for rates and detailed in Table 7.

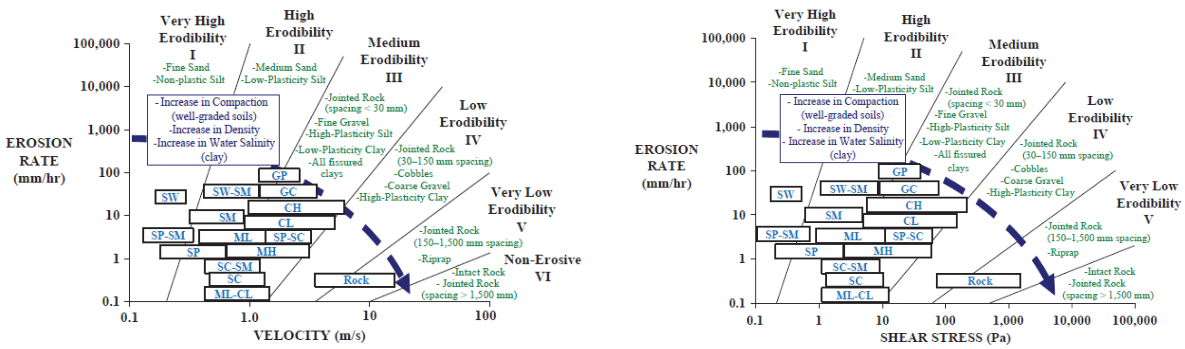

a) Velocity *b) Shear Stress*

Figure 70. Erosion Rates for Various Categories (NCHRP, 2019)

Table 7. Critical Thresholds for Various Categories (NCHRP, 2019)

Category Number	Erosion Category Description	v_c (m/s)	τ_c (Pa)
I	Very high erodibility geomaterials	0.1	0.1
II	High erodibility geomaterials	0.2	0.2
III	Medium erodibility geomaterials	0.5	1.3
IV	Low erodibility geomaterials	1.35	9.3
V	Very low erodibility geomaterials	3.5	62.0
VI	Nonerosive materials	10.0	500.0

These methods are most frequently used with soil materials and categorized using various laboratory and field methods. These methods and semi-empirical relationships provide the basis for the evaluation of scour at earthen spillways provide by NRCS (1997).

Although these methods are used extensively for channel, dam overtopping, and earthen spillway erosion, they have not been utilized directly for stilling basin erosion estimates.

3.4.2.3.3 Annandale's Erodibility Index

It was suggested by Annandale (1995) that there is a rationale correlation between the rate of energy dissipation and the erodibility of earthen materials. Although the more common hydraulic index has been related to mean channel velocity or mean boundary shear stress, these indicators do not show consistent trends related to the influence of boundary roughness and therefore the rate of energy dissipated in the near boundary region.

Annandale (1995) used various methods for computing the applied boundary stream power for multiple mechanisms of hydraulic attack/turbulence production, including turbulent stress in channels, back rollers, flow separation at grade changes impinging jets, and hydraulic jumps. These fundamental equations for applied stream power were then applied for numerous prototype case histories where scour was observed or verified that scour was negligible.

The observed cases of the presence or absence of scour were plotted against a geomechanical index for rock masses that was developed Kirsten (1982) to determine the excavation potential based on multiple properties of discontinuous rock masses. The rock mass index was a modified version of Barton's Q-system of classification (Barton, 1988); which included parameters to represent the mass strength (M_s), the block or particle size (K_b), the discontinuity/inter-particle bond shear strength number (K_d), the relative ground structure number (J_s). The basic equation for the Erodibility Index is shown in Equation 24.

Equation 24. Annadale's Erodibility Index

$$EI = M_s * K_b * K_d * J_s$$

A similar headcut erodibility index method was developed by Temple and Moore (1994) that was used in estimating unlined spillway erosion. This method used the product of the unit discharge and total head; which is representative of the available unit stream power. Schalkwyk (1995), Annadale (1995), and Kirsten et al. (1996) developed similar databases of erodibility index verse stream power. The graphical development of the EI threshold proposed by Annadale (1995) is shown in Figure 71.

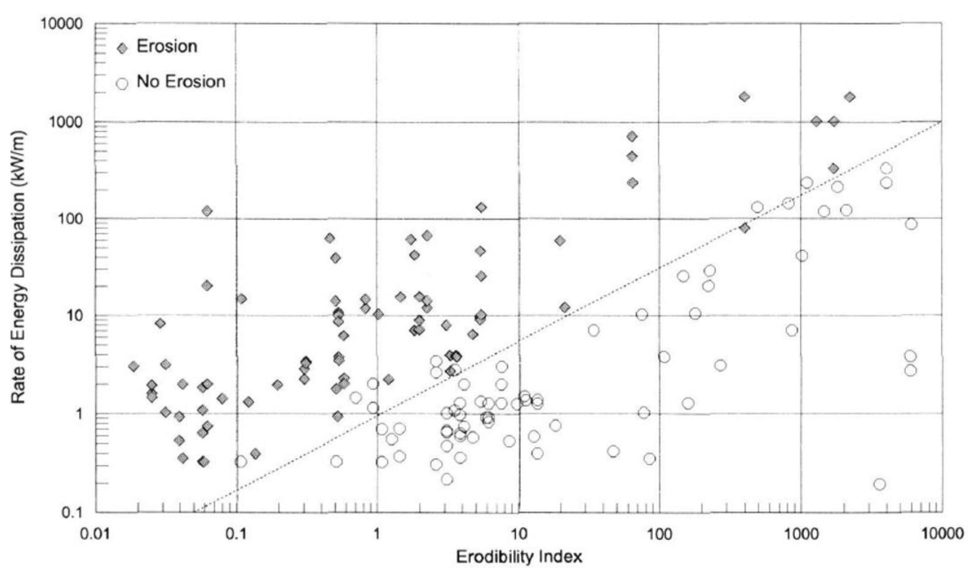

Figure 71. Annadale Erodibility Threshold (Annadale, 1995)

Annadale (2006b) combined the relevant databases and included prototype scale erosion data collected at Colorado State University into two equations for the threshold of scour. The relationship for materials with an EI < 0.1 typically representing granular and low strength soils shown in Equation 25.

Equation 25. Annadale's Scour Threshold for Low EI Materials

$$\Pi_c = 0.48(EI)^{0.44}$$

Where Π_c is the threshold applied stream power in $\frac{Kw}{m^2}$. The relationship for materials with an EI > 0.1 is shown in Equation 26.

Equation 26. Annadale's Scour Threshold for High EI Materials

$$\Pi_c = (EI)^{0.75}$$

The Erodibility Index Method has been widely used to characterize the local scour at hydraulic structures and can be used for materials ranging from granular soils to rock masses.

3.4.2.3.4 Pells Modified Geological Strength Index

Pells (2016) developed a similar semi-empirical index method to Annandale (1995) using a modified version of the Geological Strength Index (GSI). The GSI consists of two factors, the characteristic structure and the joint surface conditions of the discontinuities in the rock mass. To account for the influence of the discontinuity's orientation to flow, an adjustment factor is included; with the adjusted index termed the eGSI. The GSI developed by Hoek (2006) is shown in Figure 72 and the orientation adjustment factors shown in Figure 73.

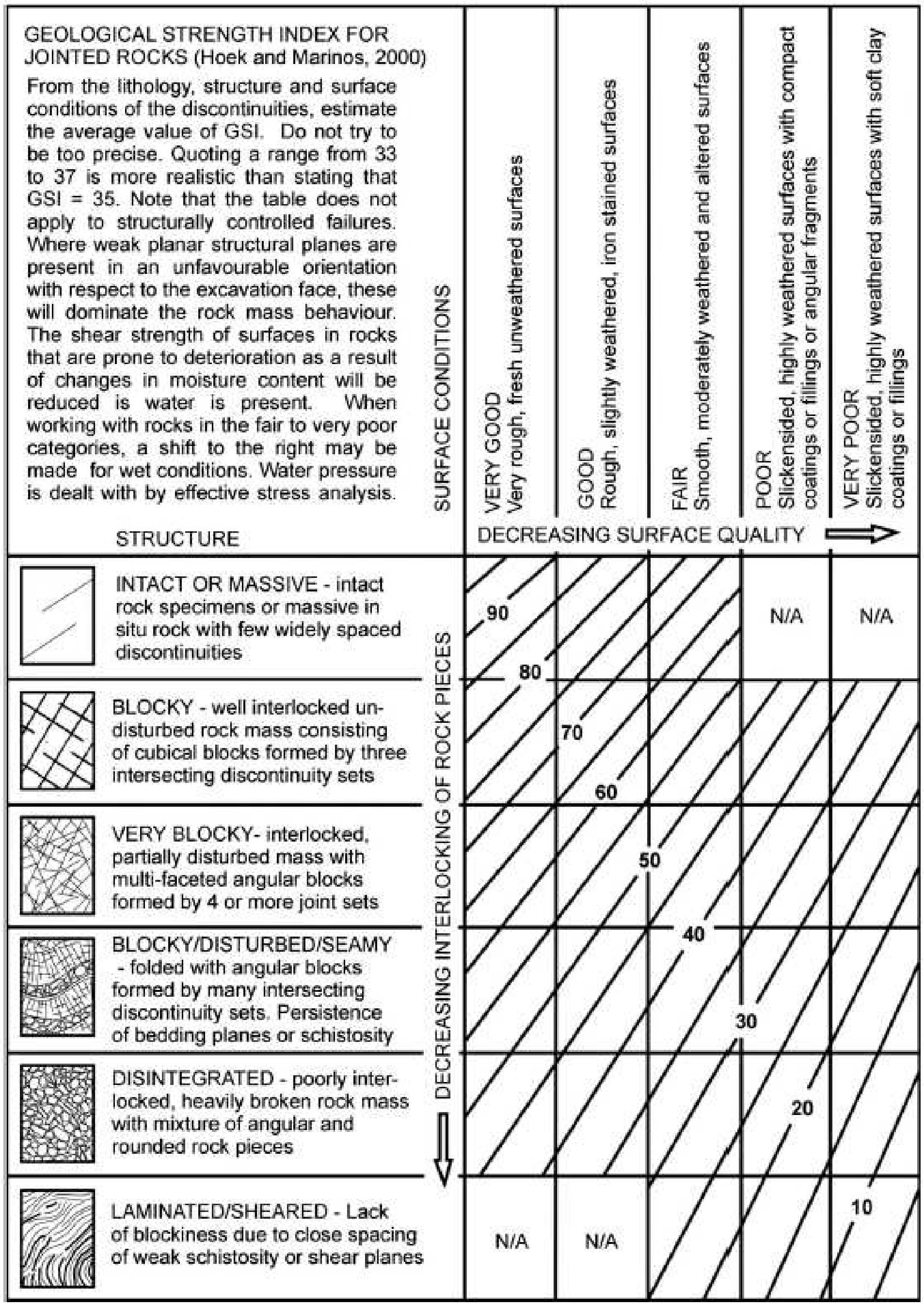

Figure 72. Geological Strength Index Chart (Hoek, 2006)

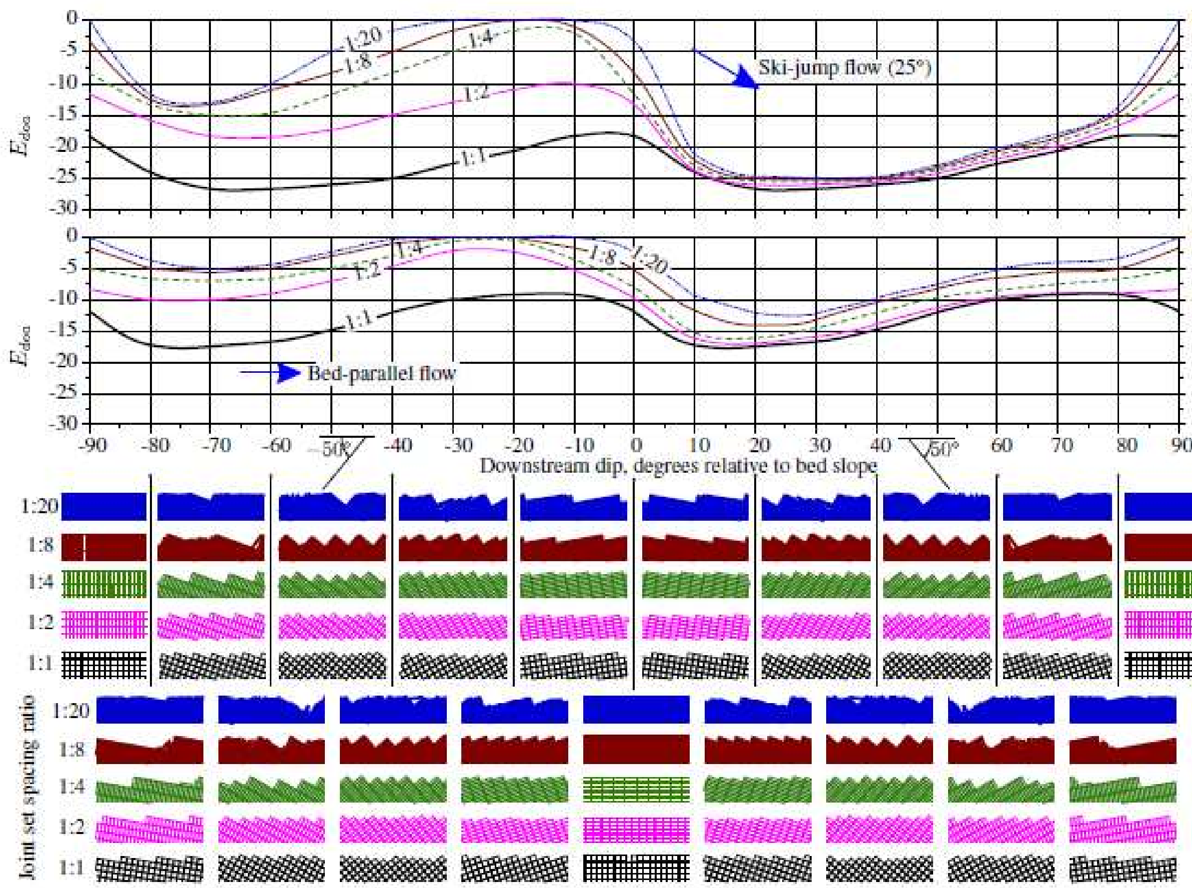

Figure 73. Discontinuity Adjustment Fator for Erosion for Horizontal Beds (Pells, 2017)

This index was estimated for 118 data points collect from 26 spillways. Both the boundary shear stress and stream power were estimated as the hydraulic index by means of 1-dimensional numerical modeling or analytical relationships for the case of a hydraulic jump.

Five erosion classes were developed to describe the prototype scour severity. The relationship for the erosion class to the eGIS is plotted as a function of boundary shear stress (a) and stream power (b) in Figure 74.

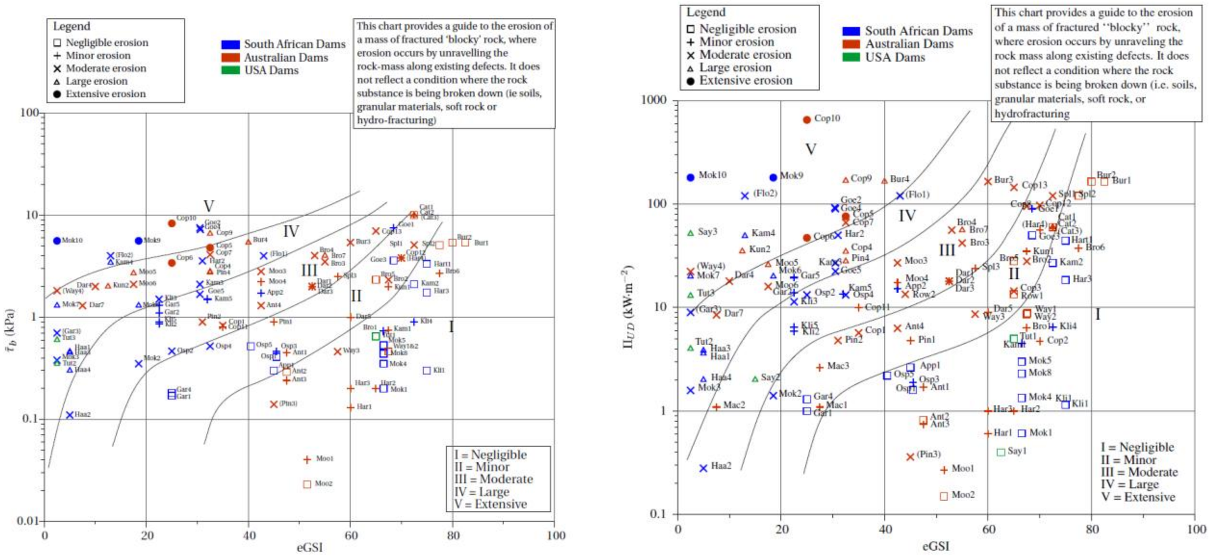

a) Shear Stress　　　　*b) Stream power*

Figure 74. eGSI applied to Spillway Scour Case Histories (Pells, 2016)

3.4.2.4 Mobile Bed as a Proxy for Prototype Thresholds

One of the primary objectives of stilling basins physical models is typically to estimate ultimate (or maximum) scour conditions likely to occur in the prototype. This has historically been achieved with an clean, fine-grained sand material as aforementioned. In instances where the erosion capacity greatly exceeds the material's resistance capacity, this provides great insights into the tendencies and anticipated downstream channel behavior in the immediate vicinity of the stilling basin. For situations where the foundation and downstream are highly resistant to scour and erosion (e.g. massive, hard rock with high unconfined compressive strength) in comparison to the expected hydraulic attack exiting the stilling basin, the results obtained from a sand bed model will not be likely to describe the scour potential or behavior within the prototype.

To relate the mobilization and/or detachment of the prototype, a velocity, shear stress, or steam power can be used. Annandale (2011) describes a method for semi-quantitative estimates of ultimate prototype scour by use of granular proxy bed material that has a threshold of motion similar to the threshold for block detachment of the rock mass or detachment of material from a cohesive soil mass. The unit stream power is scaled from the prototype to the model by using the Froude scale similitude relationship shown in Equation 27.

Equation 27. Power Similitude Relationship

$$\Pi_r = L_r^{\frac{3}{2}}$$

Where Π_r is the Froude scale ratio for stream power. The model stream power is then converted into an approximate equivalent model turbulent shear stress using the equation developed by Annandale (2006b); which is derived by integrating the universal energy balance of the near-bed region developed by Schlichting and Gersten (2017). The equation developed by Annandale is shown in Equation 28 and the graphical representation of the universal energy balance in the near-bed region shown in Figure 75.

Equation 28. Annandale's Relationship of Turbulent shear stress to Stream Power

$$\Pi = 7.853 * \rho \left(\frac{\tau}{\rho}\right)^{\frac{3}{2}}$$

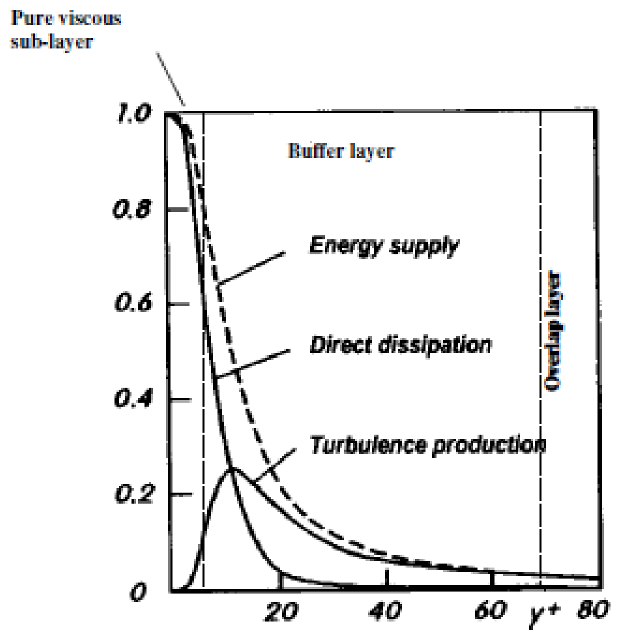

Figure 75. Universal energy balance in the near-bed region (Source: Annandale, 2006b)

Once the approximate equivalent turbulent shear stress is estimated for the model scale, a non-cohesive granular proxy material can be selected to represent the incipient stream power of the prototype rock mass.

It is worth noting that this approach is not intended to represent the transport and breakup processes associated with the detached individual blocks, only the threshold for block detachment. In addition, there are limitations associated with the incipient stress of granular materials on a non-horizontal boundary and the inability of granular materials to maintain slopes steeper than the submerged angle of repose.

The submerged incipient motion of a granular particle can be estimated using a dimensionless shear stress parameter (Julien, 2010). This parameter is often referred to as the Shields parameter (Shields, 1936) and represents the ratio of a shear stress value to the submerged density of a particle to a stability parameter defined by the submerged weight times a characteristic grain size, as previously expressed in Equation 29.

Equation 29. Shields Particle Stability Criterion

$$\Theta_c = \frac{\tau}{(\gamma_s - \gamma)d_s}$$

Where Θ_c is the shields stability parameter, γ_s is the specific weight of the bed material, γ is the specific weight of the water, and ds is the representative size of the bed material.

There are many published values and approaches to determining the shields stability parameter. Shields (1936) experimentally developed a dimensionless relationship for various grain size and submerged weights to the incipient stress required for “bed-load movement”. The dimensionless parameter is denoted the “coefficient of the critical tractive force”; but is subsequently described in literature as the Shield’s Parameter.

The boundary shear stress and particle Reynolds numbers for the Shield’s parameter are computed using mean flow parameters and attempts to correct for sidewall influences was made. The original published Shield’s relationship is illustrated in Figure 76. Shields described the boundary layer behavior similarly to that described by Nikuradse (1933) as having three distinct regimes, which also explained the shape of the values of the coefficient of the critical tractive force. Shield’s anticipated that the dimensionless parameter would maintain constant for fully developed turbulent flow conditions, although data with particle Reynolds Numbers above 1000 was not obtained.

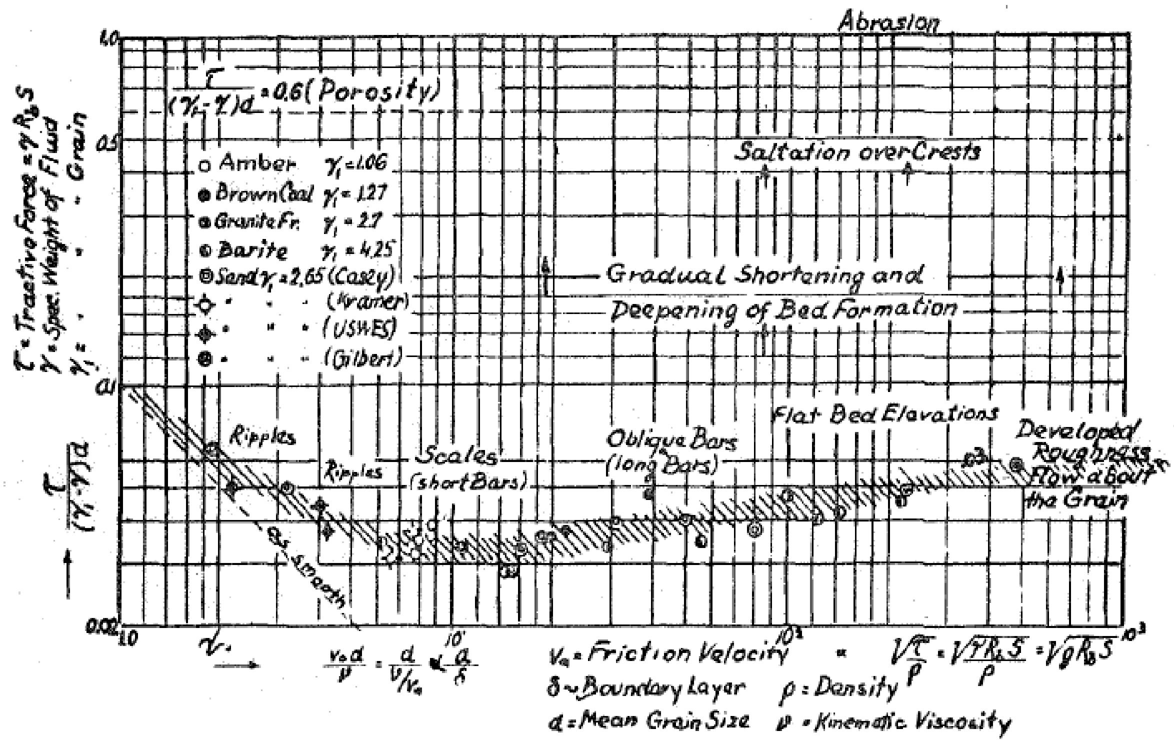

Figure 76. Experimental Data of Shields (1936)

Yalin et al. (1979) provided additional data to inform the Shield's relationship within the Laminar and Transitional flow ranges (i.e. values of Particle Reynolds Numbers ranging from 1 to 100). Yalin describes the increasing importance of turbulent boundary layer and associated macro-turbulent eddies on the inception of sediment transport as the particle Reynolds Number increases within the transitional range towards fully turbulent flow. Although the values published have varied slightly, Gessler (1971) reported a critical Shield's Parameter value of 0.046 for rough, turbulent flows.

Buffington and Montgomery (1997) systematically evaluated critical values of the Shield's Parameter report by various authors ranging over eight decades. The range of values estimated across multiple datasets is found to be 0.03 to 0.086 for the rough, turbulent flow regime. The data are farther stratified by multiple parameters such as the definition of initial motion, method of accounting for form roughness, and relative roughness/submergence ratios, allowing for identification of the potential sources of the wide range of values. The major contributing factors to a wide range of published values are the determination of the incipient motion (e.g. through direct observation of individual grain movement or through reference from measurements of equilibrium sediment transport rates) and the inclusion of form roughness into the computation of shear stress. It is also concluded that a universal value for Shield's Parameter for rough, turbulent flow does not exist which provides additional uncertainty related to use of shear stress methods for proxy material sizing.

Most of the relationships used to evaluate incipient motion of the granular proxy material are based on experimental data on a near-horizontal bed. As the slope of the material increases, the required bed shear stress decreases proportionally. The method described by Parker (2004) to adjust the Coulomb resistive force due to gravity is used to arrive at approximate adjustment factors for incipient shear stress for significant streamwise slopes. Equation 30 is adapted to provide a relative ratio of the near-horizontal to slope incipient stress.

Equation 30. Incipient Shear Stress Slope Adjustment Factor

$$\tau_r = \cos(\alpha) * \left(1 - \frac{\tan(\alpha)}{\tan(\theta)}\right)$$

Where τ_r is the shear stress ratio, α is the streamwise slope (deg), and θ is the submerged angle of repose (deg). The submerged angle of repose is measured in a tilt flume device shown in Figure 77.

Figure 77. Tilt-Flume for use in determining submerged angle of repose of bed material (Coarse Gravel Material)

It is expected that a mound of granular materials may form downstream for the more severe scour cases. This would likely not occur with cohesive soils, as observed by Stein and Julien (1993), or rock masses. This is because the threshold stress to detach the cohesive soil or rock mass from its matrix is typically much more than the stress to breakup and transport the detached blocks. Due to the low scour attack angle exiting the basins and relatively high rate of downstream transport observed in previous experiments, it is expected that the development of mounds and their influence on the hydraulic characteristics near the structure will be minimum.

USBR (1980) describes a method of using a lightly cemented cement-sand mixture may closely represent the prototype erosion if the eroding velocity of the prototype bed material is accurately estimated. The importance of sensitivity analysis covering a range of estimated critical velocities of half and double the estimate is emphasized.

3.4.2.5 Direct measurement of Dynamic Pressure Fluctuations

Given the challenges that are associated with the use of granular materials to represent cohesive matrix such as cohesive soil and rock masses and the phenomenon of dynamic turbulent fluctuations being a critical component to local scour at stilling basins; methods of utilizing direct measurement of turbulent fluctuations as an indicator of the erosion potential of flow have been developed.

The Comprehensive Scour Model (CSM) is a semi-empirical method of evaluating the major mechanisms of detachment of blocks from a discontinuous rock mass using direct measurements of pressure fluctuations as the hydraulic index (Bollaert, 2004). The CSM utilizes three methods to estimate the scour potential: the Comprehensive Fracture Mechanics, the Dynamic Impulsion, and the Quasi-Steady Impulsion methods.

Direct pressure fluctuations were utilized with the CSM for forensics investigation into the Paradise Dam after the severe prototype scour event occurred in 2013 (Lesleighter et al., 2016) The scour event occurred downstream of the unbaffled hydraulic jump stilling basin after significant abrasion damage and associated failure of the end sill occurred; with a maximum extent of scour up to 13m. The observed RMS values of the dynamic pressure fluctuations were used to calibrate the components of the CSM to replicate the scour morphology observed during the flood event.

Humphries and Annandale (2015) used the root mean square (RMS) of the turbulent pressure fluctuations to relate to the boundary shear stress (or wall shear stress, τ_w). Farabee and Casserella (1991) related the wall shear stress to the RMS of the wall pressure fluctuation as a function of Reynolds number as shown in Figure 78. The expression used by Humpries and Annandale (2015) is shown in Equation 31.

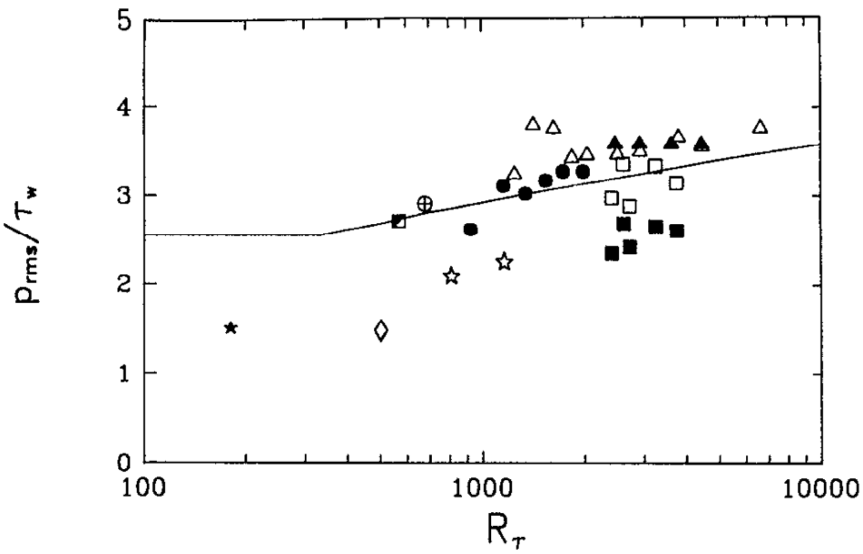

Figure 78. Relationship of the P_{RMS}/τ_w as a function of Reynolds Number (Source: Farabee and Casserella, 1991)

Equation 31. Generalized Relationship between P_{RMS} and τ_w (Source: Humpries and Annandale, 2015)

$$\tau_w = \frac{P_{RMS}}{3}$$

Where τ_w is the turbulent wall shear stress and P_{RMS} is the root mean square of the pressure fluctuations. The boundary shear stress then can be related to the applied stream power using Equation 28. Yager et al. (2018) described that the τ_w closely approximates the Reynolds Shear Stress (τ_{re}) which is a function of the product of the fluctuating velocity components in the streamwise and cross-stream directions; which has relevance to the use of Reynolds Averaged Navier-Stokes (RANS) Computational Fluid Dynamics (CFD) modeling of turbulent flows.

3.5 Recent Advances

3.5.1 Tapered Blocks and Ramp Configuration

Considering that there have been multiple published accounts of damage to baffle blocks and adjacent floor, there have been various shapes developed to reduce the damage potential. More recently, tapered blocks were evaluated and used for a new auxiliary spillway for Folsom Dam (USBR, 2012). The blocks are sized similarly to the standard USBR type III basin and consist of the sidewall and top wall being sloped away from flow and a low angle ramp in-between baffle block. The intent is even though the blocks create super-cavitation (USBR, 1990), the swarms of air bubbles can be transported away in the free stream as opposed to collapsing on the adjacent concrete surface. This block shape was tested and refined via vacuum tank experiment conducted at the USBR's Low Ambient Pressure Chamber (LAPC) facility (USBR, 2009).

USBR (2009) used visual observations of cavitation flashes and vortex formation around the baffles and ramp to position an intermittent ramp aimed at reducing the reattachment of the vortices on the horizontal floor adjacent to the baffles. The tapered blocks were aimed at reducing the potential for reattachment on the baffle sides; which were observed as damage locations for Bonneville and Claytor described previously. The tapered blocks increase the cavitation potential and incipient cavitation conditions as measured by acoustic emissions; whereas the standard block design did not vent and produce super-cavitation. An example of super-cavitation resulting from flow separation off the leading edge of a baffle block and horeshoe vortex formation upstream of the baffles are shown in Figure 79.

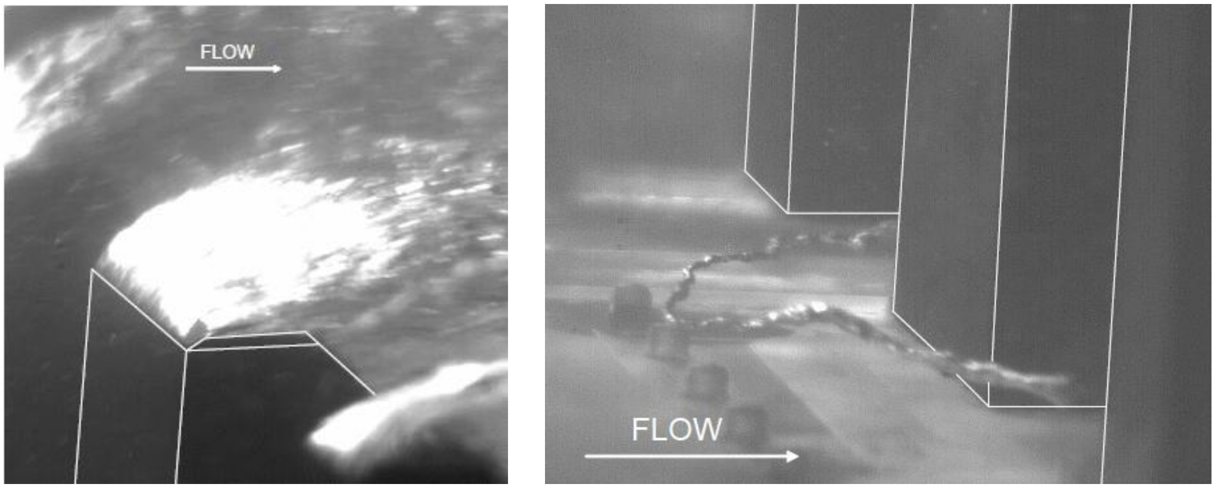

a) Super-cavitation (vented) *b) Upstream Horseshoe Vortex*

Figure 79. Observed Cavitation in Vacuum Tank Experiments (USBR, 2009)

The baffle block shape and configuration was utilized at Folsom Dam, below a high head stepped chute with a unit discharge of 1755 $\frac{\mathrm{ft}^2}{\mathrm{s}}$ and an incoming velocity of over 90 $\frac{\mathrm{ft}}{\mathrm{s}}$.

3.5.2 Baffled Roller Basin

The recent evaluation of the modifications to the Gross Dam in Colorado, owned and operated by Denver Water suggests that incoming chute slope may be influential in the hydraulic characteristics and performance of a baffled stilling basin (Ettema et al., 2019). The spillway consists of a stepped chute at a 0.5:H to 1V slope with a total hydraulic head of 486-feet and a step height of 4-feet. Evaluation of a standard USBR baffled hydraulic jump stilling basin (i.e. Type III) configuration resulted in ineffective momentum being transferred to the baffle blocks related to the steep impingement angle of the chute with the horizontal floor. To remedy the inefficiencies, the baffle blocks were moved much closer to the chute to change the overall function of the blocks and eliminate the “rooster tail” that was exhibited at the recommended location.

4 EVALUATION OF PUBLISHED DATA

4.1 General

As described in previous sections, there are wide variations in the standard baffled hydraulic jump stilling basin geometries published in USBR, USACE, and SAF guidance documents. The source of this discrepancy is not obvious based on the guidance documents themselves; therefore, additional interrogation is conducted by comparison of the source data used to develop the standard geometric relationships.

4.2 Stilling Basin Geometry

Given that there are multiple data sources utilized in the development of current standard baffled stilling basin design, it would seem prudent to perform a re-evaluation of existing data. Basco (1984) performed a similar exercise with the data contained in USACE (1964), although the USBR data for Type III basins (USBR, 1955; USBR 1984) was not included.

4.2.1 Critical Depth

If the unit discharge is held constant, the estimated baffle heights from both USACE (1992) and USBR (1984) standard guidance do not change with Fr_1; unlike the SAF basins that hold a constant baffle height equal to the incoming flow depth (i.e. baffle height = 1.0 d_1). This suggests that there may be a correlation between the unit discharge and optimum baffle geometry, irrespective of the Fr_1. There is precedence for utilizing the critical depth as a scale parameter associated with the prediction of stepped spillway flow behavior and energy dissipation, which is most often explained by a dimensionless parameter of step height divided by the critical depth (Chanson, 1996). The critical depth can be expressed as a function of the unit discharge via Equation 32.

Equation 32. Critical Depth for Rectangular Channel

$$d_c = \sqrt[3]{\frac{q^2}{g}}$$

Where d_c is the critical depth of flow.

From a theoretical standpoint, the hydraulic jump has been described as a relationship between the change in pressure and momentum prior to and after the hydraulic jump. Whereas in accordance with Newton's second law of motion, the change in the pressure must be equal to the change in momentum minus the losses occurring within the hydraulic jump (Elevatorski, 1959). Mathematical expressions of the change in pressure (ΔP) and change in momentum (ΔM) is described in Equation 33 and Equation 34 , respectively.

Equation 33. Expression for change in pressure from hydraulic jump

$$\Delta P = \frac{1}{2}\gamma\left({d_2}^2 - {d_1}^2\right)$$

Equation 34. Expression for change in momentum for hydraulic jump

$$\Delta M = \frac{\gamma \boldsymbol{q}(v_1 - v_2)}{g}$$

It can be seen Equation 34, the unit discharge (q) is a scale factor to associate the change in velocity to the change in momentum; providing a theoretical basis for the unit discharge; and therefore critical depth, as a scaler for relationships associated with the hydraulic jump.

To explore this potential in additional detail, the data utilized by USBR (1955) to establish relationships between the length of the hydraulic jump to the sequent depth (Figure 4) was compiled and evaluated utilizing the critical depth as a scale factor. If the unit discharge of all the experiments is transformed into critical depth via Equation 32, then the incoming flow depth and the sequent depth can be replaced with critical depth to represent unit discharge. The relationship between jump length and critical depth is shown in Figure 80, and demonstrates a stronger correlation than is associated with normalizing the stilling basin length with the sequent depth in-which has often been done in practice to-date (USBR, 1955; USBR 1984; USACE, 1980).

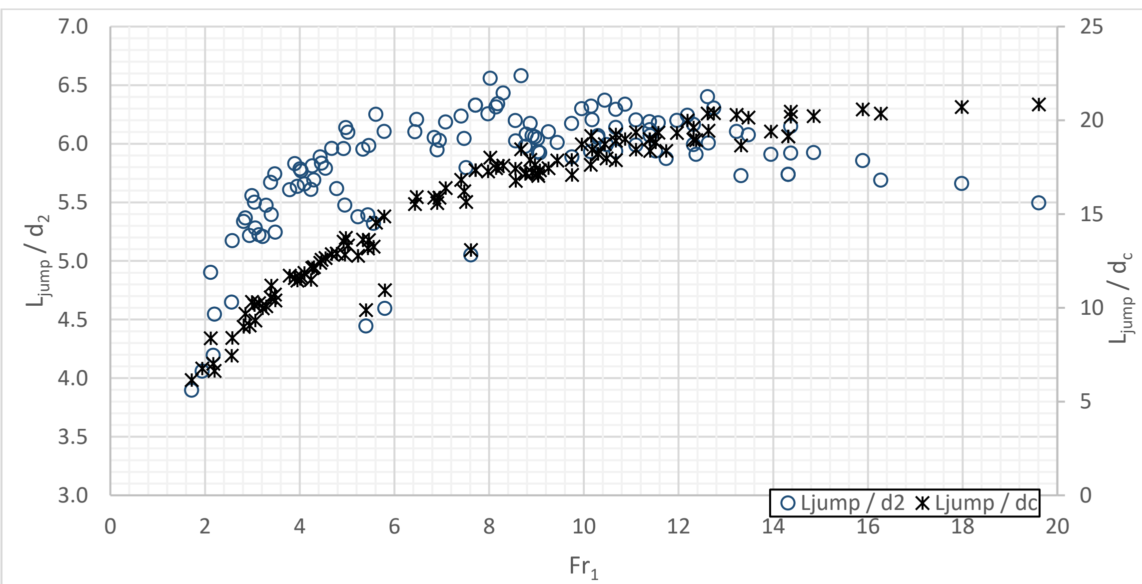

Figure 80. Re-evaluation of USBR (1955) Experimental Data Related to Free Jump Length

Considering that the presence of the baffle blocks in the stilling basin provides additional momentum transfer and therefore aids in the development of the hydraulic jump action; it is logical that the unit discharge, and critical depth by association, would be an appropriate scale factor for baffled stilling basins. To evaluate the strength of the correlation of each potential scale index parameter (d_1, d_2, and d_c) the data utilized in development of the standard USACE (1992) and USBR (1984) stilling basin geometries are plotted normalizing with each parameter.

4.2.2 Stilling Basin Length

The length of the stilling basin normalized to the sequent depth in Figure 81. There is significant variation in the data; especially regarding the USACE data. The length range is from approximately 1.0 d_2 to greater than 3.5 d_2. Basco (1970) reports that the optimum length is significantly longer than the adopted guidance and range of data evaluated by the USACE and USBR.

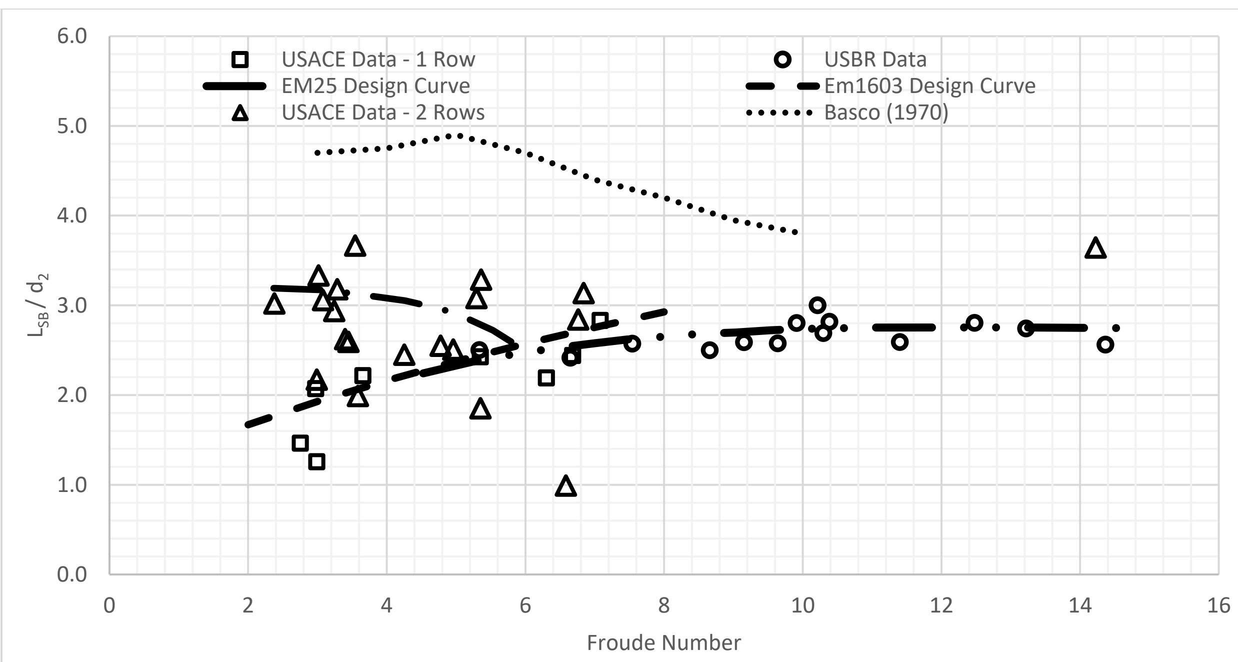

Figure 81. L_{SB}/d_2 as a Function of Fr_1

The L_{SB} is normalized to d_c in Figure 82. The data show less variation when normalized to d_c, than when normalized to d_2. This is consistent with the trend shown in Figure 80 for the re-evaluation of normalized free jump length. Unlike the relationship to d_2, there is an increasing trend with Fr_1 when normalizing to d_c.

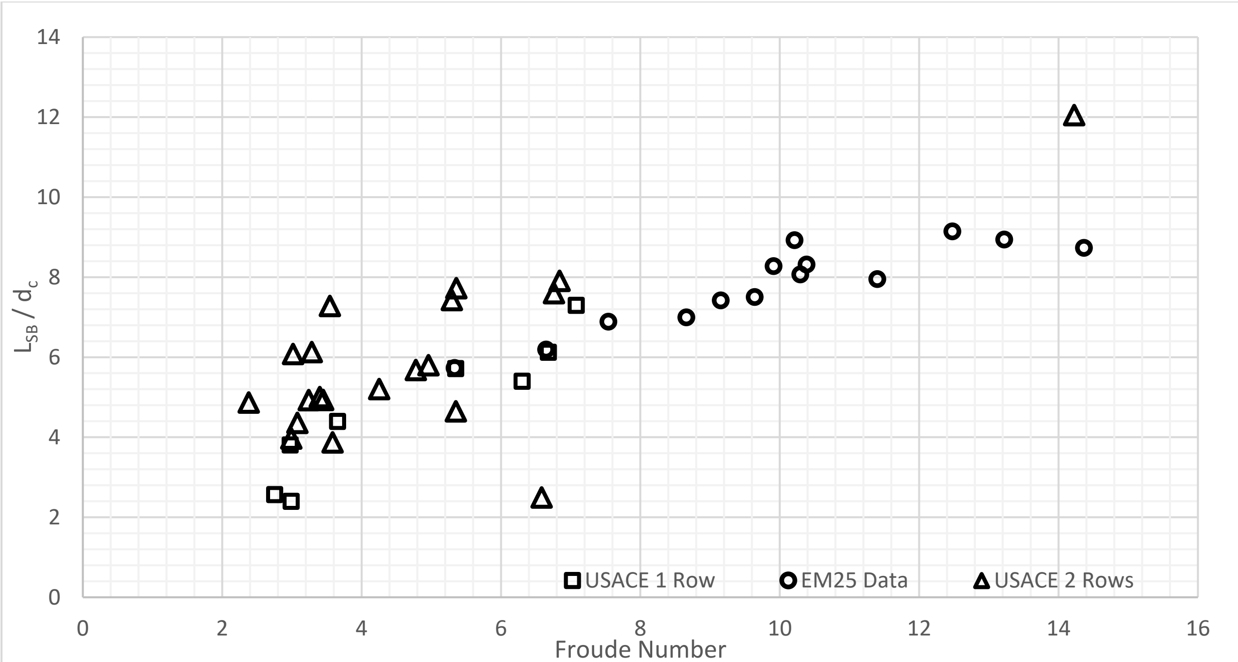

Figure 82. L_{SB}/d_c as a function of Fr_1

The L_{SB} is normalized to d_1 in Figure 83. Normalizing to d_1 results in less variation than either d_2 or d_c. There is a strong increasing trend with Fr_1 as also demonstrated with the USBR (1955) data for both free and forced jumps.

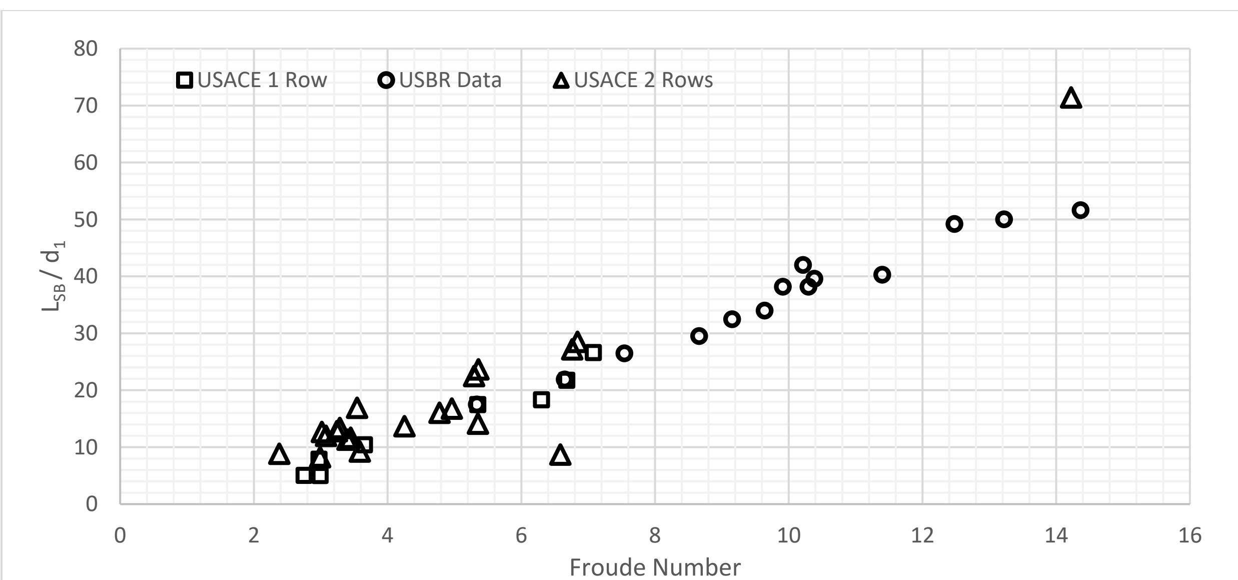

Figure 83. L_{SB}/d_1 as a function of Fr_1

The d_2 is the parameter used by USBR (1984) for all stilling basin types (Type I thru Type IV). USBR (1955) plots the experimental data in terms of both d_1 and d_2; stating that "the first is perhaps the better method while the second is more common". The USACE (1992 and 1987) utilizes d_1 as the scale parameter, although USACE (1980) utilizes d_2. No standardized guidance has evaluated the use of d_c.

Considering the consistency of the data for stilling basin length when normalized to the d_1, the use of the d_1 for the USACE (1992) length estimate, and the strong linear trend observed related to $\frac{L_{SB}}{d_1}$ the data was re-evaluated as a linear relationship and is shown in Equation 35.

Equation 35. Unified Equation for Stilling Basin Length

$$\frac{L_{SB}}{d_1} = 4.1Fr_1 - 4$$

The unified expression for stilling basin length can be shown normalized to the d_1 as a function of Fr_1 in Figure 84.

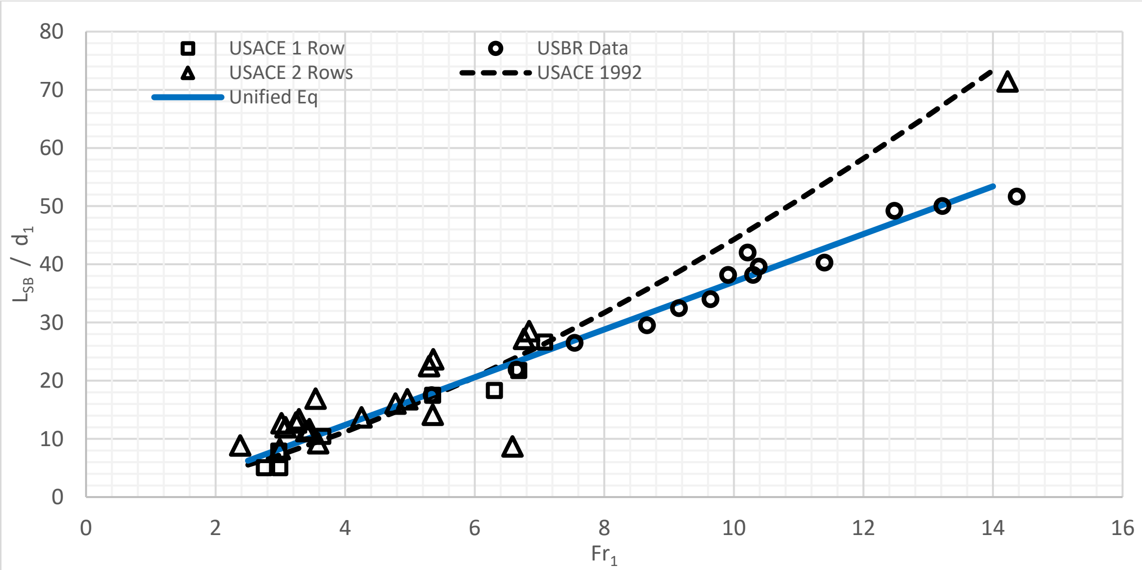

Figure 84. Comparison of Existing Data/Guidance and Unified Equation for $\frac{L_{SB}}{d_1}$

The unified expression for stilling basin length can be shown normalized to the d_1 as a function of Fr_1 in Figure 85.

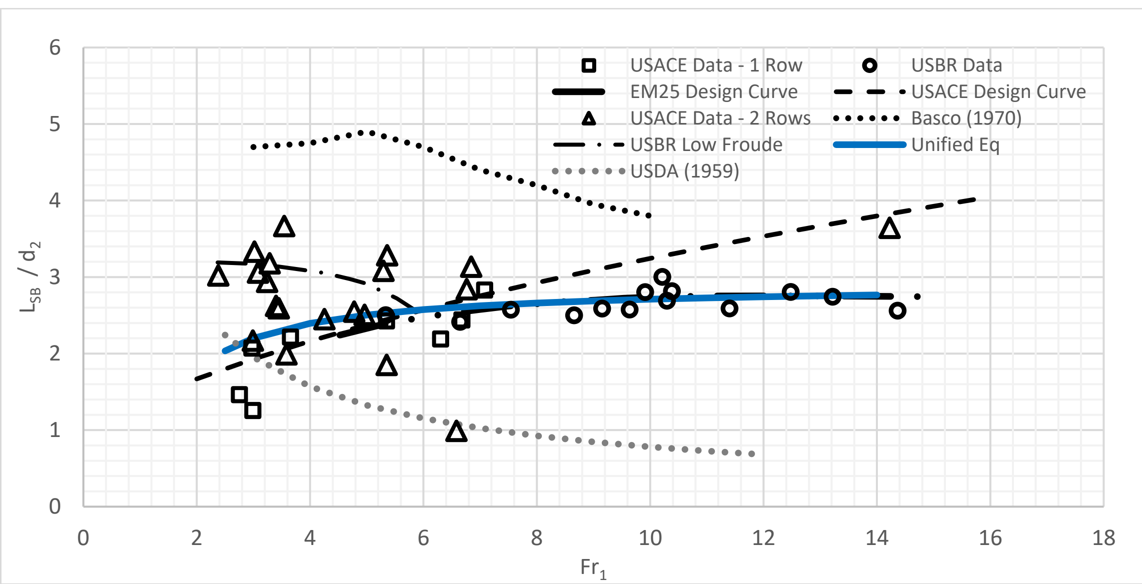

Figure 85. Comparison of Existing Data/Guidance and Unified Equation expressed as $\frac{L_{SB}}{d_2}$

4.2.3 Location of Baffle Block

The length from the Point of Intersection of the chute and the 1st row of baffle blocks (x_{B1}) is normalized by the d_2 in Figure 86. The d_2 is used to define the X_{B1} for the USACE (1992) stilling basin for Fr_1 below 4.6, above this value d_1 is used. Both the USBR (1984) and USDA (1957) use the d_2. It is demonstrated that there is little variation with the verification test of the USBR and wide variation for the USACE data.

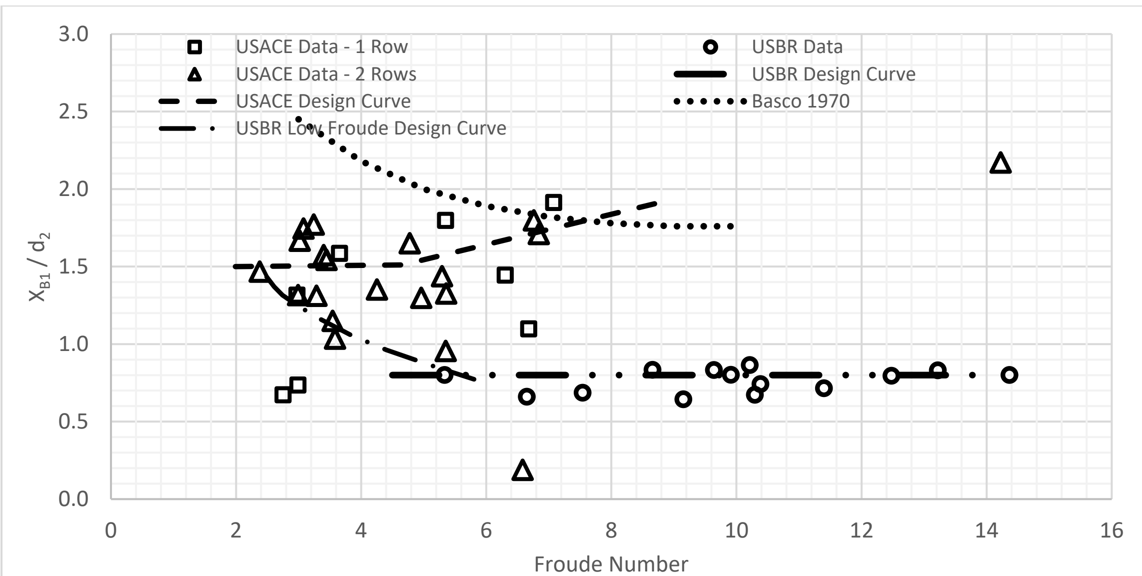

Figure 86. X_{B1} / d_2 as a function of Fr_1

The X_{b1} is normalized to the d_c in Figure 87 and d_1 in Figure 88.

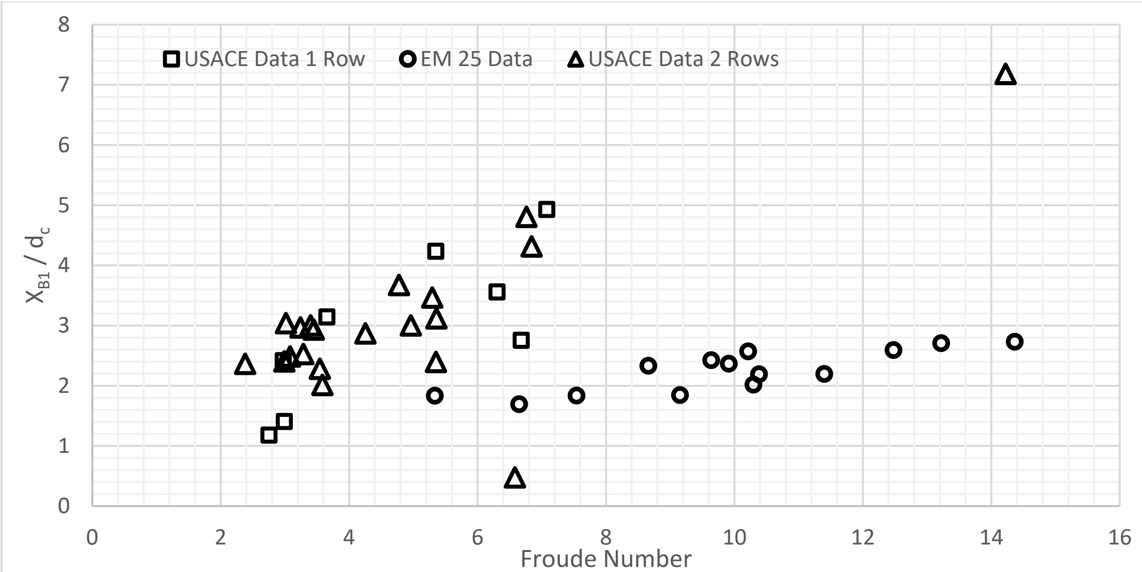

Figure 87. X_{B1} / d_c as a function of Fr_1

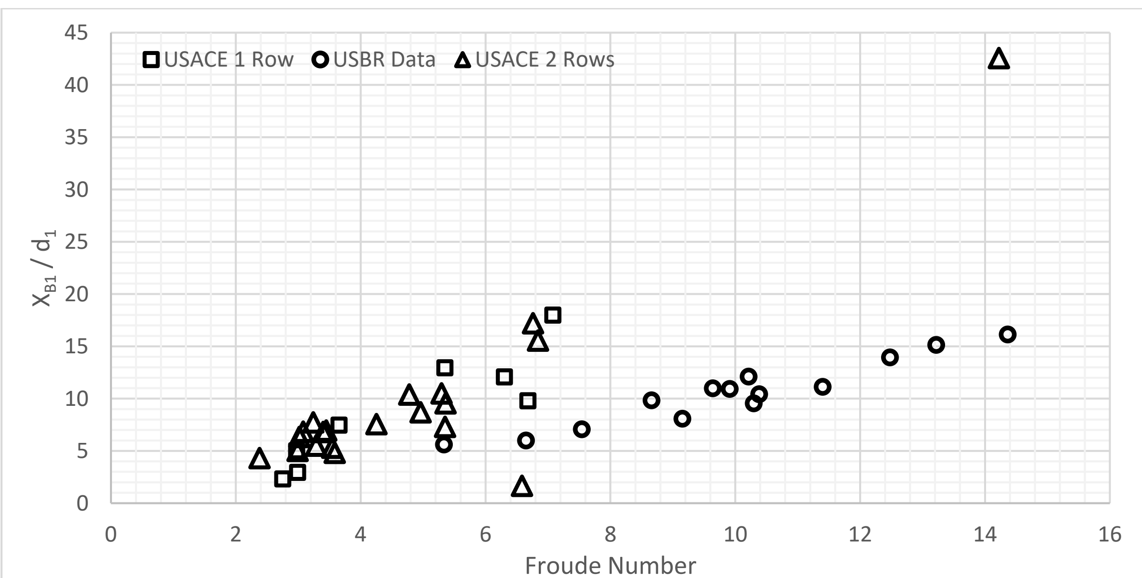

Figure 88. X_{B1} / d_1 as a function of Fr_1

It can be seen there are two distinct trends between the USACE and the USBR standard basins with the USACE data having the baffle block location significantly farther downstream.

4.2.4 Baffle Block Height

The height of the baffle block (H_B) is normalized by the d_1 in Figure 89. The d_2 is used to define the H_B for the USACE (1992) stilling basin for $Fr_1 < 4.6$, above this value d_1 is used. The USBR (1984) expresses the H_B as a function of the d_1. The H_B is shown as a function of the d_c and the d_2 in Figure 90 and Figure 91, respectively.

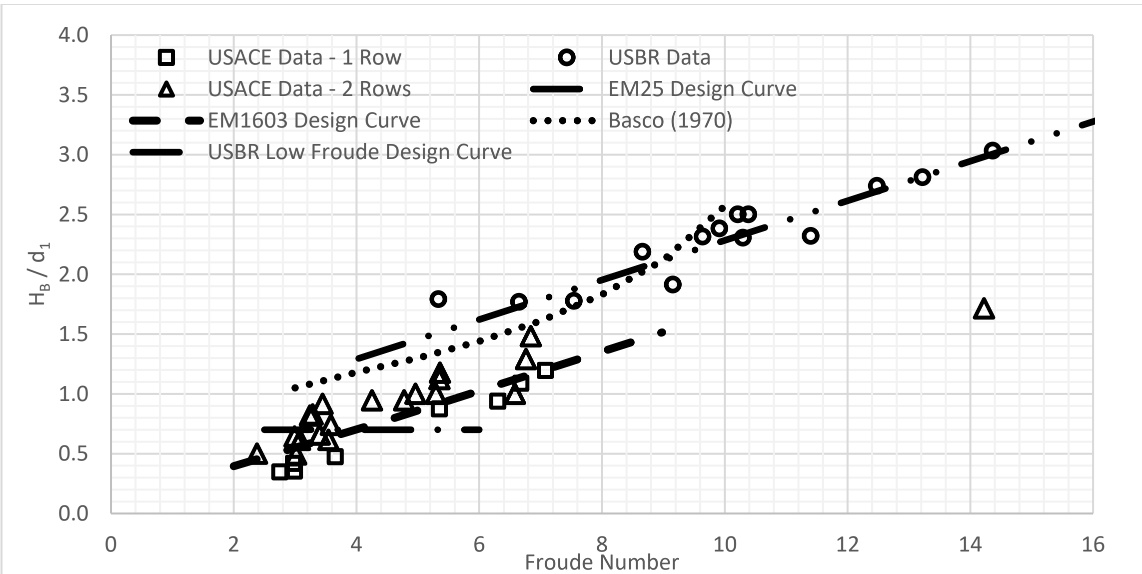

Figure 89. H_B / d_1 as a function of Fr_1

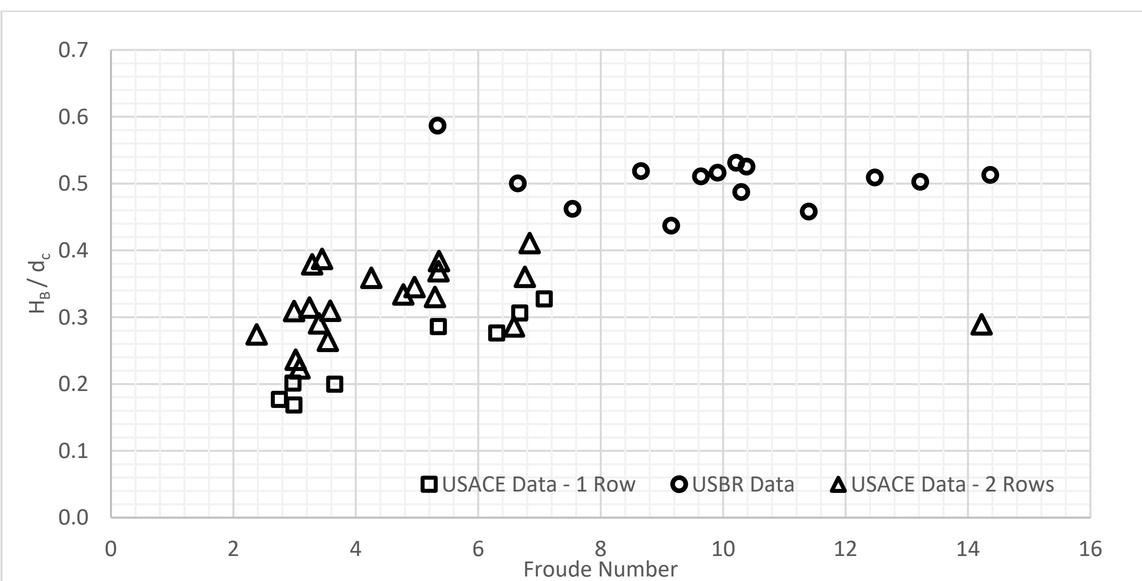

Figure 90. H_B / d_c as a function of Fr_1

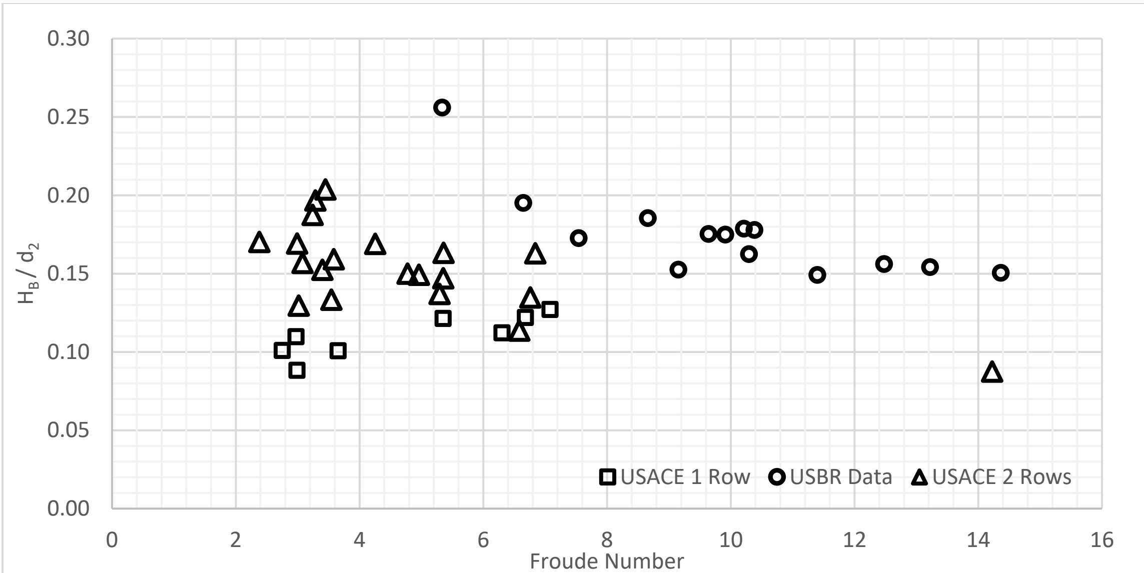

Figure 91. H_B / d_2 as a function of Fr_1

As with the baffle location, it can be seen there are two distinct trends between the USACE and the USBR standard basins in relationship to baffle block height, with the USACE data having the baffle block height significantly smaller when normalized to the d_c. When the data is normalized to the d_2 there is more of a constant relationship of block height, roughly ranging from $0.1 < \frac{H_B}{d_2} < 0.2$.

4.2.5 End Sill Height

The end sill height normalized to the d_1 as a function of Fr_1 is illustrated in Figure 92.

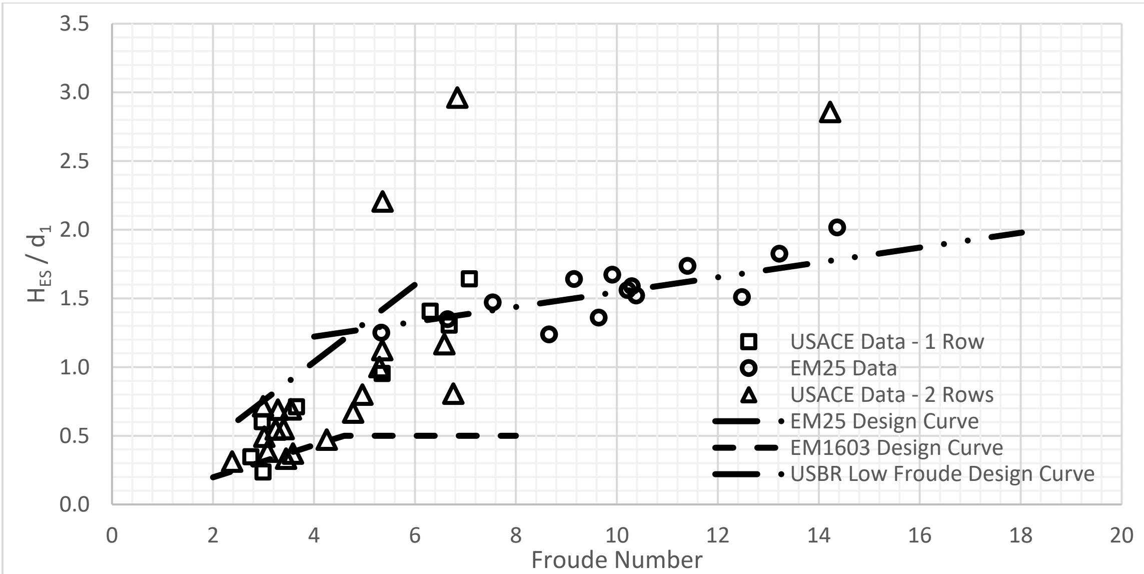

Figure 92. H_{ES} / d_1 as a function of Fr_1

The H_{ES} is normalized to the d_c in Figure 93 and d_2 in Figure 94.

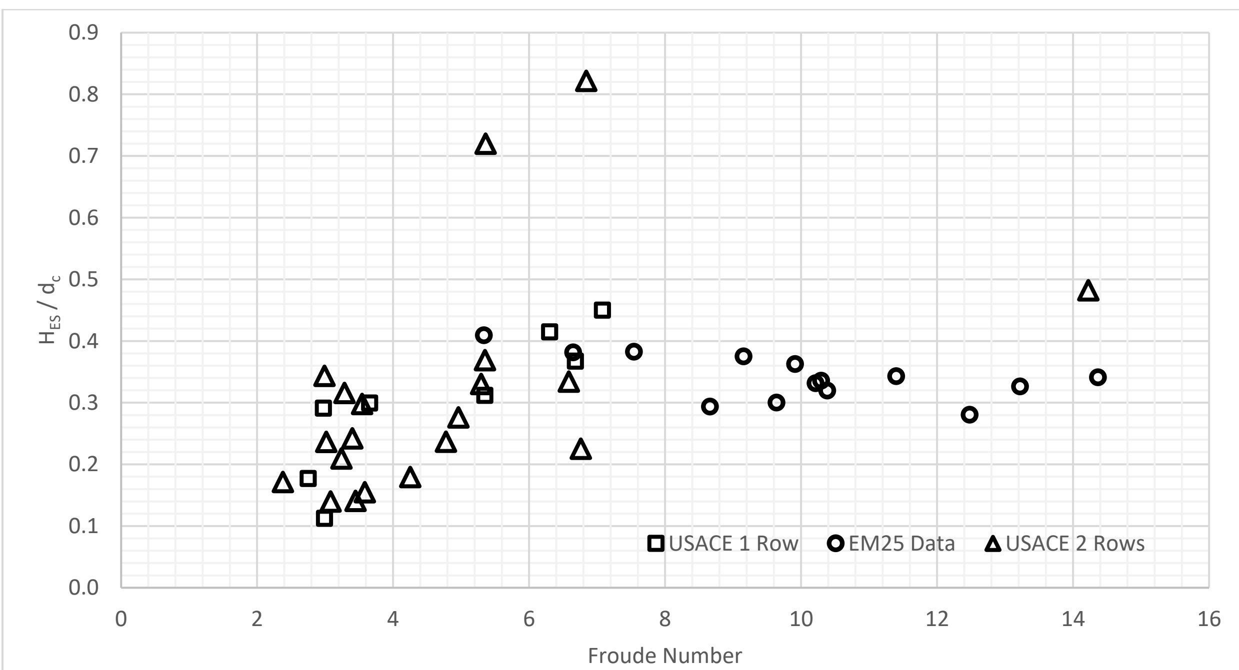

Figure 93. H_{ES} / d_c as a function of Fr_1

There is a relatively constant relationship to the end sill heights as a function of the Fr_1 for the USBR (1955) data and an increasing trend for the USACE (1969) data.

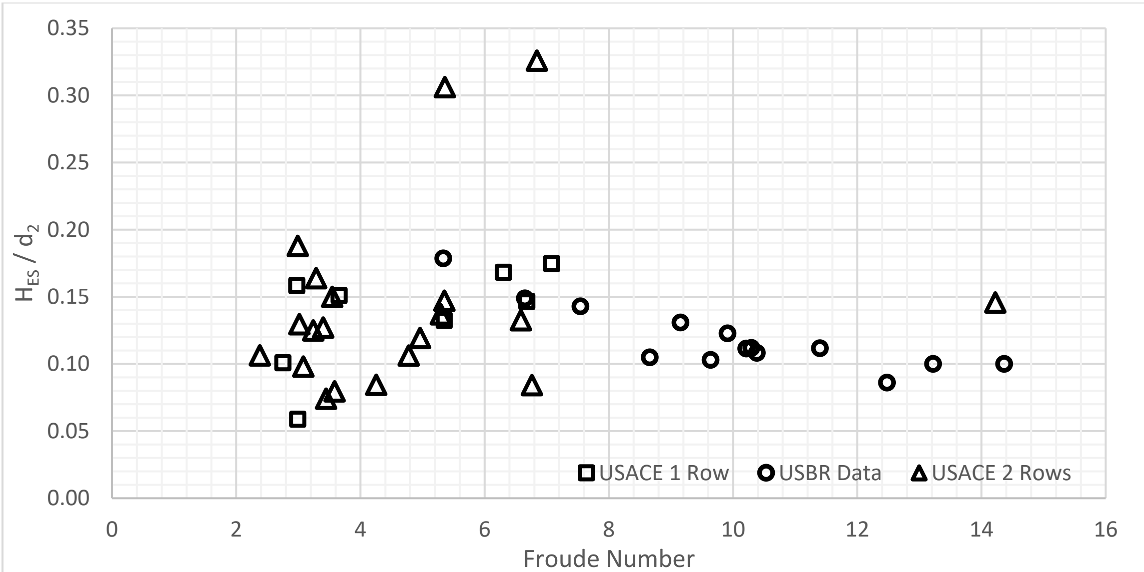

Figure 94. H_{ES} / d_2 as a function of Fr_1

There is a wide variation in end sill height, with increasing trends for the USACE (1969) data and decreasing trends with the USBR (1955) data with increasing Fr_1 when normalized to the d_2.

4.3 Required Tailwater

The design tailwater from various investigations of baffled stilling varies between complete loss of hydraulic jump action (USACE 1939) to full conjugate depth (USBR, 1984). The SAF and USACE stilling basin design guidance emphasizes a design tailwater ratio of 85 precent.

If the efficiency of energy dissipation is evaluated from a fundamental perspective, the depth average flow velocity and flow depth entering/exiting the basin can be used to estimate it's value, as demonstrated by USBR (1984). The impact of reduced tailwater on energy dissipation can be visualized by comparing a scenario with full sequent depth verse 85 percent of its value, as shown in Figure 95.

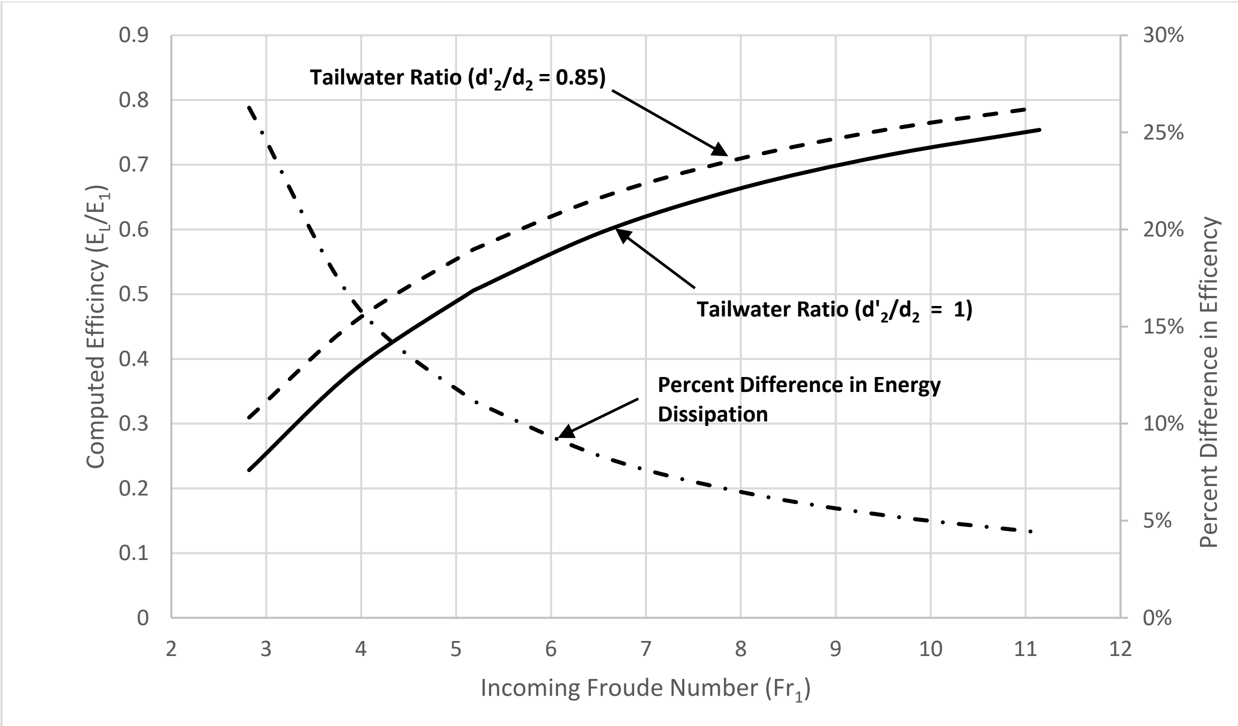

Figure 95. Efficiency of Energy Dissipation of Hydraulic Jump with Reduced Tailwater

As the momentum is transferred to the chute, baffle blocks, and end sill; the required tailwater is reduced, thereby increasing the energy loss within the hydraulic jump. As the Fr_1 increases, the relative increase in energy dissipation from reduced tailwater decreases. Also noteworthy is the observation from numerous model studies that the location of behavior of the high velocity jet exiting the stilling basin has significant impacts on the potential downstream scour and erosion, as well as downstream wave propagation.

The data from USACE (1969) and the USBR (1955) related to the required tailwater to maintain the hydraulic jump is illustrated in Figure 96.

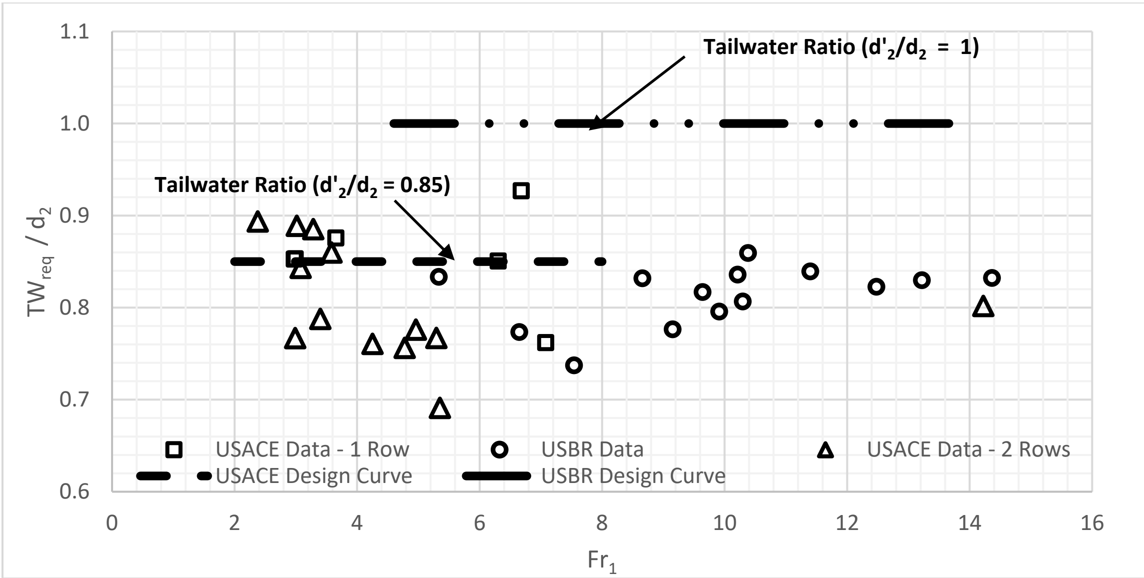

Figure 96. TW_{req} / d_2 as a function of Fr_1

There is a large amount of scatter associated with the estimate of the required tailwater to maintain the hydraulic jump action. The exact source of the variation is likely associated with various factors; but the variation does suggest that the estimate of the required tailwater to maintain the jump action is subjective, especially at lower Fr_1 where the jump action is less defined.

Considering the relationship found between the basin dimensions and the use of critical depth as the scaling parameter instead of d_1 or d_2; the required tailwater to maintain the hydraulic jump action (TW_{req}) from USACE (1969) and the USBR (1955) is plotted normalized to d_1 and d_c as shown in Figure 97 and Figure 98, respectively.

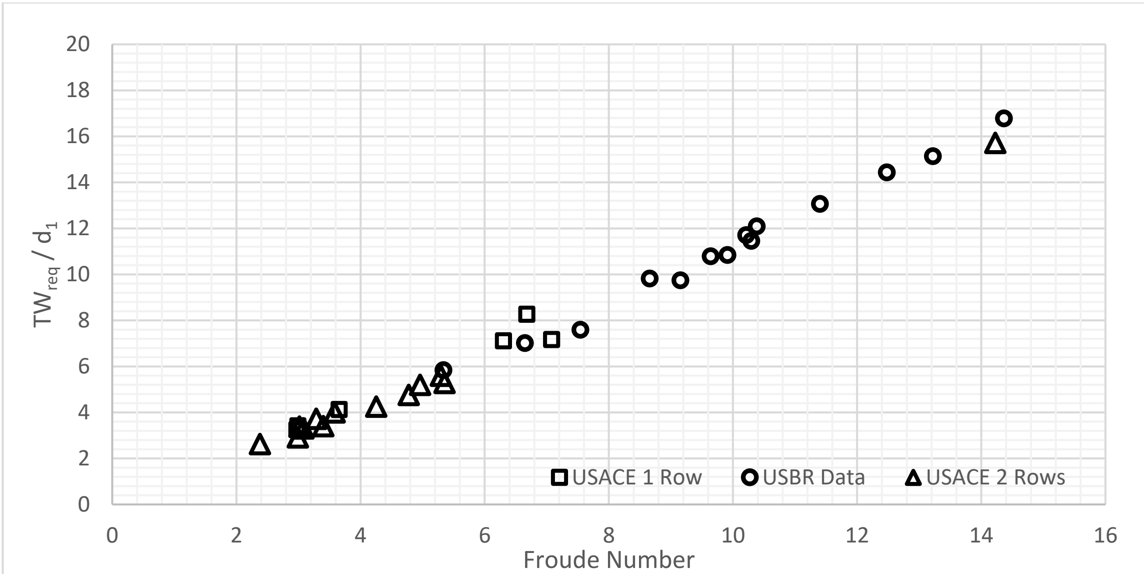

Figure 97. TW_{req} / d_1 as a function of Fr_1

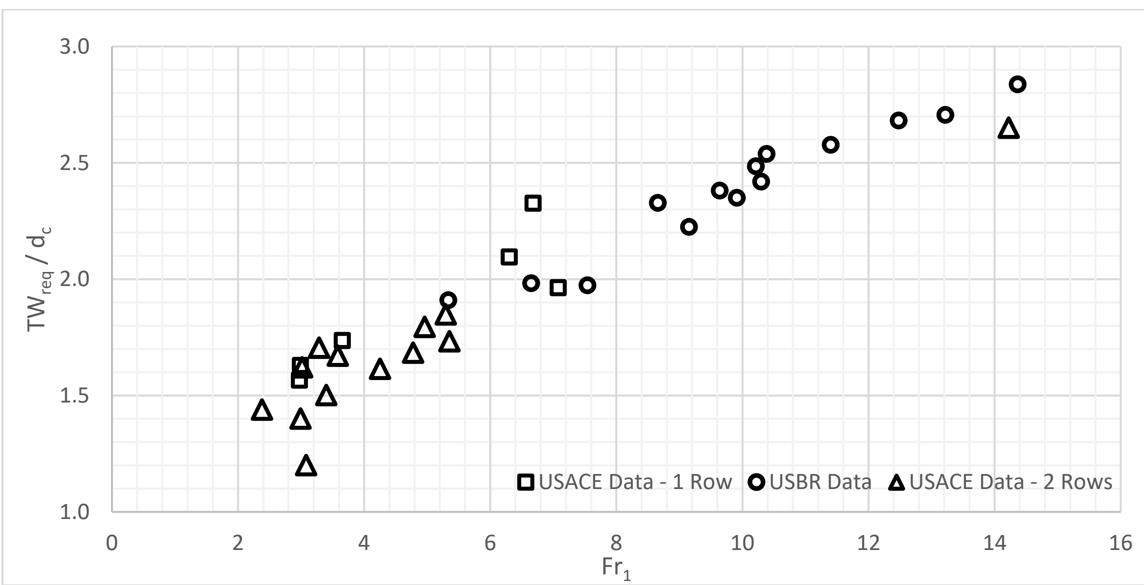

Figure 98. TW_{req} / d_c as a function of Fr_1

This illustrates that d_1 and d_c have less variation and are potentially a better scale parameter for the determination of required tailwater than the sequent depth for the standard stilling basin configurations.

Guidance provided by Blaisdell (1948) was modified by USDA (1959) for the SAF stilling basin uses a power function to describe the relationship of the Kinetic Flow number to the $\frac{TW_{req}}{d_1}$ ratio. A similar approach was taken for the current research whereas both a power and slope intercept relationship was taken to describe the required tailwater as a substantial envelop curve. It was found that a slope intercept relationship normalizing to the d_1 was most appropriate. The expression is shown in Equation 36.

Equation 36. Unified Equation for Required Tailwater Depth

$$\frac{TW_{req}}{d_1} = 1.8Fr_1 - 0.2$$

This expression is compared to the data and the standard guidance when normalizing to d_1 in Figure 99.

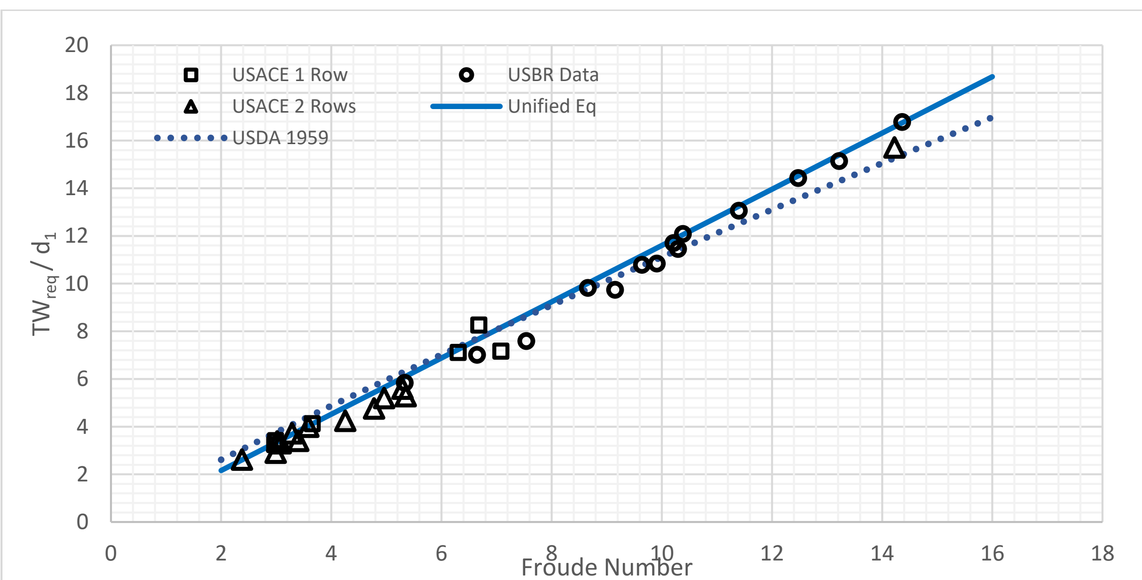

Figure 99. Comparison of Existing Data/Guidance and Unified Equation for $\frac{d'_2}{d_1}$

The Equation 36 is also compared to the data and guidance when normalized to d_2 by the use of Equation 1, and shown in Figure 100.

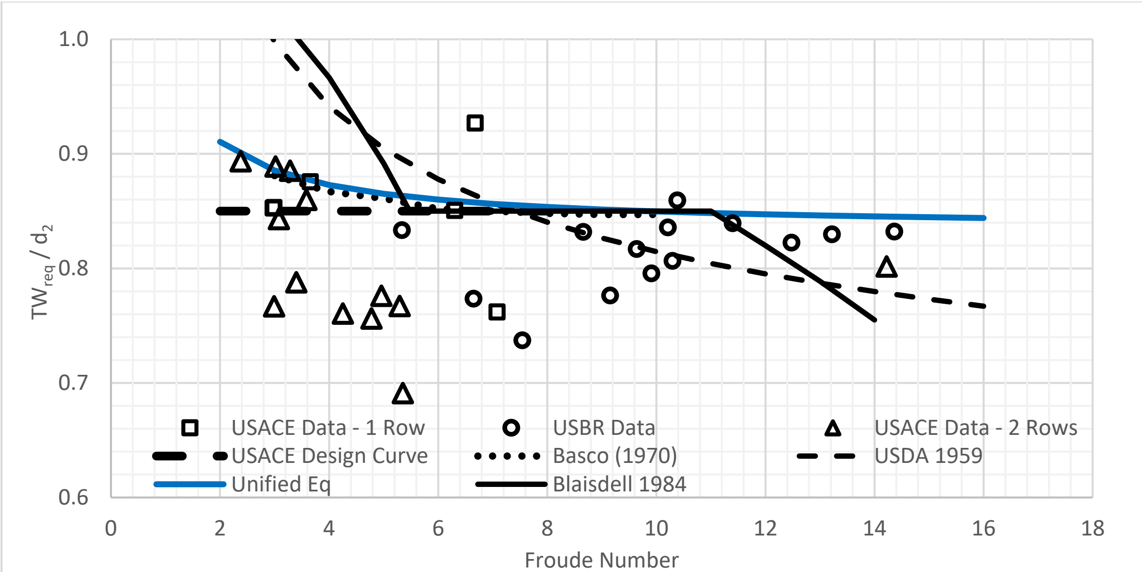

Figure 100. Comparison of Existing Data/Guidance and Unified Equation for $\frac{d'_2}{d_2}$

It can be seen that Equation 36 provides a better envelope of the empirical data and more closely matches the optimum tailwater estimated by Basco (1970).

4.4 Chute Slope

The influence of the stilling basin chute angle was evaluated by plotting the major dimensionless basin parameters versus the incoming chute angle as shown in Figure 101.

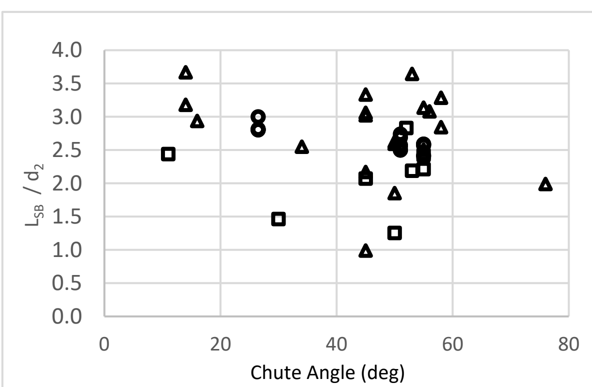

a) Length of Stilling Basin

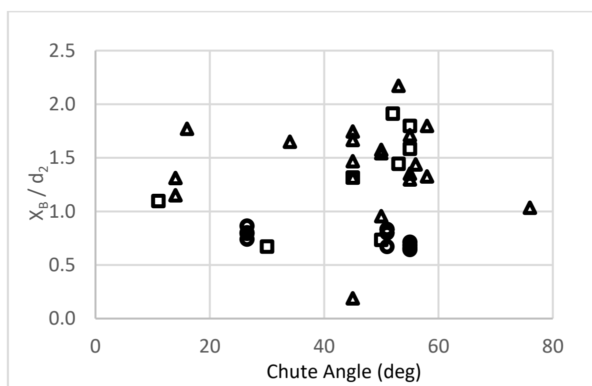

b) Distance to Baffle Blocks

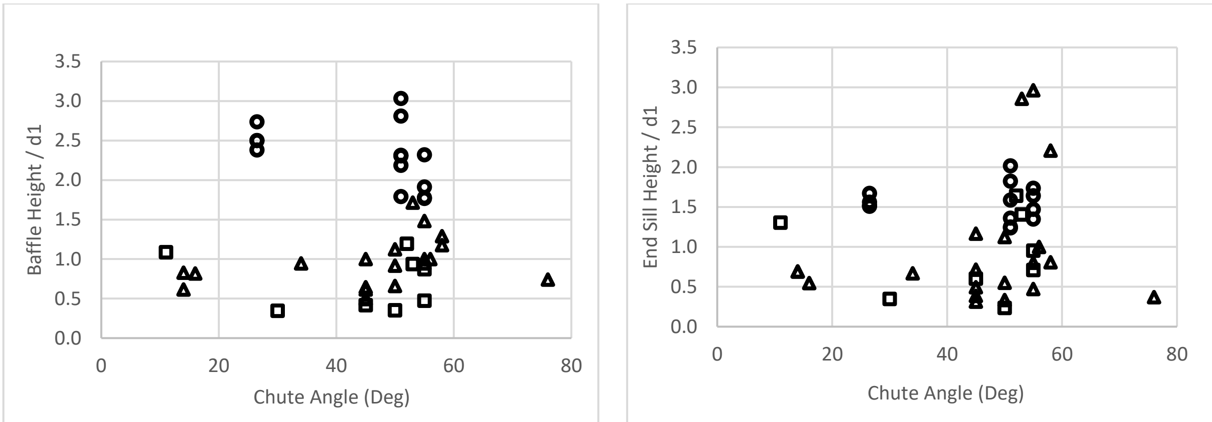

c) Baffle Height *d) End sill Height*

USACE Data - 1 Row USACE Data - 2 Rows USBR Data

Figure 101. Stilling Basin Parameters by Chute Slope (Adapted from USACE 1969 and USBR 1955)

There is not an apparent trend associated with the chute angle, although it is noteworthy that the majority of the steep chute stilling basins included a toe curve which may reduce the benefit of the momentum direction with the horizontal and the associated turbulence production and momentum transfer.

4.5 Mobile Bed Scour

4.5.1 SAF Basin

The effects of varied tailwater on downstream scour potential for a Fr_1 of 5.4 were evaluated by Blaisdell (1948). The experiments evaluate the scour characteristics and average boil heights for various ratio of actual tailwater to sequent depth. It is worth noting that no scour is observed for increased tailwater above that of sequent depth. There is also minimal scour related to a decrease in the tailwater ratio above 0.85. It is noted that for the initial loss of hydraulic jump action at relative tailwater ratio of 0.69; that there was no increase in the scour observed immediately downstream of the end sill; however, the total volume of material downstream “increased significantly”. An illustration of the centerline profile and flow conditions is shown in Figure 102 and summary of results shown in Table 8.

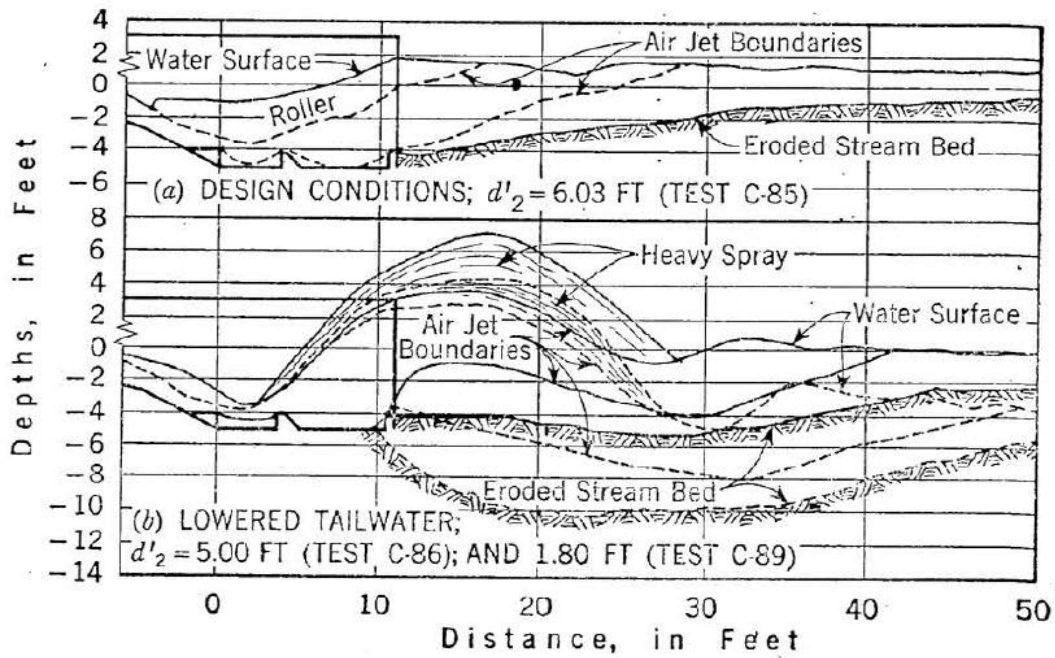

Figure 102. Proportions of the SAF Stilling Basin (Source: Blaisdell, 1948)

Table 8. SAF Stilling Basin influence of various tailwater conditions (Source: Blaisdell, 1948)

Test No.	Flow, Q (ft³/sec)	d'_2 (ft)	$\frac{d'_2}{d_2}$	Scour[a]	z_a (ft)	$\frac{z_a}{d_2}$
C92..........	277	11.49	1.60	−4.0	1.8	0.11
C91..........	274	9.56	1.33	−4.0	0.8	0.11
C90..........	277	8.54	1.19	−4.0	1.1	0.15
C83..........	286	7.71	1.07	−4.0	1.2	0.17
C84..........	280	7.08	0.98	−4.0	1.0	0.14
C85..........	272	6.03	0.84	−4.1	0.8	0.11
C86..........	280	5.00	0.69	−5.0	7.0[b]	0.97
C87..........	280	3.80	0.53	−7.0	7.1[b]	0.99
C88..........	277	2.77	0.38	−8.5	7.4[b]	1.03
C89..........	275	1.80	0.25	−10.1	7.9[b]	1.10
C98..........	284	−0.40	−0.06	−13.0	10.5[b]	1.46

[a] Elevation of maximum depth of scour, in feet, on the channel center line near the end of the stilling basin.
[b] Surface roller on hydraulic jump washed out of stilling basin.

If the scour depth is made dimensionless by the ratio of the sequent depth ($S_{end\ sill}/d_2$) there is a nearly linear relationship obtained with a coefficient of determination of 0.99. This relationship is shown in Figure 103. Although not described in Blaisdell (1948), it is assumed that the negative value of d'_2 is the result of tailwater below the stilling basin.

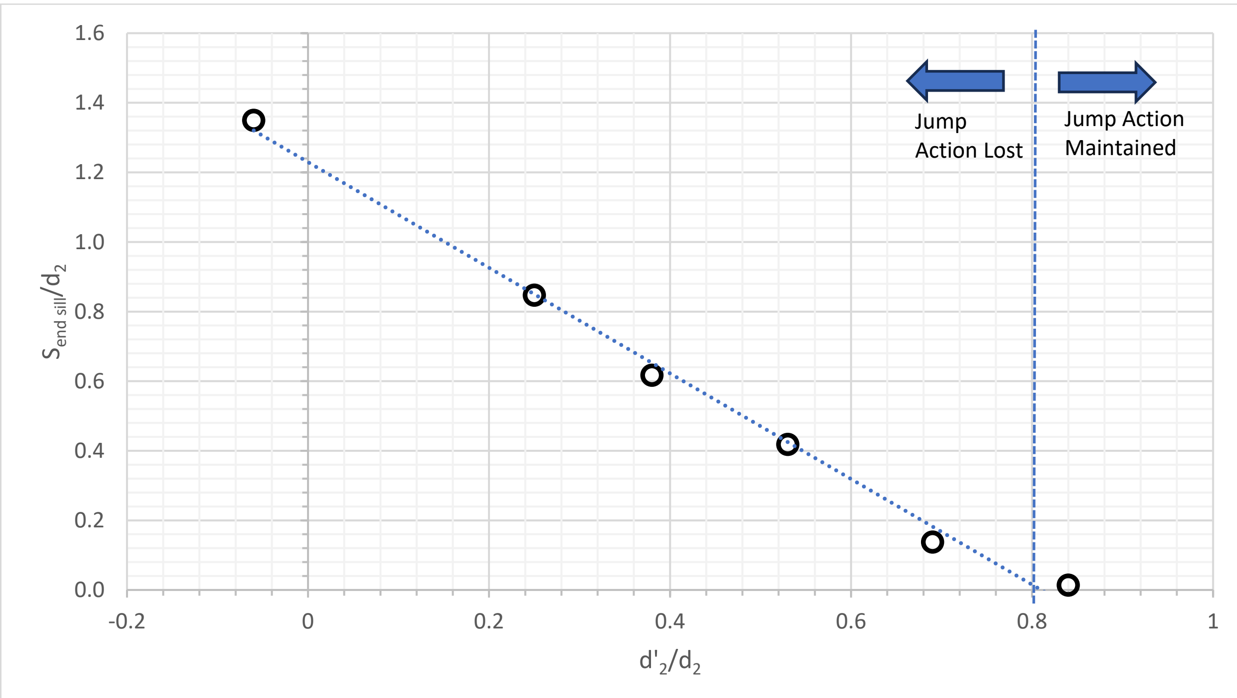

Figure 103. Evaluation of observed scour with decreasing tailwater below that required for hydraulic jump action (Adapted from Blaisdell, 1948)

4.5.2 Keystone (USACE 1960)

The stilling basin for the Keystone Dam was evaluated using a 1:36 scale mobile bed model (USACE, 1960). 12 configurations were evaluated primarily based on the downstream scour of the basin. All plans were evaluated at a design discharge of approximately 1,070-$\frac{\mathrm{ft}^2}{\mathrm{s}}$, incoming Froude No. of 4.3, and a TW/D_2 ratio of 0.87. All plans utilized two rows of standard baffle blocks with a solid vertical end sill. The primary configuration variables evaluated, and their common dimensionless parameters are summarized in Table 9.

Table 9. Keystone Dam Model Evaluation Plans (Source: USACE, 1960)

Plan	Baffle Height (H_B)	Blockout Ratio (A_b)	End Sill Height (H_s)	Basin Length (L_b)	Dist. To 1st Row Baffles (L_1)	$\frac{H_B}{D_1}$	$\frac{L_b}{D_2}$	$\frac{H_s}{D_2}$
1	8	0.50	10	174	76	0.63	2.45	0.14
2	8	0.50	10	174	96	0.63	2.45	0.14
3	8	0.50	10	174	116	0.63	2.45	0.14
4	8	0.50	14	174	96	0.63	2.45	0.20
5	8	0.50	6	174	96	0.63	2.45	0.08
6	8	0.42	6	174	96	0.63	2.45	0.08
7	10	0.42	6	174	96	0.79	2.45	0.08
8	10	0.42	10	174	96	0.79	2.45	0.14
9	10	0.42	10	213	96	0.79	3.00	0.14
10	10	0.42	10	213	135	0.79	3.00	0.14
11	12	0.42	10	174	96	0.94	2.45	0.14
12	12	0.42	6	174	96	0.94	2.45	0.08
USACE EM 1110-2-1603	11.8	N/A	5.9	158	106.5	0.93	2.23	0.08

Observations of velocity at the first row of baffles and end sill, as well as the downstream equilibrium scour utilizing a coarse sand bed material were made. The cross-stream location of the profile is not described. A typical profile is provided in Figure 104.

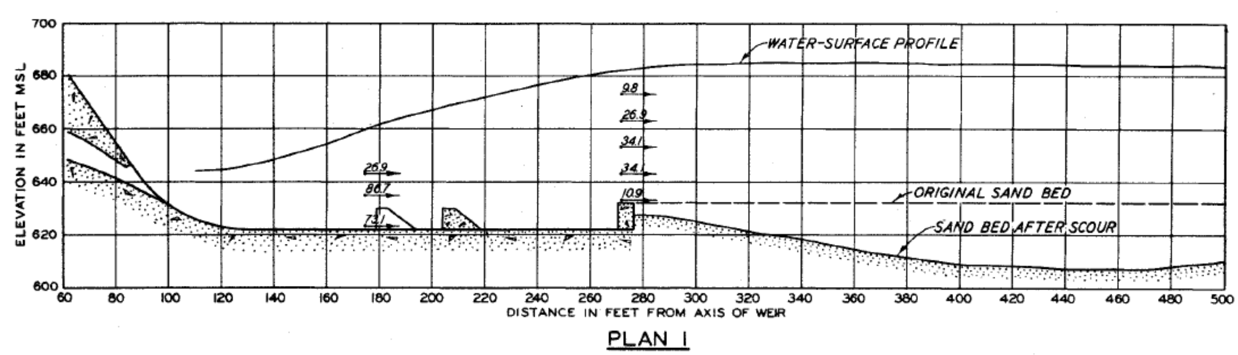

Figure 104. Keystone Dam Model Study Typical Profile (Source: USACE, 1960)

The characteristics of each scour profile were extracted, including the depth at the end sill, the maximum depth, and the characteristic scour out slope angle from the horizontal. These are provided with dimensionless parameters in Table 10.

Table 10. Keystone Dam Model (1960) Evaluation Scour Characteristics

Plan	$\frac{H_B}{D_1}$	$\frac{L_b}{D_2}$	$\frac{H_s}{D_2}$	V_{baffle} [a] (ft/s)	$V_{end\ sill}$ [b] (ft/s)	$\frac{S_{end\ sill}}{D_2}$ [c]	$\frac{S_{max}}{D_2}$ [d]	$\frac{L_{scour\ max}}{D_2}$ [e]	θ_{scour} [f]
1	0.63	2.45	0.14	86.7	10.9	0.07	0.21	2.3	10
2	0.63	2.45	0.14	62.9	6.8	0.08	0.18	2.0	8
3	0.63	2.45	0.14	62.9	16.6	0.04	0.24	2.3	8
4	0.63	2.45	0.20	51.3	26.9	0.08	Scour to rigid bed [g]		
5	0.63	2.45	0.08	77.6	22.2	0.11	0.24	2.2	8
6	0.63	2.45	0.08	64.7	30.7	0.11	0.21	2.3	9
7	0.79	2.45	0.08	74.7	22.2	0.00	0.11	1.7	7
8	0.79	2.45	0.14	76.1	8.5	0.00	0.06	1.7	10
9	0.79	3.00	0.14	68.2	3.8	0.06	0.10	1.6	11
10	0.79	3.00	0.14	62.8	8.5	0.03	0.18	2.7	7
11	0.94	2.45	0.14	77.6	11.9	0.03	0.06	1.5	6
12	0.94	2.45	0.08	71.5	15.6	0.03	0.10	1.6	6

[a] *velocity immediately upstream of baffle*
[b] *velocity immediately above end sill*
[c] *scour depth immediate downstream of end sill*
[d] *maximum scour observed*
[e] *distance from the end sill to the maximum observed scour*
[f] *characteristic scour exit slope angle*
[g] *bed scour exceeded the material depth; thereby providing error in scour prediction*

4.6 Bluestone Dam Stilling Basin Evaluation

4.6.1 Overview

Bluestone Dam has undergone five phases of upgrades associated with intolerable risk associated with overtopping and dam instability. These modifications include stabilization of the gravity dam monoliths, construction of an new auxiliary spillway, and significant modification to the existing principle spillway.

Bluestone is a concrete gravity dam located along the New River in southern West Virginia and has a drainage area of approximately 4,600 square miles. The dam has an approximate length of 2,000-feet and a structural height of 165-feet. The dam has three discharge structures: sixteen (16) 5.6 feet wide x 10 feet high sluices controlled by vertical lift gates; twenty-one (21) ogee crest spillway bays controlled with wheeled vertical lift gates; and six (6) penstock outlets that have been converted into auxiliary spillway structure controlled by fusible emergency gates (Moses and Koutsunis, 2018). The ogee crest spillway and the sluice outlets both discharge into a two-stage baffled hydraulic jump stilling basin. The general dam configuration is shown in Figure 105.

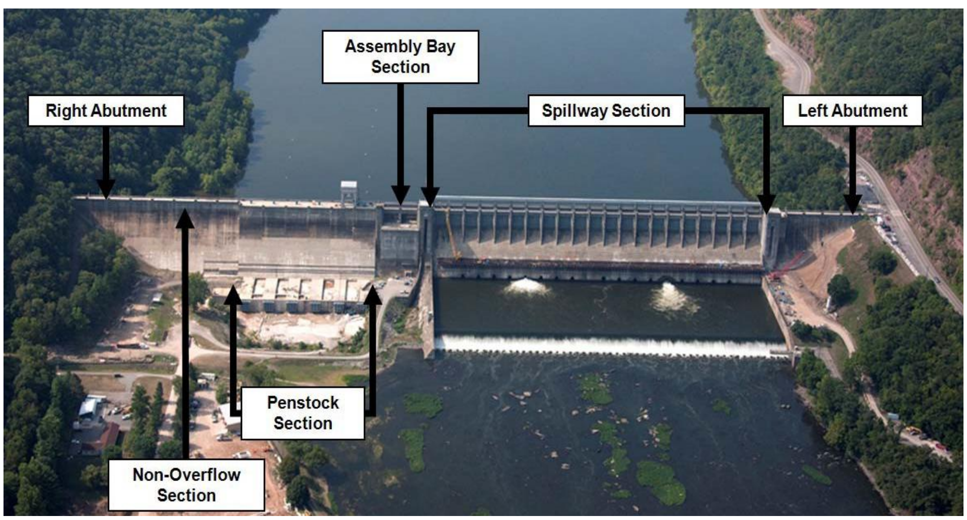

Figure 105. Bluestone Dam General Overview Aerial (Source: Moses and Koutsunis, 2018)

The primary spillway stilling basin is 798 feet wide and currently includes, upstream to downstream, a 50 feet long baffled apron, 182 feet of exposed rock, a 23 feet high ogee stilling weir and a second 50 feet long baffled apron as illustrated in Figure 106.

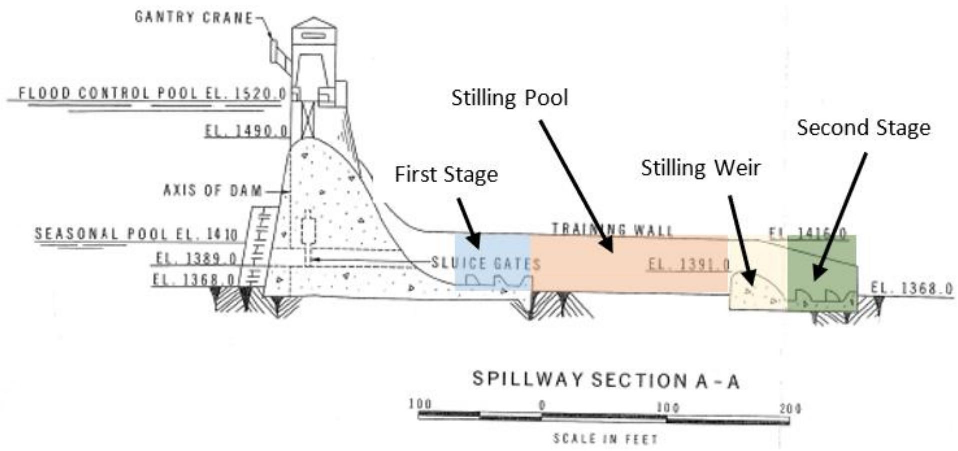

Figure 106 – Original Bluestone Dam Stilling Basin (Adapted from USACE, 1947)

The original IDF for Bluestone Dam was developed in the 1940's by transposing the largest regional storm available at the time. The resulting IDF had a peak inflow of 430,000 $\frac{\mathrm{ft}^2}{\mathrm{s}}$ In and a peak reservoir stage of 1,523 feet. The original baffled hydraulic jump stilling basin configurations were optimized through a 1:36 Froude scale mobile bed sectional model for discharges up to the original IDF.

Multiple configurations of both the first and second stage basins were incrementally evaluated with various baffle heights, baffle widths, one and two rows of baffles, baffle distance from toe, and end sill height. The recommendations of the optimization effort resulted in the following parameters: identical basin lengths of 50 feet, similar baffle heights (6.5 feet for the first stage and 6.0 feet for the second stage), and drastically different sill heights (7 feet for the first stage and 3.5 feet for the second stage).

The Fr_1 number to the primary stilling basin at the original design discharge of 430,000 $\frac{\mathrm{ft}^3}{\mathrm{s}}$ is 6.6 and the estimated required tailwater is 85 percent of the computed conjugate depth (USACE, 1969). It is worth noting that the second stage basin was configured to experience a loss of hydraulic jump action at approximately 50-percent of the original design discharge. The second stage stilling basin was configured to minimize downstream scour potential experienced during the full original design flood without the hydraulic jump occurring on the stilling basin apron.

An update to the Probable Maximum Precipitation (PMP) was performed in 1982 and the estimate of the PMF increased to approximately 1,100,000 $\frac{\mathrm{ft}^3}{\mathrm{s}}$. The PMF was re-evaluated again in 2015, resulting in a peak inflow of PMF of approximately 1,500,000 $\frac{\mathrm{ft}^3}{\mathrm{s}}$ (Moses and Koutsunis, 2019). This was more than three times the original design inflow and resulted in significant overtopping of the dam.

Evaluation of the increased spillway discharge was evaluated and resulted in loss of the hydraulic jump action within the primary spillway, creating a shooting jet that impinges immediately upstream of the stilling weir (USACE, 2003). Severe scour was estimated to occur due to the impinging jet (George and Annandale, 2010) as shown in Figure 107. The associated scour was determined to present intolerable risks associated with overflow dam section sliding/overturning stability.

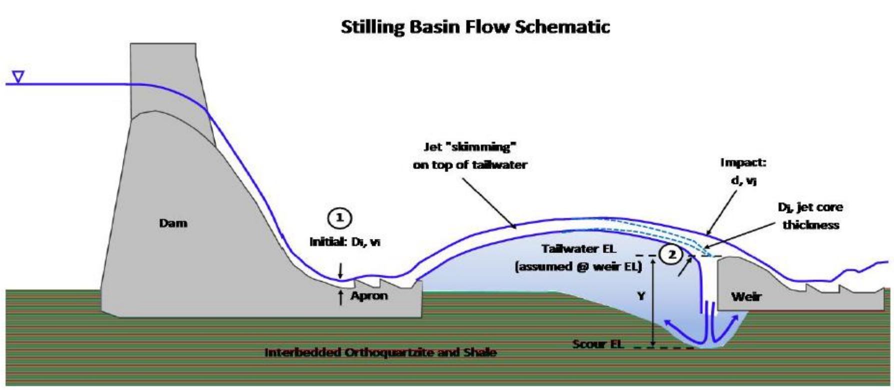

Figure 107.Shooting Jet and Associated Impingement Related Scour (Source: George and Annandale, 2010)

Even within the additional downstream scour, the dam sections themselves were determined to be unstable when loaded to the updated IDF and required significant stabilization with the utilization of pre-stressed ground anchors.

4.6.2 Hydraulic Jump Action

The original design of the two-stage hydraulic jump stilling basin was based on extensive physical modeling (USACE, 1937; USACE, 1946). The two-stage configuration was determined to be the most economical alternative to minimize excavation depths at the toe of the dam. The second stage stilling basin was also configured to provide the required tailwater for more frequent events; but not for the original design discharge. For the events approaching the original design flood, it was found that the baffle and end sill could be configured such that there were tolerable scour tendencies downstream.

Two physical models were developed by the USACE Engineering Research and Development Center (ERDC) Coastal and Hydraulics Laboratory (CHL) for evaluation of the recent modification of the spillway and stilling basin. These consisted of a 1:65 Froude scale comprehensive physical model of the approach, structure, and tailrace; and a three bay 1:36 Froude scale sectional model of the approach, spillway, stilling basin and tailrace. The 1:36 scale model included a movable bed downstream of the 2nd stage end sill to evaluate scour. The comprehensive (a) and sectional model (b) are shown in Figure 108.


a) 1:65 Scale Comprehensive Model


b) 1:36 Scale Section Model

Figure 108. Bluestone Dam Physical Models

Multiple configurations were evaluated to mitigate the potential failure modes associated with rock scour in the primary and secondary baffled hydraulic jump stilling basins. Ultimately a baffled hydraulic jump basin with tapered blocks with intermittent ramps, similar to the Folsom Dam Auxiliary Spillway was selected as a replacement of the existing first stage basin. The initial dimensions were based on the Folsom/USBR Type III baffle height and width (USBR, 1955; USBR, 2009).

The hydraulic action could be more described as an "overly forced" jump. The action was similar to the characteristics of an impact basin, although the jet is attached and relatively stable, the action produces a significant reverse roller, and secondary jump within the first stage basin, as shown in Figure 109.

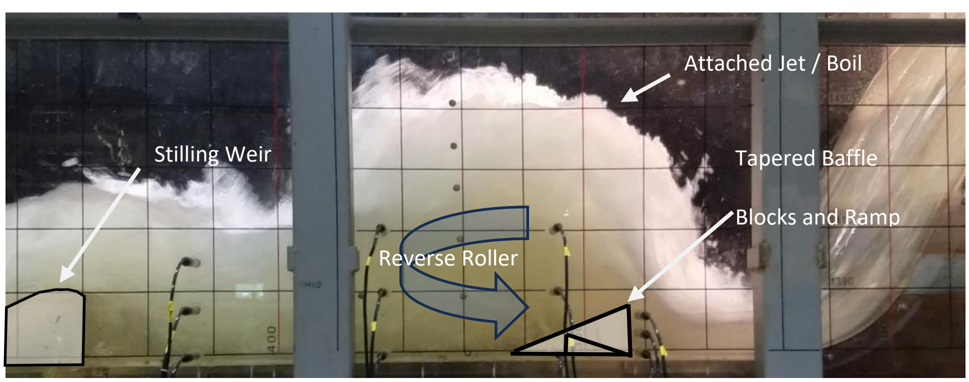

Figure 109. Overly Forced Hydraulic Jump

This configuration exhibited an ability to maintain an overly forced hydraulic jump action within the first stage for a $\frac{d'_2}{d_2}$ of approximately 0.8.

The initial configuration of block height, width, and spacing was developed based on the USBR (1984) Type IIII. It was found that this configuration produced an unstable and surging hydraulic jump, whereas a significant boil would develop and transition into a detached shooting jet. Through multiple iterations of block height, width, and spacing; it was determined that a slenderer baffle block with an increased blockage ratio produced the most stable overly forced hydraulic jump with no detachment and development of a shooting jet. The initial and final baffle block dimensions are shown in Table 11.

Table 11. Initial and Optimized Baffle Block Geometry

Parameter/ Configuration	Initial	Optimized
Baffle Height (H_B)	17	16.5
Baffle Width (W_B)	13	11
Baffle Space (W_S)	12.4	8
Baffle Blockage Ratio (R_B)	0.49	0.58
Baffle Slenderness Ratio (R_s)	1.31	1.5

There were differences in the behavior of the exiting flow conditions between the sectional model and the general model worth noting. First is the impact of the additional effective tailwater created by the interaction of the flows exiting the stilling basin and the adjacent flows. This interaction results in asymmetrical location of the jump with increasing sweep towards the middle of the basin, as shown in Figure 110. Under specific flow conditions the angle of the toe location on the right descending side of the basin would move towards and away from the basin at a relatively constant period, in association with interactions with the flow exiting the adjacent Penstock Stilling Basin.

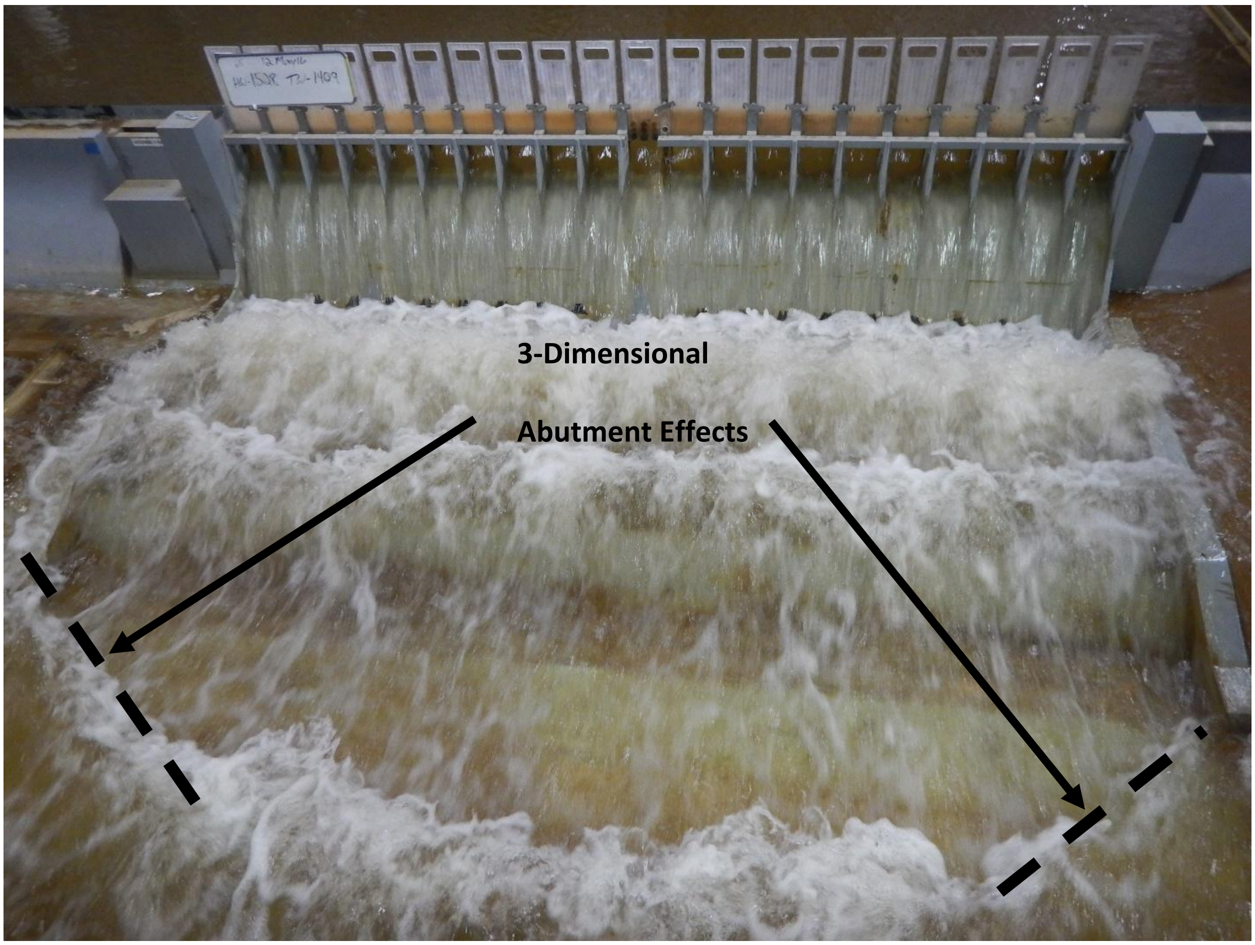

Figure 110. Bluestone Dam General Model Asymmetric Jump Location

The second observation is that the loss of the hydraulic jump moves rapidly downstream for a rigid bed experiment, as opposed to the rapid adjustment of the bed materials to obtain the equivalent depth required to produce the jump action immediately downstream of the end sill for that of the mobile bed experiments in the section model. This can be seen by the significant difference in distance before the secondary jump between the mobile bed section model (Figure 108 (b)) and the rigid bed comprehensive model (Figure 110).

4.6.3 Hydrodynamic Forces

An extensive instrumentation effort was undertaken to better understand and refine the hydraulic loading on structural elements association with modification of the first and second stage stilling basins. This included evaluation of loads on various features with both submersible high precision pressure transducers and standard pressure taps and manometer board readings.

The experiments were conducted primarily within the 1:36 sectional model; with loading conditions of a permanent center divider wall were conducted in the 1:65 Froude scale comprehensive model. Preliminary estimates of the forces acting on the blocks were provided by the use of Equation 19 (USBR, 1987); and were very substantial. Based on theoretical rationing it was determined that the factor of 2 in Equation 19 may be excessive; so instead it was proposed that a value equal to full stagnation pressure plus the vapor pressure would be utilized as having more physical basis of the hydrodynamic loading for design purposes, as expressed in Equation 37 (Moses, 2016).

Equation 37. Physically Based Maximum Baffle Block Load

$$F_B = \gamma A_B(h_{v1} + P_v)$$

Given the current state of stability of the dam and stilling basin features and the novelty of the block and ramp configuration; the block and ramp loads were a primary focus of the investigation. A special manifold system was developed and constructed with additive manufacturing to accommodate pressure readings at very close proximity; that would not otherwise be possible with pressure transducers or pressure taps. The ports on the end of the manifold were configured to be used with both pressure transducers and pressure taps. The baffle block manifold is shown in Figure 111 with the location within the section model illustrated in Figure 112.

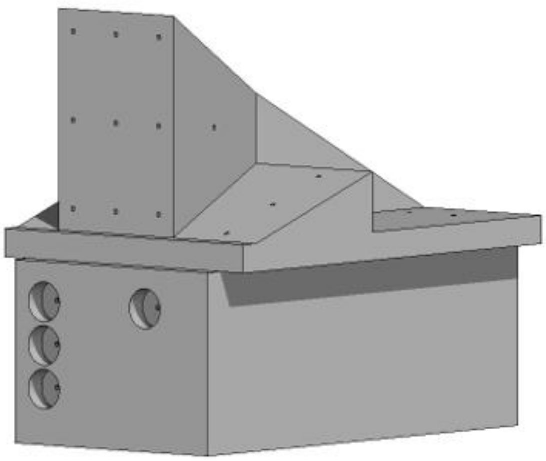

a) Solid view

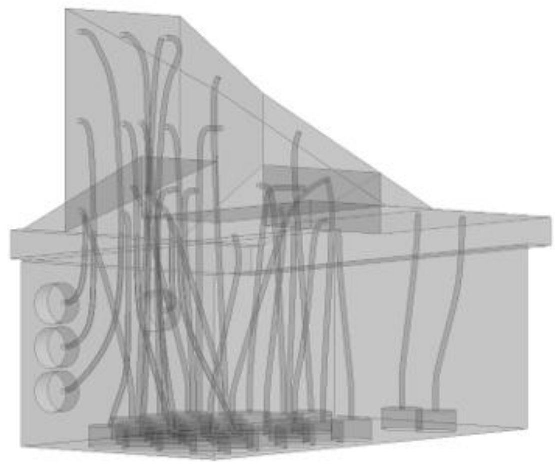

b) Transparent view

Figure 111. Isometric views of Baffle Manifold System (USACE, 2018)

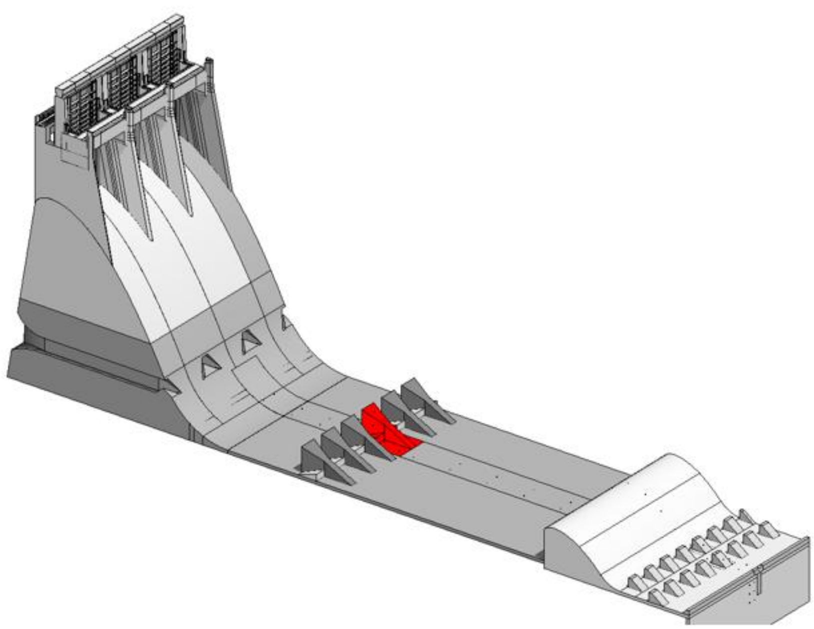

Figure 112. Location of Instrumented Baffle Block within Sectional Model (USACE, 2018)

The fabricated baffle is shown in Figure 113.

a) After Fabrication

b) Pressure Tap Configuration

Figure 113. Fabricated Baffle and Manifold (photos by author)

The experiments were conducted with both pressure transducers and pressure taps, allowing for direct comparison. In general, there was good agreement, although several locations recorded variation of greater than 10-percent, whereas the data from the pressure transducers were determined to be unreliable.

The instantaneous time-synchronized data from each of the valid transducers was then converted into its corresponding vector unit force for each timestep by normalizing to each reading's contributing area in the plane of action of the baffle and ramp elements. The statistical evaluation of the instantaneous computed force vectors is shown in Table 12.

Table 12. Bluestone Dynamic Baffle Forces (Modified from USACE, 2018)

	Headwater (feet)	Stream-wise[1] (feet of water)	Vertical[2] (feet of water)	Cross-Stream[3] (feet of water)
Min	1520	16	-41	-120
	1524	20	-39	-173
	1528	25	-37	-153
	1535	57	-47	-166
5th Percentile	1520	53	-20	-53
	1524	66	-17	-59
	1528	80	-15	-60
	1535	96	-8	-61
50th Percentile	1520	74	-7	-7
	1524	90	-3	-11
	1528	106	1	-8
	1535	123	8	-3
95th Percentile	1520	94	8	41
	1524	113	14	39
	1528	129	19	43
	1535	146	28	55
Max	1520	133	29	34
	1524	145	29	137
	1528	162	29	151
	1535	180	29	163

From Table 12, there is a significant lateral (cross-stream) vector component to the force. This is associated with macro-scale fluctuations occurring in the stilling basin, which results in a fluctuation of force in the cross-stream direction. There was also loading associated with unbalanced flow conditions due to the spillway pier wake. This was observed with the negative

[1]Downstream is Positive
[2] Upward is Positive
[3] Right is Positive

value of the median cross-stream vector and by observing an unbalanced load on the baffle face; whereas the side of the baffle aligned near the center of the spillway bay consistently observed a higher force.

Under the current research effort, the data presented in Table 12 is compared to the computed forces by means of USBR (1987), USACE (1965), USACE (1970), and USACE (2016) in Table 13.

Table 13. Comparison of Estimated and Observed Baffle Block Forces

Pool Elevation (ft)		1520	1524	1528	1535
Q (cfs)		452,000	543,000	644,000	836,000
Q (cs/ft)		566	680	807	1048
Z (ft)		152	156	160	167
H (ft)		30	34	38	45
V_A / V_T		0.95	0.96	0.97	0.98
V_T (ft/s)		94	95	95	96
V_1 (ft/s)		89	91	92	95
D_1 (ft)		6.3	7.5	8.7	11.1
H_{v1} (ft)		123.6	128.1	132.7	138.8
Fr_1		6.2	5.8	5.5	5.0
D_2 (ft)		53	58	64	73
Equation 19 (lbf/ft)		267,676	279,215	291,166	308,590
Equation 37 (lbf/ft)		129,174	133,766	138,466	144,758
Equation 18 (lbf/ft)		76,381	79,137	81,956	85,731
USACE (1970)		36,734	44,578	53,409	69,996
Observed USACE (2018) (lbf/ft)	Median	76,190	92,664	109,138	126,641
	95th Percentile	96,782	116,345	132,818	150,322
	Maximum	136,937	149,292	166,795	185,328

It is demonstrated that Equation 19 (USBR, 1987) significantly over-predicts even the maximum instantaneous baffle forces. This is expected since there is a factor of 2 placed on the total specific energy entering the stilling basin. It is also seen that Equation 18 (USACE, 1965) significantly under-predicts the median for the larger fall heights and unit discharges. The approach prescribed in USAEC (1970), which relates to the baffle force as a function of the pressure force of the sequent depth, also significantly under-predicts the observed forces. Equation 37 (Velocity Head plus Vapor Pressure) estimated values between the 95th percentile and maximum observed values for all flow scenarios.

The significant baffle size and associated force transfer requires significant means to provide internal stability of the block and external stability of the adjacent floor slabs. A robust reinforcement is required to provide internal stability within the block. The use of post-tensioned anchors was required to provide for external stability of the apron floor monolith in which the blocks is connected. In addition, the tapered blocks adopted have fragile edges as the block narrows in the stream-wise direction.

Given the high sensitivity to performance related to the baffle frontal area and the significant woody debris observed at the dam site during flood events, specific experiments were conducted to evaluate the potential for floating woody debris to impact the baffles. Characteristic tree sizes were developed from observed debris accumulations and samples of wood from characteristic trees prepared at the linear scale ratio. When the specimens were saturated, they were observed to impact the upper face of the baffle blocks as shown in Figure 114.

Figure 114. Observed Scaled Characteristic Woody Debris Impact (USACE, 2018)

To minimize the potential to lose frontal area of the block due to chipping associated with floating debris, stainless steel face plates were utilized as shown in Figure 115.

a) Stainless steel face plate *b) Tail reinforcement and post-tensioned anchor recess*

Figure 115. Stainless Steel Face Plate and Reinforcement (Photos by Author)

The wall loads were determined in the same manner, whereas both pressure transducers and pressure taps were utilized to evaluate the forces acting on the side walls. The locations of the observations are shown in Figure 116.

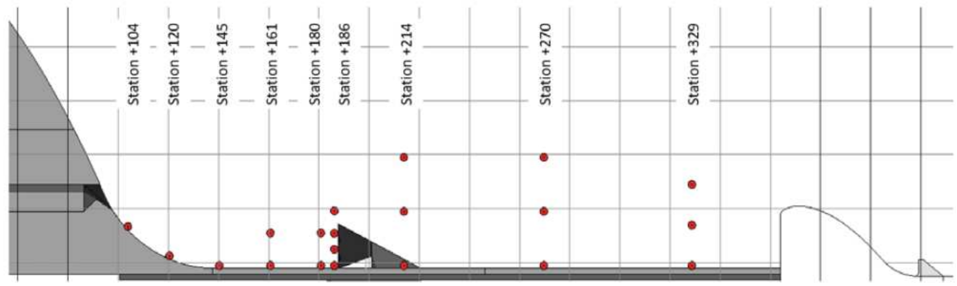

Figure 116. Locations of side wall force observations (USACE, 2018)

For the initial estimate of forces, the high and low surges observed on the sectional flume walls were used as the maximum and minimum average forcesfor the side walls adjacent to the horizontal floor. The forces on the side walls in the vicinity of the toe curve were estimated utilizing bucket pressure design charts (USACE, 1992). A comparison of the initial estimate based on minimum and maximum water surface and that observed with pressure transducers is shown in Figure 117.

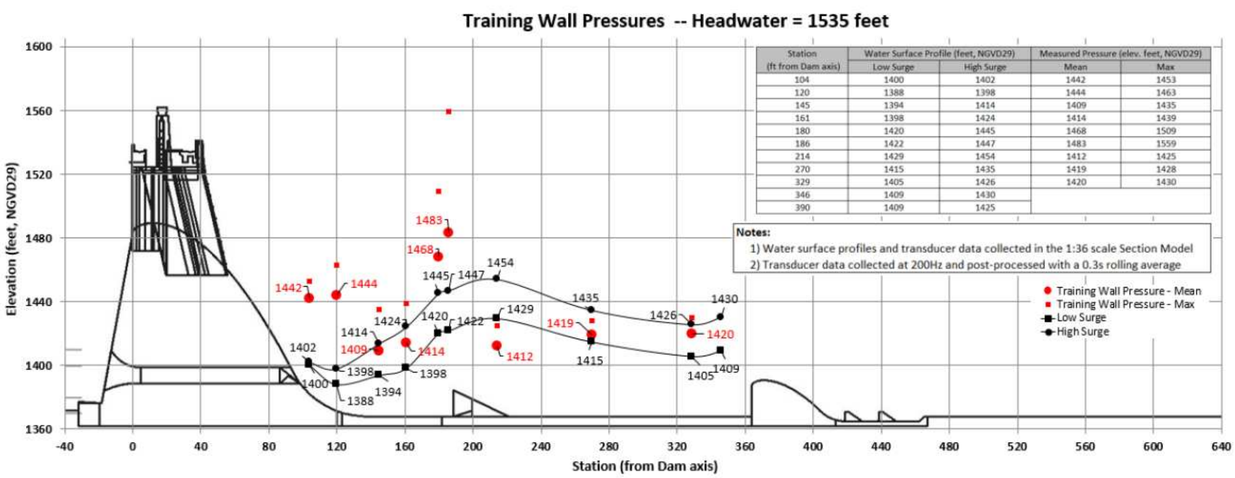

Figure 117. Comparison of pressure transducer observations and water surface profiles (USACE, 2018)

The mean values are significantly higher than the observed water surface profiles in the vicinity of the toe curve and in the area upstream of the baffles. As expected, there is a higher pressure than indicated by the water surface profile immediately adjacent to the toe curve where the centrifugal force occurs as the flow is turned to the horizontal. There was a significant high-pressure zone observed as the stagnation on the baffle face propagates out and impacts the wall. It is also worth noting that the observed mean pressure just downstream of the baffle blocks and near the point of maximum boil height as compared to the water surface profile. This is a location of significant aeration and turbulence as the flow separated off the leading edge of the baffles, which may have contributed to the readings.

4.6.4 Stilling Basin Sidewalls and Deflector

The original investigations into the required stilling sidewall heights were conducted in a 1:36 scale sectional model with the right wall modified to allow for height adjustments and observations of the overtopping flows impact to a mobile bed adjacent (USACE, 1937). It was concluded that approximately 5-feet of stilling basin overtopping was allowable with no impact on the adjacent riverbed, based on observations of the mobile bed. An isometric view of the test facility (b), section view of test flume (a), and overtopping simulation (c) are shown in Figure 118.

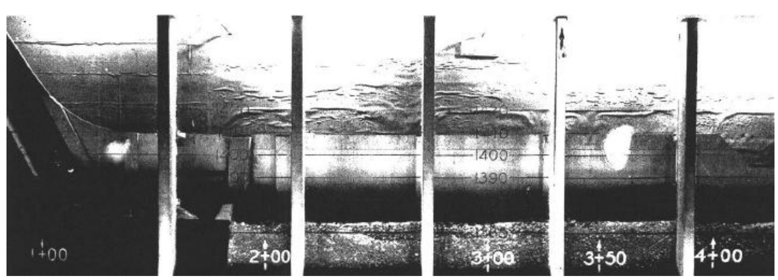

a) 1:36 scale model (section view)

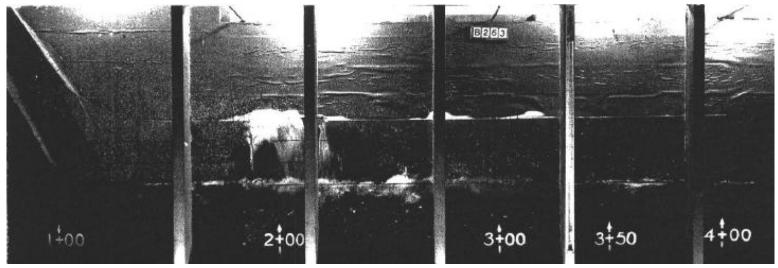

b) 1:36 scale model (iso view)

c) Allowable overtopping, Q = 300,000 cfs

Figure 118. Bluestone Stilling Basin 1:36 Scale Model for Evaluation of Sidewall Overtopping (USACE, 1937)

The current modification to the stilling basin produced a severe boil in the first stage basin due to the overly forced hydraulic jump, as shown in Figure 109. The required side wall raise associated with containment of the boil observed from the section model would have required a raise exceeding 40-feet; which would have doubled the height of the existing wall. To determine the required side wall raise, a 1:65 scale comprehensive model was utilized to evaluate the impacts of the overtopping of the existing side wall. The evaluation was focused on the potential for toe erosion of the wall and the associated impacts on stability on both the right and left sidewalls. The overtopping flows are shown in Figure 119.

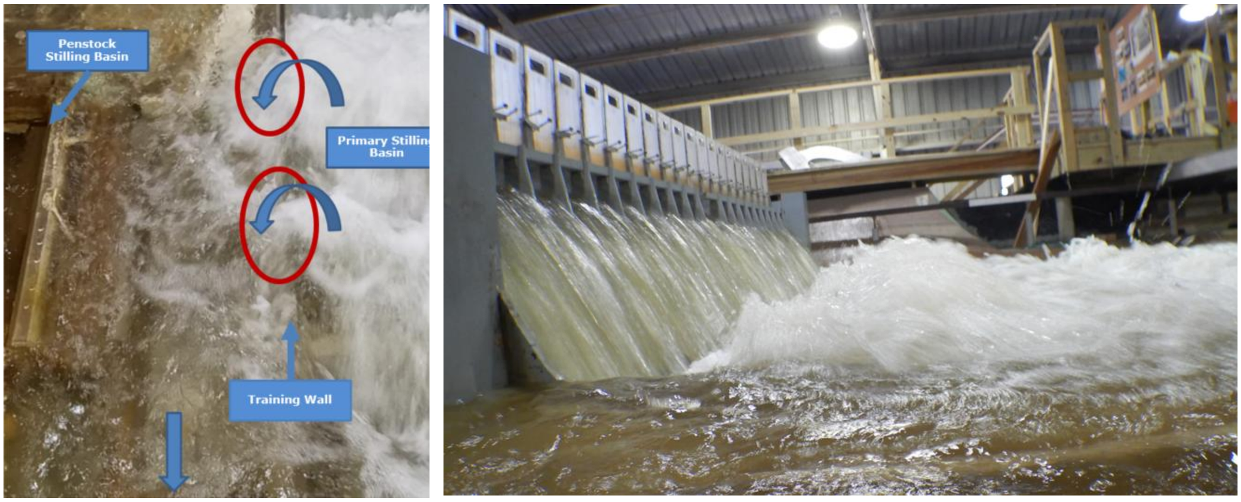

a) Plan (flow from top to bottom) *b) Section (looking at right wall and boil)*

Figure 119. Bluestone Dam Right Sidewall Overtopping Observations (USACE, 2018; Author)

The Erodibility Index method was utilized to evaluate the resistance of the rock riverbed and a combination of proxy bed material and pressure transducers was utilized to evaluate the hydraulic attack. It was determined via both the scaled mobile bed proxy and computed stream power estimates derived by the magnitude of the pressure fluctuations, that there is a high likelihood of prototype scour and potential wall instability associated with overtopping flows from the modified stilling basin with the updated inflow design flood.

Multiple side wall heights were evaluated quantitatively with observations of the turbulence at the bed made. Based on the evaluation of the behavior the diving jet that occurred along the back of the sidewall and the magnitude of the wall height required to reduce the erosion to a tolerable level, an alternative strategy was evaluated that includes a flow deflector along the back of the wall to re-direct the diving jet into the flow and minimize scour potential without a costly wall raise. The overtopping flows and the concept of the side wall deflector is shown in Figure 120.

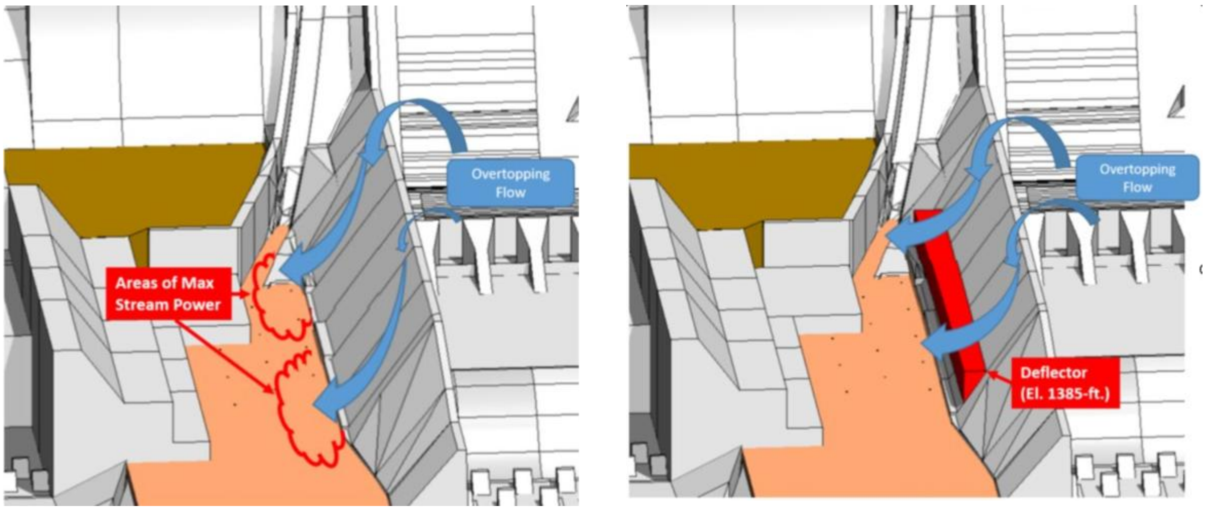

a) Without deflector *b) With deflector*

Figure 120. Comparison of Left Side Wall Overtopping Flow Behavior With and Without Deflector

The position of the deflector block was determined experimentally to reduce turbulence on the adjacent boundary, it was found experimentally that this was an elevation approximately 20-feet (prototype) below the tailwater elevation for the design flow condition, relating to approximately half of the total height of the wall.

Submersible Druck PDCR 1830 pressure transducers were utilized with the SYS6216-4D-VCS enhanced universal input module for data collection. Sensitivity analysis to collection rate was performed at 2,000, 1,000 and 200 Hz to determine if there would be impacts to the mean, standard deviation, minimum, and maximum pressures. The comparison showed little variation in key parameters; therefore, collection rate of 200 Hz was selected for efficiency of data collection and processing. The comparison is contained in Table 14.

Table 14. Sensitivity of Pressure Transducer Capture Rate for Bluestone Stilling Basin 1:65 Scale Model (USACE, 2018)

	200 Hz	1,000 Hz	2,000 Hz
Mean(psi)	0.2246	0.2360	0.2367
Standard Deviation (psi)	0.0170	0.0165	0.0161
Minimum (psi)	0.1368	0.1632	0.1645
Maximum (psi)	0.3108	0.3286	0.3238
Range (psi)	0.1740	0.1653	0.1593

The procedures described in Section 3.4.2.5 were utilized to convert the magnitude of the fluctuations to an equivalent unit applied stream power for various headwater and tailwater scenarios. The configuration of the pressure transducers for the left-side overtopping is shown in Figure 121.

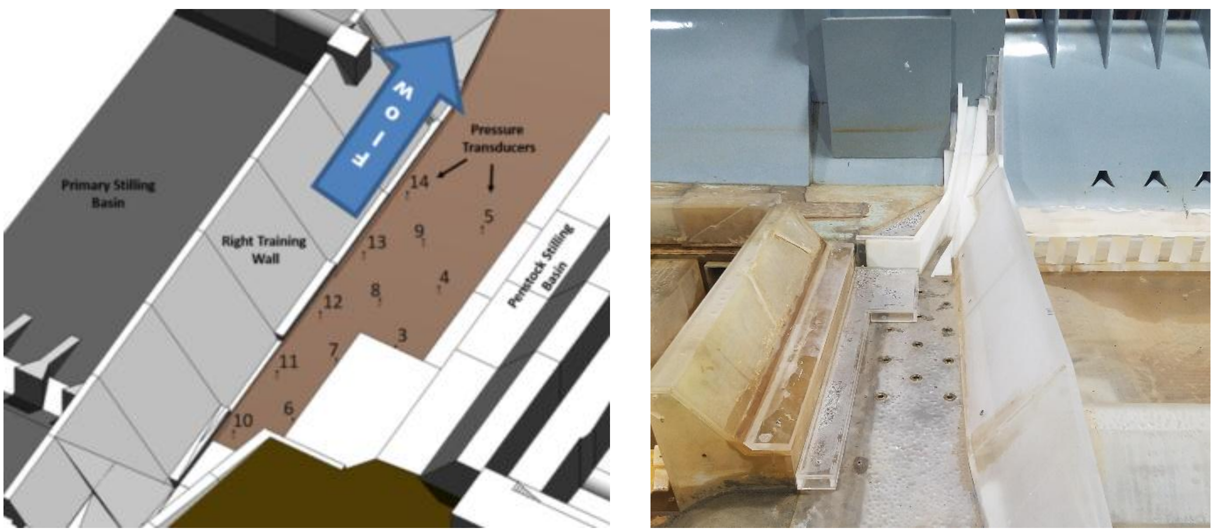

a) Isometric view of sensor locations *b) Photo of sensors (flow from top to bottom)*

Figure 121. Left Side Overtopping Pressure Transducer Locations (USACE, 2018; Author)

It was determined that the maximum headwater scenario did not produce the highest boundary applied unit stream power, that this was associated with a combination of moderate overtopping with a relatively low tailwater condition; suggesting that the depth of the plunge pool was a key factor in the boundary turbulence. An Isometric view of the computed applied boundary unit stream power ($\frac{\mathrm{Kw}}{\mathrm{m}^2}$) for the critical scenario with and without the deflector beam is shown in Figure 122.

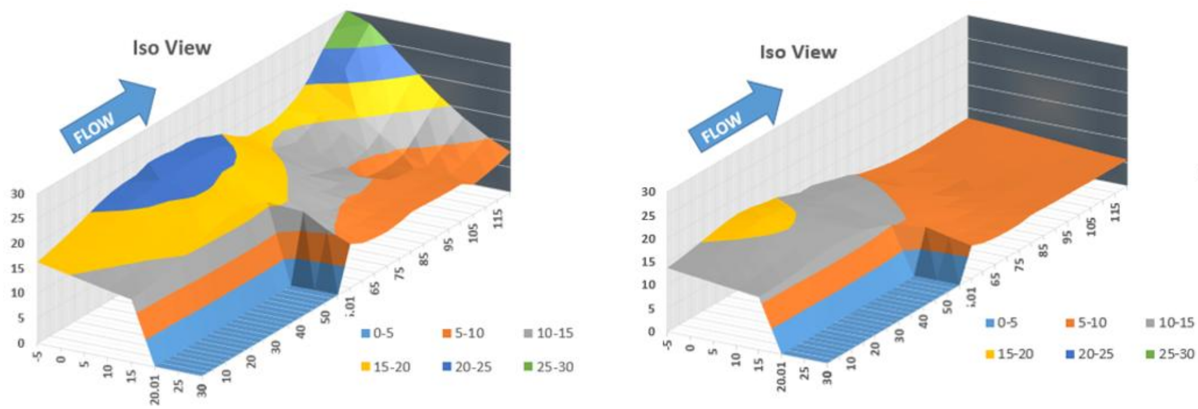

a) Without Deflector *b) With Deflector*

Figure 122. Right Side Wall Overtopping Unit Applied Stream Power Estimates (Bluestone, 2018)

The computed unit stream power for the isolated location was still above the threshold determined form the Annandale Erodibility Index (Humphries and Annandale, 2015); therefore, armor stone protection options were evaluated within the 1:65 scale physical model to decrease the potential for scour at the toe of the sidewall. A basic configuration of the sidewall armor protection and confinement wall configuration and experiment is shown in Figure 123.

a) Isometric view of configuration

b) Grid method to determine movement

Figure 123. Mobile Bed Experiments for Left Side Overtopping (USACE, 2018)

The prototype size of materials evaluated ranged from 4 to 7 feet along the intermediate axis; placing it outside the typical range for standard riprap protection design procedures. The initial estimate of stone size was completed utilizing the computed shear stress from pressure transducers (Equation 28) and utilizing shields relationship (Equation 29). To verify this relationship and account for a single mattress of material on a relatively smooth sliding surface, proxy material was evaluated for zero movement of the individual stones as compared in the grid from the pre- and post-experiment conditions. Using a zero-movement threshold was adopted as a criterion for linear particle size scaling to account for any discrepancies between model and prototype size, specific weight, and gradation and given the minimal interlock provided. In addition, the stone confinement wall on the downstream end ensures no sliding of the armor stone mattress can occur.

The right-side sidewall has substantial backfill on the outside and removal of this material would impact slope stability on the adjacent hillside. It was determined the removal of significant backfill to construct a deflector and armor stone apron similar to the left side would require significant stabilization efforts and braced excavation, therefore alternate overtopping strategies were evaluated. Several surface protection configurations were evaluated, although ultimately deemed too expensive and not a robust solution. Two examples of surface protections evaluated are illustrated in Figure 124.

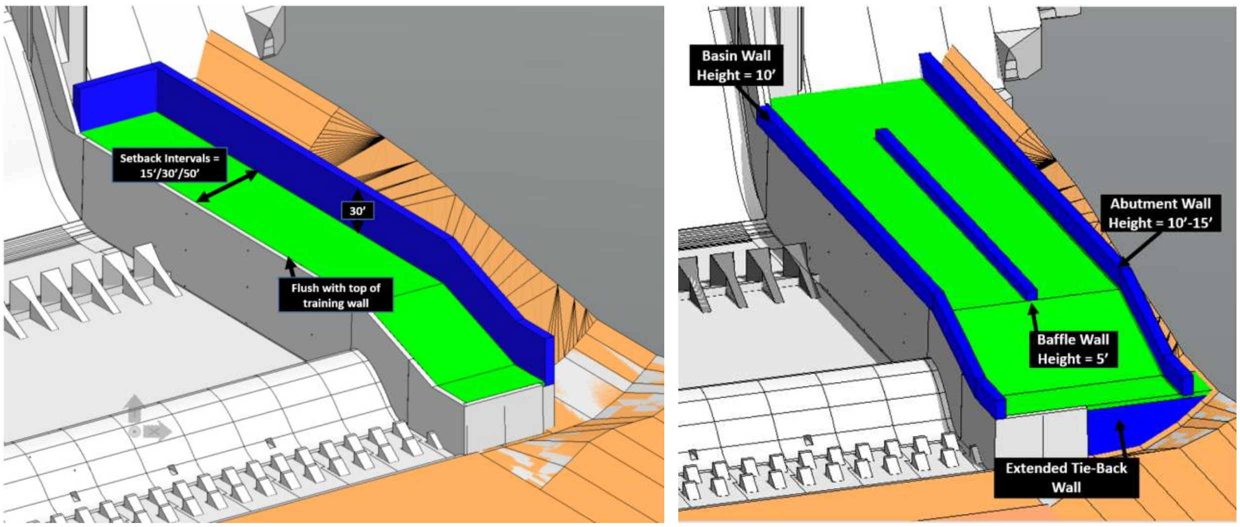

a) Full surface containment *b) Raise and surface containment*

Figure 124. Surface Protection Configurations

With an updated objective of developing a configuration that reduced the stream powers to below the in-situ rock at the toe of the side wall, multiple wall raise and top width alternatives were evaluated. These alternatives were intended to limit overtopping flows and break up the plunging jet on the top of the wall itself. Using the method described by Annandale (ref), granular material was selected based on scaled threshold stream power based on the most erodible rock conditions foreseeable in this location. A zero-movement threshold was set for conservatism. The experiments are highlighted in Figure 125.

a) Aerial b) Section c) Pre-Experiment d) Post-Experiment

Figure 125. Left-Side Wall Overtopping Experiments (Photos by author)

The final configuration resulted in a wall raise of 10 feet and a horizontal wall top width of 11 feet. The recently constructed wall modifications are illustrated in Figure 126.

a) Right deflector wall *b) Left raise and top deflector*

Figure 126. Construction Photos of Constructed Sidewall Modifications (Photos by Author)

4.6.5 Downstream Scour Behavior

The rock downstream of the primary stilling basin consists of Interbedded Orthoquartzite and Carbonaceous Shale; with observed significant faulting on the right side of the river channel.

The rock mass properties were utilized by Humphres and Annandale (2015) to characterize three distinct categories of rock encountered. The lower end of the Interbedded Orthoquartzite was utilized for sizing of a proxy bed material and had a lower limit threshold stream power determined to range from 1.8 $\frac{kW}{m^2}$. The estimated range of EI values and corresponding threshold stream powers are shown graphically in Figure 127.

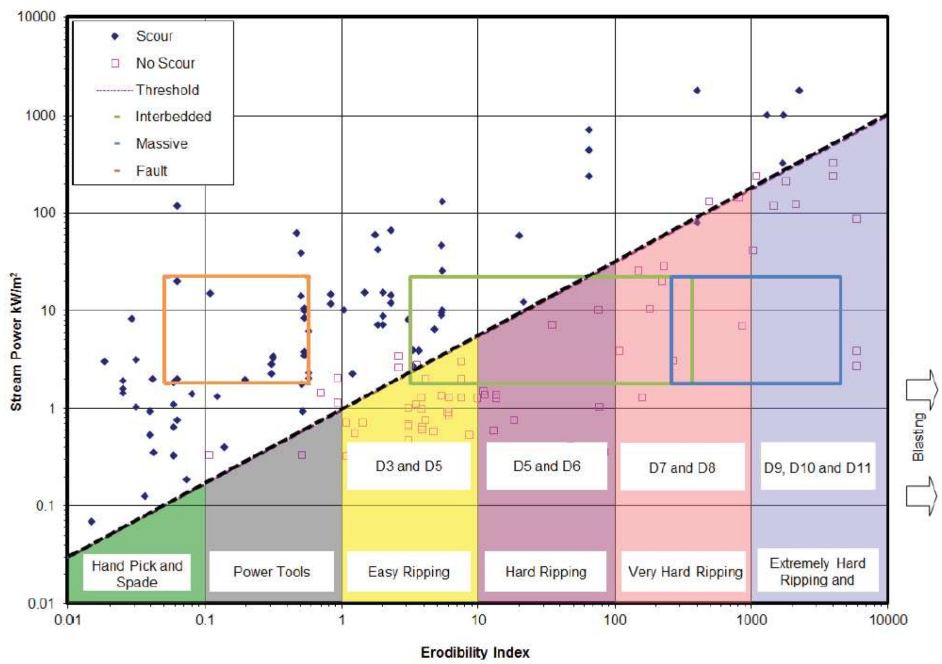

Figure 127. Erodibility Index for Bluestone Dam Scour Estimates (Source: Humphries and Annadale, 2015)

When applying the method described in Section 3.4.2.4 this results in a median grain size material of 12-mm. The final material utilized for the subsequent evaluation in the 1:36 scale section model had a median particle size of 17-mm.

As noted previously, the second stage basin utilized a similar configuration as the first stage and was designed considering the loss of the jump action at approximately 300,000 $\frac{\mathrm{ft}^3}{\mathrm{s}}$. Scour profiles were observed for spillway discharges up-to 1,100,000 $\frac{\mathrm{ft}^3}{\mathrm{s}}$with the hydraulic jump action lost, without significant increase in depth immediately downstream of the end sill with increasing unit discharge.

This suggests that the combination of the two rows of baffles and end sill work together to sufficiently lift the higher velocity floor jet into the flow field and away from the bed for flows many times the design value. Intermittent turbulent eddies (i.e. bursts and sweeps) are observed to dive down and initiate motion and rework the mobile bed at approximately 10- to 15-degree angle from horizontal, depending on flow condition. This is depicted in the annotated photograph shown in Figure 128.

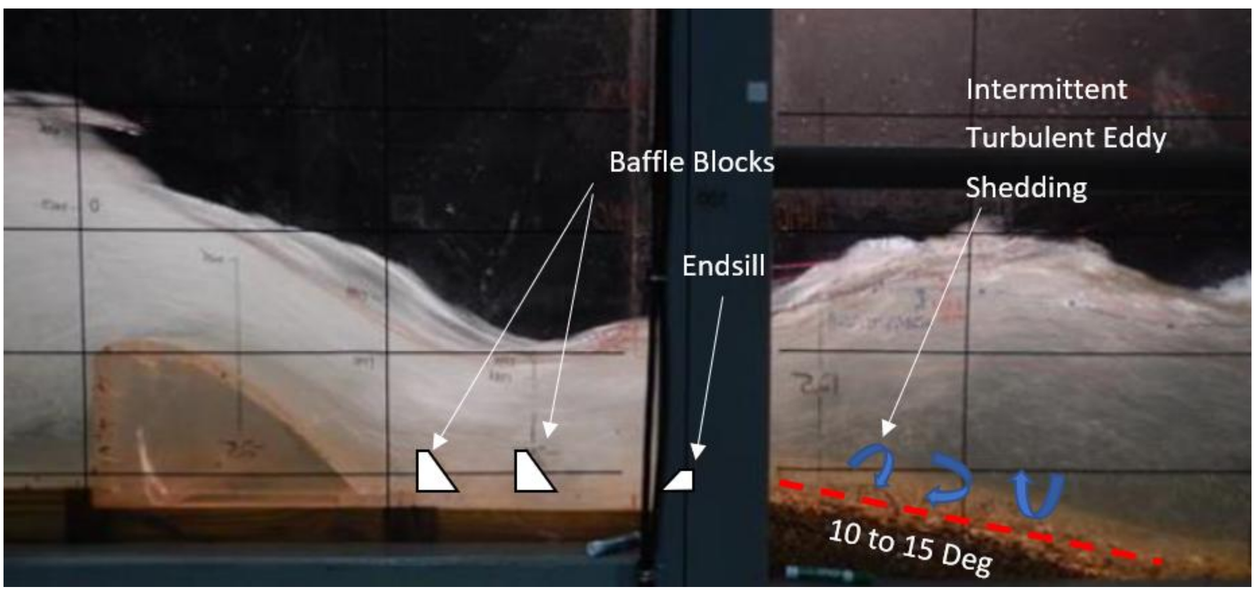

Figure 128. Turbulence and Scour Behavior Downstream of Bluestone Second Stage Basin (overview)

The macro-scale turbulent bursts (a) and the intermittent periods with no near-bed turbulence (b) are illustrated in Figure 129.

a) Macro-scale turbulent structure b) Intermittent period with no near-bed turbulence

Figure 129. Turbulence and Scour Behavior Downstream of Bluestone Second Stage Basin (Closeup)

It is worth noting that the 2nd stage stilling basin is relatively short in relation to the prescribed stilling basin length, which relates to a ratio of $\frac{L_{SB}}{d_2}$ of < 1 for the updated design discharge. The scour depths were greater for the scenario where the tailwater depth was sufficient to maintain the hydraulic jump in the downstream extent of approximately the d_2. This was true for all discharge scenarios and is believed to be related to the shortness of the basin and the significant lifting of the high velocity and related macro-turbulent structures associated with the combination of baffles and end sill when the jump action is lost.

Several iterations of reconfiguration of the second stage basin were attempted, including replacing the ogee stilling weir with a stepped weir and sizing the baffles and end sill using the USBR Type III configuration (USBR, 1984). The results of all reconfiguration attempts were increased scour at the lower discharge, resulting in the recommendation for no modification of the second stage stilling basin.

In an effort to compensate for limitations with representing rock mass scour with a granular proxy material, the potential for undermining of the downstream apron was evaluated with flush mounted pressure transducers on the vertical downstream face of the stilling basin, as shown in Figure 130. The steam power on the vertical face was estimated using the method described in Section 2.4.2; the maximum stream power values were below the anticipated threshold for concern.

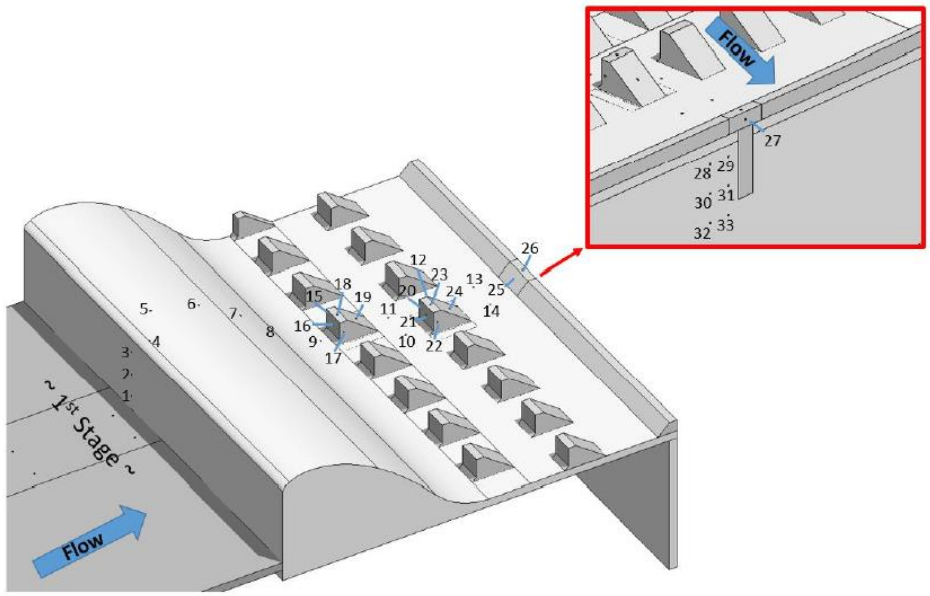

Figure 130. Location of Pressure Transducers in Downstream Face of Second Stage Stilling Basin

5 PHYSICAL MODEL EVALUATION

5.1 Mobile Bed Evaluation

Mobile bed experiments were performed for the Keystone Dam project as part of operational research and development associated with the current research.

5.1.1 Methods

Keystone Dam is in Tulsa County, OK at mile 539 on the Arkansas River approximately 15 miles west of the City of Tulsa. The project is located approximately 2 miles downstream from the confluence of the Cimarron and Arkansas Rivers. The dam consists of a primary overflow spillway gravity dam section, two non-overflow gravity dam sections, two flanking earthen dam embankment sections, and a two-unit power plant. An aerial image of the project is shown in Figure 131.

Figure 131. Keystone Dam Overview (Adapted from USACE, 2012)

The original stilling basin design philosophy was to accept unfavorable performance for the rare to extreme flood load scenarios, that approach the spillway design flood. The original design intentionally designed the appurtenant features (baffles and end sill) and raised the stilling basin invert to have favorable performance for a flood loading of lessor magnitude; but have marginal performance at the original maximum flood load case, as described in the original design physical modeling report (USACE, 1960).

Both the original (USACE, 1960) and the experiments conducted as part of the current research were performed at the USACE Engineering Research Development Center's, Waterways Experiment Station in Vicksburg, MS. The original physical model consisted of a 1:36 Froude scale hydraulic model representing 2 full spillway bay and 2 half spillway bay sections. The width of the sectional model was 4 feet, which represents 144 feet in the prototype. The current model study adopted the same extents and length scales as the original model to minimize the potential for addition confounding variables in evaluating the required tailwater and hydraulic performance, although conformance to major similitude standards-of-practice at this scale and flow conditions were confirmed outside the roughness similitude for the acrylic construction materials for the chute. The Froude scale parameters are provided in Table 15.

Table 15. Keystone Dam Model Froude Scale Similitude

Variable	Froude Similitude Scale
Length	L_r = 36
Velocity/Time	$L_r^{0.5}$ = 6
Discharge	$L_r^{2.5}$ = 7,776
Volume/Force	L_r^{3} = 46,660
Pressure/Stress	L_r = 36
Power/Reynolds	$L_r^{1.5}$ = 216

The relevant flow parameters and model similitude numbers are summarized in Table 16. The original design scenario is condition 3 with an incoming Froude number of 4.2 and a unit discharge of approximately 1,070 cfs/ft. The conditions evaluated represent a range from 55- to 124-percent of the original design discharge.

Table 16. Keystone Dam Model Flow Parameters

	Flow Parameter	Cond. 1	Cond. 2	Cond. 3[a]	Cond. 4	Cond. 5
Prototype	Prototype Headwater (NGVD 29 - Feet)	752	759	766	772	777
	Unit Discharge (cfs/ft)	588	812	1,069	1,218	1,327
	Incoming Froude No.	5.4	4.7	4.2	4.0	3.9
Model	Model Unit Discharge (cfs/ft)	2.7	3.8	5.0	5.6	6.1
	Incoming Flow Depth (ft)	0.20	0.27	0.35	0.40	0.43
	Incoming Flow Velocity (ft)	13.6	13.8	14.0	14.2	14.4
	Reynolds Number	253,078	349,589	460,142	523,785	570,696
	Head on Crest (ft)	0.9	1.1	1.3	1.5	1.6
	Weber Number Over Crest	3,132	4,931	7,270	8,354	9,062

[a] *Original Design Discharge*

The model configuration is illustrated in Figure 132.

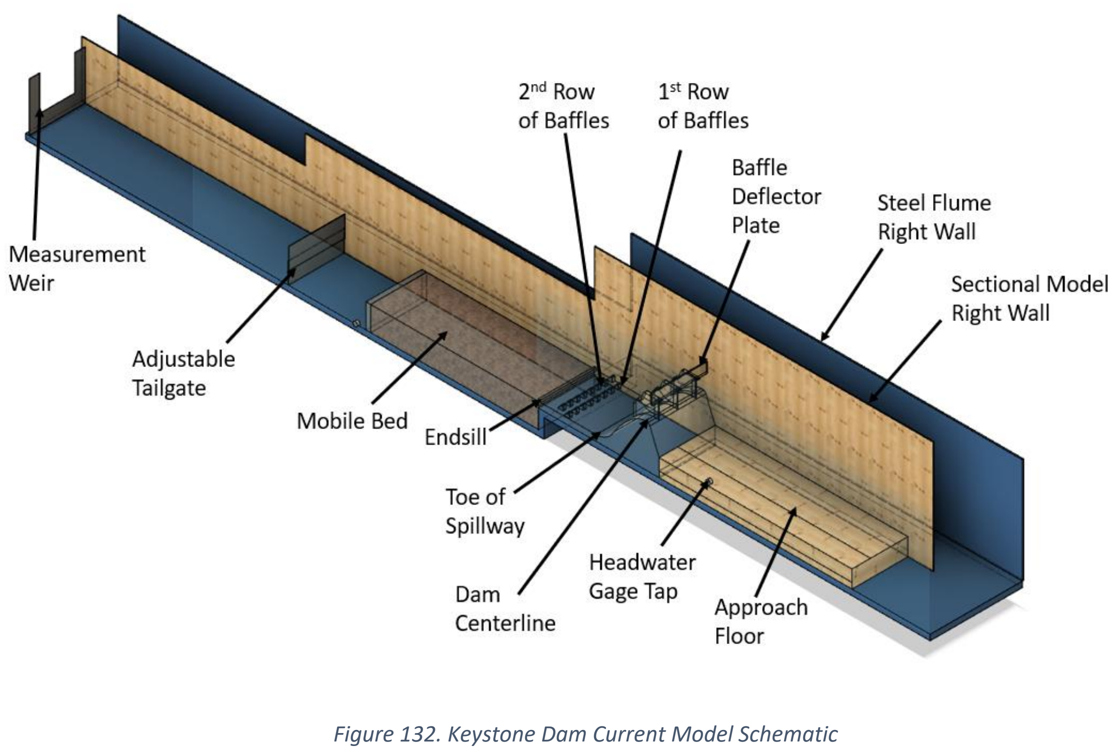

Figure 132. Keystone Dam Current Model Schematic

5.1.2 Results

5.1.2.1 Hydraulic Jump Action

The tailwater required to maintain the hydraulic jump condition up to the new estimate of the PMF was evaluated with a coarse-grained mobile bed. The data obtained under the current effort corroborated the original design physical model values, except for the original spillway design discharge (largest discharge evaluated in the original study). The values from the new physical model study agree with the lower discharges from the original study. The flow parameters and observational data of the current study are summarized in Table 17 and results compared to the original study in Figure 133.

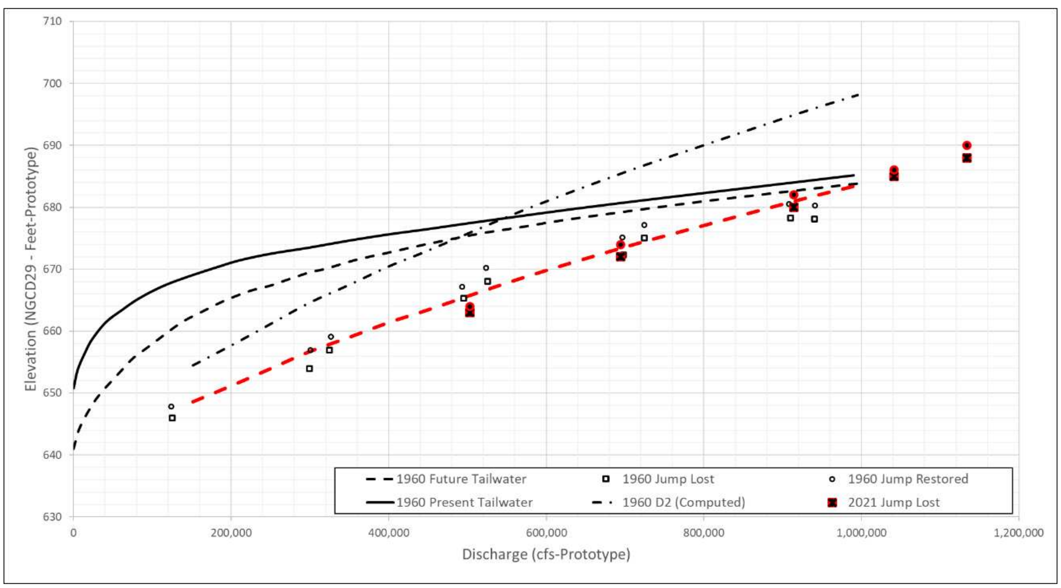

Figure 133. Keystone Dam Updated Required Tailwater Curve

It is found for the Keystone baffled hydraulic jump stilling basin configuration and the flow conditions evaluated, that the determination of the hydraulic jump action being lost or maintained is subjective and a transitional range exits whereas the flow surges and the regime is unstable. This is illustrated in Figure 134 through Figure 136.

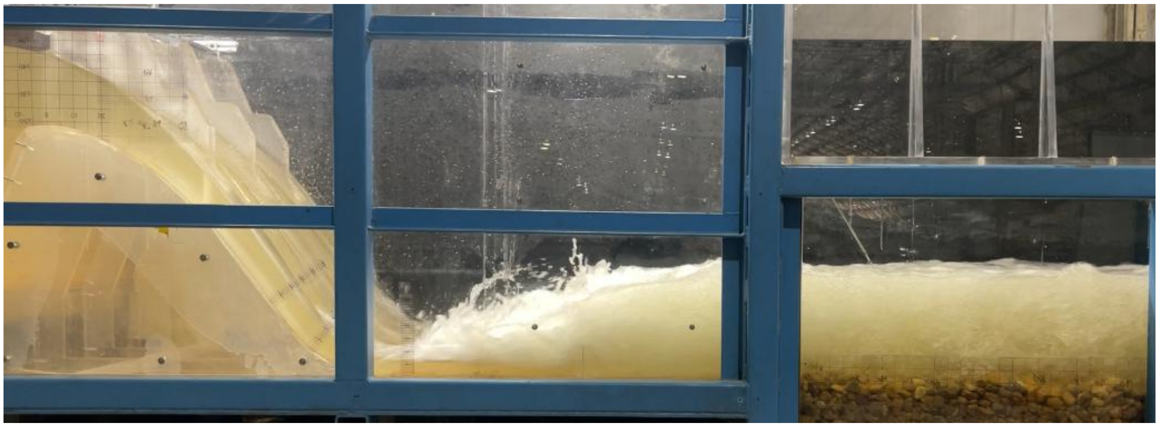

Figure 134. Hydraulic Jump Action Maintained

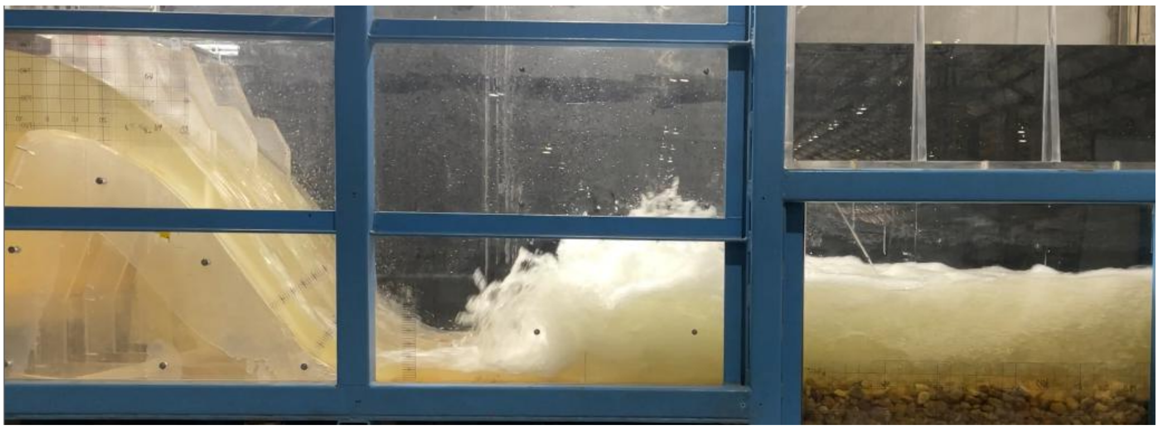

Figure 135. Transitional Jump Action

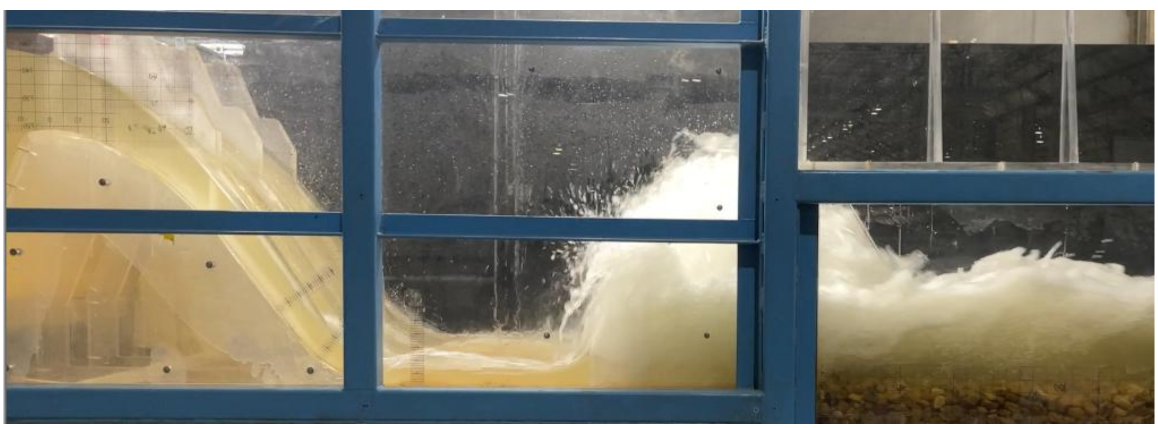

Figure 136. Hydraulic Jump Action Lost

This is illustrated in Figure 137 and Figure 138.

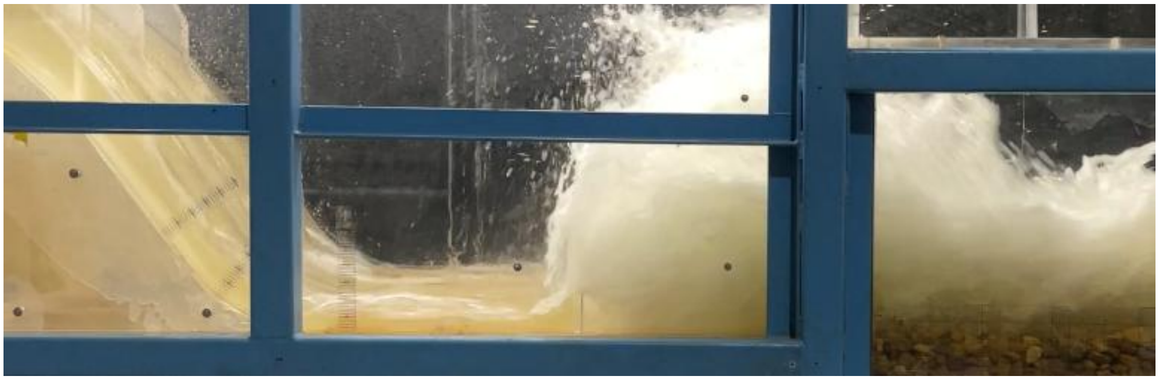

Figure 137. Jump Action Lost, Lower Unit Discharge (High Froude)

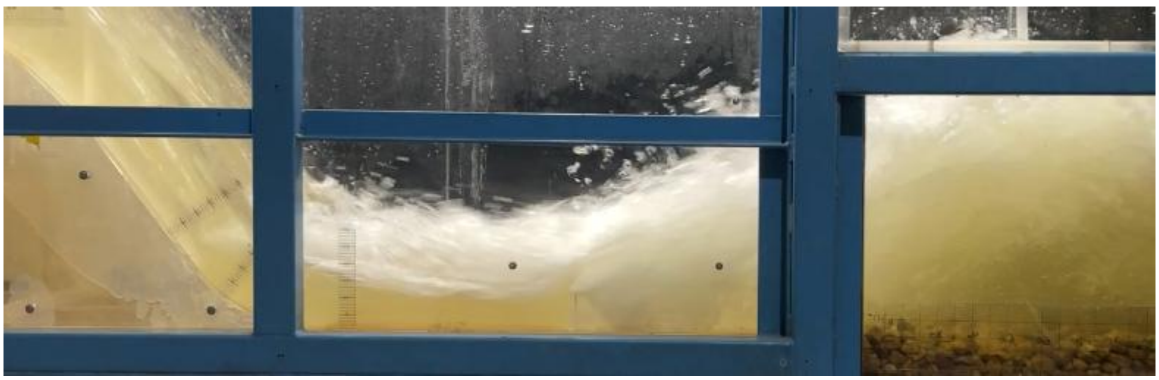

Figure 138. Jump Action Lost, Higher Unit Discharge (Low Froude)

There was an intermittent behavior identified associated with the separation flashes that occur off the baffle when the jump action was lost, and the high velocity jet was directly impacting the baffles. This can be observed in Figure 139; whereas the separation went from a fully developed state to minimal appearance in a duration of less than 1-second. The condition of the separation from the baffle block directly influenced the jet behavior whereas it steepened the jet. The transient between these conditions resulted in strengthening of macro-scale turbulence structures as the jet angle fluctuates.

a) Significant separation *b) Apparent lack of separation*

Figure 139. Transient Nature of Baffle Block Separation

As unit discharge is increased, the d_1 , v_1 , and the Fr_1 reduces; especially for higher heads where velocity only slightly increases with increasing drop height and flow depth. The computed values for these parameters and the associated observations of required tailwater to maintain the hydraulic jump action are given in Table 17.

Table 17. Keystone Dam Hydraulic Jump Action Data Summary

		Cond. 1	Cond. 2	Cond. 3	Cond. 4	Cond. 5
Flow Parameters	Unit Discharge (cfs/ft)	588	812	1,069	1,218	1,327
	Critical Depth (ft)	22.1	27.4	32.9	35.8	37.9
	Incoming Depth (ft)	7.2	9.8	12.7	14.3	15.4
	Incoming Froude No.	5.5	4.8	4.3	4.1	4.0
	Sequent Depth (D2) (ft)	52.8	62.0	71.0	76.0	79.5
Maintain Jump Action	Require TW	38	47	55	60	63
	Ratio (TW/D2)	0.72	0.76	0.77	0.79	0.79
	Ratio (dc/TW)	0.58	0.58	0.60	0.60	0.60
Restore Jump Action	Required TW	664	674	682	686	690
	Require TW	39	49	57	61	65
	Ratio (TW/D2)	0.74	0.79	0.80	0.80	0.82
	Ratio (dc/TW)	0.57	0.56	0.58	0.59	0.58

The current Keystone values are plotted in against the USACE and USBR data described in Figure 140. As the unit discharge increases and Froude number decreases, the required $\frac{TW_{req}}{d_2}$ to maintain the hydraulic jump increases near linearly from the evaluated 55- to 124-percent of design discharge.

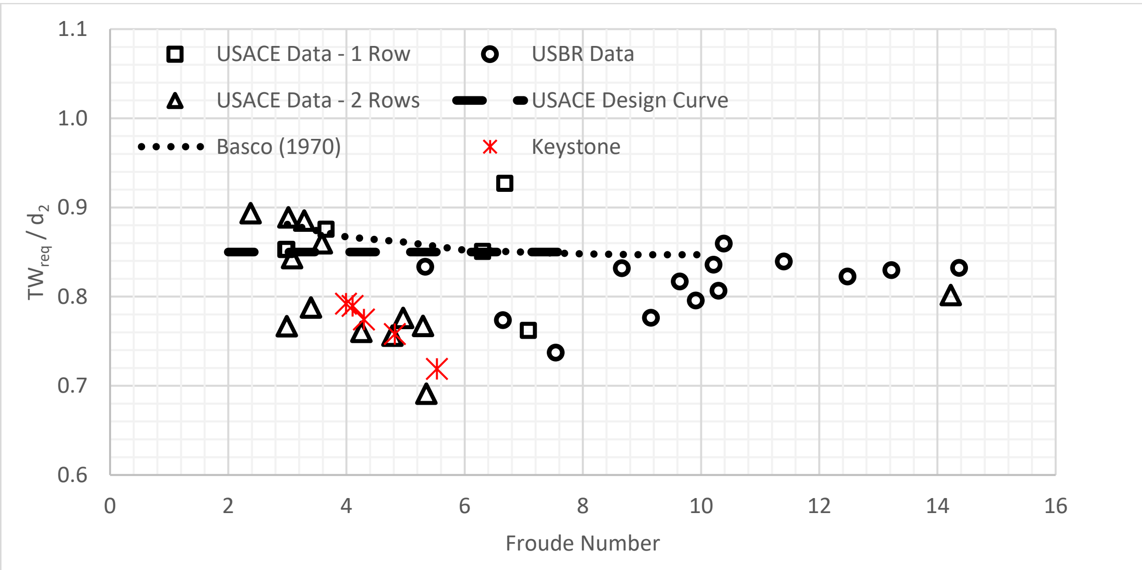

Figure 140. Comparison of Keystone Findings and Combined Required Tailwater/D2 Ratio Data from USBR and USACE

It is found that plotting the ratio of the required tailwater to the critical depth produces a reasonably consistent predictor of required tailwater for the Keystone stilling basin when subjected to flow conditions that are above/below the original design conditions. This is graphically illustrated in Figure 141.

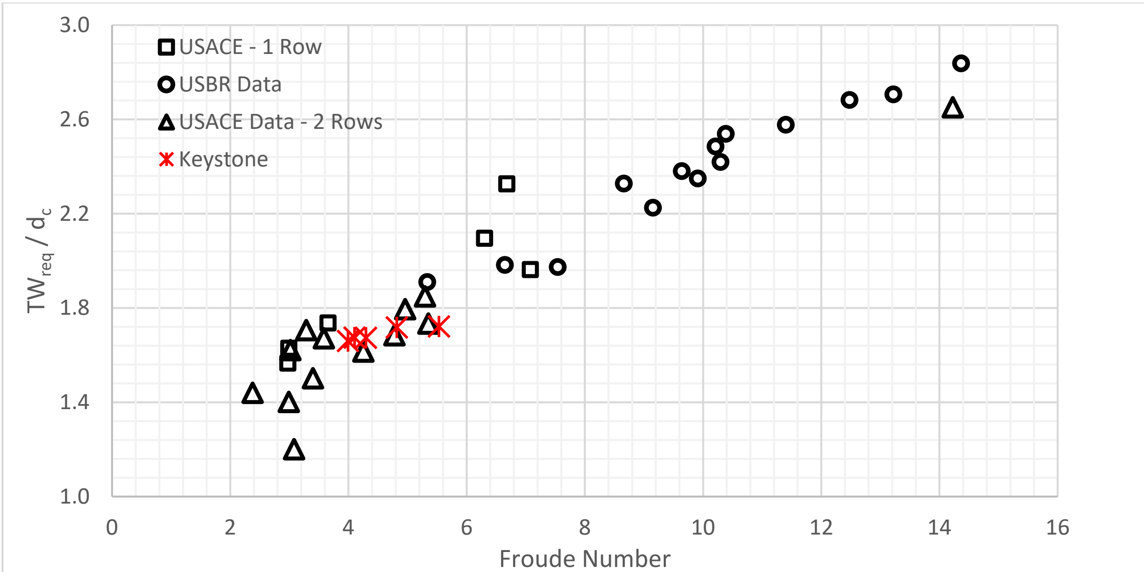

Figure 141. Comparison of Keystone Findings and Combined Required Tailwater/Critical Depth Ratio Data from USBR and USACE

Since the configuration is not modified in comparison to the incoming flow conditions, it is demonstrated in Figure 142 that the relative basin length decreases with an increase in unit discharge/decreasing Fr_1.

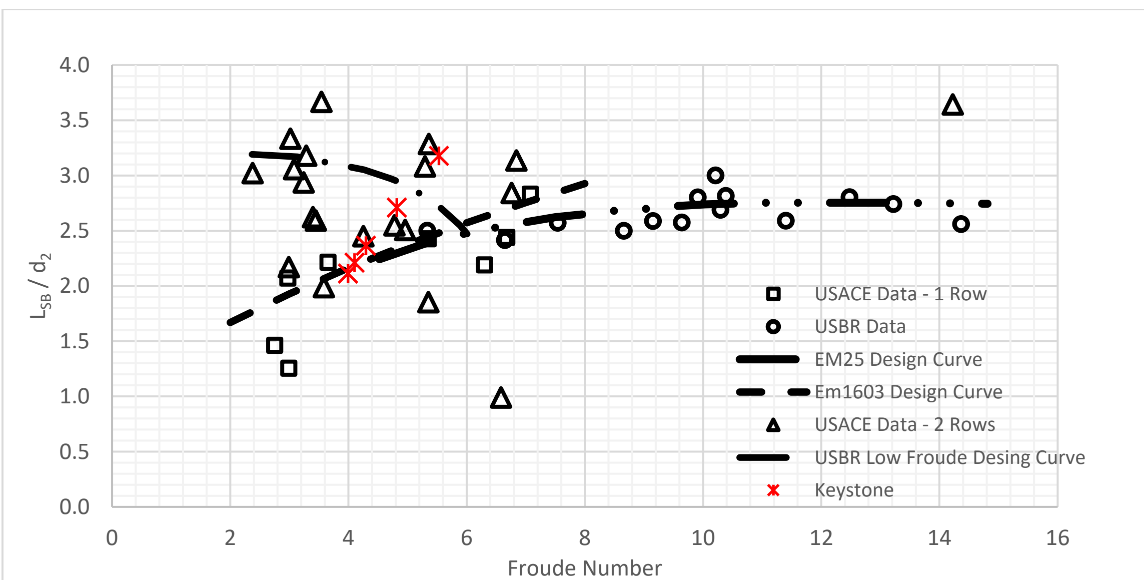

Figure 142. Comparison of Keystone Findings and Combined Stilling Basin Length / Sequent Depth Ratio Data from USBR and USACE

Unlike the Bluestone Second Stage Stilling basin, the minimum basin length is still within the range of recommended guidance and other projects. If the unit discharge was increased significantly more, then the basin length is expected to then be a controlling factor in performance.

5.1.2.2 Downstream Scour Behavior

The original model study utilized a sand bed to estimate the general downstream scour tendencies associated with the various stilling basin designs under consideration. The current study objective was to evaluate the scour potential with mobile-bed materials representing a range of threshold erodibility of the more susceptible rock mass units present at the dam.

The downstream bed material consists of nearly horizontally bed sedimentary sequences of shale and sandstone. There are two main geologic units in the elevation range anticipated to be susceptible to scour, an upper and lower Shale units; interbedded with a thin sandstone layer. The excavation of the stilling basin (a) and downstream cutoff key (b) are shown in Figure 143.

a) Stilling Basin Floor

b) Cutoff Key

Figure 143. Keystone Dam Stilling Basin Construction Photos

The rock mass erodibility for these units was estimated utilizing both the methods described by Annadale (1995) and Pells (2016). The range of values estimated for the units ranges from approximately 1 to over 200 for the EI and approximately 10 to 70 for the eGSI. When considering erosion threshold stream power associated with these geomechanical index values, the range is 0.3- to 10- $\frac{\mathrm{kW}}{\mathrm{m}^2}$ and 1- to 50- $\frac{\mathrm{kW}}{\mathrm{m}^2}$, for the EI and the eGSI; respectively. The values for the EI (a) and the eGSI (b) are illustrated graphically with red highlights in Figure 144.

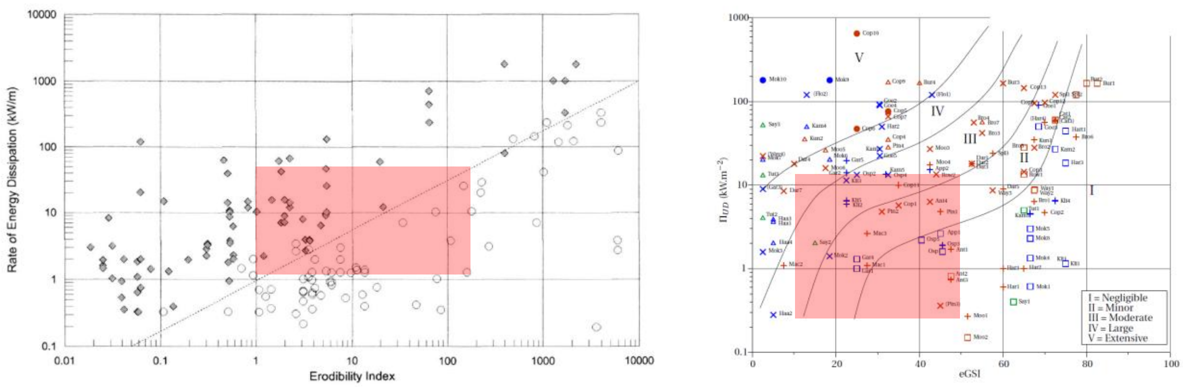

a) Method of Annadale (1995) *b) Method of Pells (2016)*

Figure 144. Graphical Illustration of Threshold Stream Power

Using the methods described in Section3.4 provides a range of materials with median particle sizes ranging from 40 to 87 mm. Considering uncertainty in the scaling process and the available materials, the materials utilized in the experiments had geometric mean particle size of 28 and 88 mm, shown in Figure 145 a) and b); respectively.

a) b)

Figure 145. Keystone Mobile Bed Material Proxy

The larger material demonstrated insignificant scour potential, even when the hydraulic jump action was lost in the basin due to insufficient tailwater. The smaller material had a scour pattern similar to the scour pattern of the sand bed from the original model study (USACE, 1960).

The scour pattern near the end sill follows the same slope in the downstream direction, although the overall scour depth increases for increasing discharges as shown in Figure 146.

It is not known why the sand bed profile exhibited lower scour depths as compared to the gravels used in the current study; although the fact that is approximately 2-feet lower suggest it could potentially be a relic of adjustments to the bed made when the prototype stilling basin invert elevation was adjusted two feet up to increase economy of construction excavation. The equilibrium scour condition for the coarse gravel was not able to be determined for the design discharge and above due to limitations of mobile bed depth.

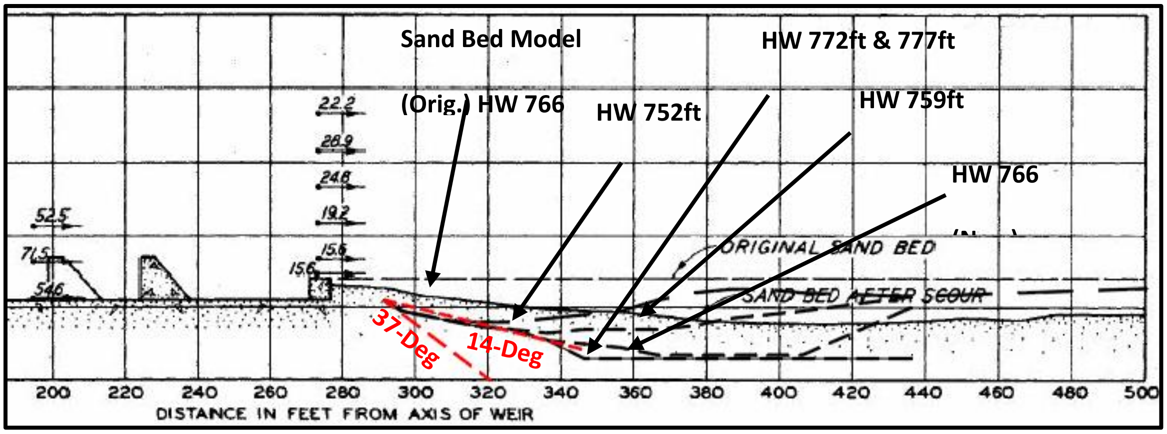

Figure 146. Keystone Basin Mobile Bed Scour Patterns, geometric mean = 28mm (Adopted from USACE, 1960)

The process of intermittent eddies being shed off the end sill reworking the material at an approximately 14-degree angle from horizontal, which is significantly less than the minimum submerged static angle of repose of 37 degrees measured.

To determine the influence of the grain size on ultimate scour and to understand the scour evolution in additional more detail, another series of experiments is conducted specifically related to the current research. A granular material with geometric mean particle size of 3.7 mm and a submerged static angle of repose of ~ 38 degrees was used. The static angle of repose was determined via tilt box apparatus; although the observed angle of repose of material deposited downstream of the mobile bed is observed to be 32.6 degrees. The tilt box a) and downstream deposition b) are illustrated in Figure 147.

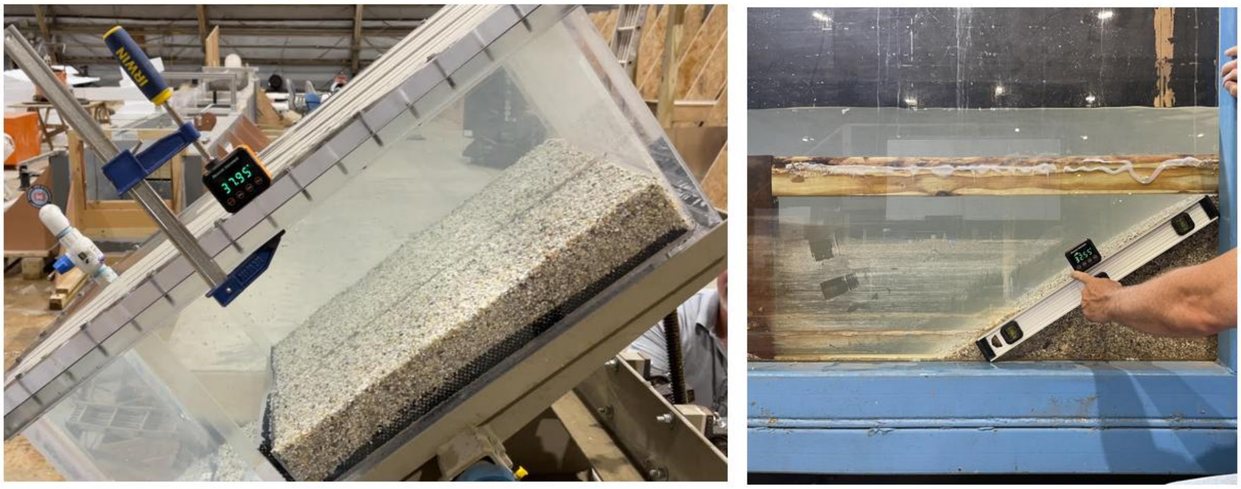

a) b)

Figure 147. Observational Methods of Submerged Angle of Repose

To understand the scour evolution, experiments were performed at the design discharge for the tailwater for two tailwater scenarios. A tailwater ratio ($\frac{d'_2}{d_2}$) of 0.83; which is the approximate minimum required to maintain the hydraulic jump and that in which the hydraulic jump is not maintained. The simulation was conducted with the small bed material with the bed being reset between experiments.

The results indicated that the scour evolution involves the deepening of the scour hole along a relatively constant exit angle, that was equal to 15 degrees when the hydraulic jump action is maintained. This is very similar to the 14 degrees observed for the previous experiment with a larger median grain size and the 6- to 11-degrees measured from the 1960 sand bed experiments for various configurations. The observed scour depths along the side wall for the condition with the hydraulic jump action maintained are detailed in Table 18 and illustrated in Figure 148.

Table 18. Mobile Bed Scour Evolution, Design Discharge, Maintained Jump Action

	Duration (min) / Scour Elevation (Prototype)					
Station	0	0.25	0.5	0.75	1	1.25
5	631	628	628	628	628	628
25	631	624	624	624	624	624
50	631	620	620	620	620	620
75	631	617	615	615	612	612
100	631	615	612	609	606	605
125	631	615	610	608	606	603
175	631	618	613	610	607	604
200	631	621	618	613	610	608
225	631	624	620	618	614	613
250	631	627	624	621	621	621
Max Depth		16	21	23	25	28

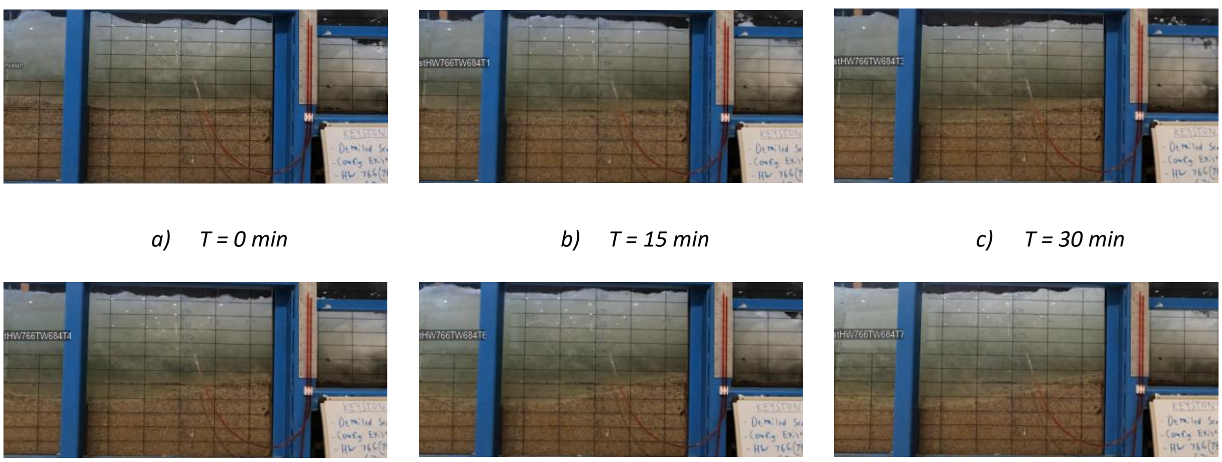

a) T = 0 min *b) T = 15 min* *c) T = 30 min*

d) T = 45 min *e) T = 60 min* *f) T = 75 min*

Figure 148. Mobile Bed Scour Evolution, Design Discharge, Maintained Jump Action

The results were similar for the scenario where the hydraulic jump was lost. The exit slope for the lost jump action is near constant at an angle of 10 degrees. This is noticeably shallower than that of the scenario with the hydraulic jump is maintained. The observed scour depths along the side wall for the condition with the hydraulic jump action maintained are detailed in Table 19 and illustrated in Figure 149.

Table 19. Mobile Bed Scour Evolution, Design Discharge, Lost Jump Action

	Duration (min) / Scour Elevation (Prototype)				
Station	0	0.25	0.5	0.75	1
5	631	629	629	629	629
25	631	625	626	626	626
50	631	623	624	624	624
75	631	619	619	620	620
100	631	615	614	616	616
125	631	611	609	611	611
175	631	608	607	607	607
200	631	610	608	608	608
225	631	614	612	610	610
Max Depth		23	24	24	24

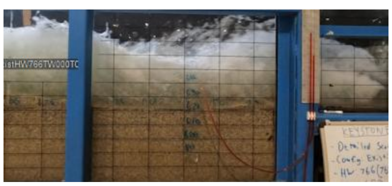

a) T = 0 min

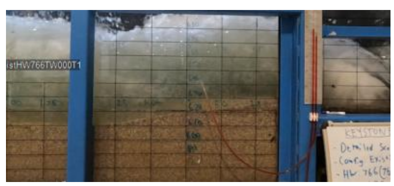

b) T = 15 min

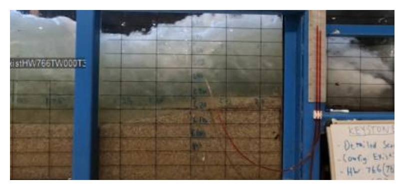

c) T = 30 min

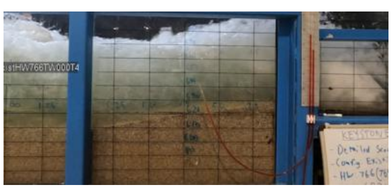

d) T = 45 min

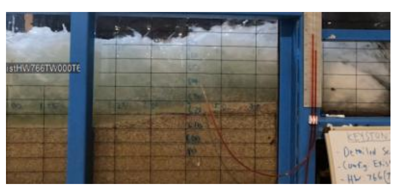

e) T = 60 min

Figure 149. Mobile Bed Scour Evolution, Design Discharge, Lost Jump Action

A comparison of the scour patterns at quasi-equilibrium are shown in Figure 150 for the condition of a maintained hydraulic jump (a) and a lost hydraulic jump (b).

a) Jump Action Maintained *b) Jump Action Lost*

Figure 150. Existing Stilling Basin, Design Discharge

Similar to scour patterns observed for the Bluestone spillway sectional model, there were distinct ridge and valley topography in the cross-stream direction as a result of the forcing of a secondary turbulence structure that forms as a result of the macro-scale turbulent fluctuations interact with the side wall; as shown in Figure 151.

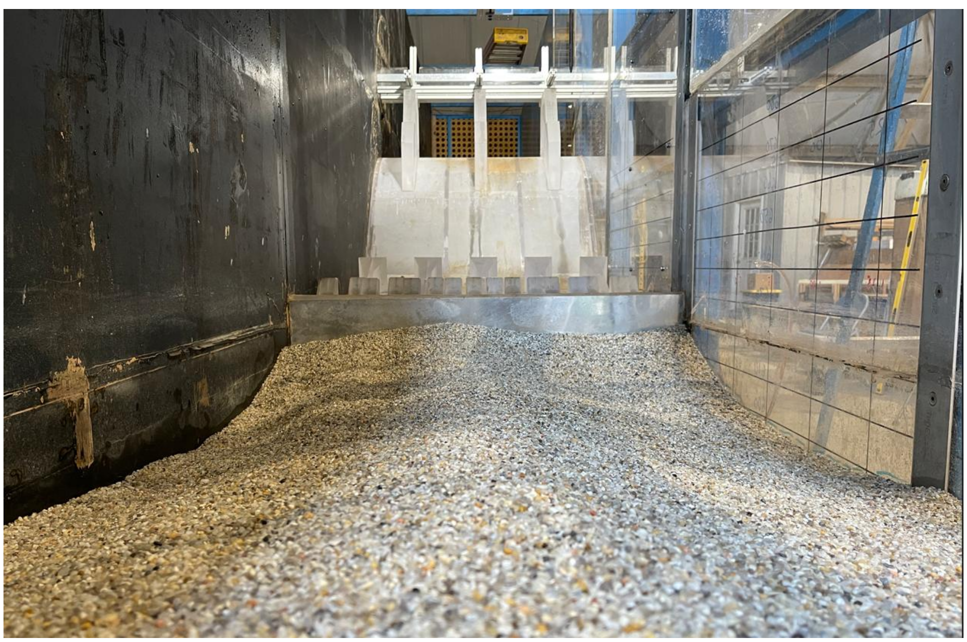

Figure 151. Typical Ridge and Trough for Mobile Bed Downstream of Hydraulic Jump

5.2 Rigid Bed Evaluation

Approximately 450 individual experiments were performed to evaluate various aspects of standard baffled stilling basin configurations, along with permutations of these based on recent findings. These experiments range over two crest heights and variable unit discharges, which produce Fr_1 ranging from 4.02 to 11.3. A total of 15 individual stilling basin configurations were evaluated. Each configuration was evaluated across six unit discharges and a varied tailwater from the sequent depth to that in which the hydraulic jump action was lost.

5.2.1 Methods

5.2.1.1 General

The physical model experiments were conducted at the US Army Corps of Engineers Coastal and Hydraulics Laboratory, of the Engineering Research and Development Center. The facility is located on the Waterways Experiment Station campus in Vicksburg, Mississippi. Given limited funding to complete the experiments, the design and execution of the experimental campaign was developed to be implemented by the author without the need for additional staff.

The same flume described above for Keystone Dam was modified to conduct the experiments described herein. The flume consists of a steel section that has been modified with a wood false wall to have a width of 4-feet and an overall length of 61 feet. The flow provided to the flume is provided by a constant head tank that extends the length of the facility, providing flow to all models within the facility. Flow to the head tank is provided by four constant speed pumps with a total discharge capacity of approximately 45 cfs to the multiple physical modeling bays within the building. Excess flows provided to the constant head tank are returned to the sump area by a return line whereas the water level in the tank is maintained constant.

Four inflow lines are provided flow into the sectional flume, each controlled by a gate valve. These lines discharge into the upper wall of the flume. A head tank and perforated wall provide uniformly distributed velocities in the upper approach channel. The water levels in the approach channel are controlled by the Control Weir, which replicates the effects of an overfall dam and spillway. An elliptical allows for a smooth transition into the constant slope chute that is 0.7 horizontal to 1 vertical, which is in the typical range for a concrete gravity overflow section. The flow then transitions to a baffled hydraulic jump stilling basin that exits into a rigid tailrace section that is level with the stilling basin floor. The flow exits to the stilling pool that is controlled with a variable height vertical leaf gate exiting into a second stilling pool used for flow measurement via a rectangular contracted weir. Flow exits the measurement weir and is conveyed to the sump where it is recirculated to the constant head tank. An Illustration of the sectional flume is shown in Figure 152.

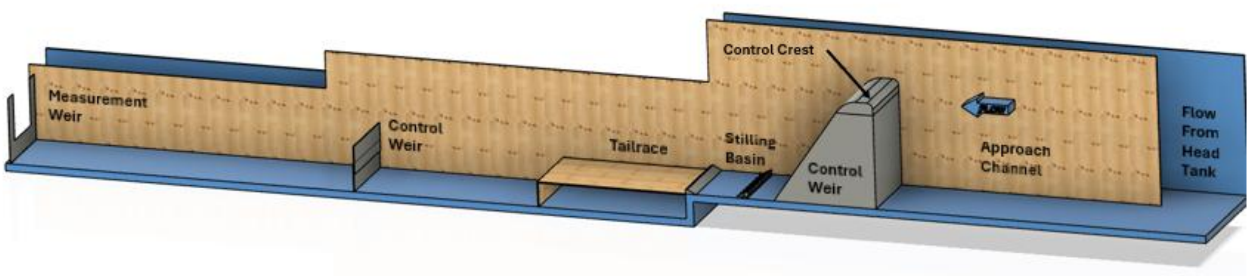

Figure 152. Sectional Flume Configuration, Shown with High Fr_1 Crest

The experiments are conducted in a sectional flume that represents significant upstream and downstream domains to provide for relatively uniform inflow and exit conditions. Since the transition of the basin into the channel is not represented in the sectional model, the prediction of required tailwater to maintain the hydraulic jump action and scour to the extents will represent that of the center of a prototype stilling basin.

The Fr_1 has been demonstrated by many (Riegel and Beebe, 1917; USBR, 1955; USDA, 1959; and USACE, 1965) to be a primary explanatory parameter for the characteristics of the hydraulic jump and the optimum geometry of a baffled hydraulic jump stilling basin. Two Fr_1 were selected for experimental design based on the range of experimental data described in previous sections and the operational range of most baffled hydraulic jump stilling basins for large dams.

5.2.1.2 Similitude

The proposed use of the data obtained is to develop dimensionless parameters that can be scaled to reasonable prototype magnitude. This implies that the laws of Froude similitude must be meet and some major considerations and criteria are subsequently described.

As detailed in Section 5.2.1.5, the minimum Reynolds number within the flume is 171,000. This value is well above the targets identified in Section 2.4 related to viscosity (Re > 10,000) and to represent the advective diffusion layer and air-concentrations within the hydraulic jump (Re > 25,000); although it is not anticipated that the aeration process is fully replicated to the extent expected in typical prototype scales.

The minimum total head on the crest is 0.65 feet (7.8-inches); which is above the 2-inch target to minimize scale effects. This flow-condition corresponds to a Weber number of 2,100 which is significantly above the minimum recommended related to surface tension effects on free overflows (We > 100).

Table 20 details the typical range of flow rates, dimensions, and velocities in which the model data described herein can be applied to prototype conditions.

Table 20. Parameters for Application within Typical Range of Model Scales

Application	Range	Unit Discharge (cfs/ft)	Crest Height (ft)	Incoming Velocity (ft/s)	Incoming Flow Depth (ft)
Model	Min	1.8	1.7	11	0.09
	Max	4.9	5.7	20	0.41
Lr = 15	Min	107	25	43	1.4
	Max	284	85	78	6.2
Lr = 30	Min	301	50	61	2.8
	Max	804	170	111	12
Lr = 60	Min	853	101	86	5.6
	Max	2274	339	156	25

5.2.1.3 Videography

High speed cameras are synchronized to read both the manometer board and capture the flow conditions along the sidewall and from a perspective above the stilling basin and tailrace. These video's are used to document and systematically describe the hydraulic characteristics within the basin and tailrace. Video data is taken for each experiment via time synchronized GoPro Hero 9/10 high capture rate cameras. The cameras were set for a minimum capture rate of 120 frames per second. A total of 3 synchronized cameras were utilized to record an aerial view of the stilling basin, a profile view of the downstream bed and piezometer board (pressure taps and pitot tubes), and a profile view of the full chute/basin/tailrace.

The time synchronization allows for consistent description of the general flow conditions, as well as the propagation of macro-scale turbulent structures as they propagate through the basin and impact the downstream bed. The video were analyzed at scaled speeds to estimate the relative magnitude and quantify the shedding frequency of large turbulent structures and their impact on mobile bed materials. Care was taken to ensure that each experiment will have video capture from the same vantage point.

The positions of the cameras are illustrated in Figure 153 and a typical view from each camera is shown in Figure 154.

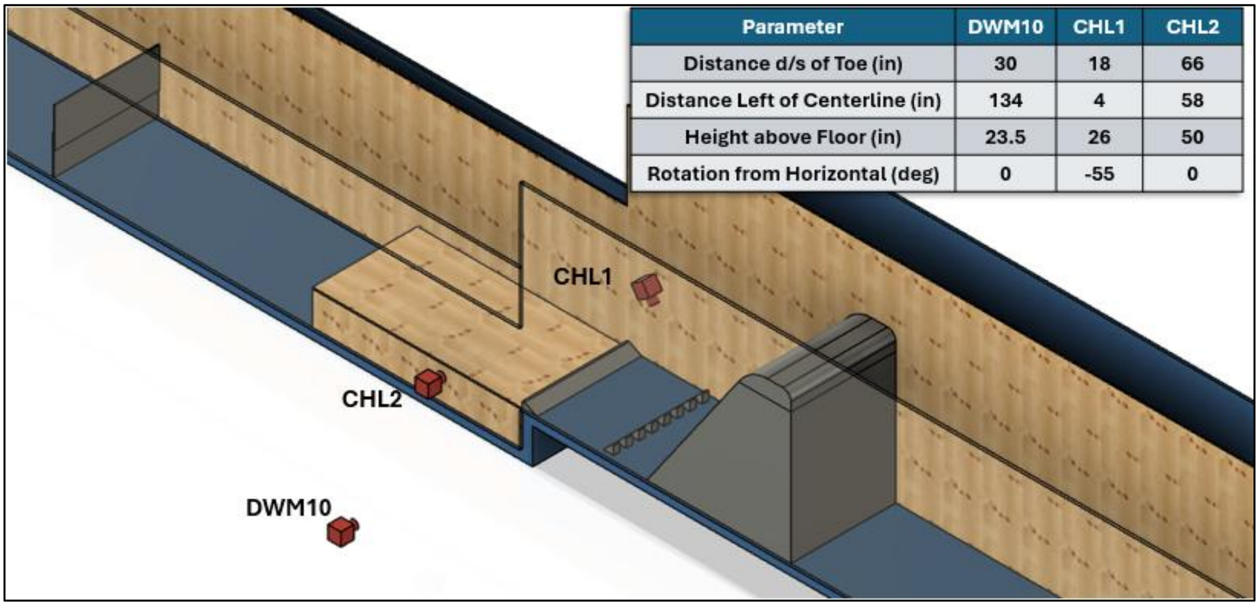

Figure 153. Video Recording Camera Locations

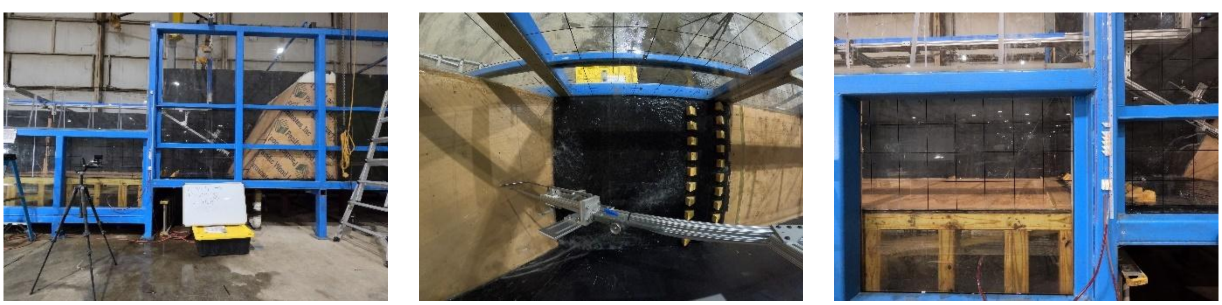

a) Camera DWM10 *b) Camera CHL1* *c) Camera CHL2*

Figure 154. Typical Camera Views

5.2.1.4 Instrumentation and Data Collection

5.2.1.4.1 Headwater

The headwater elevation upstream of the control weir was measured by means of a piezometer tap located approximately 3 feet upstream of the high control weir. A staff gage was mounted on the sidewall for a redundant check on headwater conditions. Once the required static headwater was determined via pre-experiment trials, the readings were marked for each flow condition evaluated. The piezometer board is shown in Figure 155.

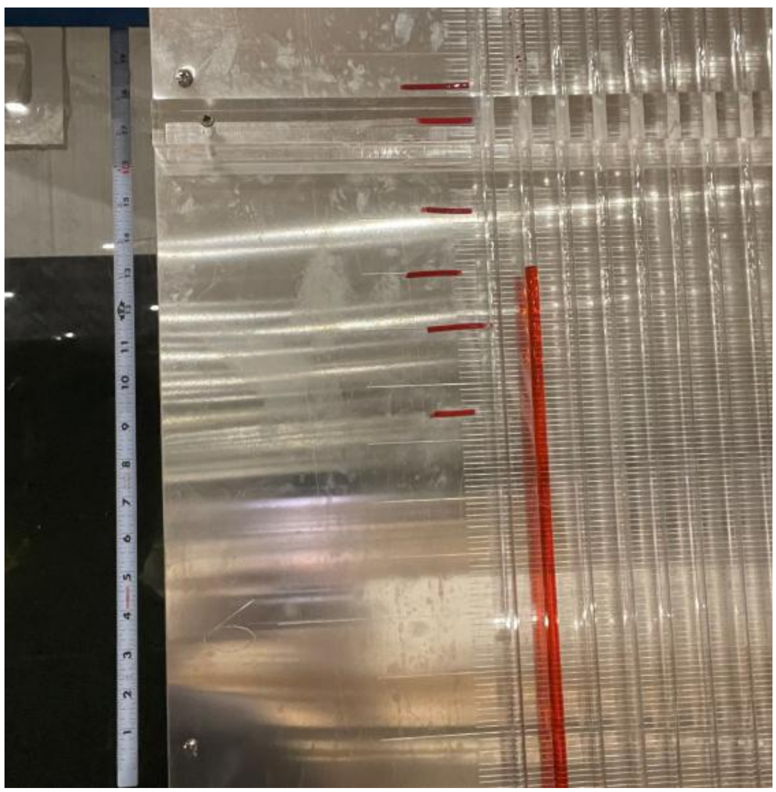

Figure 155. Headwater Piezometer Board

5.2.1.4.2 Incoming Flow Conditions

A movable pitot tube and point gage system was mounted at the base of the chute near the centerline of the flume to measure the velocity and depth of the incoming flow. Both the point gage and pitot tube were mounted perpendicular to the chute and depths are adjustable. The pitot tube and point gage were positioned as close to the toe of the chute as possible with the pitot tube positioned at a height normal to the chute that is 60 percent of the depth gage set to the computed depth.

For the high Fr_1 /weir configurations pre-experiment trials, it was noted that the velocity head measured on the pitot tube at the was nearly identical to the measured hydrostatic head measured upstream of the crest; suggesting that there were negligible losses due to surface roughness. There were no visual observations of turbulence, separation, or other form related losses due to the control crest. The incoming pitot tube and point gage system are shown in Figure 156.

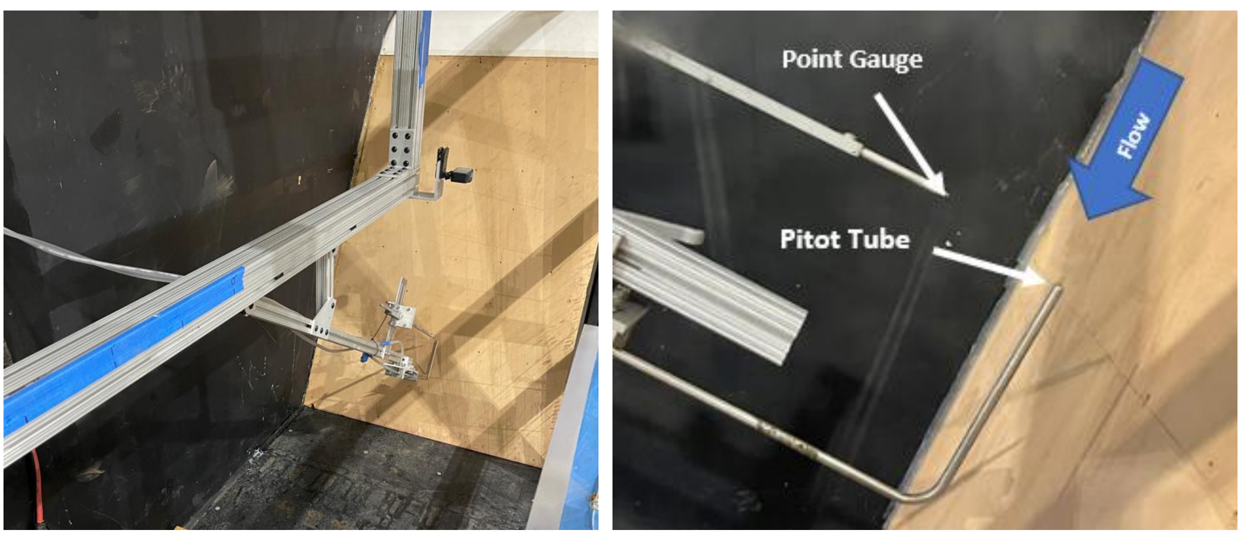

a) Overview *b) Closeup*

Figure 156. Incoming Flow Instrumentation with High Crest

Reliable velocity estimates were not possible for the low Fr_1 / low head crest configuration given the location of the pitot tube was too close to the crest and the flow velocity had not become uniformly aligned normal to the chute. The location of the lowest possible pitot tube setting in relation to the crest is shown in Figure 157.

Figure 157. Incoming Flow Instrumentation with Low Crest

5.2.1.4.3 Within the Stilling Basin

It was planned to use standard pitot tubes and point gages to collect velocity and water surface information throughout the hydraulic jump and tailrace. A carriage mounted system was developed consisting of a combination of a point gage and pitot tube mounted on a level horizontal aluminum beam. The system can slide in a stream-wise direction and the pitot tube was mounted on a point gage so that the exact depth of the instrument could be determined. The system is shown in Figure 158.

a) Overview *b) Closeup*

Figure 158. Instrumentation Carriage for Hydraulic Jump and Tailrace Observations

The velocity within and exiting the baffled hydraulic jump stilling basin was highly turbulent and aerated. The standard Pitot Tube was attempted to collect velocity profiles within and downstream of the stilling basins; although the significant aeration and high turbulence intensity rendered the Pitot Tubes ineffective. An acoustic doppler apparatus and standard velocity meter were attempted as well without reliable velocity measurements. Other means of obtaining detailed velocity estimates within the hydraulic jump where considered, such as Particle Image Velocimetry (PIV); but the significant additional cost and complexity of data collection and analysis was determined not to be commensurate to the knowledge gained in relation to the research objectives. The point gage carriage system was used farther downstream to corroborate the estimate of downstream water surface elevation determined by the piezometer taps.

5.2.1.4.4 Tailwater

A rigid platform is located downstream of the stilling basin at the level of the stilling basin apron, extending for 8 feet downstream. Two piezometers are utilized to measure tailwater, one immediately downstream of the end sill at the centerline of the flume and a second that was approximately 12-feet downstream of the stilling basins and upstream of local influence of the tailgate. The pressure taps and pitot tubes were read on a manometer board that was placed on the beam within the field of view of the tailwater camera so that tailwater readings can be synchronized with the three cameras and that experiments can be conducted by the author without additional staff requirements. Magnetic markers were fabricated so that the tailwater targets for each experiment could be set and checked ahead of the experiment also allowing for additional quality control during review and evaluation of videos. The piezometer system is shown in Figure 159.

Figure 159. Tailwater Piezometer Configuration

5.2.1.4.5 Flow Measurement Weir

A point gage on a mounted carriage system was utilized to measure the static head on the downstream rectangular contracted flow measurement weir. The carriage system allowed for multiple reading to be taken to ensure the measurements are taken at the prescribed distance upstream of the contracted weir. The weir and point gage carriage system are shown in Figure 160.

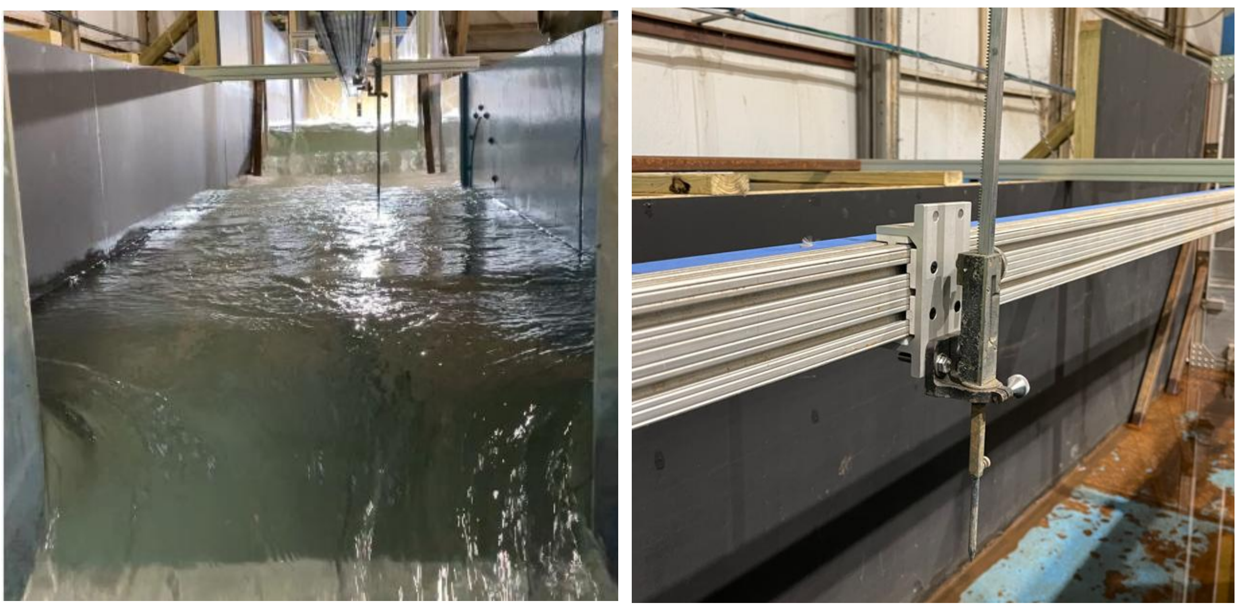

a) Overview *b) Closeup*

Figure 160. Flow Measurement Weir Point Gauge Carriage System

5.2.1.4.6 Procedures and Limitations

For any observation involving the piezometer readings, the piezometer was primed from the manometer board by injecting water via a custom nozzle until the line was full and without air. Then red dye was injected into the piezometer so that readings could be captured on the videography. For all flow conditions, the target headwater piezometer and staff gage stage was verified and corroborated with a point gage reading for the downstream measurement weir.

The only reliable velocity measurements were taken at the chute pitot tubes, near the toe of the chute. The conditions were not conducive to velocity measurement by acoustic doppler, standard velocity measurements, or pitot tubes within the jump and immediately downstream. In addition, the vicinity had significant aeration and separation of the water surface making water surface observations via the point gage carriage system not feasible. Within the exit channel, both the downstream piezometer and the point gage were interpreted as highly accurate and corroborated each other to a high precision. The near structure tailwater piezometer tap within the rigid floor showed inconsistent readings, often lower than the point gage and downstream piezometer tap. This piezometer was prepared for each experiment, although not utilized to set tailwater or determined required tailwater.

USBR (1980) determined that the surge and wave heights within stilling basins can be more accurately determined from slow motion video than from direct measurement, as well as the observational nature of performance associated with spillways and energy dissipators. Also, the determination of the turbulent conditions downstream of the basin and the loss of the hydraulic jump action was determined to be most accurately evaluated via slow motion replay of the experiments from multiple camera angles.

5.2.1.5 Flow Conditions

The discharges for both "High" and "Low" Fr_1 basins were held constant, while the v_1 and d_1 were varied with the use of different crest heights. The design unit discharge for all the basins q_D, for both incoming Froude numbers is 12.2 $\frac{\mathrm{ft}^3}{\mathrm{s}}$. This results in a unit discharge of 3.1 $\frac{\mathrm{ft}^3}{\mathrm{s}}$. This unit discharge was selected to enable the evaluation significantly above and below the design discharge, while maintaining the guidelines and recommendations for Froude scale modeling to meet the dynamic similitude previously described for the lower flow conditions. The maximum discharge of the experiments is 19.6 $\frac{\text{ft}^3}{\text{s}}$; which provides for evaluation of each basin to a unit discharge of 60 percent greater than that of design. The flow conditions evaluated and the corresponding depth averaged Reynolds number assuming the kinematic viscosity of water at 20 deg C is detailed in Table 21.

Table 21. Flow Conditions for the Evaluation of Various Stilling Basin Configurations

Ratio of Design Discharge (q_a/q_D)	Flow Description	Unit (cfs/ft)	Unit (m^2/s)	Total (cfs)	Reynolds Number (Re)
0.6	q_{60}	1.83	0.17	7.34	1.71E+05
0.8	q_{80}	2.45	0.23	9.78	2.27E+05
1.0	q_D	3.06	0.28	12.23	2.84E+05
1.2	q_{120}	3.67	0.34	14.68	3.41E+05
1.4	q_{140}	4.28	0.40	17.12	3.98E+05
1.6	q_{160}	4.89	0.45	19.57	4.55E+05

For the High Fr_1, the total approach head on crest associated with various discharge values were estimated using the standard equation for a broad crest weir and the discharge coefficients from Brater and King (1996). The incoming flow conditions were estimated utilizing the empirical method from USBR (1984) described in Section 1.2, assuming a total loss of 5 percent down the chute.

During the pre-experiment trials, the static headwater was determined through trial and error based on the depth and velocity observations near the toe of the chute. The observations of velocity head and static head in the approach channel were nearly identical, with the largest variation being 0.03 feet between the static head on the crest and the dynamic pitot tube reading (representing the velocity head). This suggests that no loss should be applied when using the USBR (1984) empirical method to determine the incoming flow conditions.

The partially contracted rectangular sharp-crest weir was fabricated and installed on the downstream end of the flume. The weir was designed to fit within the 4-feet width of the flume; while providing adequate contraction and fit within the available operating depths available. The weir and rating curve was developed in accordance with the criteria outlined in USBR (2001) and with the assistance of the USBR technical centers sharp-crest weir spreadsheet tool which is based on the procedures outlined therein.

During the pre-experiment trials, measurements of the head on the measurement weir and associated discharge values were compared with those derived based on continuity with the pitot tube velocity estimates and depth observations. The target discharge, estimated discharge based on the measurement weir, estimated discharge from the incoming flow conditions, and the percent difference between the measurement weir and the incoming flow condition observations are presented in Table 22.

Table 22. Measurement Weir and Incoming Flow Conditions Discharge Estimate Summary

Flow Desc.	Target q_T (cfs/ft)	Trial 1				Trial 2			
		Calc. from Pitot q_P (cfs/ft)	q % Diff $(\frac{q_P-q_T}{q_T})$	Calc. from Weir q_W (cfs/ft)	q % Diff $(\frac{q_W-q_T}{q_T})$	Calc. from Pitot q_P (cfs/ft)	q % Diff $(\frac{q_P-q_T}{q_T})$	Calc. from Weir q_W (cfs/ft)	q % Diff $(\frac{q_W-q_T}{q_T})$
q_{60}	1.83	1.86	2%	1.82	-1%	1.87	2%	1.84	<1%
q_{80}	2.45	2.50	2%	2.61	6%	2.50	2%	2.55	4%
q_D	3.06	3.11	2%	2.87	-7%	3.12	2%	3.02	-1%
q_{120}	3.67	3.76	2%	3.71	1%	3.76	3%	3.83	4%
q_{140}	4.28	4.41	3%	4.53	6%	4.41	3%	4.57	6%
q_{160}	4.89	5.04	3%	5.06	3%	5.04	3%	5.02	3%

A comparison of the target unit discharge, average estimated based on incoming flow conditions, and average estimated from partially contracted rectangular sharp-crest weir is shown in Figure 161.

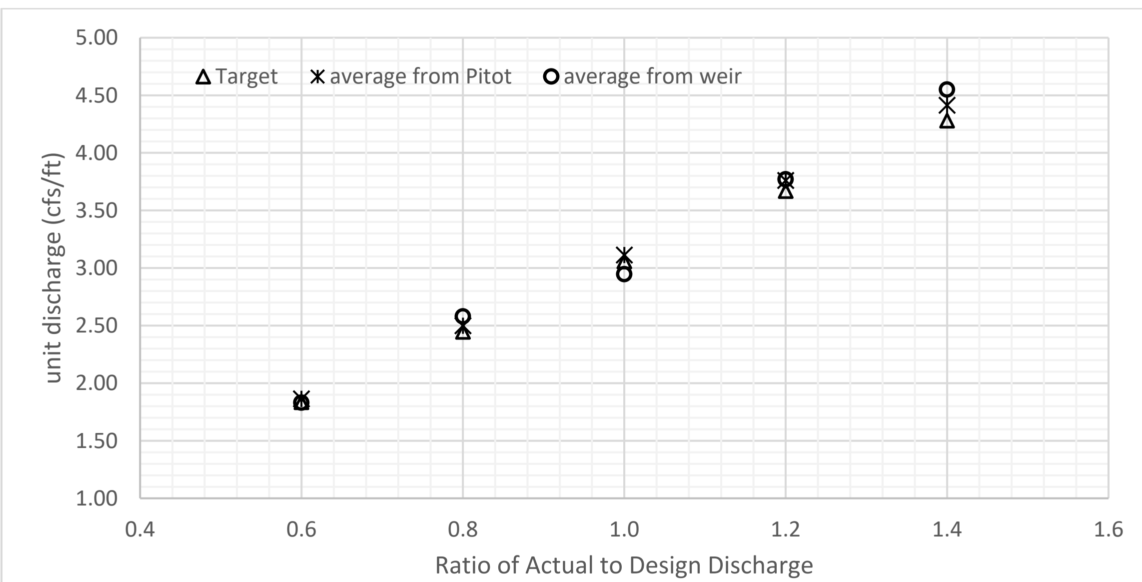

Figure 161. Plot of Target, Avg. Est. from Incoming Flow Conditions, and Avg. Est. from Measurement Weir

As described in Section 5.2.1.4.2, the incoming flow conditions for the Low Fr_1 could not be estimated reliably from the pitot tube and depth gage due to the required distance from the floor of the stilling basin to the tip of the pitot tube. To match the discharge values used for the

High Fr_1, the headwater readings for the Low Fr_1 were based on the average observations from the measurement weir. The headwater condition for each configuration was established by increasing flow until the average observed stage on the measurement weir point gage from the pre-experiment trials was achieved. This was to ensure that the unit discharges were the same between the High- and Low- Fr_1 experiments. The incoming v_1 and d_1 for the Low Fr_1 experiments was based on the procedure for short spillways prescribed in USACE (1987) and shown in Equation 5.

5.2.1.6 Tailwater

The tailwater is controlled via a two leafed vertical slide gate shown in Figure 162.

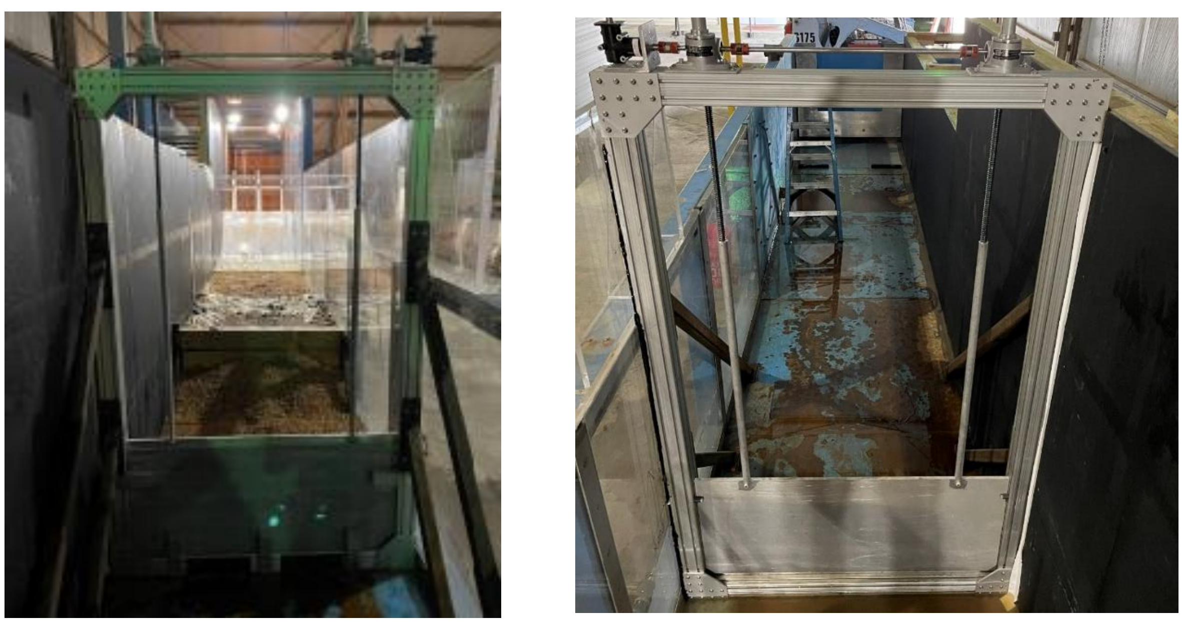

a) Looking Upstream, Keystone Configuration   *b) Looking Downstream*

Figure 162. Tailgate for Control of Stilling Basin Tailwater

The tailwater varies from the computed sequent depth to the point of loss of the hydraulic jump. These are computed for each crest (High and Low Fr_1) and flow condition ($q_{60,}$ q_{80}. Q_D q_{120} q_{140} q_{160}).

5.2.1.6.1 High Froude Number Configurations

The Tailwater used for the High Fr_1 experiments for each ratio of tailwater are based on the planned incoming flow conditions and using the sequent depth as computed in Equation 1. Initially, the tailwater scenarios were meant to represent ratios of the $\frac{d'_2}{d_2}$ of 1.0, 0.9, 0.85, 0.8, 0.75, and 0.70; but due the discrepancies from the planned to updated incoming flow parameters, alphabetic descriptor will be used subsequently to describe the tailwater scenarios. The tailwater depths used for the High Fr_1 experiments are detailed in Table 23.

Table 23. Tailwater Depths used for High Froude Number Configurations

Tailwater Scenario / Flow Ratio (q'/q)	Tailwater Depth Used (ft)					
	1	0.6	0.8	1.2	1.4	1.6
A	1.81	1.40	1.62	1.98	2.13	2.28
B	1.63	1.26	1.46	1.78	1.92	2.05
C	1.54	1.19	1.38	1.68	1.81	1.94
D	1.45	1.12	1.30	1.58	1.70	1.82
E	1.36	1.05	1.22	1.49	1.60	1.71
F	1.27	0.98	1.13	1.39	1.49	1.60

The tailwater ratios reported and plotted subsequently are based on the updated estimate of the d_2 for each flow condition. The tailwater depths for each High Fr_1 scenario represent the ratios of $\frac{d'_2}{d_2}$ detailed in Table 24.

Table 24. Tailwater Ratios for High Froude Number Configurations

Tailwater Scenario / Flow Ratio (q'/q)	Ratio of d'/d_2 for High Fr_1 Experiments					
	1	0.6	0.8	1.2	1.4	1.6
A	0.97	0.97	0.97	0.97	0.96	0.97
B	0.87	0.87	0.87	0.87	0.87	0.87
C	0.82	0.82	0.82	0.82	0.82	0.82
D	0.77	0.77	0.77	0.77	0.77	0.77
E	0.73	0.72	0.73	0.73	0.72	0.72
F	0.68	0.68	0.68	0.68	0.68	0.68

5.2.1.6.2 Low Froude Number Configurations

The tailwater depths used for the Low Fr_1 configurations were developed in the same manner as the High Fr_1 configurations and are detailed in Table 25.

Table 25. Tailwater Depths used for Low Froude Number Configurations

Tailwater Scenario / Flow Ratio (q'/q)	Tailwater Depth Used (ft)					
	1	0.6	0.8	1.2	1.4	1.6
A	1.48	1.13	1.29	1.64	1.78	1.91
B	1.33	1.01	1.17	1.47	1.60	1.72
C	1.26	0.95	1.10	1.39	1.51	1.63
D	1.18	0.90	1.04	1.31	1.42	1.53
E	1.11	0.84	0.97	1.22	1.33	1.43
F	1.04	0.79	0.91	1.15	1.24	1.34

The tailwater ratios reported and plotted subsequently are based on the updated estimate of the d_2 for each flow condition based on the actual specific head upstream of the crest and Equation 5. The tailwater depths for each Low Fr_1 scenario represent the ratios of $\frac{d'_2}{d_2}$ detailed in Table 26.

Table 26. Tailwater Ratios for Low Froude Number Configurations

Tailwater Scenario / Flow Ratio (q'/q)	Ratio of d'/d_2 for High Fr_1 Experiments					
	1	0.6	0.8	1.2	1.4	1.6
A	1.02	1.01	1.00	1.02	1.02	1.02
B	0.92	0.91	0.90	0.91	0.92	0.92
C	0.86	0.86	0.85	0.87	0.86	0.87
D	0.81	0.81	0.80	0.81	0.81	0.82
E	0.76	0.76	0.75	0.76	0.76	0.77
F	0.71	0.71	0.70	0.71	0.71	0.72

5.2.1.7 Basin Geometry

The baffle hydraulic jump basins for evaluation consist of the standard USACE basin described in USACE EM 1110-2-1603 (1992), the Standard USBR Type III (USBR, 1955; USBR, 1984), and the USBR Type III with tapered blocks and intermittent ramp (USBR, 2009; USBR, 2012). The selection of these three basins is based on the wide number of existing basins for large dams are of the USACE or Standard USBR Type III type; and the limited data on the tapered block as it compares to the other two types.

The basin parts are fabricated from acrylic, wood, and smaller pieces are 3D printed. The parts (excluding the toe-curve and chute blocks) are connected to the basin floor via strong magnets for ease of adjustment. The basin floor is comprised of thick steel plate to allow for magnetic connections and rigidity with dynamic pressure fluctuations. It was found to be critical that each baffle block was secured in place with a small amount of silicon and allowed to cure prior to experiments to minimize the potential for baffle block movement.

Examples of baffle blocks proposed for use in experiments are shown in Figure 163 and Figure 164. These blocks represent the same incoming flow conditions for various design guidance.

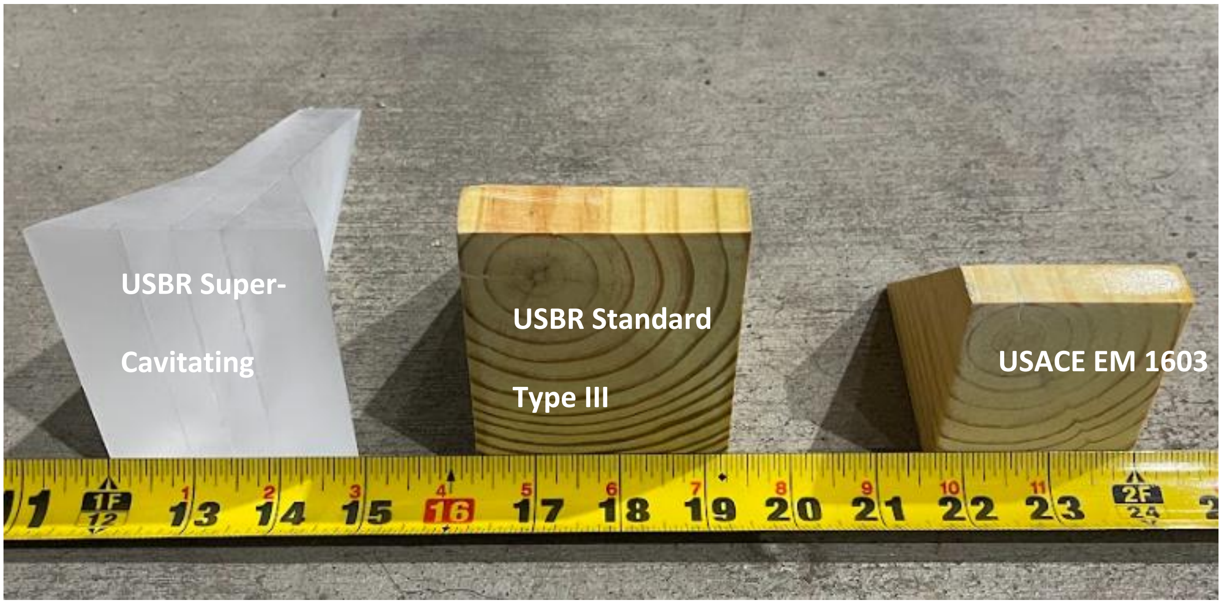

Figure 163. Baffle Block Geometries

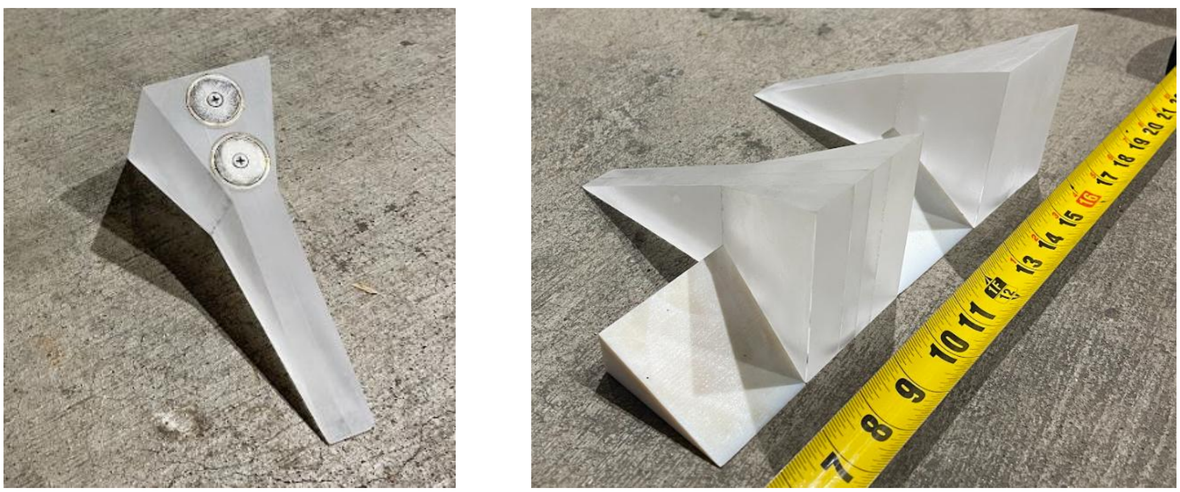

Figure 164. Baffle Magnetic Connection (left) and Intermittent Ramps (right)

The variation in Fr_1 was established by adjusting the drop height via the construction of two different crest heights. The high crest provides a drop height of 5.65 feet from the crest to the basin apron, producing an estimated incoming Froude number of approximately 8 for the basin design discharge. The low crest has a drop height of 1.65 feet and produced an estimated Fr_1 of approximately 4 for the design discharge. Both control weirs have a rounded upstream shape and a parabolic downstream shape to provide for smooth transition into the chute section. A broad crest weir was attempted but resulted in separation and severe disturbance down the chute.

It is worth noting that a range of Fr_1 were simulated as the incoming unit discharge is adjusted. Increasing unit discharge will result in decreasing Fr_1 as the flow depth increases for similar velocities.

5.2.1.7.1 Toe Curve

To better understand the influence of impingement angle of the chute with the horizontal apron of the Basin, a removable toe curve is utilized. USACE (1992) states that a minimum bucket radius of 4 times the flow depth should be used for trajectory buckets. USBR (1987) states a minimum radius of 5 times the flow depth "…have been found acceptable" for the reverse curve at the lower end of the Ogee Crest. For concave curves in general, it is recommended a minimum radius of 10 times the flow depth (USBR, 1987). The adopted toe curve radius is 20 inches, representing 10 times the estimated incoming flow depth for the design discharge for the high Froude number basins. An illustration of the toe curve for the USBR Type III stilling basin is provided in Figure 165.

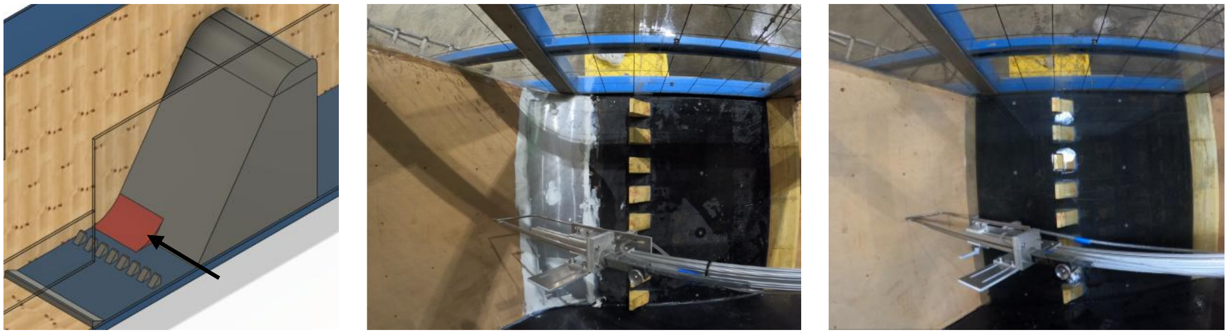

a) CAD Isometric View *b) With Toe Curve (3c)* c) *Without Toe Curve (3a)*

Figure 165. Comparison of with and without Toe Curve

Based on the limited influence determined from the High Fr_1 experiments and the relatively short weir height, no toe curve was used for the Low Fr_1 experiments. USACE (1987) states that "Toe curves at the intersection of the downstream spillway face and the stilling basin floor are not widely used in low-head navigation dams."

5.2.1.7.2 High Froude Number Configurations

There were 10 configurations evaluated with a design Fr_1 of 8.2 illustrated in Figure 166, with detailed dimensions provided in Table 27.

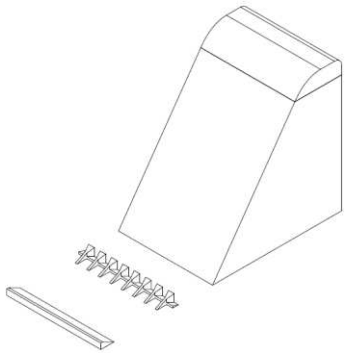

a) Configuration 1a

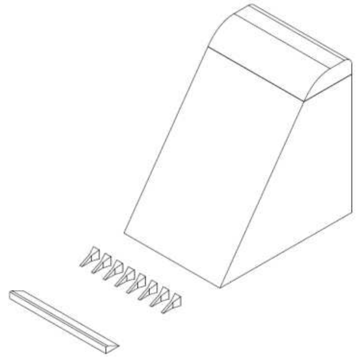

b) Configuration 2a

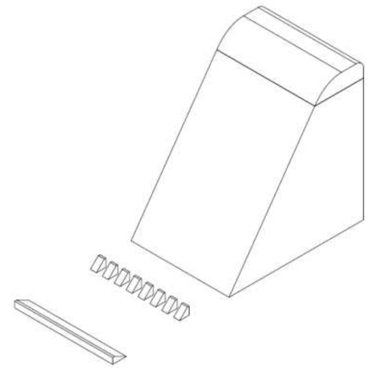

c) Configuration 3a

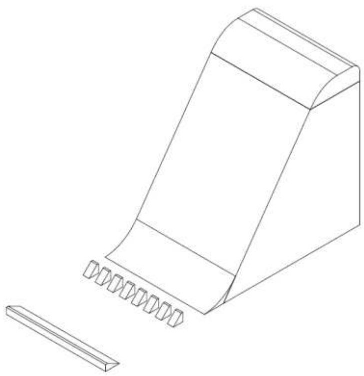

d) Configuration 3c

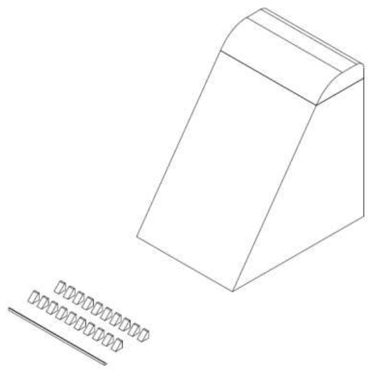

e) Configuration 4a

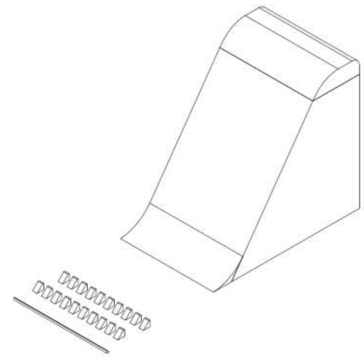

f) Configuration 4c

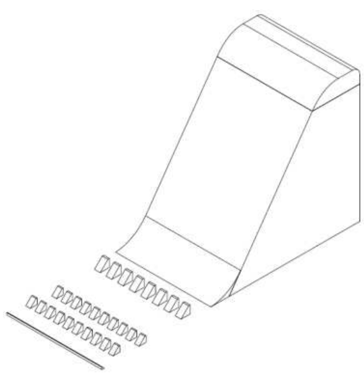

g) Configuration 5c

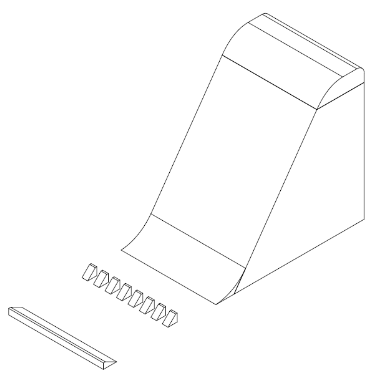

h) Configuration 6c

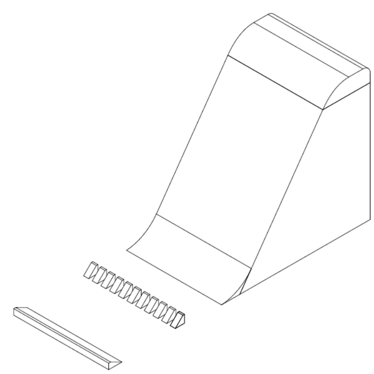

i) Configuration 7c

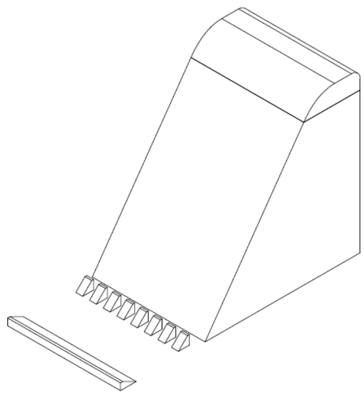

j) Configuration 8a

Figure 166. High Froude Number Stilling Basin Configurations

Table 27. Dimensions of High Froude Number Basin Configurations

Parameter[1]/ Configuration	1a	2a	3a	3c	4a	4c	5c[2]	6c	7c	8a
Basin Length (L_{SB})[3]	57.0	57.0	57.0	57.0	64.1	64.1	64.1	66.2	66.2	36.0
Baffle Height (H_B)	3.9	3.9	3.9	3.9	2.9	2.9	3.9/2.9	3.9	3.9	3.9
Baffle Top Width (W_T)[4]	0	0	0.78	0.78	0.58	0.58	0.78/0.58	0.78	0.78	0.78
Baffle Width (W_B)	2.91	2.91	2.91	2.91	2.32	2.32	2.91/2.32	2.91	2.59	2.91
Baffle Space (W_S)	2.91	2.91	2.91	2.91	2.31	2.31	2.91/2.31	2.91	1.79	2.91
Baffle Blockage Ratio (R_B)	0.50	0.50	0.50	0.50	0.50	0.50	0.50	0.50	0.59	0.50
Baffle Slenderness Ratio (R_s)[5]	1.33	1.33	1.33	1.33	1.25	1.25	1.33/1.25	1.33	1.50	1.33
Block Shape [6]	Tape.	Tape.	Std.	Std.	Std.	Std.	Std.	Std.	Std.	Std.
Intermittent Ramps	Yes	No	No	No	No	No	No	No	No	No
Distance to 1st Row (L_{1B})	17.4	17.4	17.4	17.4	41.04	41.04	17.4	26.59	26.59	4.5
Distance to 2nd Row (L_{2B})	N/A	N/A	N/A	N/A	51.89	51.89	41.04	N/A	N/A	N/A
Distance to 3rd Row (L_{3B})	N/A	N/A	N/A	N/A	N/A	N/A	51.89	N/A	N/A	N/A
End sill Height (H_S)	2.85	2.85	2.85	2.85	1	1	1	2.85	2.85	2.85
Exit Slope of Sill H:V (S_{ES})	2	2	2	2	1	1	1	2	2	2

[1] All dimensions are in inches
[2] Configuration 5c utilizes both USBR (1984) and USACE (1992) baffle blocks
[3] Basin length measured from point of tangency with stilling basin floor and chute to the downstream end of the end sill
[4] Top width is the flat portion of the top of the baffle (zero represents a sharp edge)
[5] Slenderness Ratio take as H_B/W_B
[6] Tapered Blocks (Tape.) include a 3H to 1V sidewall and top taper or Standard Blocks (Std.) which have parallel sidewalls and a flat top section

These configurations utilized either the USBR (1984) or the USACE (1992) standard geometries with variations to the block shape (standard/tapered), block width (standard/slender), length to the blocks, inclusion of additional row of blocks, toe curve (with or without).

The objective of configurations 1a, 2a, and 3a is to compare the relative impacts associated with the tapered blocks and intermittent ramps (USBR, 2009). All three configurations are the prescribed length, distance to blocks, block height, block width, blockage ratio, and end sill dimensions from USBR (1984); without the presence of a toe curve or chute blocks. The shape of the baffles for R1a are modified from the standard shape based on USBR (2009); consisting of a side wall and top that is tapered at a 3-horizontal to 1-vertical and has an intermittent ramp between the blocks with a height of ¼ the block height and an out slope of 3-horizontal to 1-vertical. Configuration 2a is the same configuration as 1a with the omission of the intermittent ramps. Configuration 3a has the same basin and block face dimensions; although utilizes the standard block sidewall and top shape.

Configurations 3c and 6c were developed with the objectives to evaluate the influence of the toe curve on the basin length and performance of the basins. Configuration R3c is the same basin length, distance to blocks (as measured from the point of tangency of the chute and the basin), block height, block width, blockage ratio, block shape, and end sill configuration as R3a; with the addition of the toe curve described in Section 5.2.1.7.1. Configuration R6c has the same baffle block and end sill configuration, although both the length of the basin and the distance to the blocks are increased to account for the radius of the toe curve; starting the measurement at the end of the toe curve instead of the point of tangency.

Configurations 4a and 4c were developed to evaluate the performance of the USACE (1992) stilling basin with and without the toe curve and to compare the performance to that of the standard USBR (1984) stilling basin. Both configurations consist of two rows of the standard baffle shape with the baffle height, baffle width, baffle spacing, distance to 1st row and distance to 2nd row determined by USACE (1992).

Configuration 5c was developed to determine the impact of placing USBR (1984) blocks upstream of the 1st row of USACE (1992) within a standard USACE (1992) basin. This was to provide information for modifications to Keystone Dam being considered at the time of the experiments.

Configuration 7c utilizes the prescribed basin length, distance to baffles, baffle height, and standard shape from USBR (1984); although the baffle width, baffle space, and blockage ratios are modified. The configuration provides a reduced block width and block space, resulting in a more slender block ($H_b/W_b = 1.5$) with an increased blockage ratio ($W_B / (W_B + W_S) = 0.59$).

Configuration R8a was developed with the objective of evaluating a reduced length basin similar to that developed for the Gross Reservoir enlargement project. This configuration utilizes the standard USBR (1984) block shape, block height, and block width; although the distance to the baffles was reduced from 0.8 D_2 to 0.2 D_2. The overall length of the basin was reduced from 2.6 D_2 from the prescribed length, to 1.7 D_2.

All the basin configurations were developed prior to the pre-experiment trials and final crest configurations; and therefore, an estimate of geometry based on the updated estimate of incoming velocity and the observed flow depth. This resulted in the following discrepancy between the actual tested configuration and the calibrated incoming flow conditions (Fr_1, v_1, and d_1); which are detailed in Table 28.

Table 28. Comparison of Planned verse Calibrated Incoming Flow Conditions

Parameter	Used	UPDATED	% Difference
Fr_1	8.18	8.95	9%
v_1 (ft/s)	18.8	19.9	6%
d_1 (ft)	0.163	0.154	-6%

The actual basin dimensions used in the experiments and those computed assuming the calibrated incoming flow conditions are compared in Table 29.

Table 29. Comparison of High Fr_1 Stilling Basin Dimensions (used verse estimated with calibrated incoming flow parameters)

Configuration	Dimension	USED for Experiments Fr_1, v_1, d_1 (ft)	ESTIMATED Dimension based on UPDATED Fr_1, v_1, d_1 (ft)	Percent Difference
1a, 2a, 3a, 3c, 5c, 6c, and 7c	Basin Length	4.75	4.95	4%
	Baffle Height	0.32	0.33	1%
	Sta of Baffles	1.45	1.49	3%
	End Sill Height	0.24	0.23	-3%
4a and 4c	Basin Length (L_{SB})	5.34	5.76	8%
	Baffle Height (H_B)	0.24	0.24	1%
	Sta of Baffles (1st Row)	3.43	3.71	8%
	End Sill Height	0.082	0.077	-6%

5.2.1.7.3 Low Froude Number Configurations

As previously referenced, there are many large dam spillways that have stilling basin design floods that produce incoming flow conditions with relatively low Fr_1 numbers (i.e. below 4.5). In the case of run-of-river dams associated with navigation structures, these conditions can be below the effectiveness of the hydraulic jump as an energy dissipator whereas the function of the structure is primarily to prevent scour and undermining of the structure.

Low Fr_1 basin configurations were developed for identical unit discharge (and associated critical depth). Based on the observations and comparison results from the High Fr_1 experiments, all Low Fr_1 configurations were evaluated without a toe curve. The six configurations evaluated with a design Fr_1 of ~4 is illustrated in Figure 167, with detailed dimensions provided in Table 30.

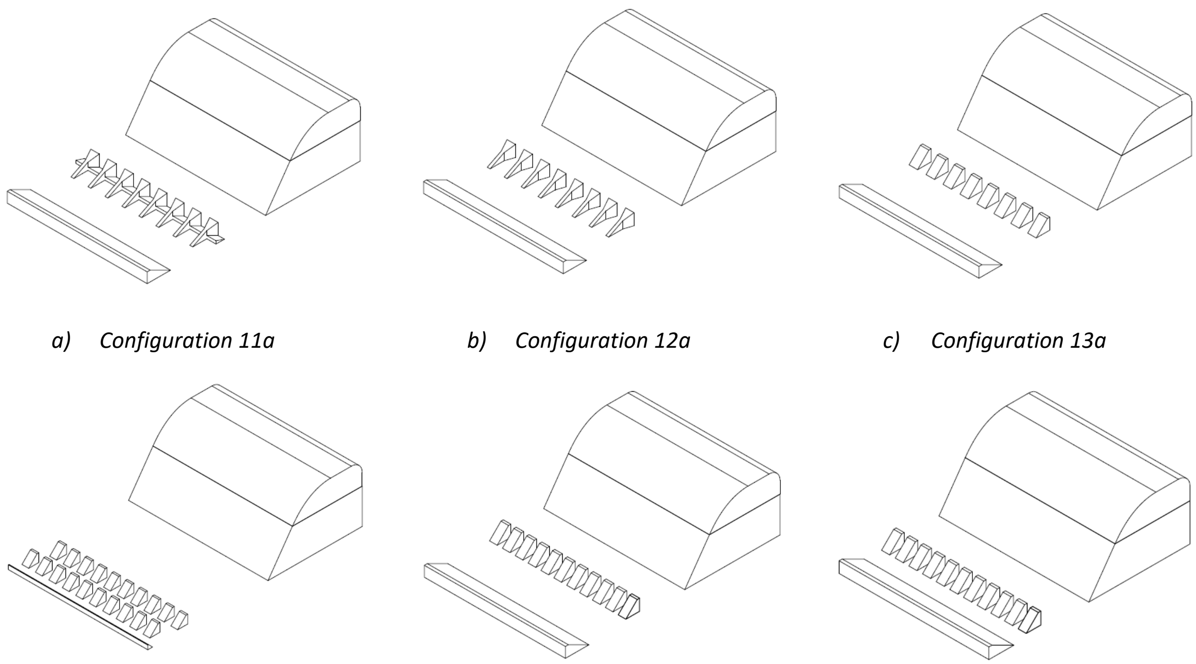

a) Configuration 11a *b) Configuration 12a* *c) Configuration 13a*

d) Configuration 14a *e) Configuration 15a* *f) Configuration 16a*

Figure 167. Low Froude Number Stilling Basin Configurations

Table 30. Dimensions of Low Froude Number Basin Configurations

Parameter/Configuration	11a	12a	13a	14a	15a	16a
Basin Length (LSB)	40.6	40.6	40.6	57.0	40.6	32.0
Baffle Height (HB)	3.9	3.9	3.9	3.9	2.9	2.9
Baffle Top Width (WT)	0.78	0.78	0.78	0.78	0.58	0.58
Baffle Width (WB)	2.9	2.9	2.9	2.9	2.3	2.3
Baffle Space (WS)	2.9	2.9	2.9	2.9	2.3	2.3
Baffle Blockage Ratio (RB)	0.50	0.50	0.50	0.50	0.50	0.50
Slenderness Ratio	1.33	1.33	1.33	1.33	1.25	1.25
Block Shape	Tape.	Tape.	Std.	Std.	Std.	Std.
Intermittent Ramps	Yes	No	No	No	No	No
Distance to 1st Row (L1B)	14.1	14.1	14.1	26.8	14.1	14.1
Distance to 2nd Row (L2B)	N/A	N/A	N/A	34.0	N/A	N/A
End sill Height (HS)	3.5	3.5	3.5	1.4	3.5	3.5
Exit Slope of Sill H:V (SES)	2	2	2	1	2	2

Similar to the High Fr_1 configurations, the incoming flow conditions planned for the low Fr_1 configurations are also slightly different. For the Low Fr_1 basins the ultimate actual velocity was slightly underestimated in planning verse those assumed for the experiments. This resulted in the following discrepancy between the actual tested configuration and the calibrated incoming flow conditions (Fr_1, v_1, and d_1); which are detailed in Table 31.

Table 31. Comparison of Planned verse Calibrated Incoming Flow Conditions

Parameter	Used	Updated	% Difference
Fr_1	4.84	4.7	-2%
v_1 (ft/s)	13.2	13.0	2
d_1 (ft)	0.23	0.24	-3

A summary of the dimensions used in the experiments based on planned incoming flow conditions, the estimated dimensions with the actual incoming flow conditions, and the percent difference is included in Table 32.

Table 32. Comparison of Dimensions Used verse those based on Updated Incoming Flow Conditions

Configuration	Dimension	USED for Experiments Fr_1, v_1, d_1 (ft)	ESTIMATED Dimension based on UPDATED Fr_1, v_1, d_1 (ft)	Percent Difference
11a, 12a,13a, 15a 16a[1]	Basin Length	3.38	3.30	-2%
	Baffle Height	0.32	0.32	0%
	Sta of Baffles	1.18	1.16	-1%
	End Sill Height	0.29	0.29	1%
14a	Basin Length (L_{SB})	3.447	3.364	-2%
	Baffle Height (H_B)	0.242	0.242	0%
	Sta of Baffles (1st Row)	0.097	0.097	0%
	End Sill Height	2.231	2.182	-2%

There is a minimal difference between the planned and updated incoming flow parameters and associated basin dimensions for the Low Fr_1 configurations.

Based on the observations of the limited influence of the end sill for the USBR (1984) configuration during the experiments, configuration 16a was developed to evaluate the impacts of moving the end sill upstream thereby shortening the basin length. The L_{SB} for configuration 16a is reduced from that of 15a by approximately 20-percent. This results in a dimensionless ratio of $\frac{L_{SB}}{d_2}$ being reduced from approximately 2.3 to 1.8.

5.2.2 Results

5.2.2.1 High Froude Number Physical Model Observations

Data collected during the experiments described in Section 5.1 were analyzed to evaluate the variations in performance related to the various basin configurations and flow conditions.

[1] The stilling basin length was experimentally derived and therefore not affected by differences in incoming flow parameters.

Principle, the high-speed capture videos were systematically evaluated to determine the following:

1) General flow conditions within and exiting the basin,
2) The required tailwater to maintain the hydraulic jump action,
3) The strength and frequency of near bed turbulence structures along the exit channel bed,
4) The maximum boil height within the stilling basin,
5) The minimum angle of the hydraulic jump within the basin,

Based on preliminary evaluation of observations, detailed data was not extracted from the videography for configurations 5c and 8a.

5.2.2.1.1 Required Tailwater

As aforementioned, the principal mechanism for energy dissipation provided by the hydraulic jump stilling basin is associated with the internal turbulence produced within the jump action along the shear layer interface. If the hydraulic jump action is lost (i.e. sweepout), there is an associated loss of energy dissipation, significant momentum transferred to the baffle blocks, loss of the weight of water in the basin to resist uplift forces on stilling basin slabs, and potential for severe erosion downstream of the basin.

To determine the tailwater required to maintain the hydraulic jump, the tailwater control gate was slowly lowered until the hydraulic jump was lost, then raised again to restore the hydraulic jump action. This was repeated a minimum of three times. The time synchronized videos are then slowed to a reduced speed of 25- to 50-percent of actual to make more precise evaluation of the tailwater condition at the time the hydraulic jump was lost. The observed tailwater documented herein represents the tailwater immediately prior to the transition into a loss of hydraulic jump action as shown in Figure 134. Camera CHL2 is positioned at a location to read the tailwater PZ board and therefore accurately measure the tailwater prior to the transition. As demonstrated in Section 5.1.2, there is a transitional range with decreasing tailwater.

An example of the conditions just prior to (top) and after the initiation of the transition into the loss of the hydraulic jump action (bottom) are shown for the multiple camera angles (a, b, c) in Figure 168. The tailwater stage is measured from the camera observations from Camera CHL2 as shown in column c.

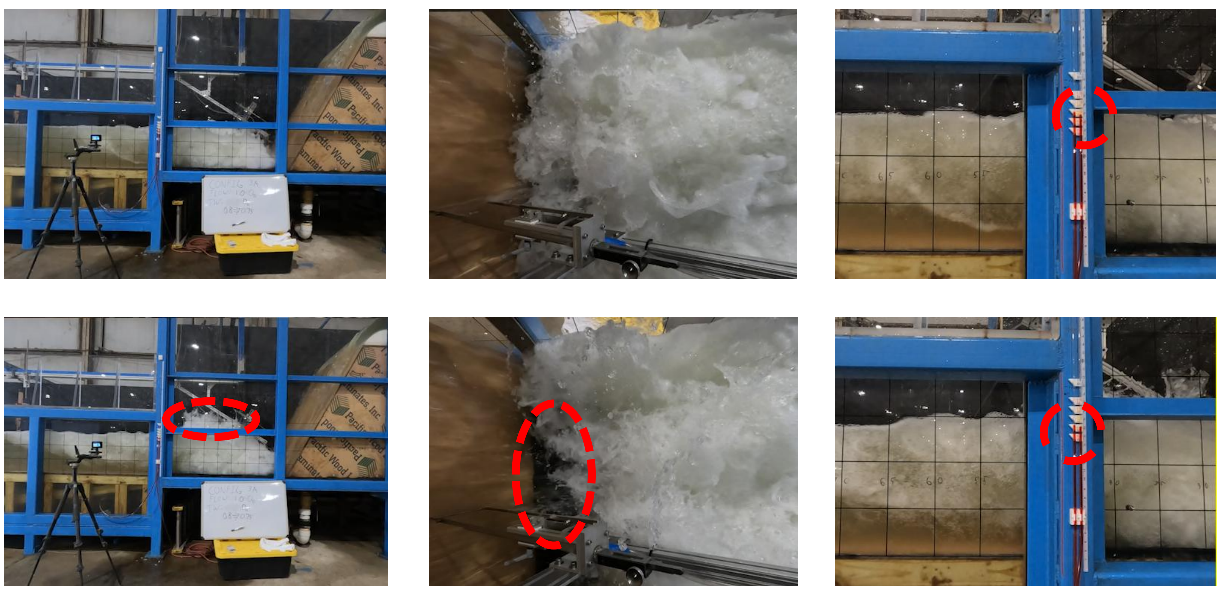

a) Side (DWM10) *b) Top (CHL1)* *c) Tailwater Piezometer (CHL2)*

Figure 168. Example of Determining Required Tailwater using Time Synchronized Cameras

The transition of the High Fr_1 configurations were determined by the combination of the excessive baffle impact and associated detached spray from the baffles that can be observed from the side view camera and the toe of the jump moving downstream from the upstream end of the basin as observed from the top view camera.

The general characteristics of the conditions upon loss of the hydraulic jump are important for both the loss of resisting force provided by the weight of water within the basin and related to the potential increase in scour potential and location associated with the resulting shooting jet. An illustration of the typical conditions immediately before and after loss of the hydraulic jump action are provided for the q_{60} for each of the High Fr_1 flow conditions in Figure 169.

a) Configuration 1a (Maintained)

b) Configuration 1a (lost)

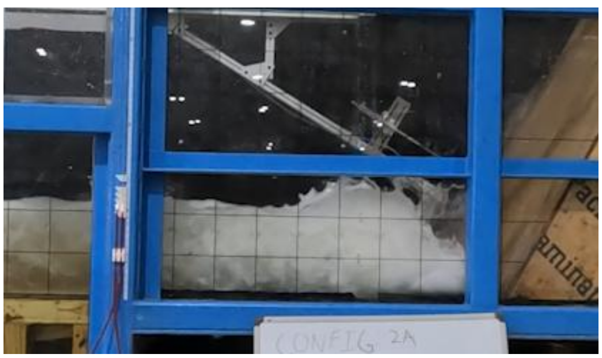

c) Configuration 2a (Maintained)

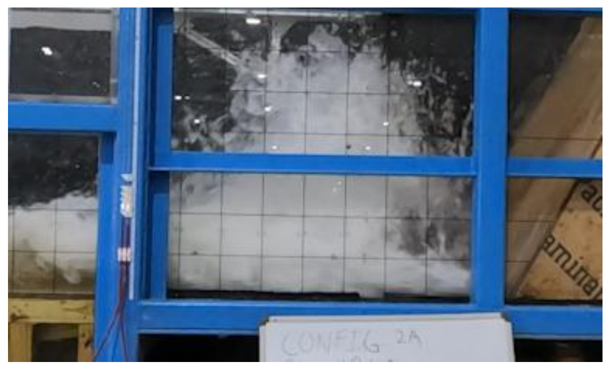

d) Configuration 2a (Lost)

e) Configuration 3a (Maintained)

f) Configuration 3a (Lost)

g) Configuration 3c (Maintained)

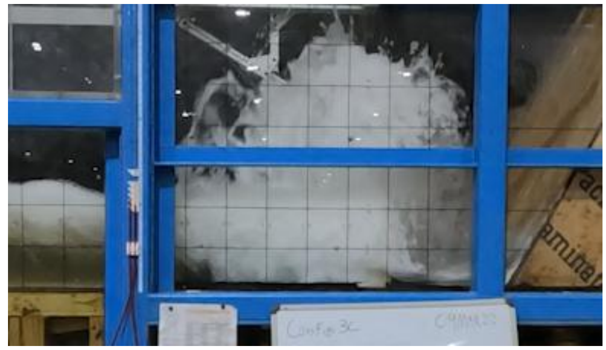

h) Configuration 3c (Lost)

i) Configuration 4a (Maintained)

j) Configuration 4a (Lost)

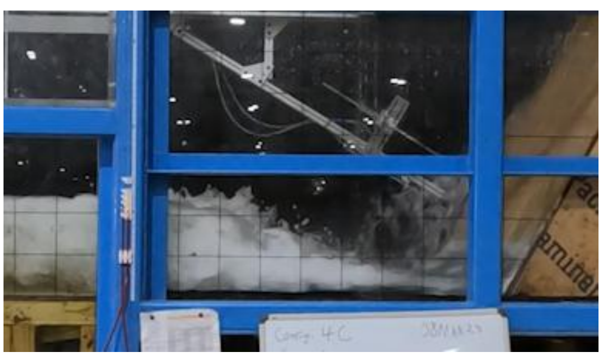

k) Configuration 4c (Maintained)

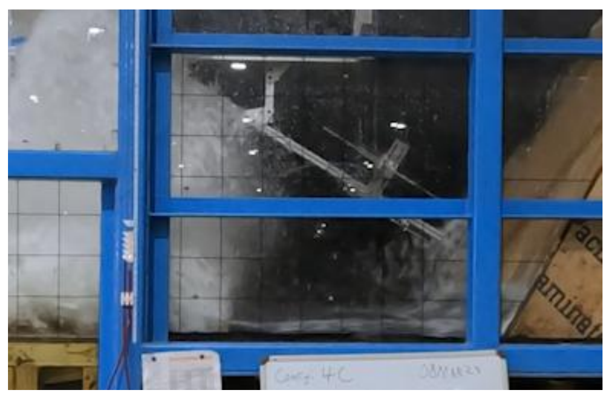

l) Configuration 4c (Lost)

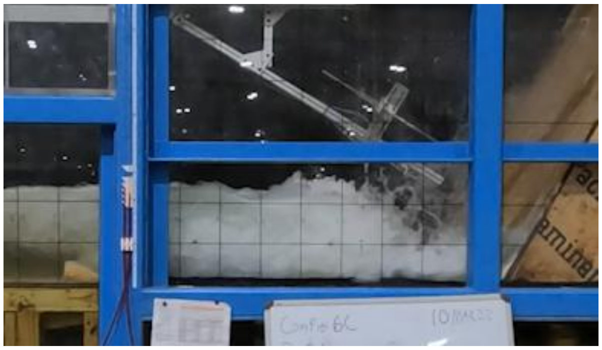

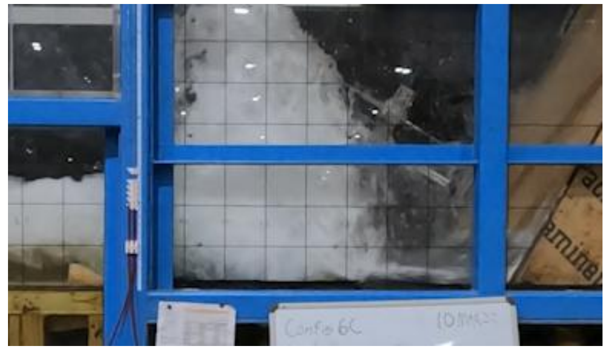

m) Configuration 6c (Maintained)

n) Configuration 6c (Lost)

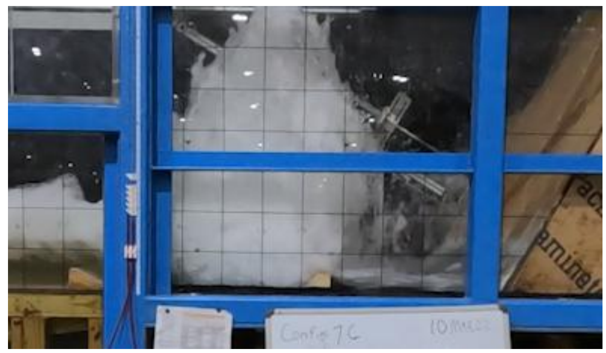

o) Configuration 7c (Maintained)

p) Configuration 7c (Lost)

Figure 169. High Froude Configurations, Before and After Loss of Hydraulic Jump Action, q_{60}

For each of the High $Fr_{1,}$ the loss of the hydraulic jump action resulted in significant spray action that is multiple times the tailwater depth. The behavior was relatively similar, although the spray position changed with block location.

The configurations 2a and 7c both seemed to have a more disintegrated jet projecting off the baffles. The spray for configurations 4a and 4c were severe against the right wall; where the 1^{st} row of baffles abutted the wall; suggesting that additional momentum transfer occurring against the wall from the confinement.

As the hydraulic jump action was lost, there was more of an unstable transition region when comparing configurations with/without a toe curve (Configurations 3a, 3c, 6c, and 4a, 4c).

An illustration of the typical conditions immediately before and after loss of the hydraulic jump action are provided for the q_D for each of the High Fr_1 flow conditions in Figure 170.

a) Configuration 1a (Maintained)

b) Configuration 1a (lost)

c) Configuration 2a (Maintained)

d) Configuration 2a (Lost)

e) Configuration 3a (Maintained)

f) Configuration 3a (Lost)

g) Configuration 3c (Maintained)

h) Configuration 3c (Lost)

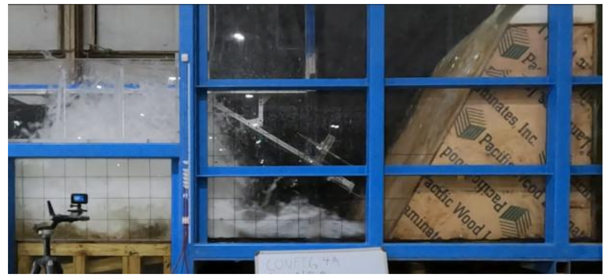

i) Configuration 4a (Maintained)

j) Configuration 4a (Lost)

k) Configuration 4c (Maintained)

l) Configuration 4c (Lost)

m) Configuration 6c (Maintained)

n) Configuration 6c (Lost)

o) Configuration 7c (Maintained)

p) Configuration 7c (Lost)

Figure 170. High Froude Configurations, Before and After Loss of Hydraulic Jump Action, q_D

The shooting jet exhibited a significantly higher projection and jet disintegration for the q_D as compared to the q_{60}. Similar to the q_{60}, the characteristics of the shooting jet was similar for each of the configurations with the exception of Configuration 7c. There was significantly less change from the characteristics before and after loss of the hydraulic jump action for configuration 7c as shown in Figure 170 (o and p). It is also worth noting that there is significantly less turbulence downstream of the end sill for both configurations 6c and 7c. There is also an area of relatively low turbulence immediately downstream of the end sill for configurations 4a and 4c; apparently resulting from a lifting of the jet by the combined effect of the two rows of baffles and end sill.

Similar to the q_{60} scenarios, the configurations with toe curve have a more unstable and larger range of transition between the hydraulic jump maintained and lost. The transition and associated surging produced the most severe turbulence conditions immediately downstream of the end sill. In other words, the transition was more severe than both the hydraulic action being maintained, and the hydraulic jump being fully lost.

An illustration of the typical conditions immediately before and after loss of the hydraulic jump action are provided for the q_{160} for each of the High Fr_1 flow conditions in Figure 171

a) Configuration 1a (Maintained)

b) Configuration 1a (lost)


c) *Configuration 2a (Maintained)*

d) *Configuration 2a (Lost)*


e) *Configuration 3a (Maintained)*

f) *Configuration 3a (Lost)*


g) *Configuration 3c (Maintained)*

h) *Configuration 3c (Lost)*


i) *Configuration 4a (Maintained)*

j) *Configuration 4a (Lost)*


k) Configuration 4c (Maintained) *l) Configuration 4c (Lost)*

m) Configuration 6c (Maintained) *n) Configuration 6c (Lost)*

o) Configuration 7c (Maintained) *p) Configuration 7c (Lost)*

Figure 171. High Froude Configurations, Before and After Loss of Hydraulic Jump Action, q_{160}

The shooting jet was observed to have a lower trajectory angle from horizontal (more downstream vector) for the q_{160} experiments. In addition, the height of the shooting jet was similar, and lower in some cases, than the q_D experiments even though the unit discharge was 60-percent higher. This suggests that the ratio of incoming flow depth to baffle height likely influences the behavior of the shooting jet.

The transition for the q_{160} was the most severe and unstable, this instability was much worse for the configurations with a toe curve. An example of the unstable transition and associated surging for configuration 3c is provided by time-lapse in Figure 172; whereas the characteristics transitioned from jump action to severe shooting jet, and back to jump action within an 8 second period. This would mean that if the unstable surging phenomenon where scaled up to a prototype scenario based on a length scale of 55; the entire surge would occur in under 1-minute. A similar unstable transition was observed for Configuration 6c and 4c.

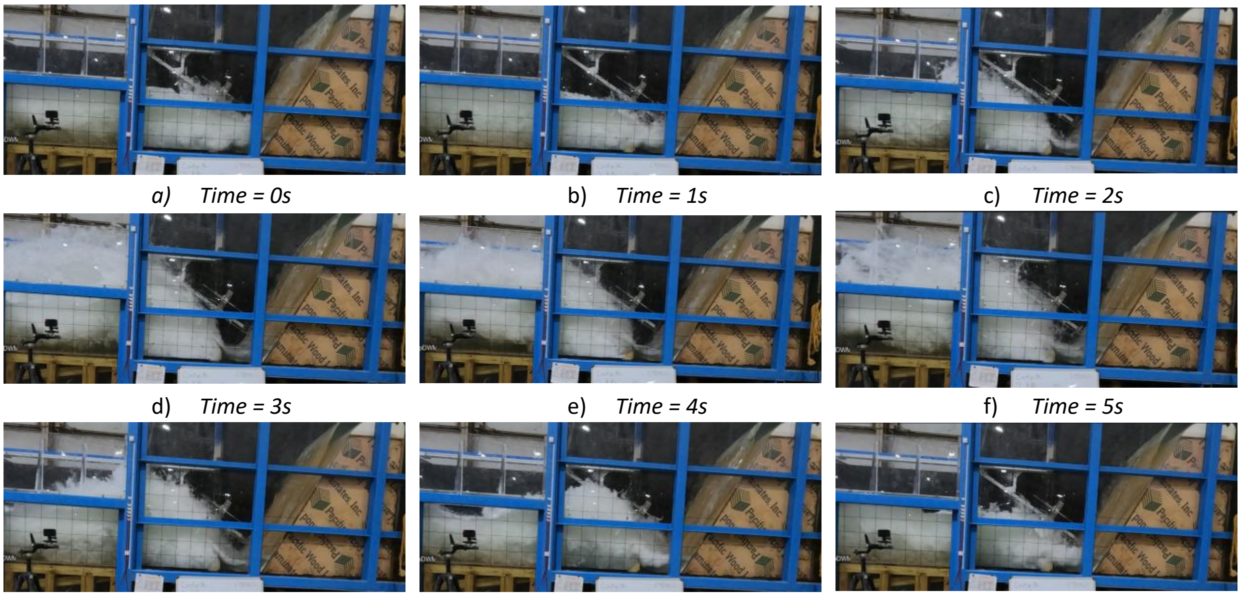

a) Time = 0s b) *Time = 1s* c) *Time = 2s*

d) *Time = 3s* e) *Time = 4s* f) *Time = 5s*

g) Time = 6s *h) Time = 7s* *i) Time = 8s*

Figure 172. Dynamic and Unstable Transition Region for Configuration 3c, q_{160},

A summary of the observations of required tailwater depth to maintain the hydraulic jump action are tabulated in Table 33 and plotted in Figure 173. The tabulated values for the ratio of required tailwater to the sequent depth, critical depth, and incoming flow depth are tabulated in Table 34, Table 36, and Table 37; respectively.

Table 33. Observed TW_{req} as a Function of q_x / q_d for High Froude Number Configurations

Flow Conditions					Tailwater Required (TW_{req}) (ft)							
Flow Desc.	Fr_1	d_c (ft)	d_1 (ft)	d_2 (ft)	1A	2A	3A	3C	4A	4C	6C	7C
q_{60}	11.3	0.47	0.09	1.45	1.05	1.04	1.09	1.13	1.02	1.04	1.09	1.02
q_{80}	9.9	0.57	0.12	1.67	1.23	1.22	1.23	1.31	1.23	1.25	1.30	1.20
q_D	8.9	0.66	0.15	1.87	1.39	1.41	1.39	1.43	1.41	1.41	1.43	1.34
q_{120}	8.2	0.75	0.18	2.05	1.58	1.56	1.58	1.60	1.56	1.58	1.58	1.47
q_{140}	7.7	0.83	0.21	2.21	1.79	1.77	1.79	1.83	1.79	1.81	1.79	1.68
q_{160}	7.2	0.91	0.24	2.36	1.98	1.96	1.96	1.98	1.94	1.96	1.96	1.87

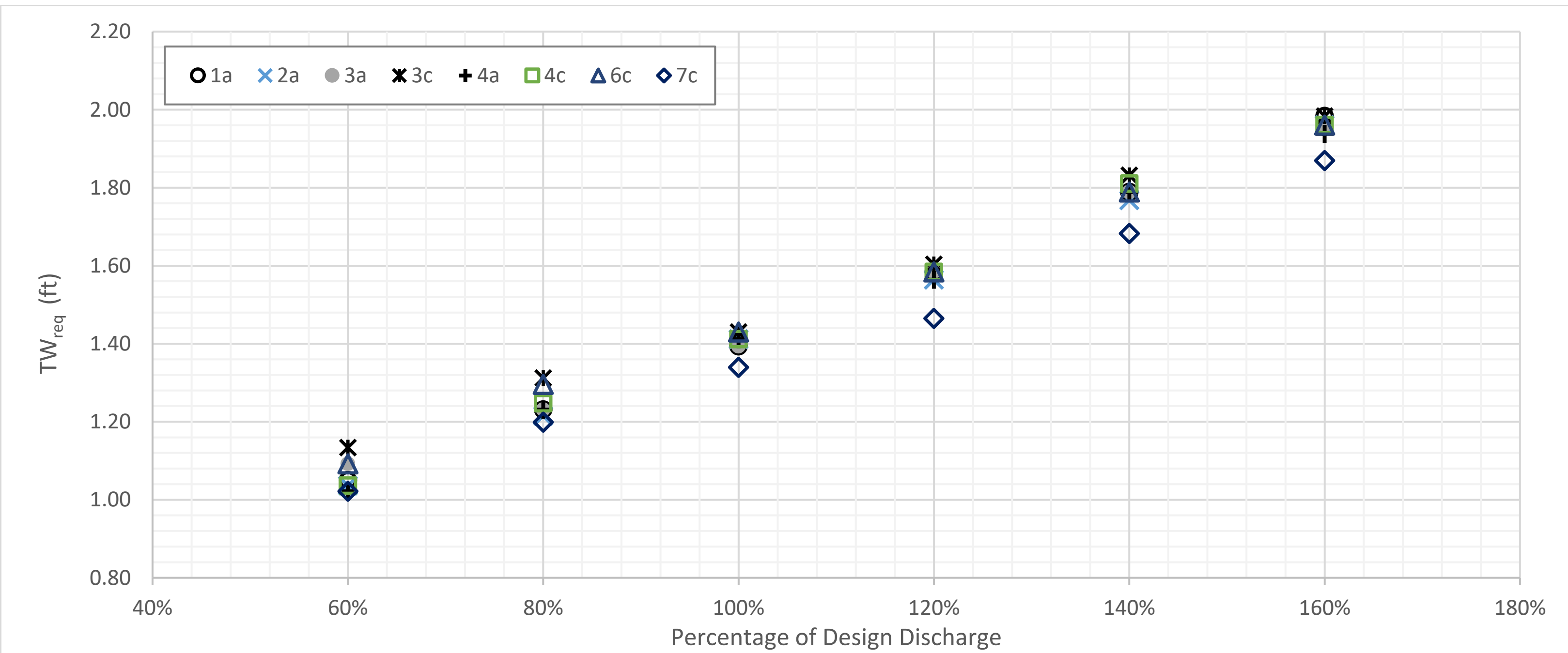

Figure 173. Observed TW_{req} as a Function of q_x / q_d for High Froude Number Configurations

Table 34. TW_{req} / d_2 as a Function of q_x / q_d for High Froude Number Configurations

Flow Conditions					Ratio of Tailwater Required to Sequent Depth (TW_{req} / d_2)							
Flow Desc.	Froude Number	Critical Depth (ft)	Incoming Depth (ft)	Sequent Depth (ft)	1A	2A	3A	3C	4A	4C	6C	7C
q_{60}	11.3	0.47	0.09	1.45	0.72	0.71	0.75	0.78	0.70	0.71	0.75	0.70
q_{80}	9.9	0.57	0.12	1.67	0.74	0.73	0.74	0.78	0.74	0.75	0.77	0.72
q_D	8.9	0.66	0.15	1.87	0.75	0.76	0.75	0.77	0.76	0.76	0.77	0.72
q_{120}	8.2	0.75	0.18	2.05	0.77	0.76	0.77	0.78	0.76	0.77	0.77	0.72
q_{140}	7.7	0.83	0.21	2.21	0.81	0.80	0.81	0.83	0.81	0.82	0.81	0.76
q_{160}	7.2	0.91	0.24	2.36	0.84	0.83	0.83	0.84	0.82	0.83	0.83	0.79

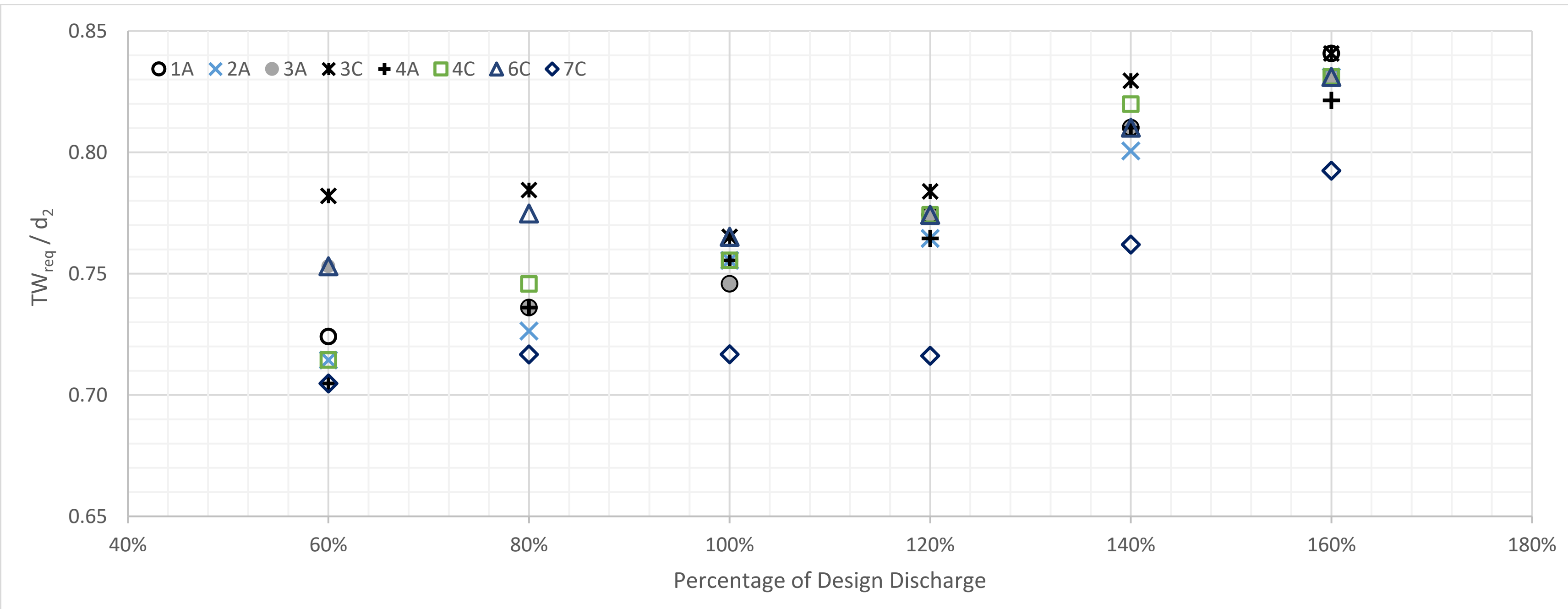

Figure 174. TW_{req} / d_2 as a Function of q_x / q_d for High Froude Number Configurations

Table 35. TW_{req} normalized to TW_{req} at q_d

Flow Conditions					$((TW_{req} @ q_d) / (TW_{req} @ q_x))$							
Flow Desc.	Froude Number	Critical Depth (ft)	Incoming Depth (ft)	Sequent Depth (ft)	1A	2A	3A	3C	4A	4C	6C	7C
q_{60}	11.3	0.47	0.09	1.45	73.4%	78.4%	79.3%	72.4%	73.4%	76.4%	76.3%	73.4%
q_{80}	9.9	0.57	0.12	1.67	86.1%	88.3%	91.8%	87.2%	88.4%	90.6%	89.5%	86.1%
q_D	8.9	0.66	0.15	1.87	100.0%	100.0%	100.0%	100.0%	100.0%	100.0%	100.0%	100.0%
q_{120}	8.2	0.75	0.18	2.05	110.8%	113.7%	112.2%	110.8%	112.2%	110.8%	109.4%	110.8%
q_{140}	7.7	0.83	0.21	2.21	125.2%	128.4%	128.1%	126.7%	128.2%	125.1%	125.6%	125.2%
q_{160}	7.2	0.91	0.24	2.36	138.9%	140.7%	138.7%	137.3%	138.9%	137.1%	139.6%	138.9%

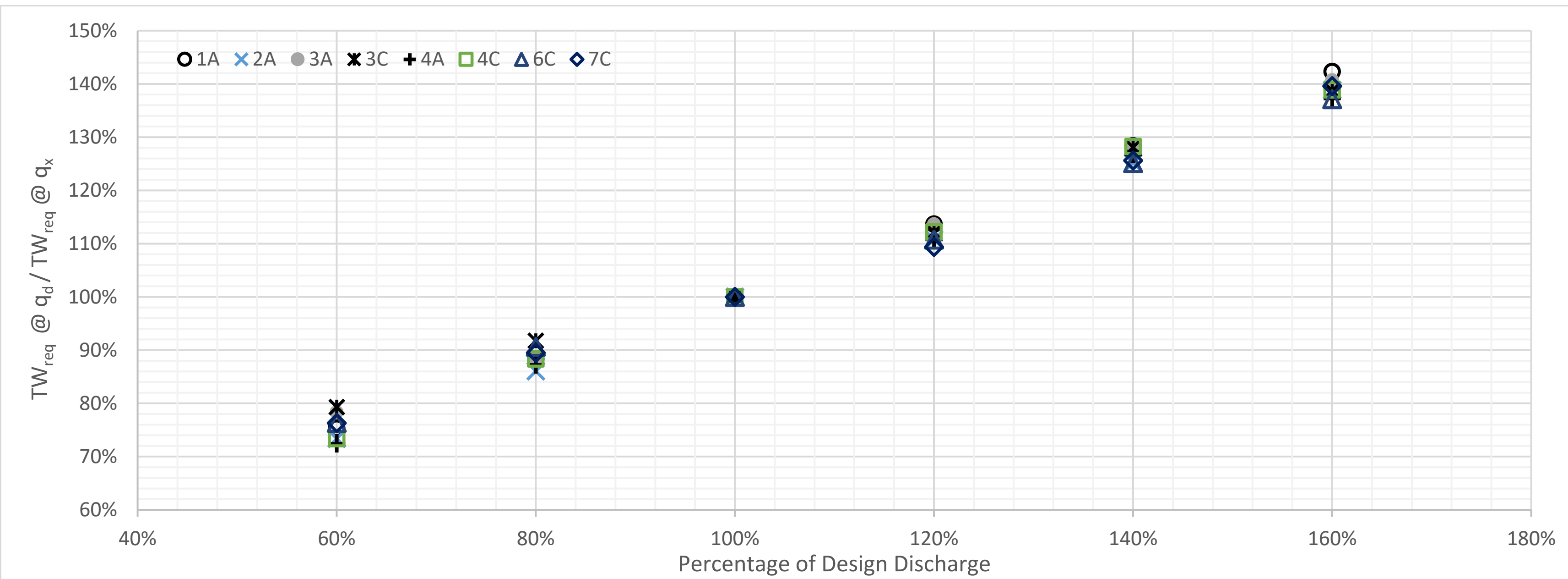

Figure 175. TW_{req} normalized to TW_{req} at q_d

The impacts of the tapered blocks on the required tailwater in negligible at the design discharge. Configuration 2a (tapered blocks without intermittent ramps) exhibits the lowest required tailwater of the three USBR (1984) configurations without toe curve. Configuration 1a (tapered blocks with intermittent ramps) exhibits the highest required tailwater. For the design discharge, configurations 1a, 2a, and 3a all match the observations of the closest Fr_1 from the USBR (1955) data.

The comparison suggests that there is little difference in the required tailwater between the USBR (1984) stilling basin configurations without a toe curve, for variation in block shape (i.e. tapered verse standard), and with/without an intermittent ramp. The tapered blocks with intermittent ramp demonstrate less resilience to unit discharges higher than design than the other two baffle shapes.

The impact of the toe curve is evaluated for the USBR (1984) basin by comparing configuration 3a (no toe curve), with configuration 3c (toe curve without adjusting stilling basin length) and configuration 6c (toe curve with adjustment to stilling basin length).

The comparison suggests that there is moderate variation in the required tailwater between these configurations, with the configuration without the presence of a toe curve requiring less tailwater to maintain the hydraulic jump for all flow conditions. In addition, the configuration without adjustment (increase) in the stilling basin length requires significantly more tailwater to maintain the hydraulic jump action for the low discharge ratios.

Comparison of configurations 3a, 4a, 4c, and 6c is utilized to evaluate the differences in the required tailwater between the USBR (1984) and the USACE (1992) stilling basin configurations.

There is little difference in the required tailwater for discharges above the design discharge (q_{120}, q_{140}, and q_{160}) although there is a significant increase in the required tailwater for the q_{60} and q_{80} flow conditions for the USBR (1984) configuration with a toe curve and an adjusted stilling basin length (6C).

A comparison of configurations 4C, 6C, and 7C is utilized to evaluate the impacts of the modified stilling basin slenderness ratio and blockage ratio; demonstrating that there is a significant reduction in the required tailwater for the modified USBR (1984) block configuration over the standard USBR (1984) and the USACE (1992) configuration.

The prediction ability of the d_c and d_1 was also evaluated by using them as a scale parameter. The results of this evaluation is tabulated in Table 36 and Table 37 and illustrated in Figure 176 and Figure 177; for the d_c and d_1, respectively.

Table 36. TW_{req} / d_c as a Function of q_x / q_d for High Froude Number Configurations

Flow Conditions					Ratio of Tailwater Required to Sequent Depth (TW_{req} / d_c)							
Flow Desc.	Froude Number	Critical Depth (ft)	Incoming Depth (ft)	Sequent Depth (ft)	1A	2A	3A	3C	4A	4C	6C	7C
q_{60}	11.3	0.47	0.09	1.45	2.23	2.20	2.32	2.41	2.17	2.20	2.32	2.17
q_{80}	9.9	0.57	0.12	1.67	2.16	2.13	2.16	2.30	2.16	2.19	2.27	2.10
q_D	8.9	0.66	0.15	1.87	2.10	2.13	2.10	2.16	2.13	2.13	2.16	2.02
q_{120}	8.2	0.75	0.18	2.05	2.12	2.09	2.12	2.14	2.09	2.12	2.12	1.96
q_{140}	7.7	0.83	0.21	2.21	2.16	2.13	2.16	2.21	2.16	2.18	2.16	2.03
q_{160}	7.2	0.91	0.24	2.36	2.19	2.16	2.16	2.19	2.14	2.16	2.16	2.06

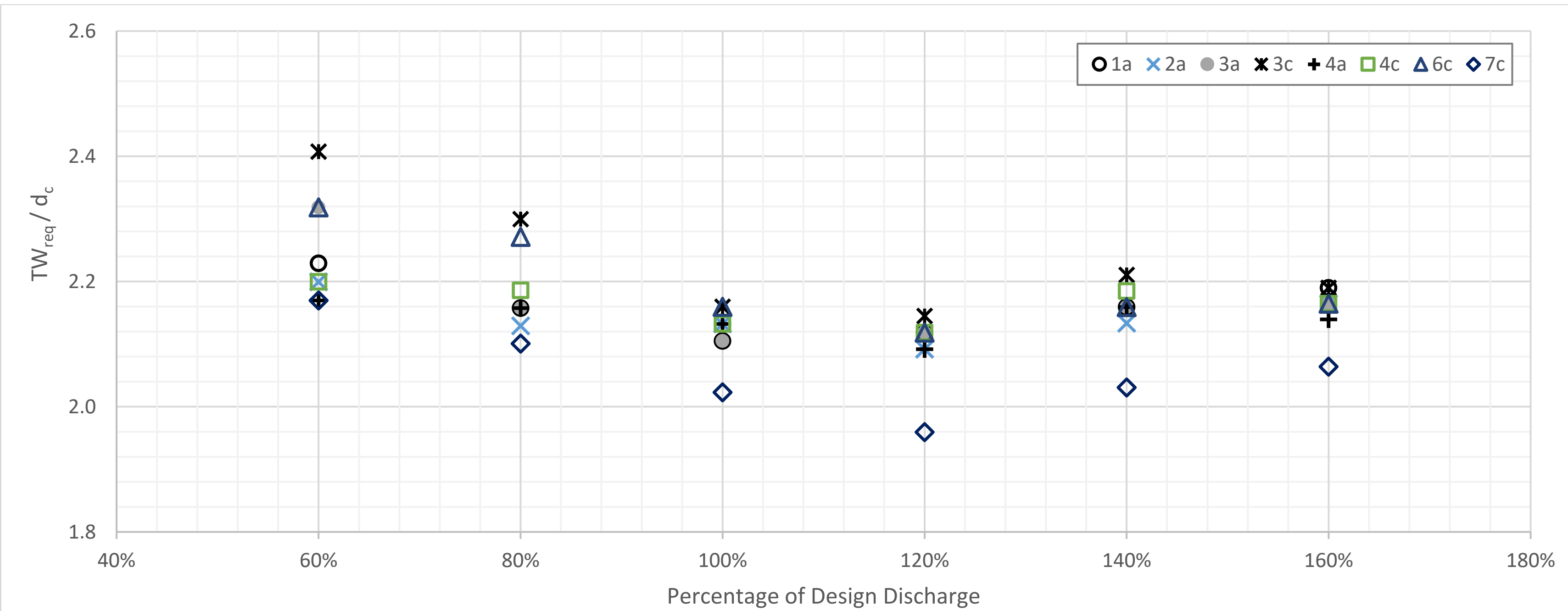

Figure 176. TW_{req} / d_c as a Function of q_x / q_d for High Froude Number Configurations

Table 37. TW_{req} / d_1 as a Function of q_x / q_d for High Froude Number Configurations

Flow Conditions					Ratio of Tailwater Required to Sequent Depth (TW_{req} / d_1)							
Flow Desc.	Froude Number	Critical Depth (ft)	Incoming Depth (ft)	Sequent Depth (ft)	1A	2A	3A	3C	4A	4C	6C	7C
q_{60}	11.3	0.47	0.09	1.45	11.24	11.09	11.69	12.14	10.94	11.09	11.69	10.94
q_{80}	9.9	0.57	0.12	1.67	9.96	9.82	9.96	10.61	9.96	10.09	10.48	9.69
q_D	8.9	0.66	0.15	1.87	9.07	9.19	9.07	9.31	9.19	9.19	9.31	8.72
q_{120}	8.2	0.75	0.18	2.05	8.64	8.53	8.64	8.75	8.53	8.64	8.64	7.99
q_{140}	7.7	0.83	0.21	2.21	8.41	8.31	8.41	8.61	8.41	8.51	8.41	7.91
q_{160}	7.2	0.91	0.24	2.36	8.19	8.10	8.10	8.19	8.00	8.10	8.10	7.72

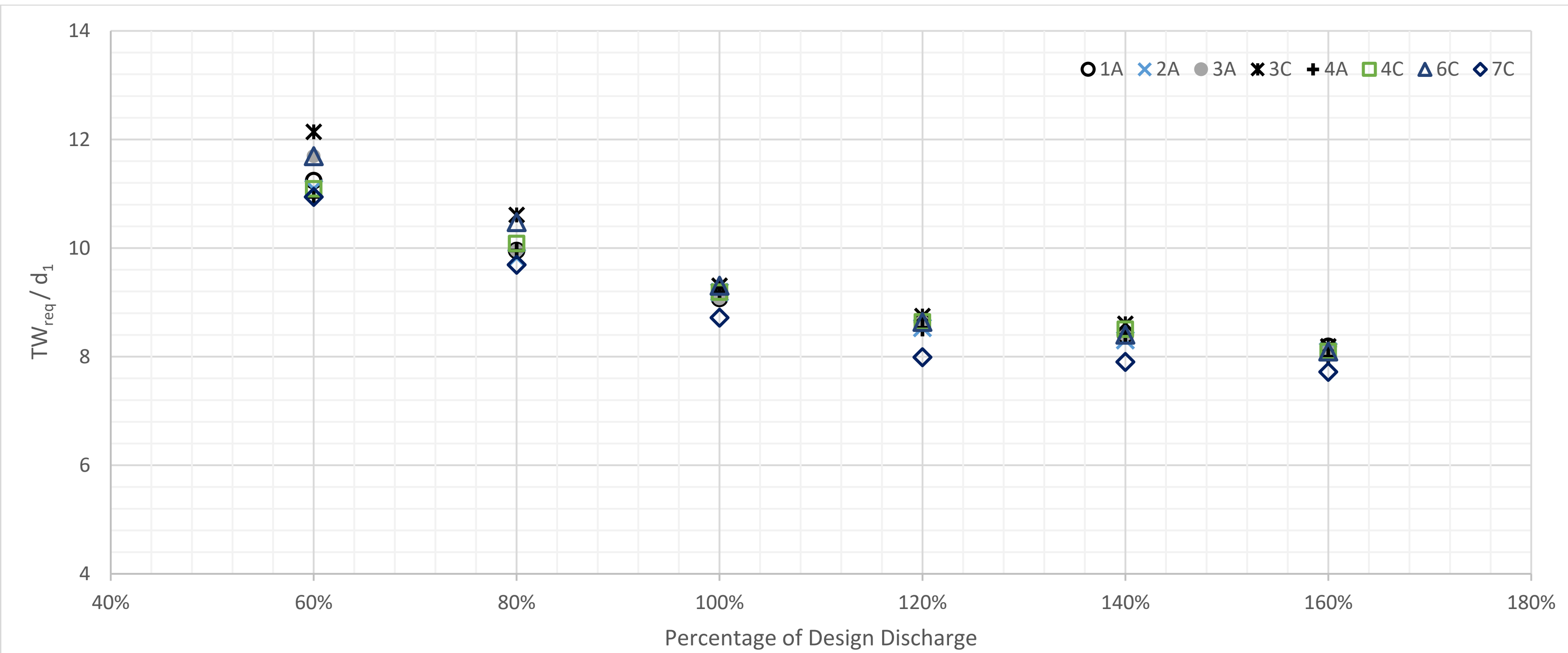

Figure 177. TW_{req} / d_1 as a Function of q_x / q_d for High Froude Number Configurations

5.2.2.1.2 Local Scour Potential

The experiments are made with a rigid downstream bed with an elevation of that of the horizontal apron within the stilling basin. A semi-quantitative method was used to describe the near-bed turbulent structures that a responsible for the local scour observed near the structure. The method uses a combination of the observed strength of the turbulent structures and the frequency of these structures in the near boundary region within a distance equal to D_2 downstream. The combination of these observations are categorized into a turbulence severity index that detailed in Table 38.

Table 38. Semi-Quantitative Near-Bed turbulence severity index

Index Number	Index Descriptor	Index Description
1	Low	Diffused turbulence exiting basin, with minimal defined structures/vorticity
2	Low-Moderate	Mostly diffused with some defined turbulent structures, boundary turbulent impacts less than 0.25 Hertz
3	Moderate	Defined turbulent structures with vorticity with an axis perpendicular to flow, boundary turbulent impacts greater than 0.25 Hertz
4	Moderate-High	Defined turbulent structures, some well-defined or exhibit multiple directions. Boundary turbulent impacts frequency generally 0.25 to 0.5 Hertz
5	High	Well Defined turbulent structures, often in swarms and exhibits secondary vorticity at boundary, boundary turbulent impacts greater than 0.5 Hertz
6	High-Severe	Impacting boundary greater than 50-percent of the time, High boundary turbulence in multiple orientations that are chaotic to determine discrete turbulent structure impact frequency.
7	Severe	Continuous, high boundary turbulence in multiple orientations, too chaotic to determine discrete turbulent structure impact frequency.

This index is assigned to each of the configurations for each flow condition and tailwater in which the hydraulic jump is maintained to be used for relative comparisons of local scour potential. Examples of the categories of turbulence utilized in the severity index are provided in Figure 178.

a) Diffused turbulence

b) Defined turbulent structures in one direction

c) Chaotic turbulent structures in multiple directions

Figure 178. Examples of Qualitative Turbulence Intensity

The frequency of the impact of the turbulent structures is defined by the number of structures counted divided by the duration of the experiment video. For the case of High-Severe and Severe, the nature of turbulence is such that no defined impacts can be counted due to the chaotic nature of the turbulent bursts and the near constant impacts.

The results of the semi-quantitative evaluation of the downstream near-bed turbulence severity index is provide in Table 39 and illustrated in Figure 179.

Table 39. Summary Table for Near-Bed Turbulence Severity Index for High Froude Configurations

$\frac{q}{q_D}$	TW ID	$\frac{d'}{d_2}$	Configuration / Observed Turbulence Index Value							
			1a	2a	3a	3c	4a	4c	6c	7c
0.6	A	0.97	Low-Mod	Low	Low	Mod-High	Mod	Mod	Low	Low
	B	0.87	Mod	Low	Low-Mod	Mod-High	Mod	Mod	Low-Mod	Low
	C	0.82	Mod	Low	Mod	High	Mod	Mod-High	Mod	Low
	D	0.77	Mod	Low-Mod	Mod	High	Mod	Mod-High	Mod	Low
	E	0.72	Mod-High	Mod	*Jump Lost*	*Jump Lost*	Mod	Mod-High	*Jump Lost*	Low
0.8	A	0.97	Mod	Low	Mod-High	High-Sev	High	Mod-High	Mod-High	Low
	B	0.87	Mod	Low-Mod	Mod-High	High-Sev	High	Mod-High	Mod-High	Low
	C	0.82	Mod	Low-Mod	High	High-Sev	High	Mod-High	High	Low
	D	0.77	Mod-High	Mod	High	High-Sev	High	High	High	Low
	E	0.73	Mod-High	Mod	*Jump Lost*	*Jump Lost*	*Jump Lost*	*Jump Lost*	*Jump Lost*	Low
1	A	0.97	High	Low	Mod-High	High	High	Mod-High	Mod-High	Low
	B	0.87	High	Low-Mod	Mod-High	High	High	High	Mode-High	Low
	C	0.82	High	Mod	High	High-Sev	High	Mod-High	High	Low
	D	0.77	High	Mod -High	High	High	High	High	High	Low-Mod
	E	0.73	*Lost*	*Jump Lost*	*Jump Lost*	*Jump Lost*	*Jump Lost*	*Jump Lost*	*Jump Lost*	Low-Mod
1.2	A	0.97	High-Sev	Mod-High	High	High	High	High	High	Low-Mod
	B	0.87	High-Sev	High	High	High-Sev	High	High	High	Mod
	C	0.82	High-Sev	High	High-Sev	High-Sev	High	Mod-High	High	Mod
	D	0.77	High-Sev	High	*Jump Lost*	*Jump Lost*	High-Sev	High	*Jump Lost*	Mod-High
	E	0.97	*Jump Lost*	*Jump Lost*	*Jump Lost*	*Jump Lost*	*Jump Lost*	*Jump Lost*	*Jump Lost*	Mod-High
1.4	A	0.96	Severe	High	High	High-Sev	High	High	High	High
	B	0.87	Severe	High	High-Sev	High-Sev	High	High	High-Sev	High
	C	0.82	*Jump Lost*	High	*Jump Lost*	*Jump Lost*	High-Sev	High-Sev	High-Sev	High
	D	0.77	*Jump Lost*	*Jump Lost*	*Jump Lost*	*Jump Lost*	*Jump Lost*	*Jump Lost*	*Jump Lost*	High
1.6	A	0.97	Severe	High	High	High-Sev	High	High	High-Sev	High
	B	0.87	Severe	High	High-Sev	High-Sev	High-Sev	High-Sev	High-Sev	High
	C	0.82	*Jump Lost*	High	*Jump Lost*	*Jump Lost*	*Jump Lost*	*Jump Lost*	*Jump Lost*	High

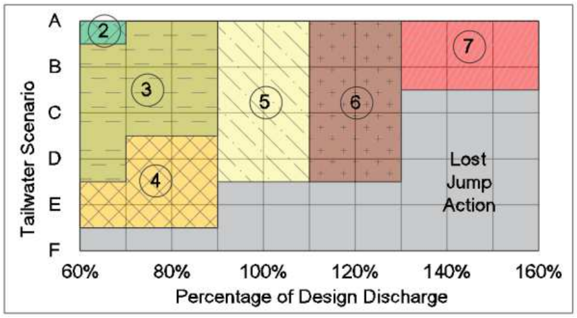

a) Configuration 1a

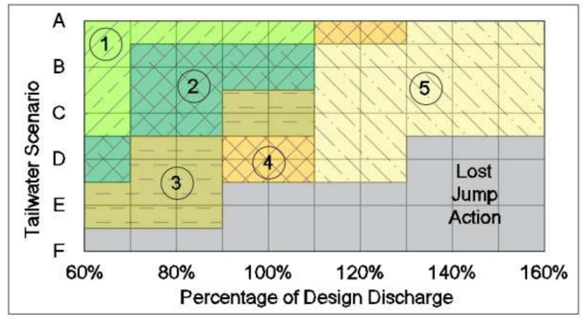

b) Configuration 2a

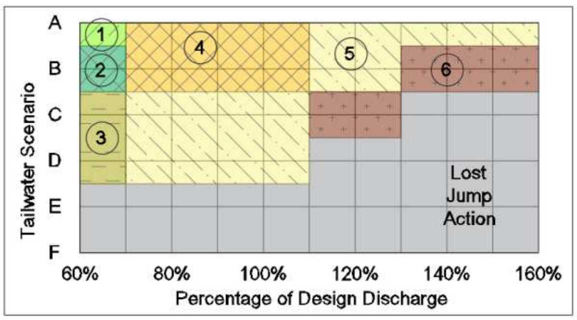

c) Configuration 3a

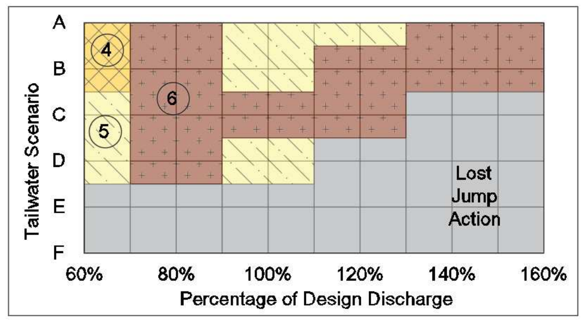

d) Configuration 3c

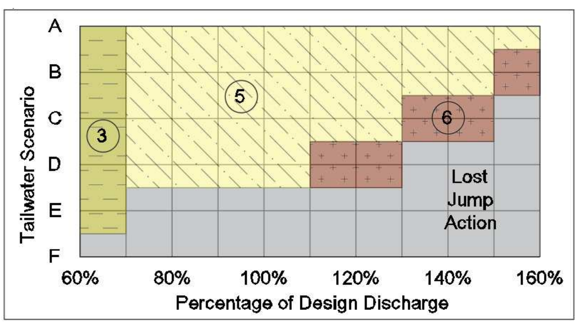

e) Configuration 4a

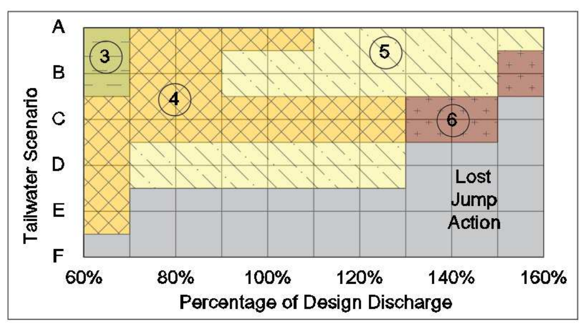

f) Configuration 4c

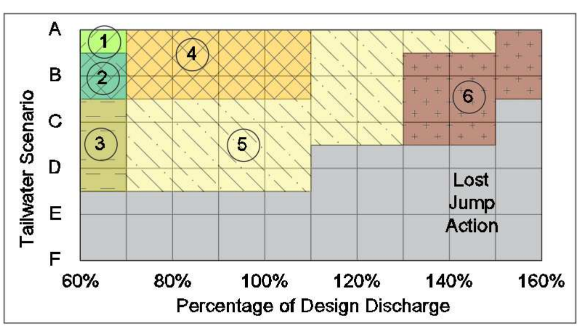

g) Configuration 6c

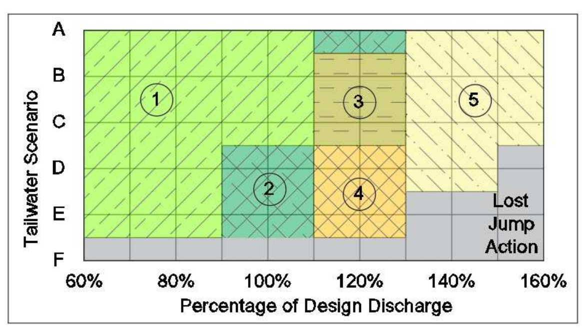

h) Configuration 7c

Figure 179. Graphical Matrix for Near-Bed Turbulence Severity Index for High Froude Configurations

5.2.2.1.3 Maximum Boil Height

The maximum boil height within the basin was determined by observing the dynamic fluctuations in water surface level within the stilling basin. The conditions within the stilling basin are very turbulent and can result in large 3-dimensional concentrations of surface waves that result in dynamic surges, often resulting in smaller bodies of water detaching. It is worth noting that smaller bodies of water are often projected above the elevation of the incoming water surface (i.e. above the height of the average specific energy head), although this is observed in the model; it is not expected under most prototype conditions related to surface tension scale effects limiting droplet size in the prototype. For the purposes of determining the maximum boil height within the stilling basin, the detached waves or isolated dynamic explosions are omitted. An example of the dynamic surge prior to detachment and the corresponding recorded boil height is shown in Figure 180.

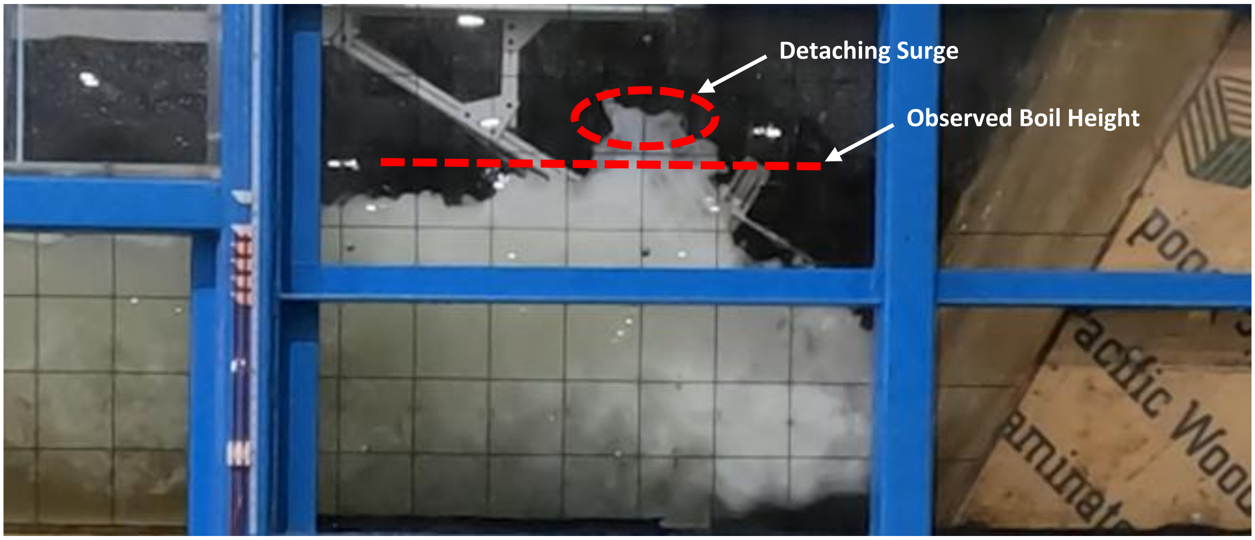

Figure 180. Example of Boil Height Observation

The horizontal beam obstructed view between a depth ranging just above 1.5 to just below 1.7 feet, and observations in this range were not made. The values are detailed in Table 40. The values were plotted against d_2 as a scale parameter for each observation, similar to that of Blaisdell (1948). These were then plotted by the discharge ratio scenario and are illustrated in Figure 181.

Table 40. Observed Maximum Boil Heights for High Froude Configurations

Flow Conditions						Maximum Boil Height - Zmax(ft)							
Flow	Fr_1	d_1	TW ID	d'	TW	1A	2A	3A	3C	4A	4C	6C	7C
q_{60}	11.3	0.09	A	0.97	1.45	Obst.[1]	Obst.	Obst.	Obst.	Obst.	1.5	Obst.	1.8
			B	0.87	1.31	Obst.	Obst.	1.5	Obst.	Obst.	1.5	1.5	Obst.
			C	0.82	1.23	Obst.	Obst.	Obst.	1.5	1.5	1.4	1.5	Obst.
			D	0.77	1.16	Obst.	1.5	Obst.	0	1.4	1.4	1.5	Obst.
			E	0.72	1.09	Det.[2]	1.8	0	0	1.4	1.4	0	Obst.
q_{80}	9.9	0.12	A	0.97	1.67	Obst.	2.1	1.9	1.8	1.9	1.9	1.9	2.1
			B	0.87	1.51	Obst.	1.9	1.8	1.8	1.8	1.8	Obst.	2
			C	0.82	1.42	Obst.	1.8	Obst.	Obst.	1.8	1.7	Obst.	1.9
			D	0.77	1.34	Obst.	Obst.	Obst.	N/A	1.7	1.7	2	Obst.
			E	0.73	1.25	1.8	1.9	N/A[3]	N/A	N/A	N/A	N/A	Obst.
q_D	8.95	0.15	A	0.97	1.87	2.2	2.6	2.2	2.1	2.2	Obst.	2.1	2.5
			B	0.87	1.68	2	2.2	2	1.9	2.1	Obst.	1.9	2.3
			C	0.82	1.59	1.9	2	1.9	1.9	1.9	1.9	1.8	2.2
			D	0.77	1.49	1.8	2.6	N/A	N/A	1.8	1.8	2.2	2
q_{120}	8.24	0.18	A	0.97	2.05	2.4	2.6	2.3	2.3	Obst.	2.3	2.3	2.6
			B	0.87	1.84	2.2	2.4	2.1	2.2	Obst.	Obst.	2.1	2.5
			C	0.82	1.74	2	2.3	2.1	2.1	Obst.	Obst.	2.4	2.4
			D	0.77	1.64	2.2	2.5	N/A	N/A	1.9	1.9	0	2.2
q_{140}	7.68	0.21	A	0.96	2.21	2.5	2.6	2.6	2.5	2.3	2.4	2.4	2.8
			B	0.87	1.99	2.3	2.7	2.4	2.5	2.4	2.3	2.3	2.6
			C	0.82	1.88	N/A	2.7	N/A	N/A	Obst.	Obst.	N/A	2.5
			D	0.77	1.77	N/A	N/A	N/A	N/A	N/A	N/A	N/A	2.4
q_{160}	7.23	0.24	A	0.97	2.36	2.7	2.9	2.5	2.9	2.6	2.7	2.6	2.9
			B	0.87	2.12	2.6	2.6	2.4	2.5	Obst.	Obst.	2.3	2.8
			C	0.82	2.01	N/A	2.9	N/A	N/A	N/A	N/A	N/A	2.7

[1] View was obstructed by horizontal beam, depth is between above 1.5-feet to below 1.8-feet
[2] Boil was frequently detaching and a consistent boil height could not be determined
[3] The hydraulic jump action was lost

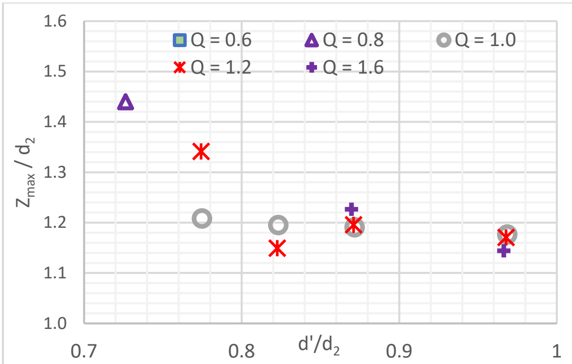

a) *Configuration 1a*

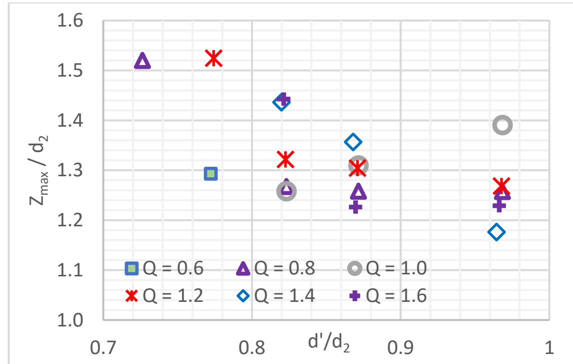

b) *Configuration 2a*

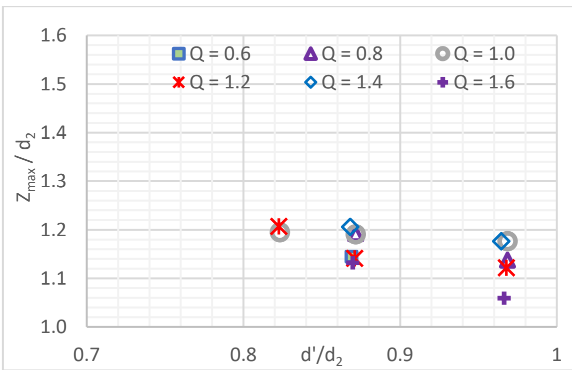

c) *Configuration 3a*

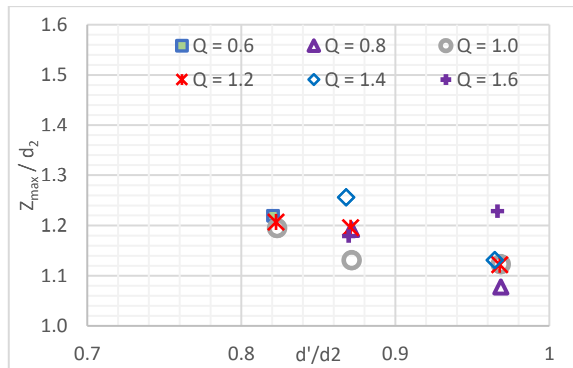

d) *Configuration 3c*

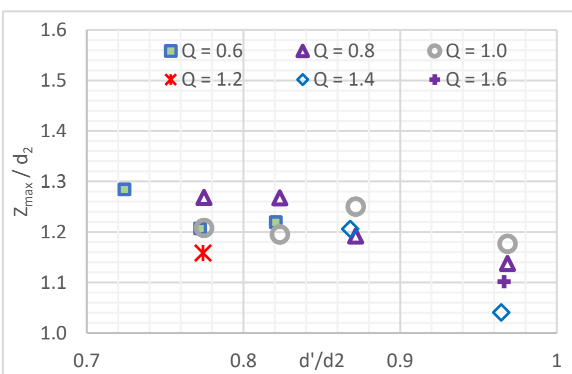

e) *Configuration 4a*

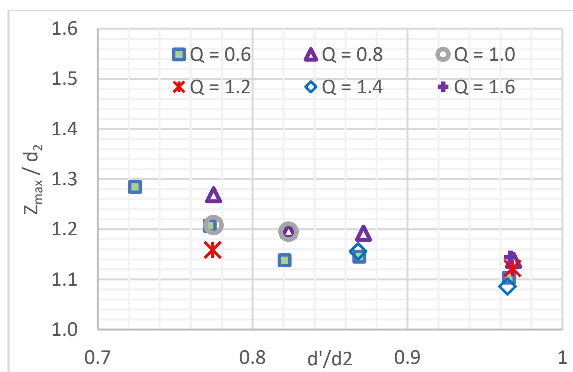

f) *Configuration 4c*

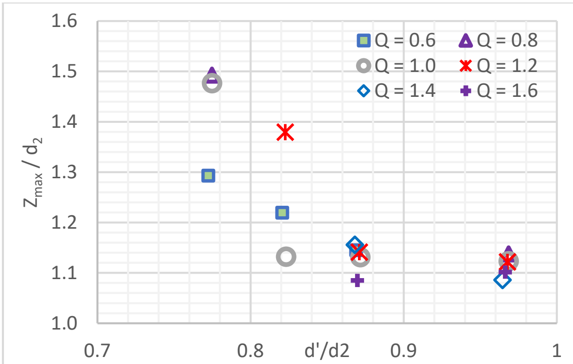

g) Configuration 6c

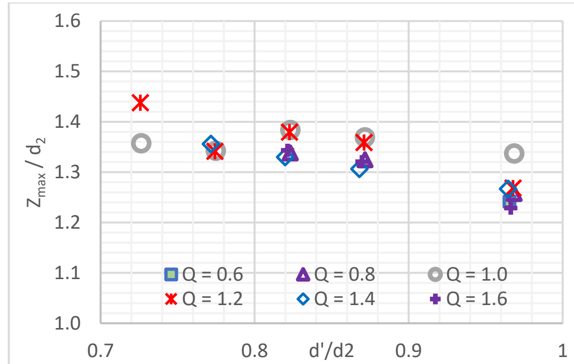

h) Configuration 7c

Figure 181. Graphical Results for Stilling Basin Boil Height Ratio $\frac{Z_{max}}{d_2}$ for High Froude Configurations

There is generally decreasing maximum boil height ratio ($\frac{Z_{max}}{d_2}$) for increasing tailwater ratio ($\frac{d'_2}{d_2}$). There is also a trend of decreasing $\frac{Z_{max}}{d_2}$ with increasing discharge ratio ($\frac{q_x}{q_D}$). The configurations with the tapered blocks (1a and 2a) and the higher blockage ratio (7c) exhibited the highest overall maximum boil heights. The typical boil conditions for the q_{60} and tailwater scenario C are presented in Figure 182.

a) Configuration 1a

b) Configuration 2a

c) Configuration 3a

d) Configuration 3c

e) Configuration 4a

f) Configuration 4c

g) Configuration 6c

h) Configuration 7c

Figure 182. Typical Boil Height Observations for High Froude Number Configurations at q_{60} and tailwater scenario C.

As illustrated in Figure 182, the configurations 4a (e) and 4c (f) have lower Z_{max} due to the location of the blocks and the reduction in momentum provided by the free jump action upstream of the baffles. Configuration 3c (d) has a significant boil that is unstable and results in detached surge; due to the minimum distance to the baffles resulting from the addition of the toe curve.

It is demonstrated in Table 40 and shown in Figure 183 (b) and (h) that the non-standard baffle shape/configurations provide the highest maximum boil height at the q_D and tailwater scenario A (~d_2). This is expected that due to the tapered shape and increased blockage ratio have a higher momentum transfer than the standard block (USACE, 1970), that this results in an increased "forcing" of the hydraulic jump action with a stronger vertical component to the dynamic surges.

The presence of the intermittent ramp (1a) reduced the Z_{max} slightly when compared to no ramp (2a). It was observed that the ramp elongates the boil projecting it farther downstream. Configuration 7c and 2a have similar Z_{max} ; with variation across the flow conditions to which is the highest. Configuration 7C exhibits the most consistent boil heights across flow conditions.

When the basin length is increased to account for the toe curve (6c), the z_{max} was slightly reduced over configuration 3a. It is not clear if the reduction is a result of the toe curve or the increased basin length. Configuration 4a and 4c have very similar $Z_{max,}$ with slightly lower Z_{max} observed for $\frac{q_x}{q_D} < q_{120}$ and slightly increased at $\frac{q_x}{q_D} > q_{120}$.

The typical boil condition for the design discharge (q_D) and Tailwater scenario A are illustrated in Figure 183

a) Configuration 1a

b) Configuration 2a

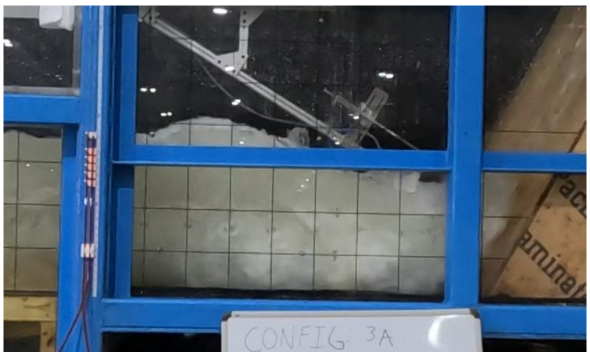

c) Configuration 3a

d) Configuration 3c

e) Configuration 4a

f) Configuration 4c

g) Configuration 6c *h) Configuration 7c*

Figure 183. Typical Boil Height Observations for High Froude Number Configurations at q_D and tailwater scenario A.

5.2.2.1.4 Jump Angle

The average water surface profile has been used to approximate the average floor pressure profile (USBR, 1984). The minimum and maximum water surface profiles have also been demonstrated to match approximately the large-scale pressure fluctuations related to floor and sidewall loads outside the vicinity of the transition between chute and the horizontal floor and the baffle blocks (USACE, 2018).

The minimum jump angle was selected to be tabulated for each configuration since it can be used as an indicator of the minimum average resistance force acting on the stilling basin floor and can be more precisely observed than the maximum jump angle due to the dynamic nature of the surface roller as the angle steepens.

As previously described, the dynamic fluctuations in the stilling basin resulting in spatial and temporal variations across the basin; therefore, adequate safety factors should be utilized when using observed water surface elevations as an indicator of resisting loads. An illustration of the determination of jump angle is shown for configuration 3a (a) and 4c (c) in Figure 184.

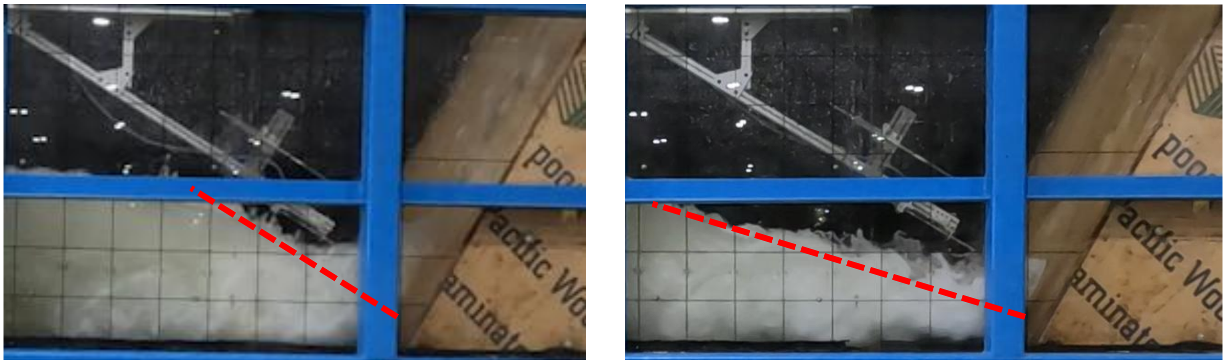

a) Configuration 3a *b) Configuration 4a*

Figure 184. Example of Minimum Jump Angle Observation

The values for jump angle are detailed in Table 41 and the results illustrated in

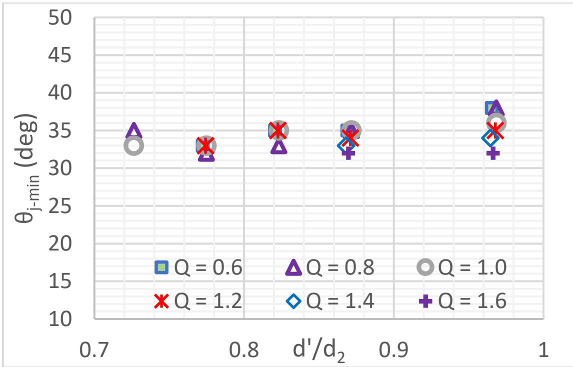

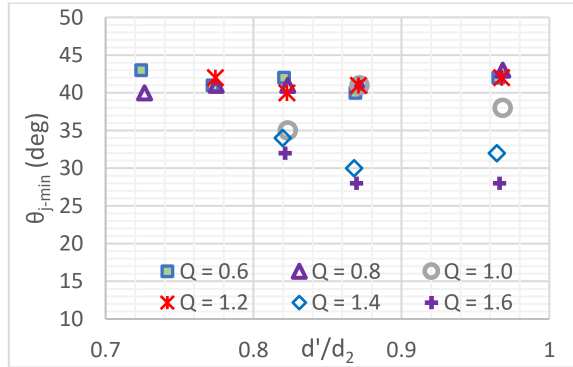

a) Configuration 1a

Configuration 2a

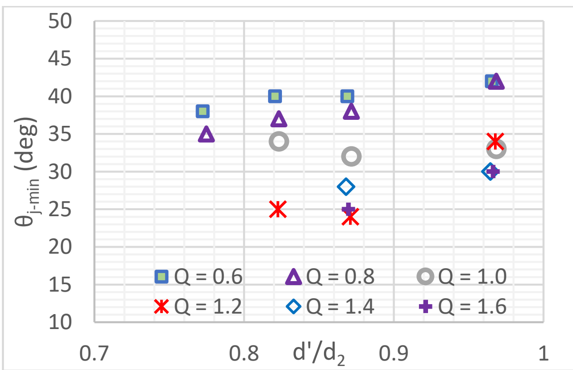

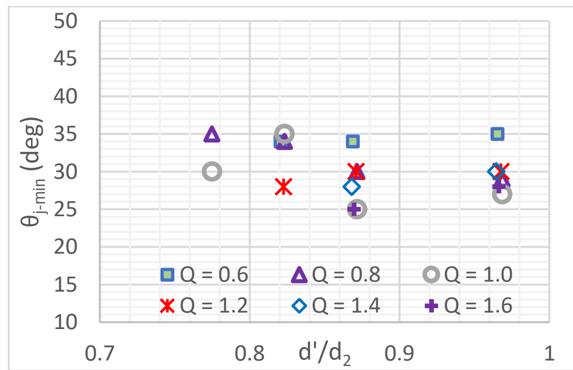

Configuration 3a

Configuration 3c

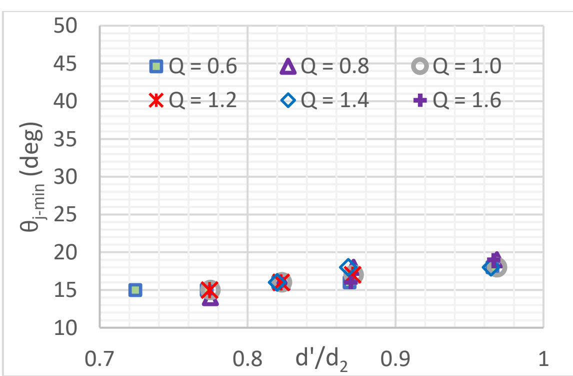

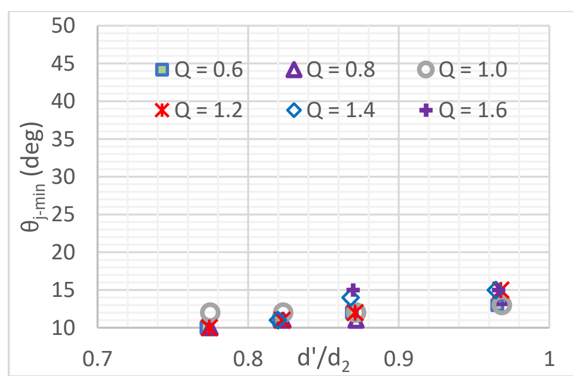

Configuration 4a

Configuration 4c

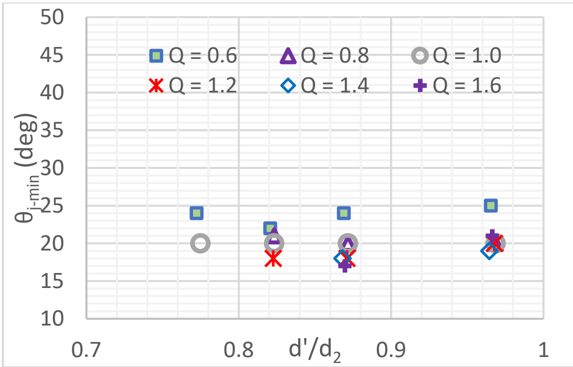

Configuration 6c

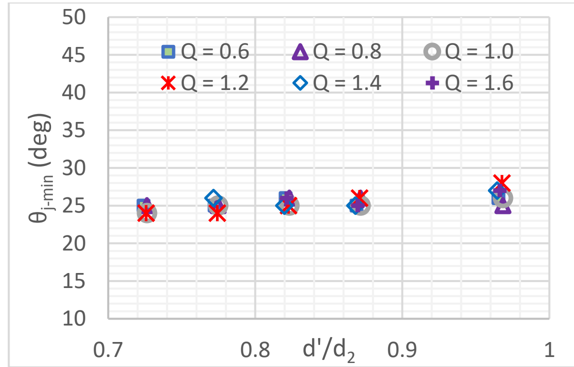

Configuration 7c

Figure 185.

Table 41. Minimum Observed Jump Angle for High Froude Configurations

Flow Conditions						Minimum Jump Angle – $\theta_{j\text{-}min}$ (deg)							
Flow Scenario	Fr_1	d_1 (ft)	TW ID	$\frac{d'}{d_2}$	TW (ft)	1A	2A	3A	3C	4A	4C	6C	7C
q_{60}	11.3	0.09	A	0.97	1.45	38	42	42	35	18	13	25	26
			B	0.87	1.31	35	40	40	34	16	12	24	25
			C	0.82	1.23	35	42	40	34	16	11	22	26
			D	0.77	1.16	33	41	38	Obst.	15	10	24	25
			E	0.72	1.09	Obst.	43	Obst.	Obst.	15	Obst.	Obst.	25
q_{80}	9.9	0.12	A	0.97	1.67	38	43	42	29	19	14	20	25
			B	0.87	1.51	35	41	38	30	18	11	20	26
			C	0.82	1.42	33	41	37	34	16	11	21	26
			D	0.77	1.34	32	41	35	35	14	10	Obst.	25
			E	0.73	1.25	35	40	Obst.	Obst.	Obst.	Obst.	Obst.	25
q_D	8.95	0.15	A	0.97	1.87	36	38	33	27	18	13	20	26
			B	0.87	1.68	35	41	32	25	17	12	20	25
			C	0.82	1.59	35	35	34	35	16	12	20	25
			D	0.77	1.49	33	Obst.	Obst.	30	15	12	20	25
q_{120}	8.24	0.18	A	0.97	2.05	35	42	34	30	Obst.	15	20	28
			B	0.87	1.84	34	41	24	30	17	12	18	26
			C	0.82	1.74	35	40	25	28	16	11	18	25
			D	0.77	1.64	33	42	Obst.	Obst.	15	10	0	24
q_{140}	7.68	0.21	A	0.96	2.21	34	32	30	30	18	15	19	27
			B	0.87	1.99	33	30	28	28	18	14	18	25
			C	0.82	1.88	Obst.	34	Obst.	Obst.	16	11	Obst.	25
			D	0.77	1.77	Obst.	Obst.	Obst.	Obst.	Obst.	Obst.	Obst.	26
q_{160}	7.23	0.24	A	0.97	2.36	32	28	30	28	19	15	21	27
			B	0.87	2.12	32	28	25	25	16	15	17	25
			C	0.82	2.01	Obst.	32	Obst.	Obst.	Obst.	Obst.	Obst.	26

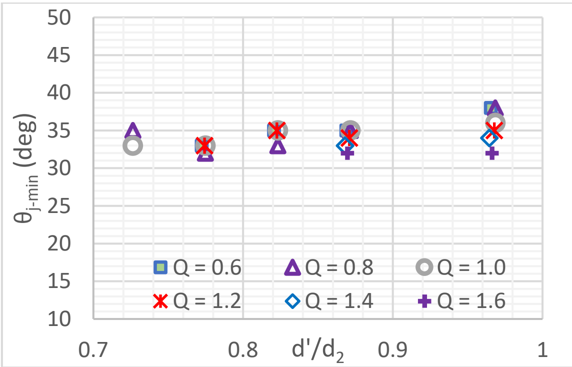

b) Configuration 1a

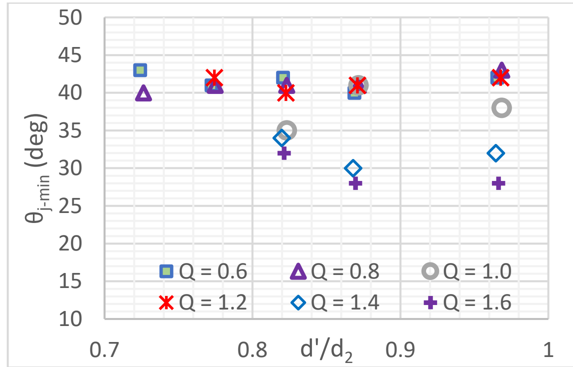

Configuration 2a

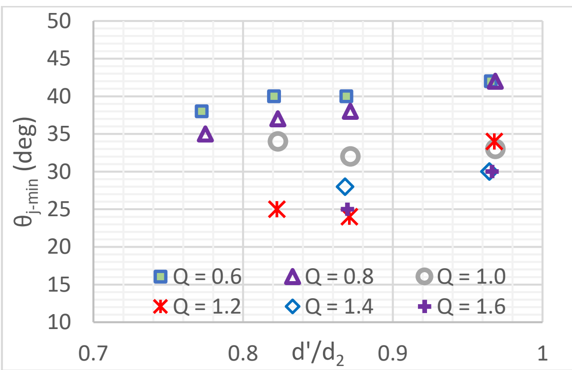

Configuration 3a

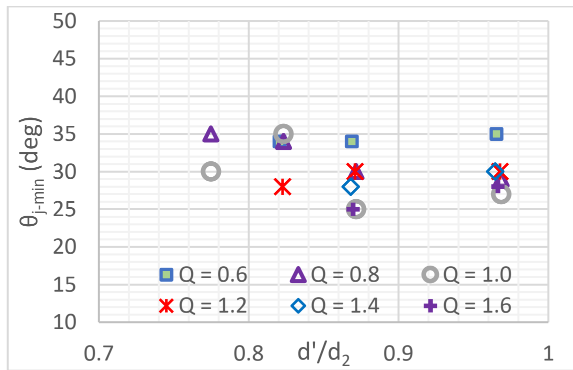

Configuration 3c

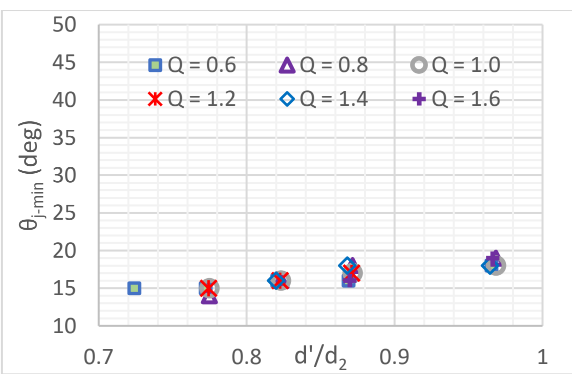

Configuration 4a

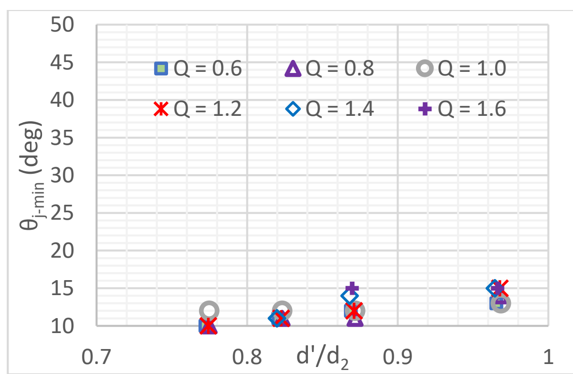

Configuration 4c

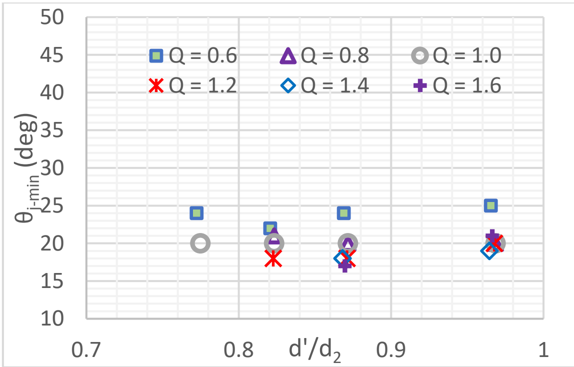

Configuration 6c

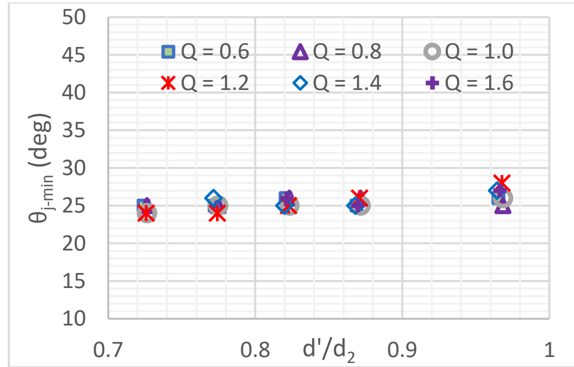

Configuration 7c

Figure 185. Minimum Observed Jump Angle for High Froude Number Configurations

Configurations 4a and 4c exhibited low minimum jump angles θ_{j-min} with consistent values across the range of $\frac{q_x}{q_D}$ and $\frac{d'_2}{d_2}$, when compared to the other stilling configurations. Configurations 1a and 7c also demonstrated higher, but consistent jump angles across the range of $\frac{q_x}{q_D}$ and $\frac{d'_2}{d_2}$. The maximum variation in minimum jump angle across all flow conditions for Configuration 7c was 4-degrees, ranging from 25- to 28-degrees. Configurations 2a, 3a, and 3c all showed a decreasing trend in jump angle with increasing $\frac{q_x}{q_D}$ and increasing $\frac{d'_2}{d_2}$. It was observed that for a given q_x, that the lower tailwaters would generally result in a steeping of the jump as increased forcing occurs. Similarly, the ratio of increasing incoming flow depth to the block height resulted in a flattening of the θ_{j-min}. This trend is illustrated for configuration 3a in Figure 186 for the q_{60} (a) and q_{160} (b) for tailwater scenario C.

a) Design Discharge (q_D)

b) 160-Percent of Design Discharge (q_{160})

Figure 186. Comparison of Typical Jump Angles for Configuration 3a

Configuration 1a (with intermittent ramps) exhibited a lower and more consistent jump angle than that of 2a (without intermittent ramps).

5.2.2.2 Low Froude Number Physical Model Observations

5.2.2.2.1 Required Tailwater

The hydraulic jump action for the Low Fr_1 configurations is substantially weaker than that of the High Fr_1 configurations. The weaker jump action does not generally result in the detachment of the jet as the tailwater is reduced and the surface roller is lost; therefore the loss of the hydraulic jump action is determined by the side and aerial observation of the roller action on the toe of the chute. Upon the loss of the surface roller, there was also generally a rapid increase in surface waves in the exit channel and sudden drop in observed tailwater with the additional momentum exiting the stilling basin. The loss of a defined surface roller is shown for the aerial and side views for configuration 11a at a discharge of q_{120} in Figure 187.

 

a) Hydr. Jump Action Maintained (Side) *b) Hydr. Jump Action Lost (Side)*

 

c) Hydr. Jump Action Maintained (Aerial) *d) Hydr. Jump Action Lost (Aerial)*

Figure 187. Determination of Required Tailwater to Maintain the Hydraulic Jump Action for Low Froude Configurations

For the case of the Type III configurations (11a, 12a, 13a, 15a, 16a) the combination of the relative block height and/or end sill height was sufficient to provide the required tailwater to maintain the hydraulic jump within the basin for the q_{60}, q_{80}, and q_D discharge conditions; with no loss of the surface roller. This resulted in a weak secondary jump just downstream of the end sill. It is worth noting that the tailwater gate did not allow for evaluation of tailwater stages below a ratio of approximately 0.75 $\frac{d'_2}{d_2}$. A side view of configurations 11a, 12a, 13a, and 15a for the q_{60} and q_{80} discharge scenarios are shown in Figure 188.

a) Configuration 11a, q_{60}

b) Configuration 11a, q_{80}

c) Configuration 12a, q_{60}

d) Configuration 12a, q_{80}

e) Configuration 13a, q_{60}

f) Configuration 13a, q_{80}

g) Configuration 15a, q_{60}

h) Configuration 15a, q_{80}

Figure 188. End sill tailwater control for USBR (1984) Configurations at q_{60} and q_{80}

For the q_D case, the surface roller is maintained for configurations 11a, 12a, 13a, and 15a; although the downstream waves and hydraulic attack appear more intense; with the primary difference in the performance being associated with the behavior of the super-critical jet over the end sill. Configuration 11a (with intermittent ramps) exhibits the most adverse impingement angle of the high velocity jet, impacting the closest to the structure. Configurations 12a, 13a, and 15a exhibit similar behavior of the jet exiting the basin, with configuration 15a being slightly less adverse. The hydraulic jump action and the exiting conditions for configurations 11a, 12a, 13a, and 15a for the q_D shown in Figure 189.

a))Configuration 11a (overview)

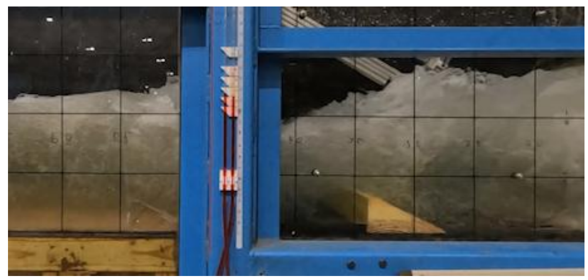

b) Configuration 11a (downstream)

c) Configuration 12a (overview)

d) Configuration 12a (downstream)

e) Configuration 13a (overview)

f) Configuration 13a (downstream)

g) Configuration 15a (overview) h) Configuration 15a (downstream)

Figure 189. Comparison of Configurations 11a, 12a, 13a, and 15a for q_D and end sill control ($d'/d_2 \sim 0.75$)

For the configuration 14a (USACE, 1992), the jump is elongated from that of the other configurations. This is characterized by a more pronounced surface roller, more like that of a free jump action. The transition from a maintained to a loss of the hydraulic jump action is similar, whereas the surface roller is lost, and all flow is directed downstream and upward by the baffles and the end sill. The flow characteristics before and after loss of the hydraulic jump for configuration 14a for the range of q_{60} through q_{160} is shown in Figure 190. In general, none of the configurations exhibited a extreme detached jet, as was the case with the high Fr_1 experiments.

a) q_{60}, jump maintained b) q_{60}, jump lost

c) q_{80}*, jump maintained*

d) q_{80}*, jump lost*

e) q_{D}*, jump maintained*

f) q_{D}*, jump lost*

g) q_{120}*, jump maintained*

h) q_{120}*, jump lost*

i) q_{140}*, jump maintained*

j) q_{140}*, jump lost*

k) q_{160}, jump maintained *l) q_{160}, jump lost*

Figure 190. Configuration 14a Before and After Loss of Hydraulic Jump Action

As shown in Figure 190, the difference in flow characteristics between the hydraulic jump action being maintained or lost decreases with increasing discharge; with the most drastic difference shown between the before (a) and after (b) condition for the q_{60} flow condition. This is similar to the finding for Keystone Dam as described in Section 5.1.2.

Configuration 16a is the same block location, shape, and configuration as configuration 15a; although the end sill is moved upstream to reduce the length of the stilling basin by approximately 20-percent. Similarly to configurations 11a, 12a, 13a, and 15a; the end sill controlled the tailwater to prevent the loss of the hydraulic jump action up through q_D. Above that the TW_{req} was similar to that of configuration 15a. The difference in the flow characteristics is shown in Figure 191.

a) q_{60}, configuration 15a

b) q_{60}, configuration 16a

c) q_{80}, configuration 15a

d) q_{80}, configuration 16a

e) q_D, configuration 15a

f) q_D, configuration 16a

g) q_{120}, configuration 15a

h) q_{120}, configuration 16a

i) q_{140}, configuration 15a   *j) q_{140}, configuration 16a*

k) q_{160}, configuration 15a   *l) q_{140}, configuration 16a*

Figure 191. Comparison of Configurations 15a and 16a at ~ 0.75 $\frac{d'_2}{d_2}$.

It can be seen from Figure 191 that the reduction in length also has a minor impact on the flow characteristics exiting the stilling basin.

A summary of the observations of required tailwater depth to maintain the hydraulic jump action for the Low Fr_1 configurations are tabulated in Table 42 and plotted in Figure 192. The tabulated values for the ratio of required tailwater to the sequent depth, critical depth, and incoming flow depth are tabulated in Table 43, Table 44, and Table 45, respectively. The graphs of the ratio of required tailwater to the sequent depth, critical depth, and incoming flow depth are illustrated in Figure 193, Figure 194, and Figure 195, respectively

Table 42. Required Tailwater Depth for Low Froude Number Configurations

Flow Conditions					TW_{req} (ft)					
Flow Desc.	Fr_1	d_c (ft)	d_1 (ft)	d_2 (ft)	11a	12a	13a	14a	15a	16a
q_{60}	5.6	0.47	0.15	1.11	SC	SC	SC	0.83	SC	SC
q_{80}	5.1	0.57	0.19	1.30	SC	SC	SC	0.99	SC	SC
q_D	4.7	0.66	0.24	1.45	SC	SC	SC	1.14	SC	SC
q_{120}	4.5	0.75	0.28	1.61	1.39	1.32	1.34	1.28	1.28	1.28
q_{140}	4.2	0.83	0.32	1.75	1.56	1.47	1.49	1.42	1.51	1.49
q_{160}	4.0	0.91	0.36	1.87	1.70	1.61	1.62	1.53	1.62	1.61

Note: "SC" represents tailwater control from end sill

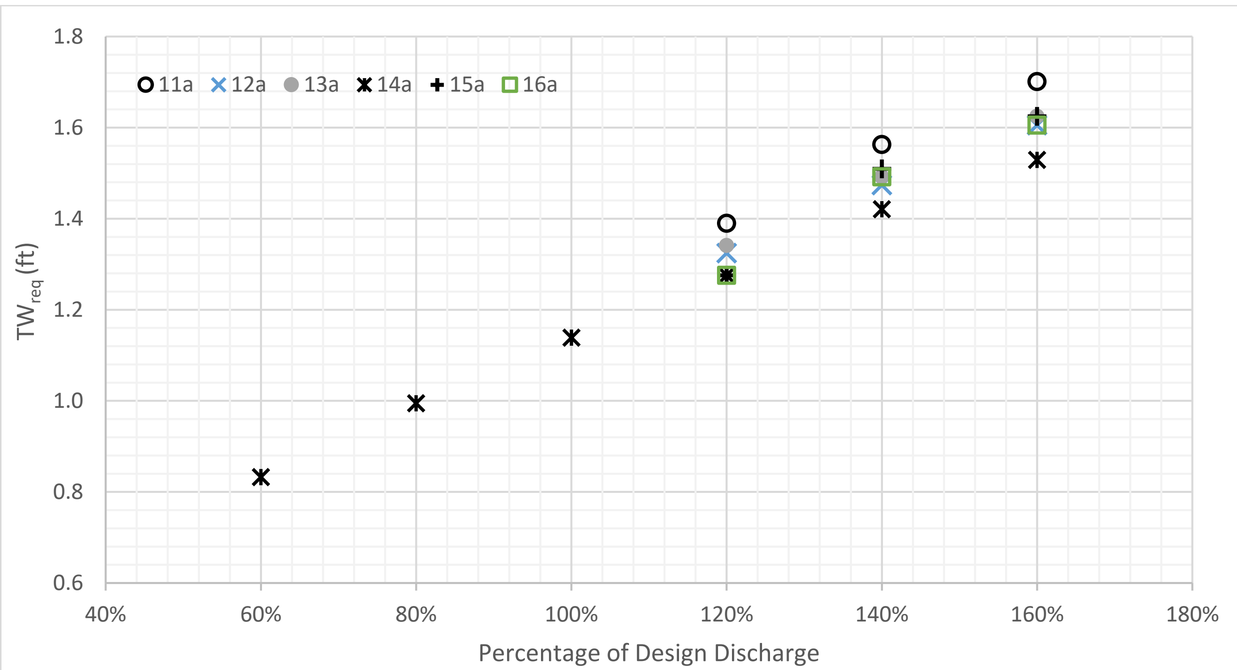

Figure 192. Required Tailwater Depth for Low Froude Number Configuration

Table 43. Ratio of Required Tailwater to Sequent Depth for Low Froude Number Configurations

Flow Conditions					$\frac{TW_{req}}{d_2}$					
Flow Desc.	Fr_1	d_c (ft)	d_1 (ft)	d_2 (ft)	11a	12a	13a	14a	15a	16a
q_{60}	5.6	0.47	0.15	1.11	SC	SC	SC	0.75	SC	SC
q_{80}	5.1	0.57	0.19	1.30	SC	SC	SC	0.77	SC	SC
q_D	4.7	0.66	0.24	1.45	SC	SC	SC	0.78	SC	SC
q_{120}	4.5	0.75	0.28	1.61	0.87	0.82	0.83	0.79	0.79	0.79
q_{140}	4.2	0.83	0.32	1.75	0.89	0.84	0.85	0.81	0.86	0.85
q_{160}	4.0	0.91	0.36	1.87	0.91	0.86	0.87	0.82	0.87	0.86

Note: "SC" represents tailwater control from end sill

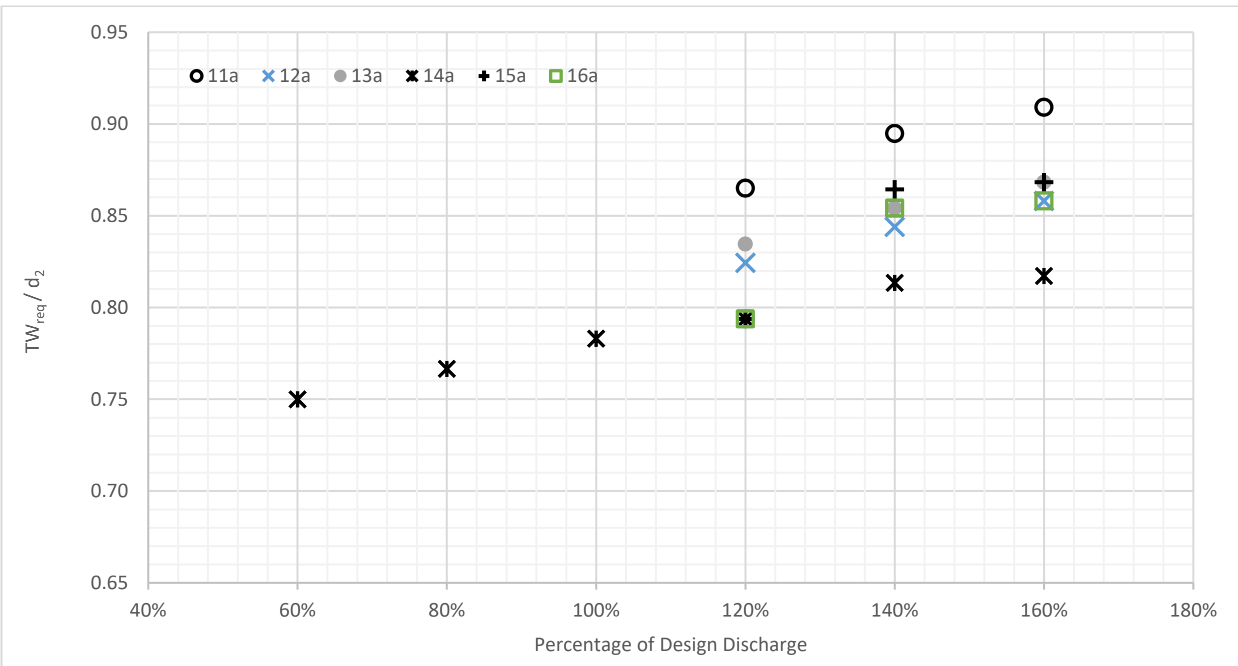

Figure 193. TW_{req} / d_2 as a Function of q_x / q_d for Low Froude Number Configurations

Table 44. TW_{req} / d_c as a Function of q_x / q_d for Low Froude Number Configuration

Flow Conditions					$\frac{TW_{req}}{d_c}$					
Flow Desc.	Fr_1	d_c (ft)	d_1 (ft)	d_2 (ft)	11a	12a	13a	14a	15a	16a
q_{60}	5.6	0.47	0.15	1.11	SC	SC	SC	1.77	SC	SC
q_{80}	5.1	0.57	0.19	1.30	SC	SC	SC	1.74	SC	SC
q_D	4.7	0.66	0.24	1.45	SC	SC	SC	1.72	SC	SC
q_{120}	4.5	0.75	0.28	1.61	1.86	1.77	1.79	1.71	1.71	1.71
q_{140}	4.2	0.83	0.32	1.75	1.89	1.78	1.80	1.71	1.82	1.80
q_{160}	4.0	0.91	0.36	1.87	1.88	1.77	1.79	1.69	1.79	1.77

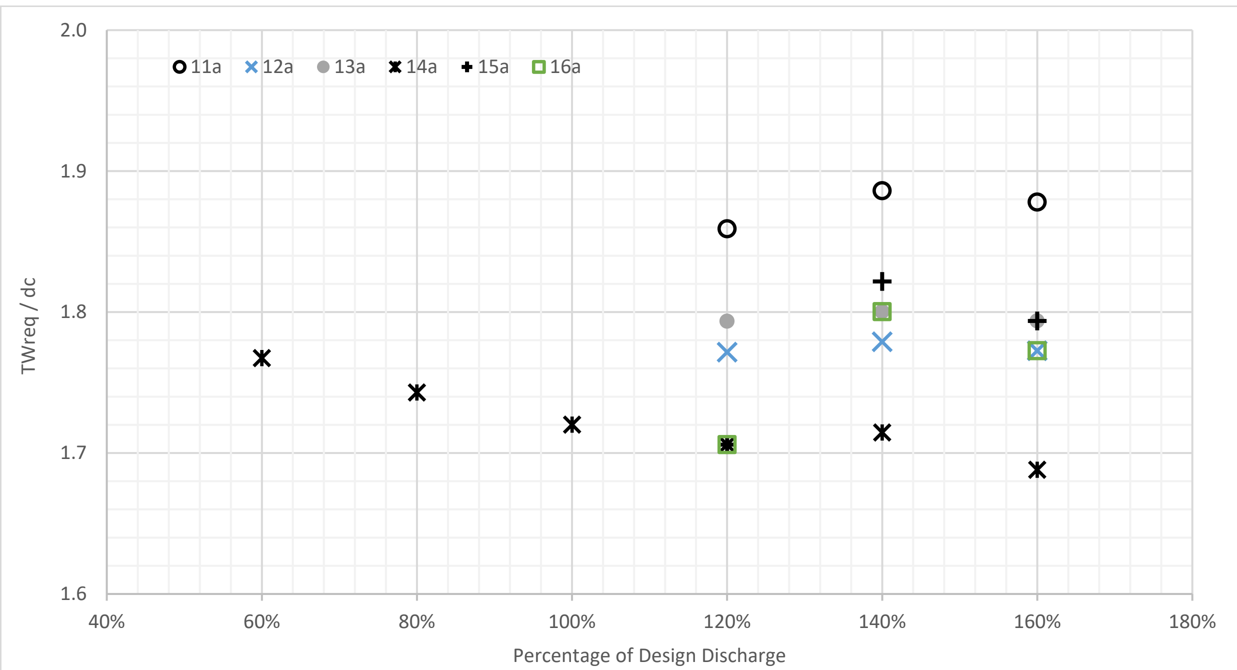

Figure 194. TW_{req} / d_c as a Function of q_x / q_d for Low Froude Number Configurations

Table 45. TW_{req} / d_1 as a Function of q_x / q_d for Low Froude Number Configurations

Flow Conditions					$\frac{TW_{req}}{d_1}$					
Flow Desc.	Fr_1	d_c (ft)	d_1 (ft)	d_2 (ft)	11a	12a	13a	14a	15a	16a
q_{60}	5.6	0.47	0.15	1.11	SC	SC	SC	5.57	SC	SC
q_{80}	5.1	0.57	0.19	1.30	SC	SC	SC	5.17	SC	SC
q_D	4.7	0.66	0.24	1.45	SC	SC	SC	4.82	SC	SC
q_{120}	4.5	0.75	0.28	1.61	5.03	4.79	4.85	4.62	4.62	4.62
q_{140}	4.2	0.83	0.32	1.75	4.95	4.67	4.72	4.50	4.78	4.72
q_{160}	4.0	0.91	0.36	1.87	4.77	4.50	4.56	4.29	4.56	4.50

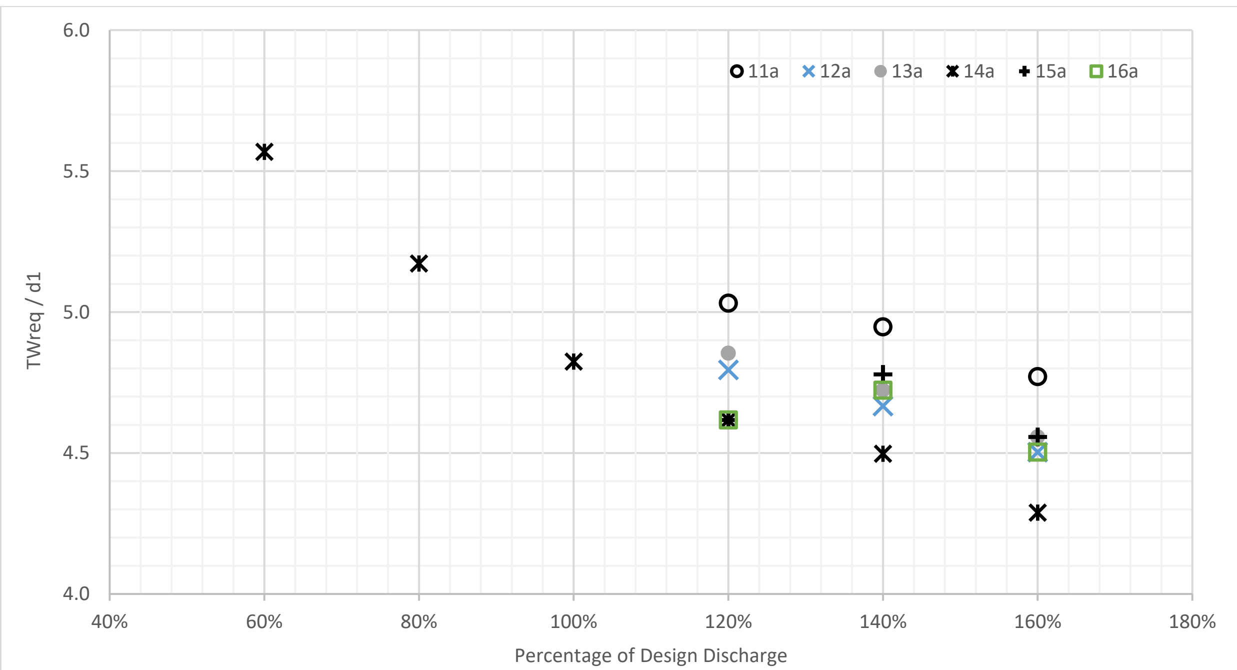

Figure 195. TW_{req} / d_1 as a Function of q_x / q_d for Low Froude Number Configurations

5.2.2.2.2 Local Scour Potential

Unlike the High Fr_1 experiments, the Low Fr_1 experiments have less aeration within the hydraulic jump, and therefore lower entrained air in the exiting flow. This results in the observation of the localized flow conditions immediately downstream more challenging. The localized turbulence is also less severe than for the equivalent $\frac{q_x}{q_D}$ and $\frac{d'_2}{d_2}$ flow condition for the High Fr_1 experiment. In addition, there is an obstruction from the vertical beam of the flume within the length of d_2 downstream of the end sill for all the configurations, except 16a. For these reasons, the semi-quantitative turbulence index was not utilized to describe the near-boundary turbulence conditions for the Low Fr_1 configurations.

5.2.2.2.3 Maximum Boil Height

The maximum boil height for the Low Fr_1 configurations was evaluated similarly to the High Fr_1 configurations; and is detailed in Table 46 and illustrated in Figure 196.

Table 46. Observed Maximum Boil Heights for Low Froude Configurations

Flow Conditions						Maximum Boil Height - Zmax(ft)					
Flow Scenario	Fr_1	d_1 (ft)	TW ID	$\frac{d'}{d_2}$	TW (ft)	11a	12a	13a	14a	15a	16a
q_{60}	5.59	0.15	A	1.01	1.13	Obs.	1.4	1.4	1.35	1.4	1.4
			B	0.91	1.01	Obs.	1.4	1.3	1.25	1.4	1.4
			C	0.86	0.95	Obs.	1.4	1.3	1.2	1.4	1.4
			D	0.81	0.90	Obs.	1.3	1.2	1.2	1.4	1.4
			E	0.76	0.84	Obs.	1.3	1.2	1.2	1.3	1.3
q_{80}	5.11	0.19	A	1.00	1.29	Obs.	Obs.	Obs.	1.5	Obs.	Obs.
			B	0.90	1.17	Obs.	1.5	1.5	1.5	Obs.	Obs.
			C	0.85	1.10	Obs.	1.5	1.5	1.35	1.5	Obs.
			D	0.80	1.04	Obs.	1.5	1.5	1.3	1.4	1.5
			E	0.75	0.97	1.8	1.5	N/A	N/A	N/A	1.5
q_D	4.70	0.24	A	1.02	1.48	2.2	Obst.	Obst.	Obst.	Obst.	Obst.
			B	0.92	1.33	2	Obst.	Obst.	Obst.	Obst.	Obst.
			C	0.86	1.26	1.9	1.5	Obst.	Obst.	Obst.	Obst.
			D	0.81	1.18	1.8	1.5	N/A	1.5	Obst.	Obst.
q_{120}	4.45	0.28	A	1.02	1.64	2.4	1.8	Obst.	Obst.	1.8	1.9
			B	0.91	1.47	2.2	1.8	Obst.	Obst.	1.9	1.9
			C	0.87	1.39	2	1.8	N/A	Obst.	N/A	N/A
			D	0.81	1.31	2.2	N/A	N/A	N/A	N/A	N/A
q_{140}	4.25	0.32	A	1.02	1.78	2.5	2	1.9	2	1.9	2
			B	0.92	1.60	2.3	2	1.9	1.8	1.9	1.9
			C	0.86	1.51	N/A	2	N/A	N/A	N/A	N/A
q_{160}	44.05	0.36	A	1.02	1.91	2.7	2.1	2.1	2.1	2	1.9
			B	0.92	1.72	2.6	2	1.9	2	2	2
			C	0.87	1.63	N/A	N/A	N/A	1.9	N/A	N/A

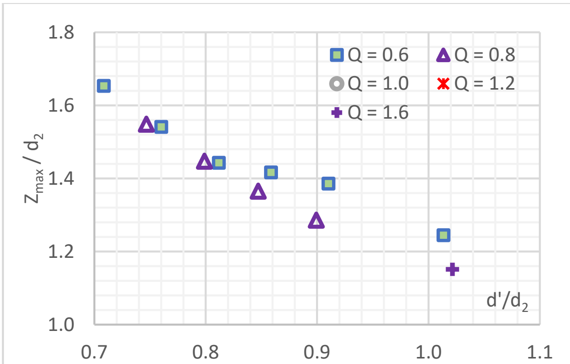

a) Configuration 11a

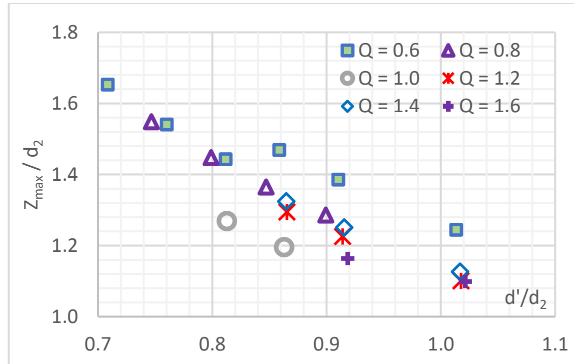

b) Configuration 12a

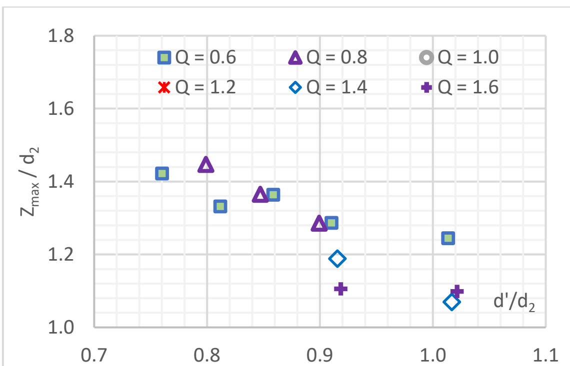

c) Configuration 13a

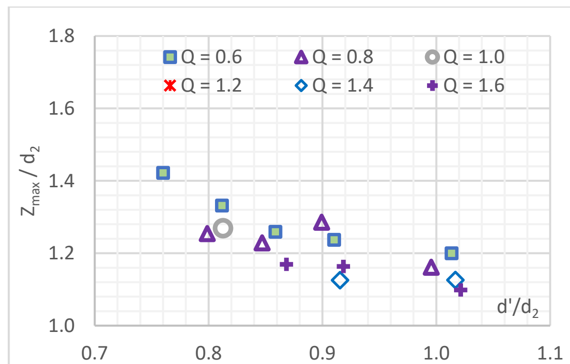

d) Configuration 14a

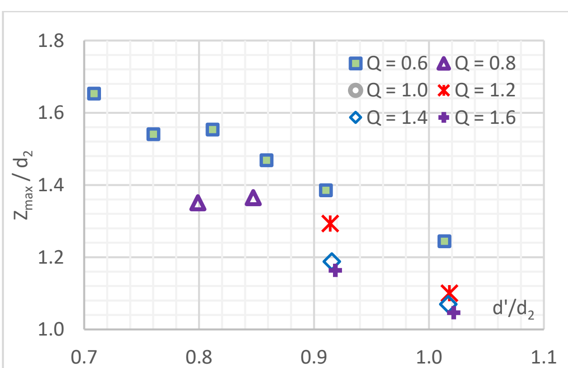

e) Configuration 15a

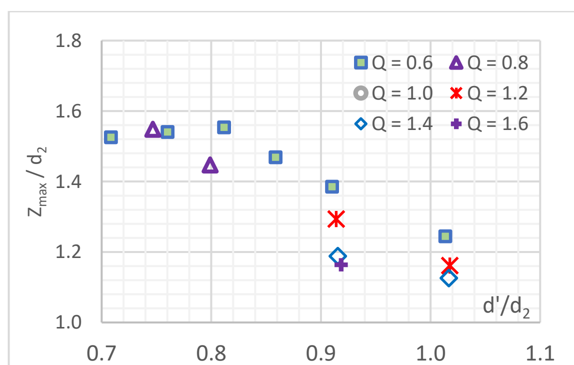

f) Configuration 16a

Figure 196. Graphical Results for Stilling Basin Boil Height Ratio $\frac{Z_{max}}{d_2}$ for Low Froude Configurations

There was a strong trend of decreasing $\frac{Z_{max}}{d_2}$ with increasing $\frac{d'_2}{d_2}$, although the absolute height stays relatively the same. An example of this trend for configuration 11a for the q_{60} flow condition is shown in Figure 197.

a) Tailwater Scenario A

b) *Tailwater Scenario B*

c) *Tailwater Scenario C*

d) *Tailwater Scenario D*

e) *Tailwater Scenario E*

f) *Tailwater Scenario F*

Figure 197. Typical High Boil for Configuration 11a at q_{60} with Varied Tailwater

There was also a general trend observed whereas the $\frac{Z_{max}}{d_2}$ reduced with increasing $\frac{q_x}{q_D}$, which may be associated with the decreasing relative baffle block height in relation to the incoming flow depth.

5.2.2.2.4 Jump Angle

The jump angle for the Low Fr_1 experiments were determined in the same way as the High Fr_1, although the d_1 values are higher making the hinge point for jump angle determination relatively high on the chute. An example of the determination of jump angle for configuration 11a, q_{140}, and Tailwater Scenario A is shown in Figure 198.

Figure 198. Example of Determination of Minimum Jump Angle for Low Fr_1 Experiments

The values for jump angle are detailed in Table 47 and the results illustrated in Figure 199.

Table 47. Minimum Observed Jump Angle for Low Froude Configurations

Flow Conditions						Minimum Jump Angle – $\theta_{j\text{-}min}$ (deg)					
Flow Scenario	Fr_1	d_1 (ft)	TW ID	$\frac{d'}{d_2}$	TW (ft)	11a	12a	13a	14a	15a	16a
q_{60}	5.59	0.15	A	1.01	1.13	29	23	24	8	28	26
			B	0.91	1.01	30	24	25	10	27	25
			C	0.86	0.95	30	24	24	10	28	25
			D	0.81	0.90	32	25	25	9	26	25
			E	0.76	0.84	32	25	25	11	28	23
			F	0.71	0.79	30	27	N/A [1]	N/A	30	25
q_{80}	5.11	0.19	A	1.00	1.29	26	26	20	9	25	22
			B	0.90	1.17	27	26	22	11	25	21
			C	0.85	1.10	28	25	22	14	24	21
			D	0.80	1.04	27	25	24	15	28	22
			E	0.75	0.97	27	27	N/A	N/A	N/A	24
q_D	4.70	0.24	A	1.02	1.48	26	21	19	15	21	21
			B	0.92	1.33	25	23	20	14	25	22
			C	0.86	1.26	25	24	20	14	26	22
			D	0.81	1.18	26	21	N/A	14	25	21
q_{120}	4.45	0.28	A	1.02	1.64	17	15	14	10	13	19
			B	0.91	1.47	16	16	14	12	15	18
			C	0.87	1.39	N/A	20	N/A	12	N/A	N/A
			D	0.81	1.31	N/A	N/A	N/A	N/A	N/A	N/A
q_{140}	4.25	0.32	A	1.02	1.78	10	11	10	9	10	10
			B	0.92	1.60	13	15	11	10	11	14
			C	0.86	1.51	N/A	19	N/A	N/A	N/A	N/A
q_{160}	44.05	0.36	A	1.02	1.91	10	10	8	10	9	12
			B	0.92	1.72	N/A	10	8	9	10	10
			C	0.87	1.63	N/A	N/A	N/A	9	N/A	N/A

[1] Hydraulic jump action lost

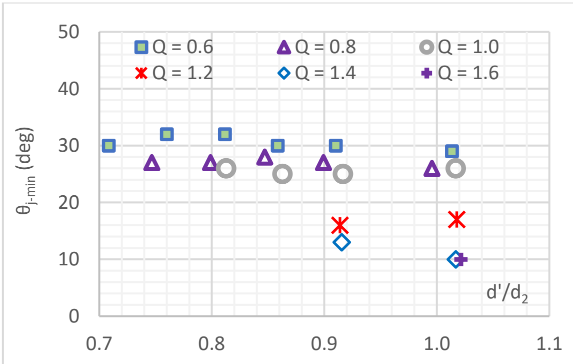

a) Configuration 11a

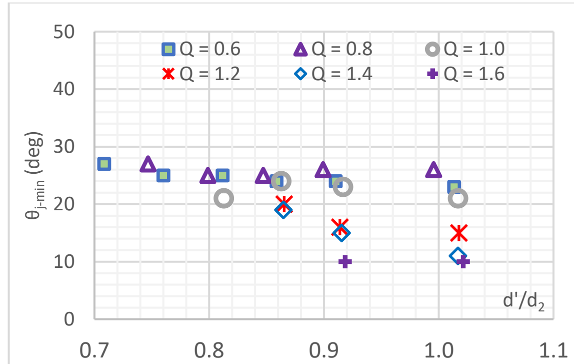

b) Configuration 12a

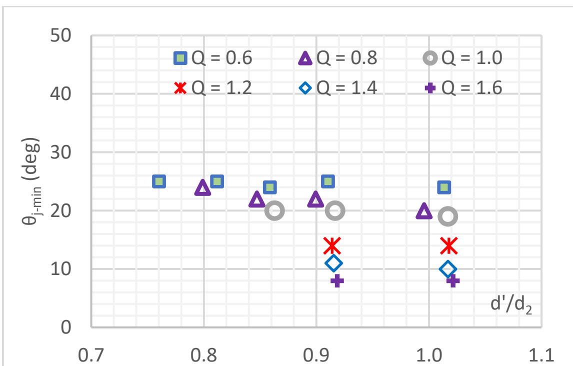

c) Configuration 13a

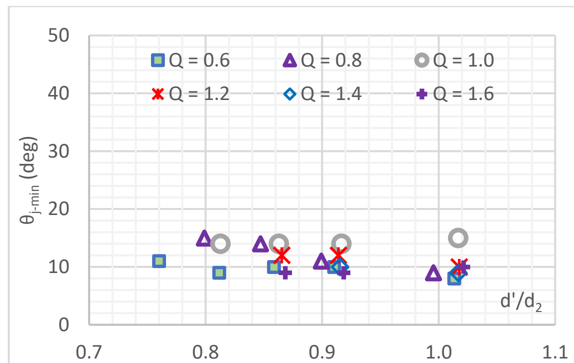

d) Configuration 14a

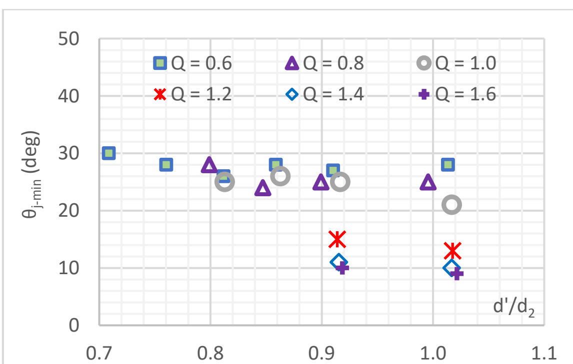

e) Configuration 15a

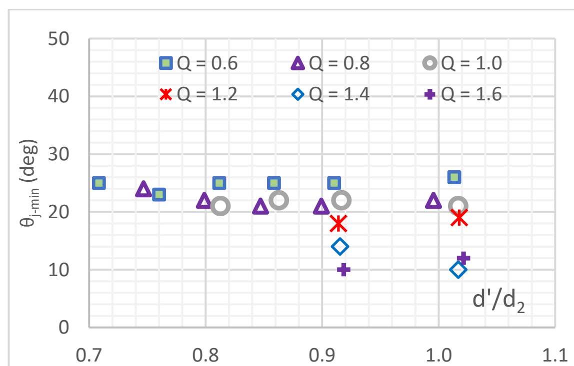

f) Configuration 16a

Figure 199. Minimum Observed Jump Angle for Low Froude Number Configurations

Similarly to the configuration 4a, 14a exhibited consistently low minimum jump angles θ_{j-min} across the range of $\frac{q_x}{q_D}$ and $\frac{d'_2}{d_2}$, when compared to the other stilling configurations.

Interestingly, the other configurations saw a significant reduction in θ_{j-min} With $\frac{q_x}{q_D} > 1$.

6 CONCLUSIONS AND RECOMMENDATIONS

6.1 Summary of Significant Findings

A numbered list of significant findings associated with the current research are provided below. Detailed descriptions of these significant findings and other conclusions and recommendations associated with the research objectives are provided subsequently.

7. The USACE (1992) stilling basin configuration is recommended for Fr_1 less than 4.5.
8. The Modified Type III stilling basin configuration is recommended for Fr_1 in the range of 4.5 to 8.
9. The stilling basin length for the USACE (1992) and USBR (1984) can be expressed by Equation 35.
10. The minimum required tailwater at the design discharge for the USACE (1992) and USBR (1984) can be expressed by Equation 36.
11. A toe curve is not recommended for the hydraulic jump basin due to increase in length required and the decrease in jump stability.
12. Intermittent ramps associated with the tapered baffle block configuration are not recommended due to increase in downstream scour potential, decreased tailwater resilience, cost, general lack of observed cavitation damage, and unproven effectiveness in reducing cavitation damage.
13. The Modified Type III is recommended over the standard or tapered block design configurations, as it has superior tailwater resilience, reduced downstream near boundary turbulence, and reduced cost and potentially maintenance requirements.

14. Macro-scale turbulent structures exiting the stilling basin are the primary phenomenon controlling downstream scour potential. A maximum downstream attack angle of 15-degrees from horizontal was determined for the USACE (1992) stilling basin configuration for Fr_1 in the range of 3 to 5.

6.2 Consolidation of Existing Guidance

6.2.1 General

The USACE (1992) and the USBR (1984) baffled stilling basins are commonly used as a terminal structure for large dams. In general, the stilling basin lengths and required tailwater are similar for both; although the baffle location, baffle block height, and end sill height vary significantly. It was determined from the current research that the stilling basin length and required tailwater for both could be unified into common expressions as a function of Fr_1 ; whereas the baffle location, baffle height, and end sill height are unique to the stilling basin type.

The development of the USACE (1992) stilling basin is not well described; the design intent was inferred from a combination of available literature (USACE, 1965; USACE, 1969), observations from case studies (USACE, 1939; USACE, 1960; USACE, 2018), and the systematic evaluation conducted as part of the current research. The design philosophy was inferred as minimizing the height of the block to reduce construction costs and minimizing scour downstream, often adding a second row of baffles to provide tailwater resilience and decrease downstream scour potential. The baffles for the USACE (1992) stilling basin are located significantly downstream as compared to the USBR Type III stilling basin. The downstream location results in the baffles and the end sill acting together to lift the high velocity floor jet away from the downstream bed in the vicinity of the structure.

It was observed that the majority of the specific projects that were used to develop the USACE (1992) configuration had Fr_1 below 4.5 and optimized for a tailwater just sufficient to maintain the hydraulic jump action at the design discharge (USACE, 1960; USACE, 1969). In fact, some stilling basins were configured in such a way as to tolerate the loss of the hydraulic jump, while minimizing the downstream erosion potential (USACE, 1939). Another common finding was that the downstream baffle location was thought to decrease the potential for cavitation damage due to the reduced velocity and observed higher sidewall and floor pressures from physical model studies (Gedney, 1961; USACE, 1965; USACE, 1970).

The development of the USBR Type III configuration as described in USBR (1955), was verified with rigid bed physical model evaluation and optimized based on minimizing the jump length at sequent depth. The baffled blocks were evaluated at a constant distance downstream of 0.8 D_2 with a block height that varies with Fr_1 and is significantly greater than the USACE (1992).

An evaluation of the data used in deriving the standard stilling basin dimensions used for the SAF (USDA, 1959), Type III (USBR, 1955), and USACE (1992) suggests that all three would provide similar energy dissipation and protection of the downstream channel when operated with the design discharge and sequent depth tailwater conditions.

In general, re-evaluation of the data suggested that all the stilling basin dimensions were described more consistently when normalized to the d_1 as a function of Fr_1. This is consistent with the findings of Blaisdell (1948) and USBR (1955).

6.2.2 Stilling Basin Length

The length of the stilling basin is a primary consideration for design. One primary benefit of a baffled hydraulic jump stilling basin is the reduction of length and associated cost and impacts to the waterway over that required for a free jump.

It is not clear in USBR (1984) if it was intended for the length of the basin to be determined by the point of intersection of the chute and the point of tangency with the horizontal when a toe curve is used. The evaluation of the point in which the stilling basin length is to be measured was conducted by comparing configurations 3c and 6c. The TW_{req} and the downstream turbulence intensity was higher for the case where the basin length was measured from the point of intersection of the chute and the horizontal floor (configuration 3c) as opposed to when the basin length is increased by measuring the length from the end of the toe curve. Also, there was a significant surging potential observed for the configuration 3c as the jump action was lost. For these reasons, the stilling basin length should be measured from the end of the toe curve for the Type III stilling basin. For the incoming flow conditions utilized for the high Fr_1 configurations, this results in an approximately 20-percent increase in the basin length. There was much less influence on the presence of a toe curve for the USACE (1992) stilling basin and no additional length is recommended.

The d_2 is the parameter used by USBR (1984) for all stilling basin types (Type I through Type IV). USBR (1955) plots the experimental data in terms of both d_1 and d_2; stating that "the first is perhaps the better method while the second is more common". The USACE (1992 and 1987) utilizes d_1 as the scale parameter, although USACE (1980) utilizes d_2.

As demonstrated by Figure 200, the use of d_1 has less variation across the data utilized in USACE (1969) and that of USBR (1955). It is recommended that Equation 35 be utilized for determination of required stilling basin length for both USACE (1991) and USBR (1984) stilling basin configurations for Fr_1 between 2.5 and 14.

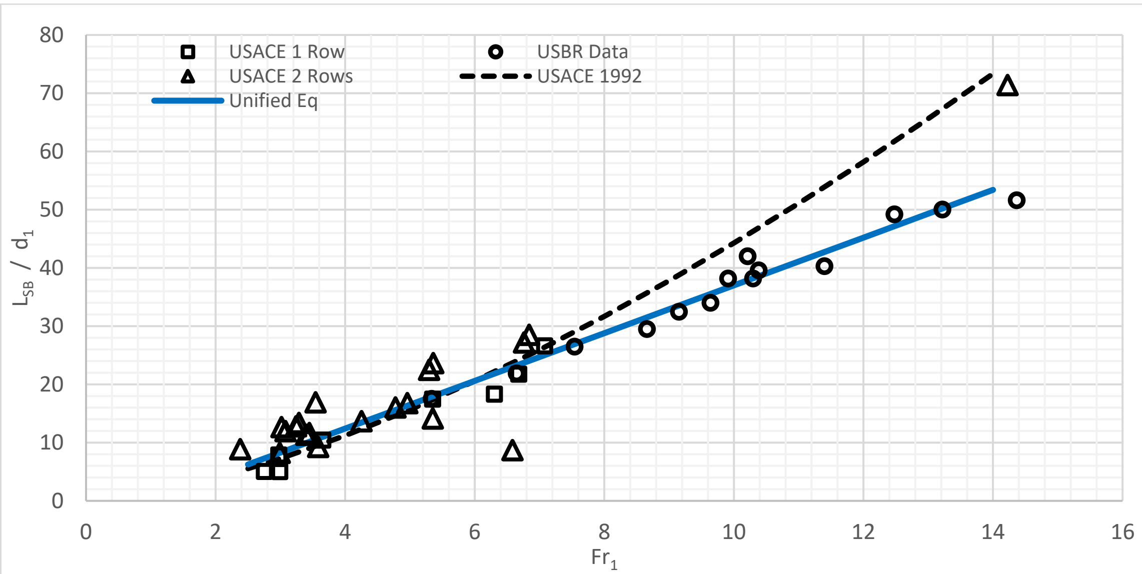

Figure 200. Figure 84. Comparison of Existing Data/Guidance and Unified Equation for $\frac{L_{SB}}{d_1}$

Equation 35. Unified Equation for Stilling Basin Length

$$\frac{L_{SB}}{d_1} = 4.1Fr_1 - 4$$

The relationship of Equation 35 to the data and existing guidance expressed as a function of $\frac{L_{SB}}{d_2}$ is shown in Figure 201.

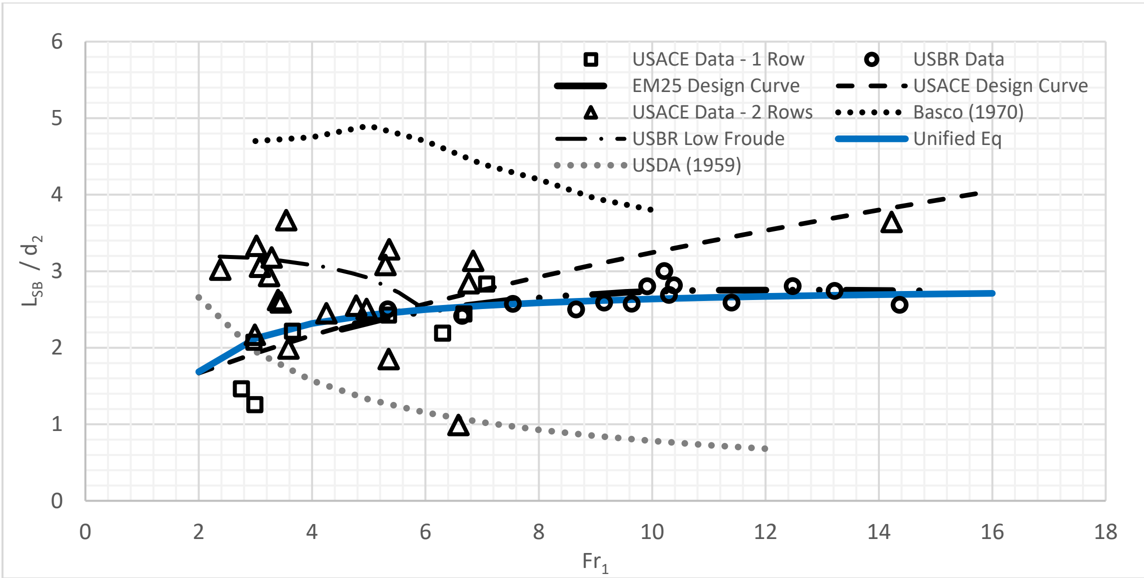

Figure 201. Comparison of Existing Data/Guidance and Unified Equation expressed as $\frac{L_{SB}}{d_2}$

When plotting the data and design guidance, it is apparent that the USACE (1992) design guidance is not adequately informed by experimental data past a $Fr_1 \sim 7$.

6.2.3 Required Tailwater

The tailwater required to maintain the hydraulic jump is of critical importance when evaluating the performance of stilling basins for potential failure modes. The "sweepout" (or loss of the hydraulic jump action), can result in a sudden change in flow characteristics inside and downstream of the stilling basin.

Inside the basin, the loss of the hydraulic jump action can result in a sudden reduction in water levels that provide resistance to stilling basin uplift and provide an increase in the lateral loads experienced by the baffle blocks and end sill. The loading and resisting on the stilling basin sidewalls are also affected. The resisting forces on the upper floor slabs in the upper basin suddenly decrease and there is potential for increased hydrodynamic loads near the locations of stagnation adjacent to baffles and the end sill. Downstream of the stilling basin, the loss of the hydraulic jump action can result a significant increase in velocity in the downstream channel and impingement of the high velocity jet near the structure resulting in increased scour potential.

The range of required tailwater ratios to maintain the hydraulic jump is relatively small across the configurations evaluated under the current research. The range within the USBR data alone is much wider for $Fr_1 > 4.5$ and USACE much wider for $Fr_1 < 7$, which suggests that there may be other factors contributing to the variation. The variation could be associated with the subjective nature of determining the required tailwater to maintain the hydraulic jump action. Another contributor to the variation may be a result of the challenges estimating the incoming flow conditions V_1, d_1, and Fr_1. Small variations in estimates of these parameters can result in large differences in the estimated d_2; in which translates to the calculated dimensionless ratio of $\frac{TW_{req}}{d_2}$.

For the low Fr_1 experiments conducted, the definition placed on determining the hydraulic jump can play a major factor in variations in estimates. There were little differences between the flow characteristics immediately prior to and immediately following the loss of the hydraulic jump action.

For the case of the Low Fr_1 configurations, the hydraulic jump is not an efficient energy dissipating structure; although it can significantly reduce the near bed hydraulic attack potential and associated local scour potential compared to a horizontal apron alone. In addition, the reduction of the tailwater below the sequent depth results in additional energy dissipation via the momentum transferred to the baffles and end sill; thereby increasing it's effectiveness as an energy dissipator.

It was determined for the current research with mobile bed experiments based on the Keystone Dam stilling basin (approximately equal in dimensions to the USACE standard configuration), that the scour potential immediately downstream of the end sill was reduced after the hydraulic jump action was lost. This was a result of the baffles and end sill acting together to lift the high velocity jet and macro-scale turbulent structures away from the bed near the end sill. This finding is consistent with evaluations of the Bluestone Dam second stage stilling basin (USACE,2018).

When applying the USBR (1984) end sill and baffle blocks to a Fr_1 of approximately 4, the tailwater created by the end sill is sufficient to maintain the hydraulic jump action up to the design discharge (q_D), although the jump action is highly "forced" and presents a significant boil and a secondary jump downstream of the basin for lower $\frac{d'_2}{d_2}$ and $\frac{q_x}{q_D} \leq 1$.

Although the data from the current research suggests that some stilling basin configurations exhibit more resilience to tailwater, the use of Equation 36 for the standard stilling basin design at the design discharge is recommended for estimating the required tailwater for standard stilling basin designs at the design discharge ($\frac{q_x}{q_D} = 1$) .

Equation 36. Unified Equation for Required Tailwater Depth

$$\frac{TW_{req}}{d_1} = 1.8Fr_1 - 0.2$$

Equation 36 is plotted against the design guidance and experimental data from USACE (1969) and USBR (1955) when normalizing to the d_1 and the d_2 in Figure 99 and Figure 100, respectively.

To account for potential observation errors, scale effects, errors in estimating the index parameters (e.g. d_1, d_2, d_c, Fr_1), and prototype tailwater errors, a reasonable factor-of-safety may be prudent. The magnitude of the safety factor should be risk-informed and should consider the frequency of use, potential for additional tailwater degradation, potential for damage to baffle blocks, unbalanced flow, downstream erodibility, impacts of cost and stability associated with increasing excavation depth, and stilling basin stability with lost jump action, at a minimum.

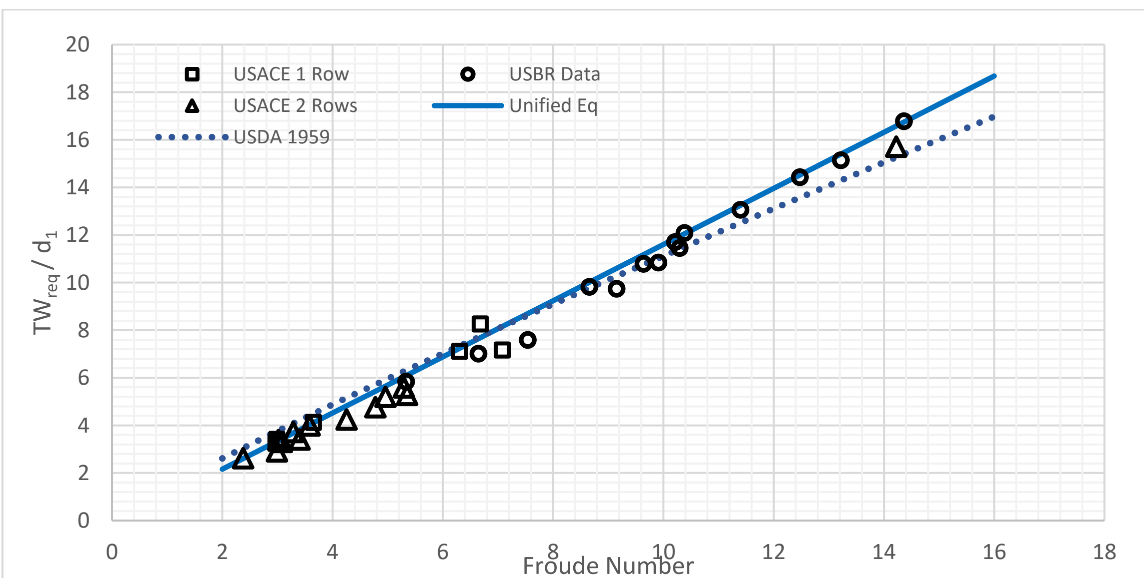

Figure 99. Comparison of Existing Data/Guidance and Unified Equation for $\frac{d'_2}{d_1}$

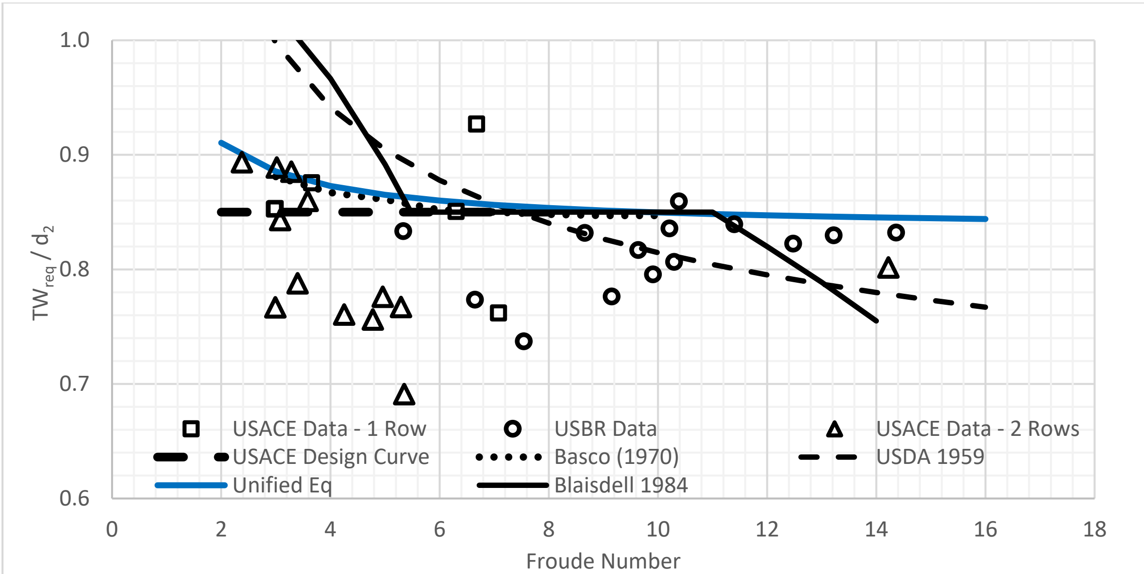

Figure 100. Comparison of Existing Data/Guidance and Unified Equation for $\frac{d'_2}{d_2}$

The use of Equation 7 (USDA, 1959) does not well represent the experimental data for the USACE (1992), USBR (1955), or current research; and therefore, is not recommended for use.

6.2.4 Block Location and Height

As mentioned previously, there are two different design philosophies for the location and size of the baffle blocks evaluated with the current research. The USACE (1992) approach utilizes a smaller baffle that is farther downstream than the USBR Type III. The USACE (1992) stilling basin was optimized for use with spillways of higher unit discharge and lower Fr_1, with a primary objective of reducing downstream scour potential while minimizing the required tailwater depth. The USBR (1984) was verified via rigid bed physical modeling with an objective of reducing the length of the hydraulic jump. These two different philosophies resulted in combinations of height and location that are unique to the stilling basin, and it is not recommended that they be unified based on the current research.

Based on the experiments conducted as part of the current research, the Modified USBR Type III (7a) demonstrated the best tailwater resilience and lowest downstream turbulence intensity for the High Fr_1 scenarios; while the USACE (1992) exhibited the best tailwater resilience and consistent boil height, without a secondary jump for the Low Fr_1 scenarios. Project specific considerations notwithstanding, it is recommended that the Modified Type III stilling basin be utilized for Fr_1 between 4.5 and 8, while the USACE (1992) configuration be utilized for Fr_1 between 2.5 and 4.5.

6.2.5 End sill

The height and shape of the end sill is critical to the potential for downstream scour. The use of an end sill downstream of the hydraulic jump stilling basin was one of the first major advances in the use of hydraulic jump terminal structures. Although the end sill was not explicitly evaluated as part of the current research; multiple items found in literature and observations through the experimentation were made.

The USBR (1984) Type III stilling basin is intended for use at Fr_1 of 4.5 to 9. Based on observations of the High Fr_1 experiments, the end sill height is sufficient to engage the high velocity jet that is redirected upward from the baffles. If the end sill were lower, or closer to the baffles, it is anticipated that it would not be sufficient height to engage the high velocity jet; especially for $\frac{d'_2}{d_2} < 0.9$. For the Low Fr_1 configurations, the end sill is sufficient to maintain the hydraulic jump action to at least a $\frac{d'_2}{d_2} = 0.75$ for the flow scenarios $\frac{q_x}{q_D} <= 1.0$. Although this is adequate for maintaining the jump action, a secondary jump occurs with this configuration, and therefore any use of this configuration should be properly investigated, including the scour potential due to the secondary jump action. Another potential would be to utilize the basin configuration by replacing the sill with a second stage weir and providing an additional downstream apron (similar to the stilling basin modification at Bluestone Dam).

For the USAEC (1992) stilling basin, the end sill is in closer proximity to the baffle blocks and works in combination with the baffle blocks to break up and lift the floor jet. An extreme case of this concept is shown by the Chief Joseph Dam (Figure 49); whereas the baffles are in very close proximity to the end sill. The majority of the stilling basins utilized in development of the guidance for the standard USACE (1992) basin had Fr_1 below 4.5. The observed action of the combination of baffle blocks and end sill for configuration (4a) seemed to achieve this goal throughout the range of experiments. This was reinforced with the observations of scour form the Keystone stilling basin configuration, with the end sill being ½ the height of the baffle blocks. For the High Fr_1 experiments, it was observed that the prescribed end sill height is too small to effectively engage the remaining high velocity floor jet. Based on these experiments and the comparison to other standard guidance as shown in Figure 16, it is recommended that the minimum of end sill height of $\frac{d_1}{2}$ be removed from the end sill height guidance in USACE (1992), so that the end sill height has a value of $0.08d_2$. The USACE (1987) states that the end sill should be half the height of the baffle; which may also provide a reasonable value for use for spillways.

6.2.6 Baffle Loads

Based on the experimental data from USACE (1970), it is demonstrated that the forces acting on baffles are directly related to the baffle location, baffle area, baffle shape, and blockage ratio. There is increasing streamwise baffle force with increasing height, increasing blockage ratio, decreasing distance to baffles, and decreasing tailwater.

Based on theoretical examinations and comparison to experimental data collect for Bluestone Dam, it is recommended that the Equation 19 (USBR, 1987) significantly overestimates forces on baffle blocks due to the factor of 2 applied to the total specific energy. Consequently, Equation 18 significantly underestimates the force on the baffle block; whereas the value estimated was less than the mean value of the experimental data.

The use of Equation 37 is recommended for the estimate of maximum sustained force on the composite baffle in the streamwise direction. This does not account for the impacts of floating debris or the potential for torsional forces resulting from unbalanced flow or from the fluctuating and lateral forces that have been observed.

Equation 37. Physically Based Maximum Baffle Block Load

$$F_B = \gamma A_B (h_{v1} + P_v)$$

Significant impact of floating debris may occur on baffle faces. Based on localized flow observations of the various stilling basin configuration and flow conditions and the simulations of floating woody debris conducted specifically for Bluestone Dam; it is expected that the potential and magnitude for impacts of floating debris increase with decreased distance to the baffles (X_{B1}) and decreasing tailwater conditions ($\frac{\mathrm{TW_{req}}}{\mathrm{d_2}}$).

6.3 Evaluation of Increased Hydrologic Loading

6.3.1 Tailwater Resiliency

It was found through the current research that the ratio of $\frac{TW_{req}}{d_2}$ generally reduced as the unit discharge decreased below the design q_D, and increased above the design discharge. The increase in the $\frac{TW_{req}}{d_2}$ increased from 9- to 13-percent when comparing a discharge that is 160-percent (q_{160}) of the design discharge (q_D) for the High Fr_1 configurations. Since the tailwater was controlled by the end sill for five out of six of the Low Fr_1 configurations for the q_D, the only ratio available is that of the 4a configuration (USACE, 2 Rows of Baffles). The increase in the $\frac{TW_{req}}{d_2}$ for configuration 4a, was only 4-percent for the q_{160}. It is worth noting that the $\frac{TW_{req}}{d_2}$ > 0.85 for all Low Fr_1 at the q_{160} ; with the exception of configuration 4a.

The relationships contained in Section 7.2.1 and Section 7.3.1 can be used to determine the required tailwater ratios for standard stilling basin configurations for various $\frac{q_x}{q_D}$ Ranging from 60 to 160-percent of the q_D. This could include the use of the data to "over" or "under" design the stilling basin; whereas the basin dimensions are scaled up and down based on considerations of a particular site and project condition.

The $\frac{TW_{req}}{d_1}$ decreased as the $\frac{q_x}{q_D}$ ratio increased for both the High- and Low- Fr_1 stilling basins. The rate of decrease was significantly less for the $\frac{q_x}{q_D}$ > 1, and nearly constant for the High Fr_1 configurations. The $\frac{TW_{req}}{d_1}$ as a function of $\frac{q_x}{q_D}$ for the Low (a) and High (b) Fr_1 are illustrated in Figure 202.

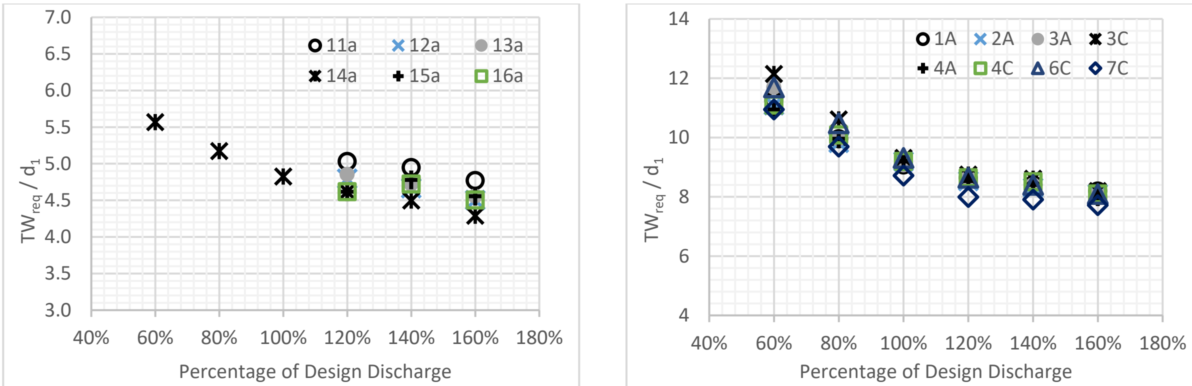

a) Low Fr_1 *b) High Fr_1*

Figure 202.Required Tailwater Ratio ($\frac{TW_{req}}{d_1}$) for Low (~4) and High (~8) Fr_1 Configuration

The $\frac{\mathrm{TW_{req}}}{\mathrm{d_2}}$ as a function of $\frac{q_x}{q_D}$ for the Low (a) and High (b) Fr_1 are illustrated in Figure 203.

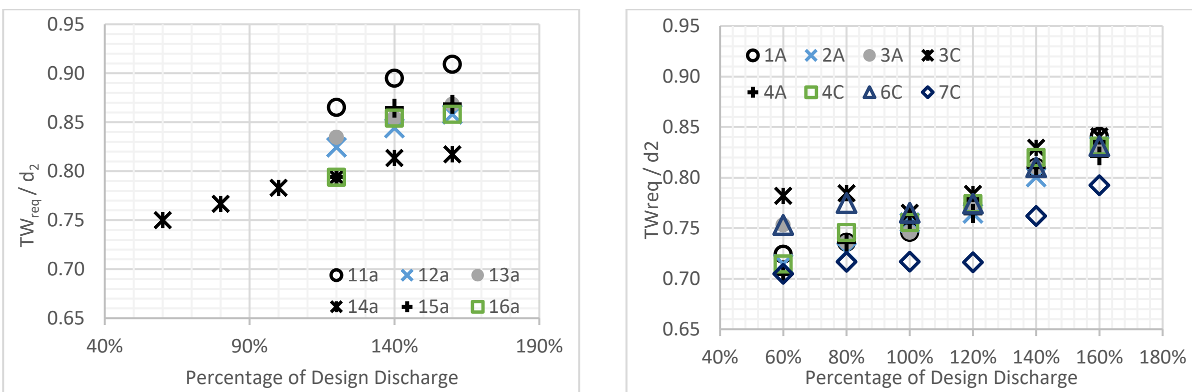

a) Low Fr_1 *b) High Fr_1*

Figure 203. Required Tailwater Ratio ($\frac{TW_{req}}{d_2}$) for Low (~4) and High (~8) Fr_1 Configuration

The $\frac{\mathrm{TW_{req}}}{\mathrm{d_2}}$ for the USACE (1992) stilling basin configurations is available for the range $0.6 < \frac{q_x}{q_D} < 1.6$ for both Low and High Fr_1 configurations. The data show consistent linear trends of increasing $\frac{\mathrm{TW_{req}}}{\mathrm{d_2}}$ increased as $\frac{q_x}{q_D}$ increases above $\frac{q_x}{q_D} > 1$, as shown in Figure 204.

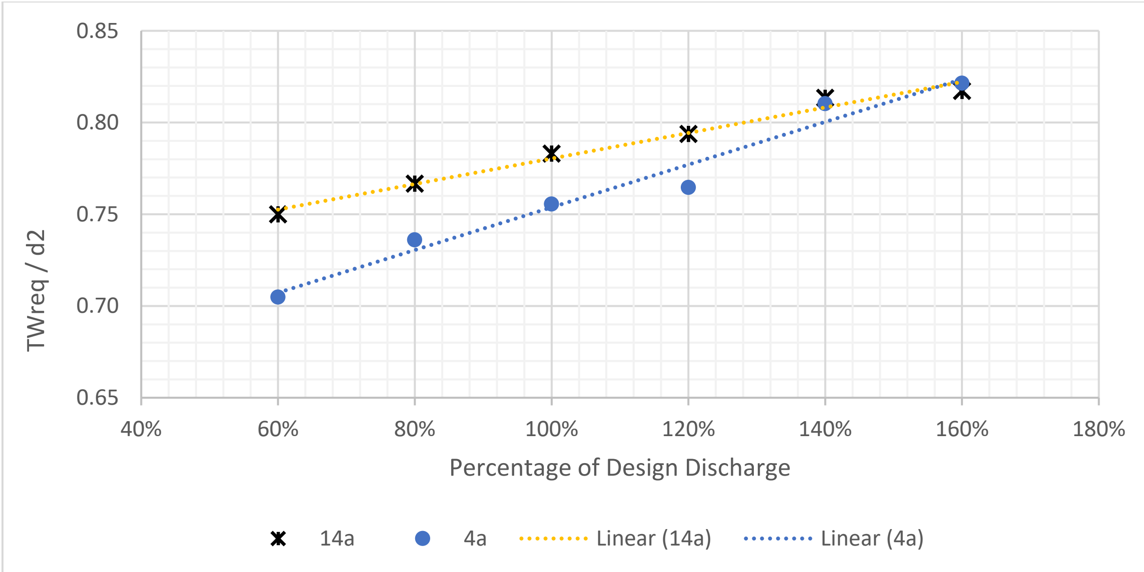

Figure 204. Required Tailwater Ratio ($\frac{TW_{req}}{d_2}$) for USACE (1992) Configurations as a Function of $\frac{q_x}{q_D}$

The equations of the linear trends are shown in Equation 38 and

Equation 39, for configuration 14a and 4a, respectively.

Equation 38. Expression for Required Tailwater for Configuration 14a

$$\frac{TW_{req}}{d_2} = 0.07\frac{q_x}{q_D} + 0.71$$

Equation 39. Expression for Required Tailwater for Configuration 4a

$$\frac{TW_{req}}{d_2} = 0.12\frac{q_x}{q_D} + 0.64$$

Results indicate that a severe condition can occur during the transition from a stable hydraulic jump action to complete loss of the hydraulic jump. This condition presents a scenario whereas the flow surges off the baffles increasing in severity resulting in a temporarily detached jet and loss of the surface roller. The detached jet varies from initially a steep angle, flattens, and then steepens again to reattach and the jump action is regained; as shown in Figure 205. The transition presented the most severe turbulence immediately downstream of the structure and has the potential to create severe unbalanced loading on the slabs as water in and adjacent to the basin fluctuate. The transition region occurred consistently through a $\frac{d'_2}{d_2}$ range of 1- to 3-percent. The transition was also noted to be less stable for the High Fr_1 configurations that included a toe curve at the transition of the sloped chute to the horizontal floor of the stilling basin.

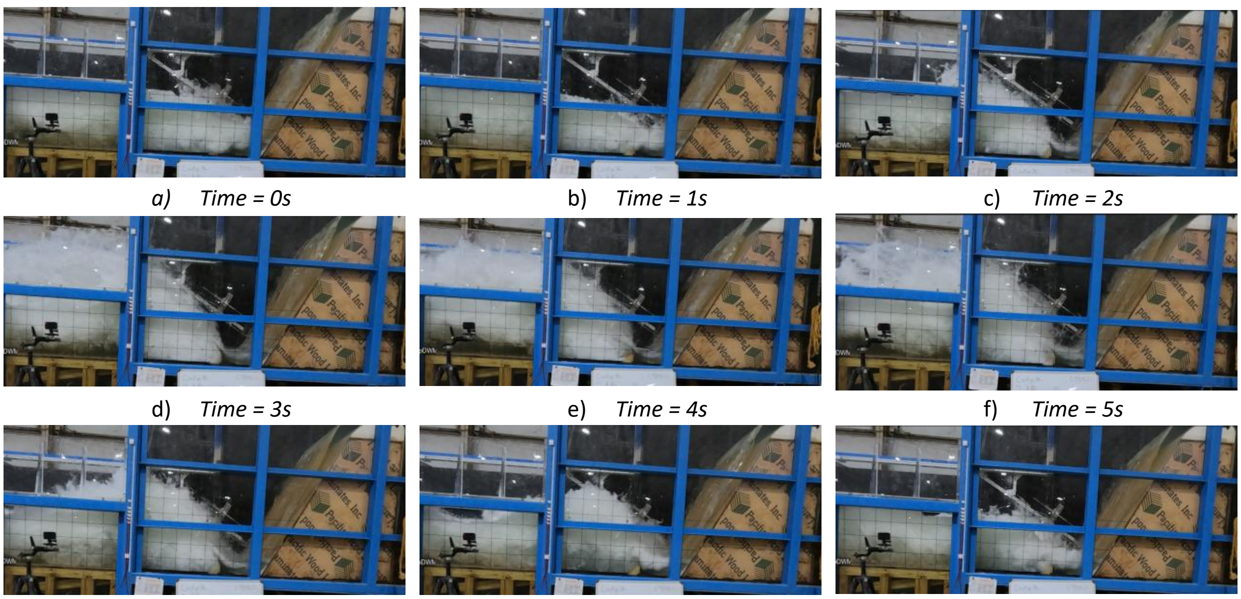

a) Time = 0s b) *Time = 1s* c) *Time = 2s*

d) *Time = 3s* e) *Time = 4s* f) *Time = 5s*

g) Time = 6s *h) Time = 7s* *i) Time = 8s*

Figure 205. Dynamic and Unstable Transition Region for Configuration 3c, q_{160},

6.3.2 Boil Height

The boil height resulting from the "forcing" of the hydraulic jump can lead to overtopping of chute walls if not appropriately accounted for. Blaisdell (1948) found that the ratio of the maximum boil height (z_{max}) to the sequent depth is independent of Fr_1 and a prescribed a recommended freeboard height value equal to one-third d_2.

There is a strong trend of decreasing $\frac{Z_{max}}{d_2}$ with increasing $\frac{d'_2}{d_2}$. This trend was observed for both High- and Low- Fr_1. The $\frac{Z_{max}}{d_2}$ Increased with decreasing $\frac{q_x}{q_D}$; whereas the lowest unit discharge correlated to the highest relative boil height. The maximum boil heights for the high- and low Fr_1 are shown in Figure 181 and Figure 196, respectively.

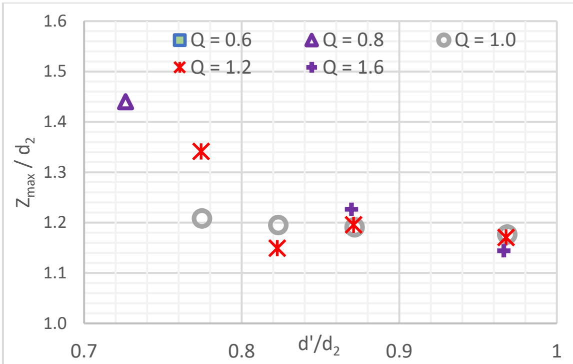

a) Configuration 1a

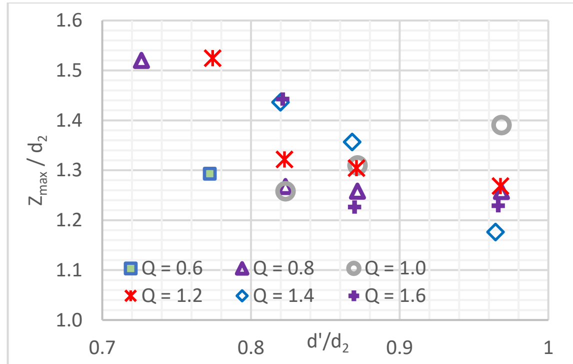

b) Configuration 2a

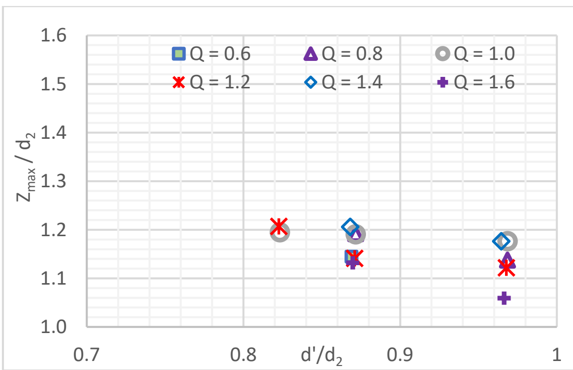

c) Configuration 3a

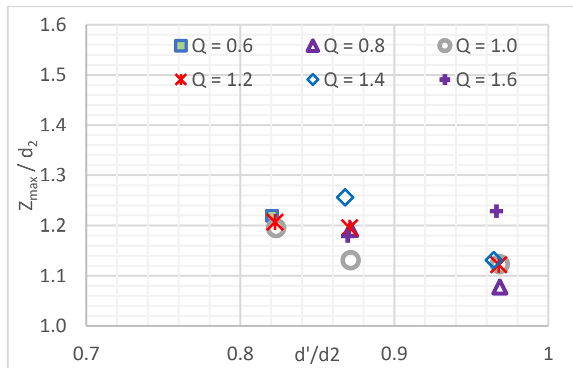

d) Configuration 3c

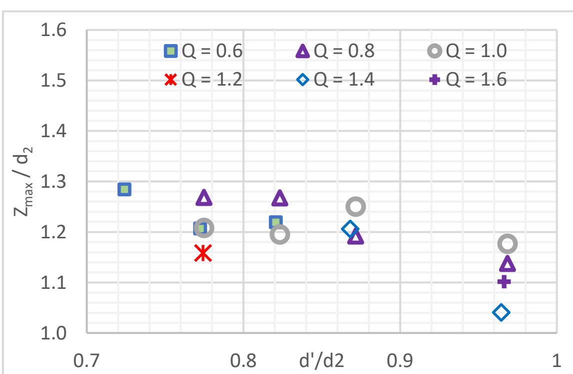

e) Configuration 4a

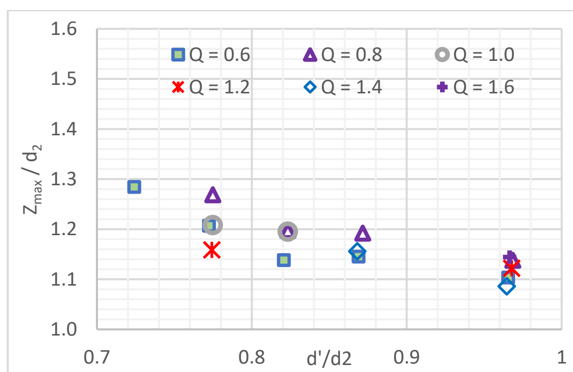

f) Configuration 4c

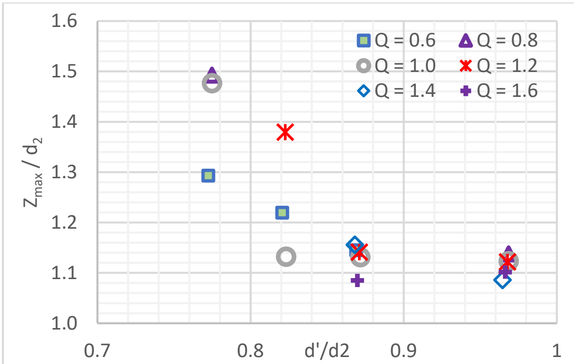

g) Configuration 6c

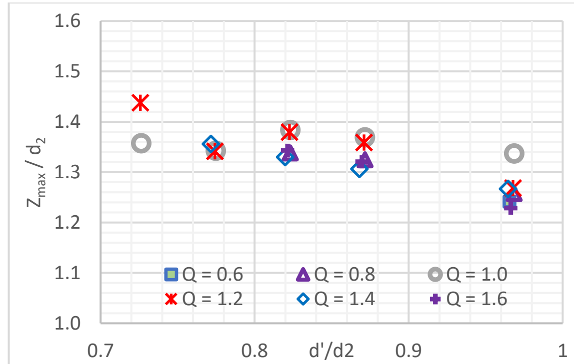

h) Configuration 7c

Figure 181. Graphical Results for Stilling Basin Boil Height Ratio $\frac{Z_{max}}{d_2}$ for High Froude Configurations

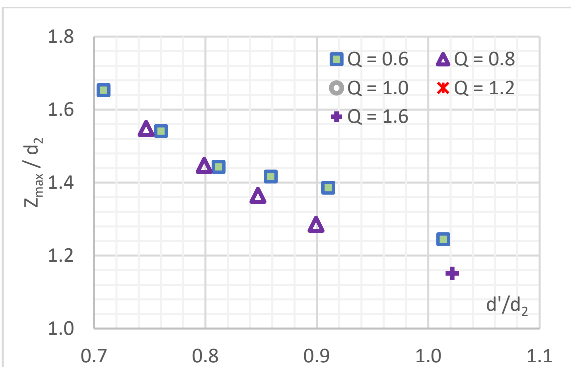

a) Configuration 11a

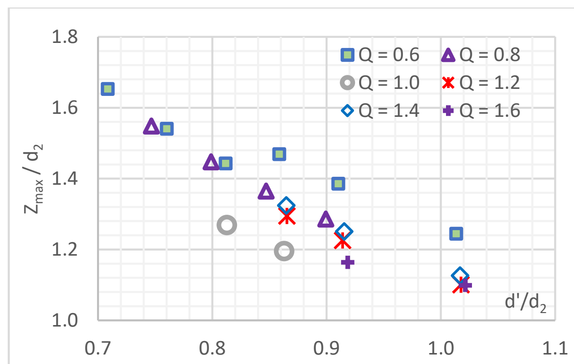

b) Configuration 12a

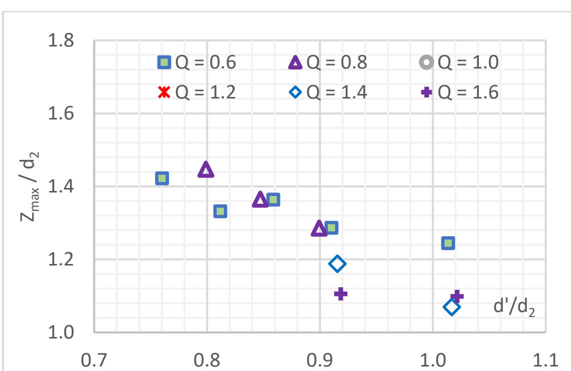

c) Configuration 13a

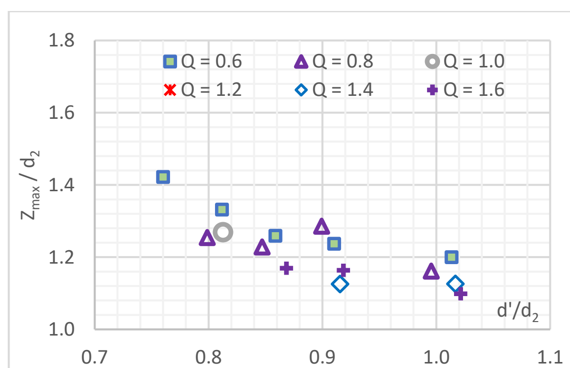

d) Configuration 14a

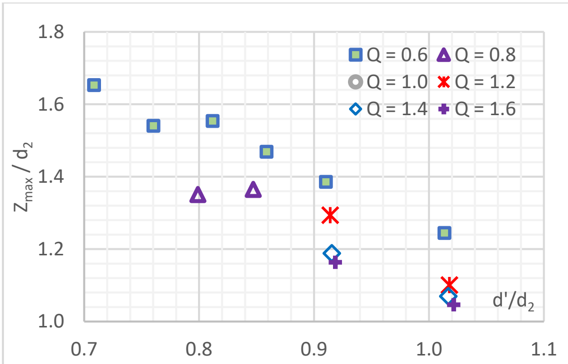

e) Configuration 15a

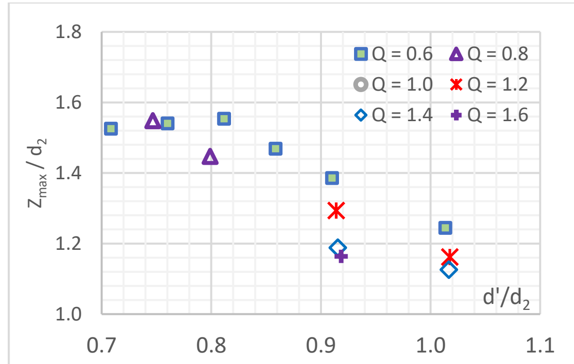

f) Configuration 16a

Figure 196. Graphical Results for Stilling Basin Boil Height Ratio $\frac{Z_{max}}{d_2}$ for *Low Froude Configurations*

Although most standard guidance prescribes minimizing the potential for overtopping of stilling basin sidewalls; numerous applications of reduced wall heights are found in literature and practice (USACE, 1937; USACE, 1964; USACE, 1992).

There are multiple examples of allowing overtopping of stilling basin side walls where the potential for erosion does not present a significant risk to the dam or other critical infrastructure. There are also mitigation strategies to allow for wall overtopping while minimizing the potential toe erosion of the side wall, such as deflectors and increasing the top width.

The data contained herein can be utilized to evaluate the wall heights required to contain the stilling basin boil resulting from baffle block forcing, and to make risk informed decisions related to allowable overtopping.

6.3.3 Jump Angle

The average water surface profile has been used to approximate the average floor pressure profile (USBR, 1984), while the minimum and maximum water surface profiles have been used to approximate the large-scale pressure fluctuations related to floor and sidewall loads (USACE, 2018). The minimum jump angle was selected as an evaluation metric as an indicator of the minimum average resistance force acting on the stilling basin floor.

The jump angle was relatively constant for variations in $\frac{q_x}{q_D}$ and $\frac{d'_2}{d_2}$ for each configuration, except for the in $\frac{q_x}{q_D} > 1$ for the Low Fr_1 application of the Type III configurations. For these scenarios, the minimum jump angle reduced from approximately 25 degrees to less than 15 degrees. In general, the USACE (1992) configurations demonstrated a much lower minimum jump angle, as compared to the Type III configurations.

The minimum jump angles for the High and Low- Fr_1 are shown in Figure 185 and Figure 199, respectively.

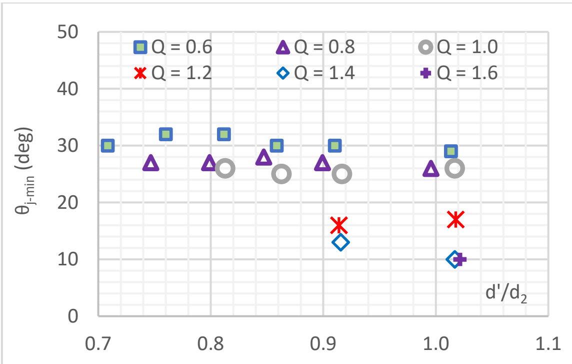

a) Configuration 11a

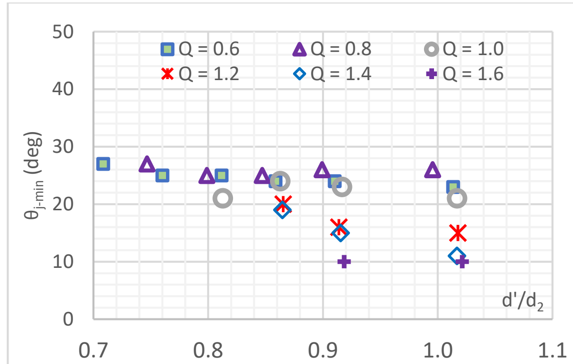

b) Configuration 12a

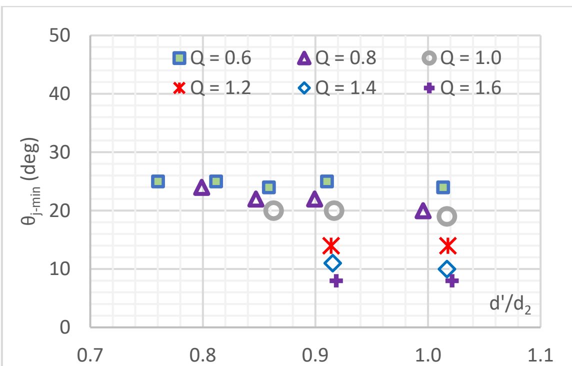

c) Configuration 13a

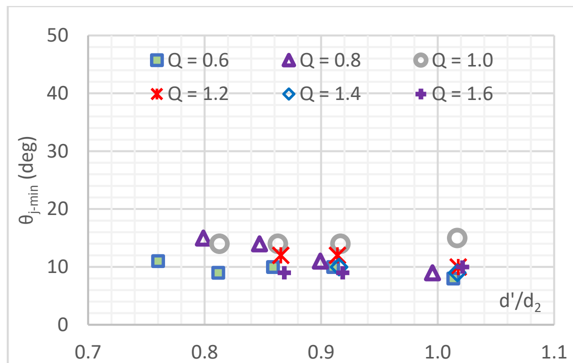

d) Configuration 14a

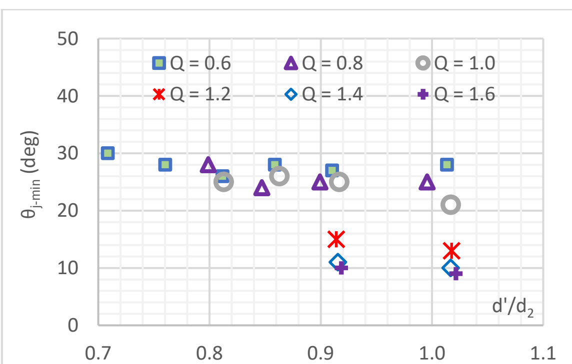

e) Configuration 15a

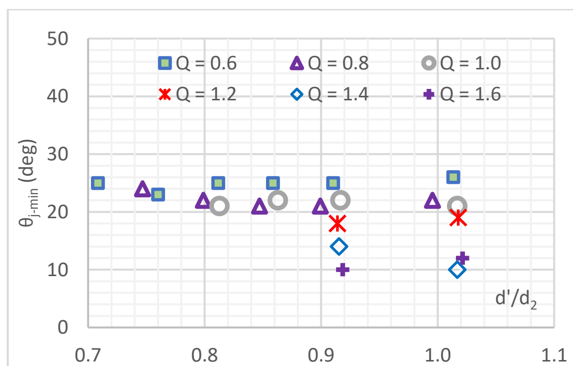

f) Configuration 16a

Figure 199. Minimum Observed Jump Angle for Low Froude Number Configurations

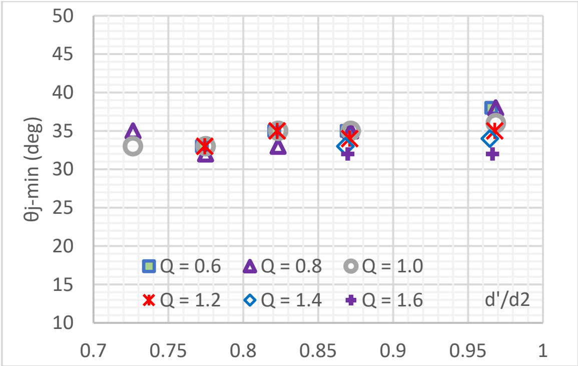

a) Configuration 1a

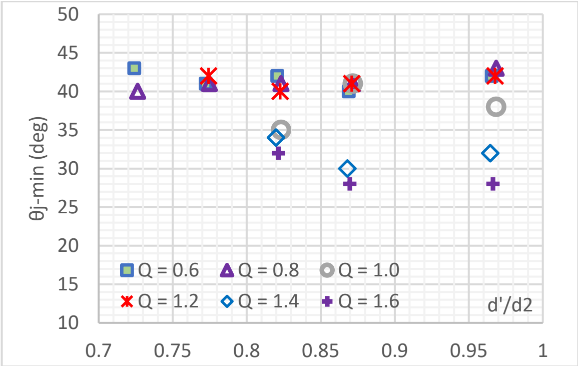

Configuration 2a

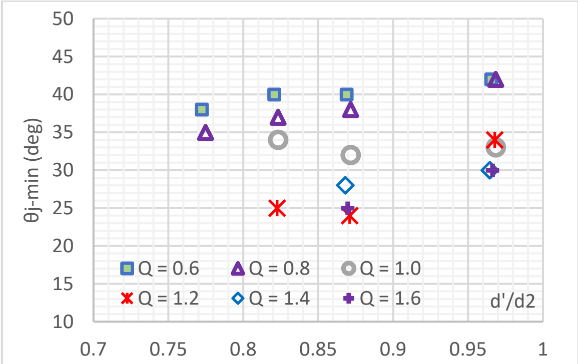

Configuration 3a

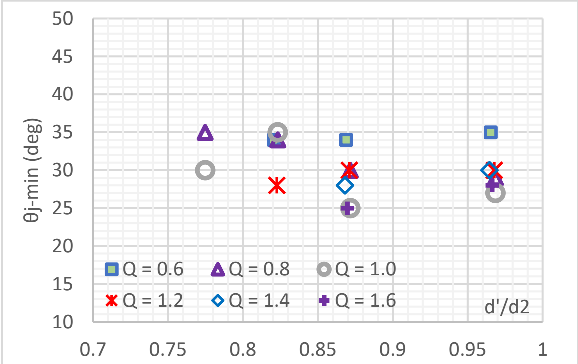

Configuration 3c

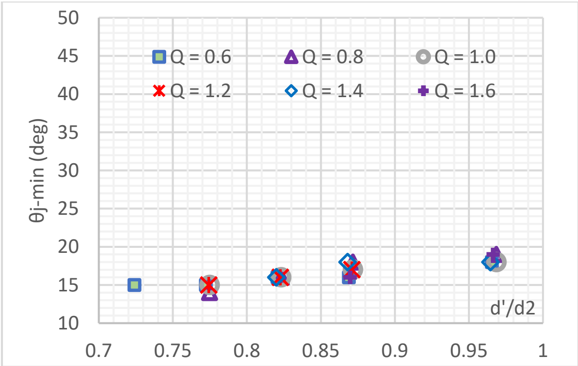

Configuration 4a

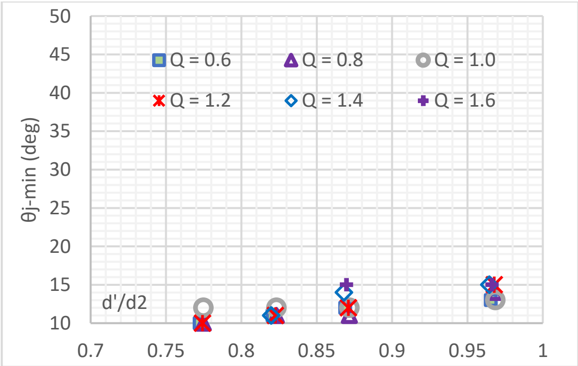

Configuration 4c

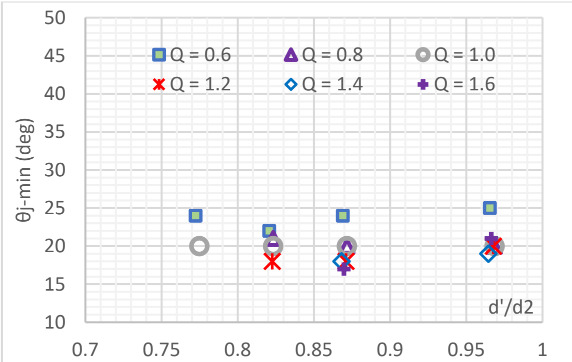

Configuration 6c

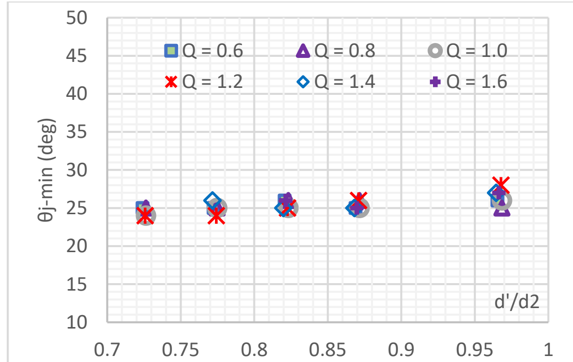

Configuration 7c

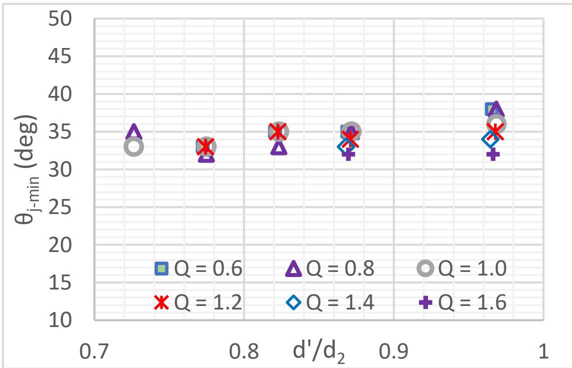

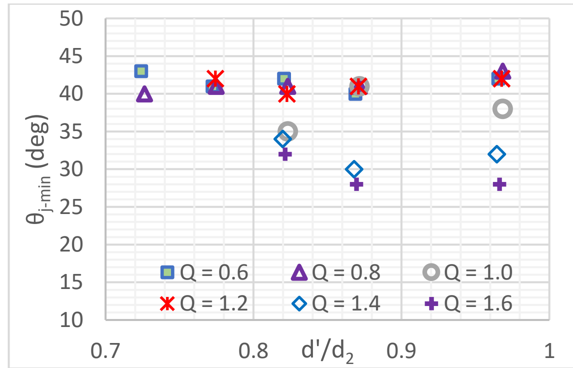

c) Configuration 1a

Configuration 2a

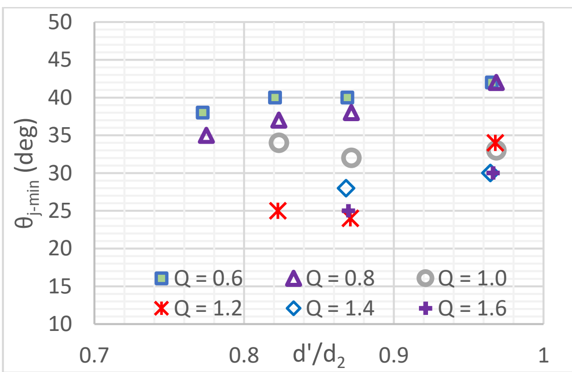

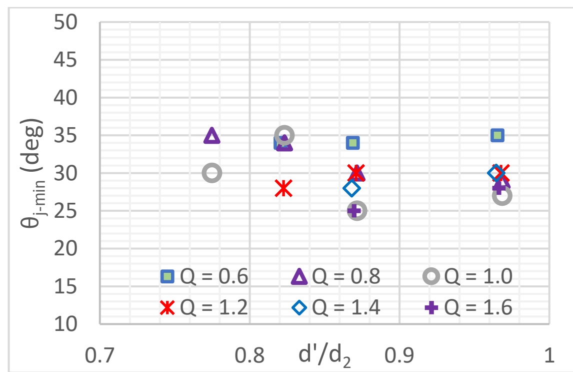

Configuration 3a

Configuration 3c

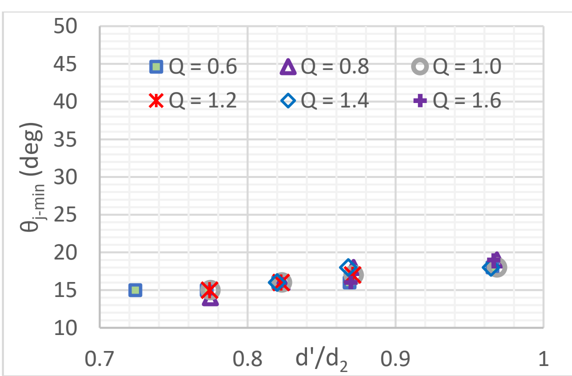

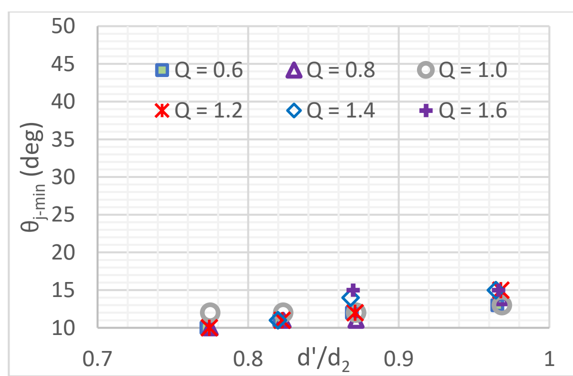

Configuration 4a

Configuration 4c

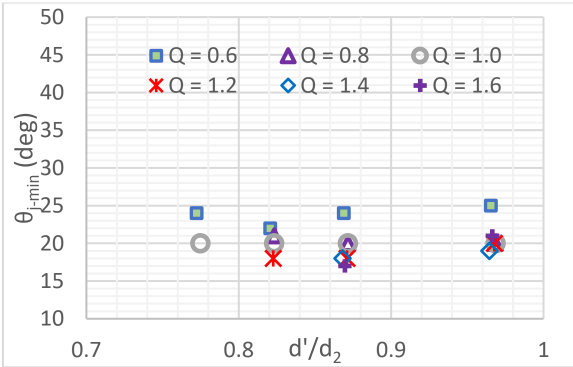

Configuration 6c

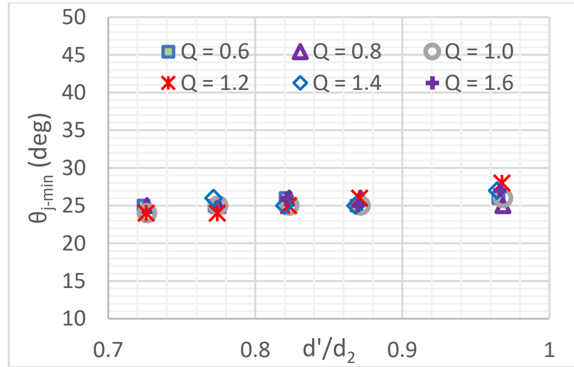

Configuration 7c

Figure 185. Minimum Observed Jump Angle for High Froude Number Configurations

The minimum jump angle is taken from the intersection of the d_1 with the point of intersection of the chute and the horizontal stilling basin floor as shown in Figure 206. The use of the minimum jump angle presented herein may be utilized to estimate the minimum water surface profile. The use of the water surface profile for the average minimum resisting force should include engineering judgment and accounting for dynamic loads due to changes in momentum at the toe and adjacent to baffles and dynamic pressure fluctuations occurring both temporally and spatially across the stilling basin.

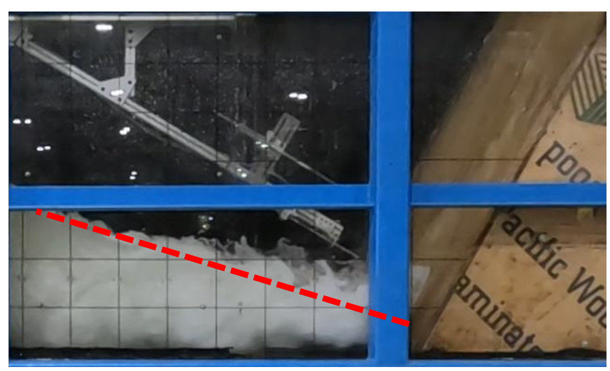

a) Configuration 3a *b) Configuration 4a*

Figure 206. Example of Minimum Jump Angle Observation Figure 184. Example of Minimum Jump Angle Observation

6.4 Baffle Shape

The tapered baffle blocks configuration (1a, 2a, 11a, and 12a) were based on experiments performed for the design of the stilling basin for the Folsom Dam Auxiliary Spillway (USBR, 2009); which is located downstream of a stepped chute. This general configuration consists of tapered side and top and intermittent ramps; developed using a vacuum tank with the goal to reduce the potential for cavitation flashes (separation off the face of the baffle) to reattach to the side of the baffle and floor. This is the location where cavitation damage has been reported, primarily associated with damage to the Bonneville pyramid shaped blocks.

The observations from the current research suggest that there is an increased momentum transfer associated with the tapered blocks, in comparison to the standard blocks as observed in the general reduction of TW_{req} and the increase in $\theta_{j\text{-}min}$ and Z_{max} for the tapered blocks (1a, 2a, 11a, 12a) over the standard blocks (3a, 3c, 6c, 13a). This is also consistent with the findings of USACE (1970); whereas it was found that the drag coefficient was consistently higher for a similar "T" shaped block to that of the standard block. The magnitude of the increase of momentum transfer was not evaluated in the current research.

During design experimentation for the Bluestone Dam Stilling Basin Modification (USACE, 2018), the use of the tapered baffle blocks and ramps with the block height, width, and spacing prescribed in USBR (1984) resulted in significant surging and instability in the jump behavior. It was determined experimentally that the negative impacts of surging could be eliminated by modifying the slenderness ratio ($\frac{H_B}{W_B}$) of the baffle blocks from the 1.33 prescribed in USBR (1984), to 1.5 and increasing the blockage ratio. This concept is represented in configurations

7c, 15a, and 16a with standard blocks shape. The current research suggests that the increase in momentum transfer can also be achieved by increasing the blockage ratio $(\frac{W_B}{W_S})$, as demonstrated by USACE (1970).

A very similar geometry to the tapered block and intermittent ramp (USBR, 2009) was evaluated by Rozanov and Kaveshnikov (1973) in a vacuum tank; whereas material properties were adjusted to capture a relative cavitation damage thresholds and rates. The erosion resistance of the model baffle block and ramp surface was adjusted so that concrete erosion would not occur without the presence of super-cavitation impacting the surface. The results of the testing demonstrated that there is still damage-potential from reattachment of the separation zone at the leading edge of the baffle onto the block and on the ramp floor itself, as shown in Figure 35.

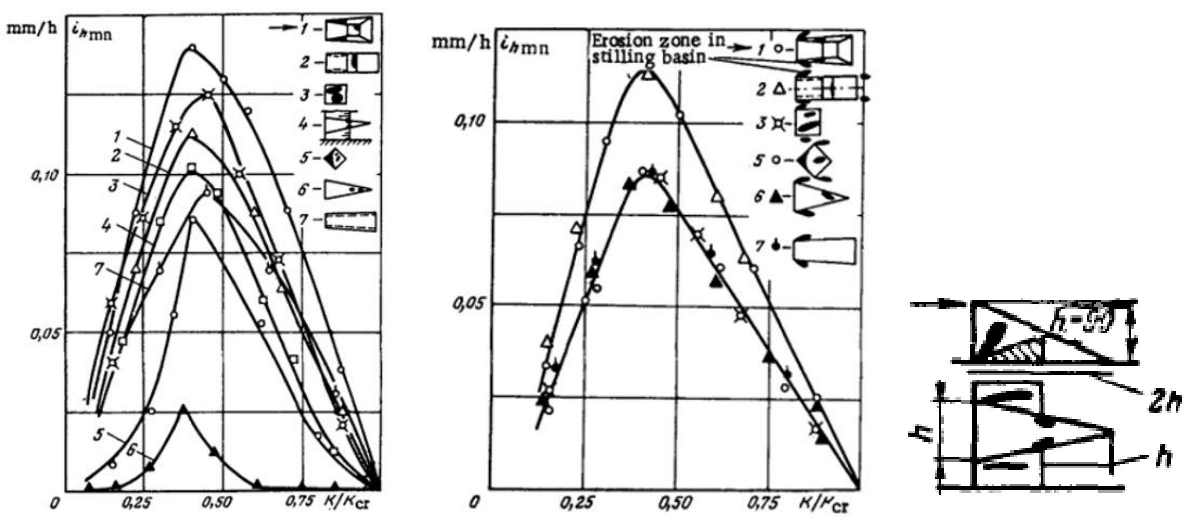

a) damage to Baffle Blocks *b) damage to basin floor* *c) damage locations*

Figure 35. Relationship of Damage Intensity to Cavitation Index Ratio (Source: Rozanov and Kaveshnikov, 1973)

The Folsom and Hinds Dam application are both downstream of stepped spillways; where it is anticipated that high aeration would result in low cavitation potential. The Bluestone Spillway

Modification is under construction and the spillway will only activate for rare events for short durations. Based on this, it is unlikely that prototype observations on damage potential will be available in the near future.

Given the increased construction challenges with a tapered block, the vacuum tank experiments of Rozanov and Kaveshnikov (1973) showing limited reduction in damage potential with the tapered blocks, and the general lack of observed cavitation damage with baffled stilling basins; the use of an increased blockage ratio should be considered when additional tailwater resilience is required.

A second row of baffle also aid in momentum transfer (USACE, 1970), which was also observed in the fact that the USACE (1992) basin showed lower required tailwater for the Low Fr_1 configurations. In addition, the two-row configuration demonstrated remarkable downstream scour resiliency for Bluestone and Keystone stilling basins with reduced tailwater conditions.

6.5 Intermittent Ramp

The use of an intermittent ramp is for the tapered block configuration is intended to lift the vortex that occurs at the edge of the baffle, upward so that the super-cavitation that forms at the flow separation along the leading edge of the baffle; thereby reducing the cavitation damage potential. The geometry evaluated for configuration 1a and 11a is based on the tapered block geometry developed for Folsom Dam Auxiliary Spillway Project.

As discussed previously and detailed subsequently, there is a general lack of cavitation damage found in prototypes for low to moderate head baffled stilling basins; with several of the often-cited instances likely being more of a result of poor concrete quality and/or abrasion than that of cavitation damage. There is a significant portion of baffled stilling basins that have been damaged by hydro-abrasion from bed load or entrapped materials. The influence of the ramps associated with hydro-abrasion (ball milling) have not been investigated, although the large-scale reverse roller and wake observed immediately downstream of the intermittent ramp has a potential to entrain/entrap material and create turbulence for hydro-abrasion of the floor downstream of the block.

Similarly to the tapered baffle blocks, the study by Rozanov and Kaveshnikov (1973) demonstrated that there was still damage potential on the ramps due to the separation off the baffle face reattaching to the ramp surface.

Configurations for Low- and High- Fr_1 were evaluated with and without intermittent ramps (1a, 2a, 11a, 12a). For all but one experiment ($Fr_1 = 8.9$, q_D), the configuration with intermittent ramps (1a and 11a) exhibited higher required tailwater. For the Low Fr_1 configuration, the impact on TW_{req} was significant, with configuration 11a (with intermittent ramps) requiring the highest value of the six Low Fr_1 configurations evaluated for the flow scenarios of $\frac{q_x}{q_D} > 1$.

Configuration 1a (with intermittent ramps) also exhibited the most severe turbulence intensities out of the eight High Fr_1 configurations evaluated. This is in sharp contrast to configuration 2a (without intermittent ramps); which exhibited one of the lowest turbulence intensities across the range of flow conditions.

Interestingly, the boil height was similar for the Low Fr_1 configurations; but lower for all scenarios for the High Fr_1 scenarios. The jump angle for configuration 11a was slightly lower than 12a for $\frac{q_x}{q_D} <= 1.2$, with the opposite observed for $\frac{q_x}{q_D} > 1.2$.

Considering that there is generally a lack of observed cavitation damage on baffle blocks and adjacent stilling basin floor, the negative impacts on tailwater resiliency, higher turbulence observed downstream, damaged observed during vacuum tank experiments, unknown prototype performance, potential for increased abrasion damage, and the increase in cost of construction; intermittent ramps are not recommended for use.

6.6 Modified Type III

The modified Type III stilling basin has the same basin length and block heights as prescribed in USBR (1984); although the blocks have an increased $\frac{H_B}{W_B}$ ratio from 1.3 to 1.5. In addition, the Blockage ratio was increased from 0.5 to 0.59. The standard (a, c) and modified (b, d) configurations are illustrated in Figure 207.

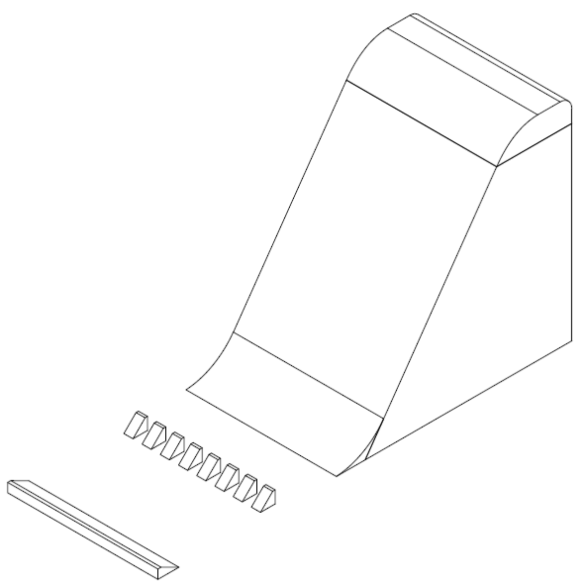

c) Standard Type III (High Fr_1)

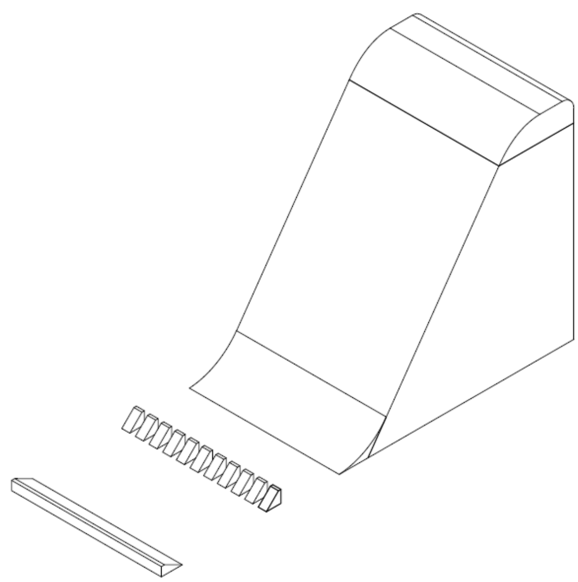

d) Modified Type III (High Fr_1)

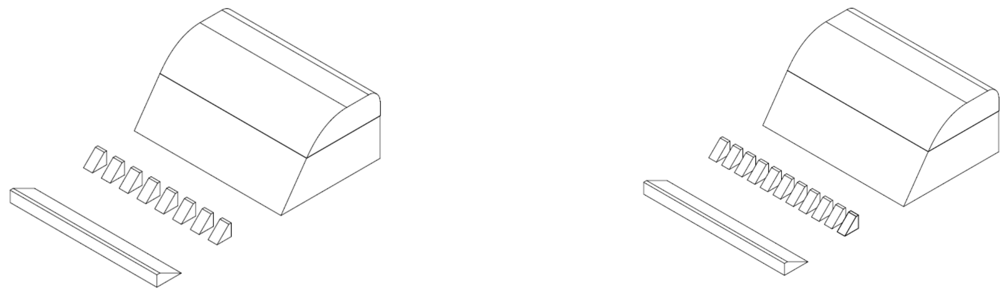

e) Standard Type III (Low Fr_1) *f) Modified Type III (Low Fr_1)*

Figure 207. Standard and Modified Type III Baffled Stilling Basin

For the Low Fr_1 application (16a), the sill controlled the hydraulic jump for $\frac{q_x}{q_D} < 1.2$. For the $\frac{q_x}{q_D}$ >= 1.2 the basin showed similar tailwater resilience to the tapered blocks without intermittent ramps (Configuration 12a) and less resiliency than the USACE (1992) stilling basin (configuration 14a). For the High Fr_1 application (configuration 7c), the stilling basin demonstrated superior tailwater resilience to the other configurations evaluated. The comparison of tailwater resiliency to other stilling basins evaluated is shown in Figure 208, with the Modified Type III configuration (15a and 7c) shown as red squares.

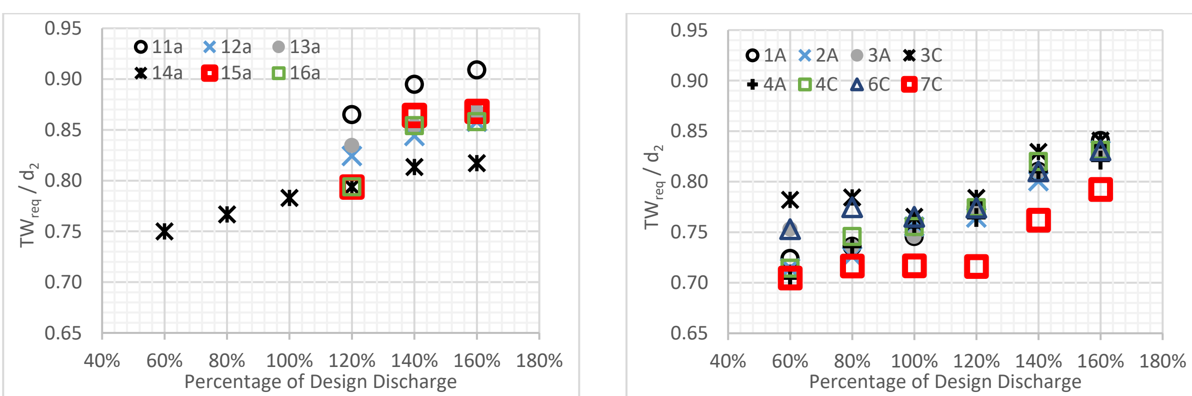

a) Low Fr_1 *b) High Fr_1*

Figure 208. Tailwater Resiliency for Modified Type III Stilling Basin

For the High Fr_1 application, the configuration 16a also exhibited the lowest downstream turbulence intensities throughout the range of $\frac{q_x}{q_D}$ and $\frac{d'_2}{D_2}$; as shown in Table 39. The general trends of observed turbulence intensities are shown in Figure 209.

Index Number	Index Descriptor
1	Low
2	Low-Moderate
3	Moderate
4	Moderate-High
5	High
6	High-Severe
7	Severe

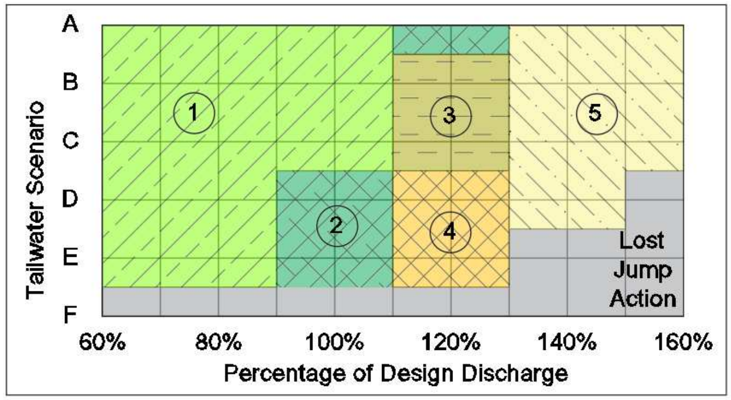

a) Turbulence Intensity Index *b) Configuration 7c Turbulence Intensity Matrix*

Figure 209. Configuration 7c Turbulence Intensity

The maximum boil heights for the modified Type III configuration were significantly higher than those of the USACE (1992), slightly higher than the Standard Type III (Configurations 3a, 3c, 6c, 13a), and lower and more consistent than the Type III with tapered baffle blocks (2a, 12a). The relative maximum boil height ($\frac{Z_{max}}{d_2}$) showed a consistent decrease with increasing $\frac{d'_2}{d_2}$ and increasing $\frac{q_x}{q_D}$, as shown in Figure 210. In many instances, the stilling basin walls are not required to completely contain the maximum boil height and the walls should be established using a risk-informed design approach and may include mitigation strategies such as those presented in Section 6.

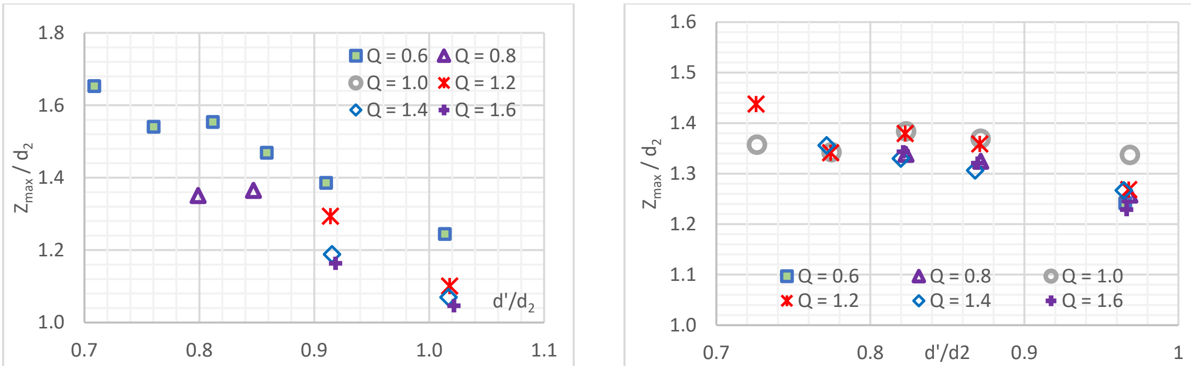

a) Configuration 15a (Low Fr₁)

b) Configuration 7c (High Fr₁)

Figure 210. Boil Heights for Modified Type III Configuration

The minimum jump angles ($\theta_{j\text{-min}}$) for the Modified Type III configuration were very consistent between 20- and 30-degrees across flow conditions, with the exception of the Low Fr_1 application for $\frac{q_x}{q_D} > 1$; whereas the jump angle is significantly lower. The lower jump angles for the Low Fr_1 application with $\frac{q_x}{q_D} > 1$ was consistent for all Type III variations (11a, 12a, 13a, 15a, 16a), with the USACE (1992) stilling basin have a consistent jump angle of 10- to 15-degrees for the full range of $\frac{q_x}{q_D}$ and $\frac{d'_2}{d_2}$. The minimum jump angles for the Modified Type III stilling basins are shown in Figure 211.

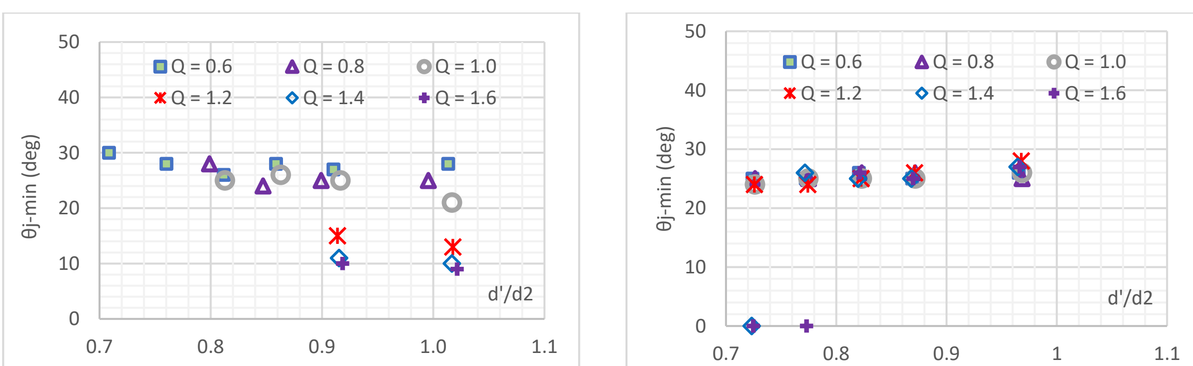

a) Configuration 15a (Low Fr₁)

b) Configuration 7c (High Fr₁)

Figure 211. Minimum Jump Angle for Modified Type III Stilling Basin

Based on the data and analysis performed as part of the current research, the Modified Type III has demonstrated advantages over both the Standard Type III and the Type III with tapered blocks; most notably the tailwater resilience. It is believed that the additional tailwater resilience is a result of additional momentum transferred to the baffle blocks with the additional blockage ratio (USACE, 1970). It was found experimentally that the increased slenderness of the blocks reduced the potential for surging and detachment of the jet with reducing tailwater (USACE, 2018). For design Fr_1 of approximately 8; it is recommended that the Modified Type III be utilized for applications with the potential for reduced tailwater and/or increased unit discharge in the future due to changes in operation, climate change, watershed changes, and/or updated understanding of extreme floods within the watershed. For Fr_1 below 4.5, it is recommended that the USACE (1992) stilling basin be utilized over the Standard or Modified Type III.

6.7 Toe Curve

It is common practice to include toe curves at the intersection of chutes and the stilling basin floor. USBR (1984) recommends that a toe curve of a radius greater than 4 times the flow depth be used when the intersection angle is greater than 45-degrees. It is also common for the chute and basin intersection for outlet works to intersect via a parabolic drop with an abrupt intersection between the chute and the basin without a toe curve (USACE, 1997). Similarly for short spillways like those associated with navigation dams, it is common to not include a toe curve at the intersection of the chute and the horizontal floor (USACE, 1987).

The inclusion of the toe curve for the USACE (1992) High Fr_1 stilling basins (Configurations 4a and 4c) resulted in a slightly lower turbulence intensity index and maximum boil height for the

$\frac{q_x}{q_D}$ <= 1.2. Above $\frac{q_x}{q_D}$ > 1.2, the turbulence intensity index was the same and the boil height increased slightly. The minimum jump angle ($\theta_{j\text{-}min}$) was consistently lower with inclusion of the toe curve. For comparison of the USBR (1984) stilling basins, there were similar findings related to the decrease in Z_{max} with decreases below $\frac{q_x}{q_D}$ <= 1.2; and increases above as well as consistently lower jump angles.

A consistent finding was that the use of a toe curve (even with increasing basin length for configuration 6c) resulted in a higher required tailwater to maintain the hydraulic jump. In addition, the use of a toe curve resulted in a significant increase in the magnitude and slight increase in the range of a transition zone between a stable hydraulic jump and complete loss of jump action. This finding is consistent with those of researchers in Europe during the early 20th century (Freeman, 1929), that the use of a straight intersection of the chute and the horizontal floor increases the stability of the jump.

Given the increase in stilling basin length, minor benefits associated with boil heights, and the significant increase in the severity of the unstable action during the transition region from maintained to lost jump; it is generally not recommended to include a toe curve at the base of the chute for hydraulic design purposes.

6.8 Cavitation and Abrasion

Cavitation has been a source of significant maintenance to hydraulic structures; especially those associated with high head dams. There are numerous case histories associated with damage immediately downstream of gates/valves, along high velocity chute inverts, along radial transitions, and at the sudden termination of a high velocity jet at deflector blocks and on the end of flip buckets.

There are multiple documented cases of damage on baffle blocks found in literature. Interestingly, most are minor damage consisting of removal of the surficial fine aggregate and exposing coarse aggregate. The most notable exception to this is the case of the pyramid shaped baffles at Bonneville Dam and the damage mentioned in USACE (1992) related to the baffled blocks at Chief Joseph Dam. Review of the relevant documentation at the time of observed damage and subsequent forensics investigations suggest that poor concrete quality and abrasion during river diversion during construction was the more likely primary factor in the damage to the baffle and floor of these two projects (USACE, 1937; USACE, 1943; Gedney, 1961). There are also documented cases of baffled stilling basins with standard blocks operating at velocities up to 25 m/s and a cavitation index of 0.33 for three decades without any damage (Khatsuria, 2005).

Given the general lack of prototype cavitation damage to baffle blocks, the adoption of special mitigation techniques (e.g. tapered or rounded blocks, intermittent floor ramps, steel armoring) do not seem supported for low to moderate head stilling basins.

The streamwise location of the baffle block also has a rationale correlation to the damage potential. There is a decrease in velocity, increase in baffle side pressure, and increase in aeration with increasing distance from the chute, which has been correlated to a decreased concern for damage potential (USACE, 1970; USACE, 1965; Chanson, 2015).

It is worth noting that a more complete survey of conditions in which successful use of baffled stilling basins without cavitation damage has not been performed; therefore, caution should be taken when selecting baffled hydraulic jump stilling basins above prescribed limits (USBR, 1987).

Abrasion damage has been a significant source of damage to baffled hydraulic jump stilling basins (ACI, 1999; USACE, 1937; USACE, 1943; USACE, 1981; USBR, 1978; USBR, 2019). The sources of the abrasion damage have typically been associated with entrainment of durable armor stone from the downstream exit channel, steel and other construction materials left in the stilling basin, bed load from river diversions, and durable stone materials thrown into the basin by vandals. The USBR (2019) has developed mitigation strategies for the Type III stilling basin, that includes a flow deflector to eliminate the ground roller entraining downstream armor stone. Also, durable patches have been implemented with various degrees of success to reduce the rate of damage and associated repairs.

6.9 Local Scour Potential

6.9.1 General

Based on the experiments described herein and relevant literature on the subject (e.g. Annandale, 2006a; Bollaert, 2010) downstream of stilling basins is typically associated with high exiting velocities and macro-turbulent structures. There were two primary observed mechanisms associated with the mobile bed scour and near bed interactions described herein;

1) An *impingement jet* of a high velocity jet that is projected off the baffles (either detached or shooting separated jet) that impacts downstream of the stilling basin (as

shown in Figure 103). This case was seen associated with low tailwater scenarios whereas the jump was lost or not effective and the momentum of the incoming jet was lifted by the baffles and/or end sill. This mechanism similar to the wall jet scour described by Annandale (2006a) associated with plunge pool terminal structures (e.g. ski jump and flip bucket). The position of the baffles seemed to be an important consideration associated with the severity and location of impingement.

2) An s*ubmerged jet* whereas the near bed turbulence provides hydraulic attack. It was also observed and described in Sections 4.6.5, 5.1.2.2, and 5.2.2.1.2 that there are large macro-scale fluctuations that are linked to the dynamic nature of the hydraulic jump. These fluctuations result in macro-scale turbulent eddies that exit the stilling basin and produce turbulent bursts and sweeps in the near-bed region. The axis of the eddies is generally in perpendicular to flow and appeared to approach a limiting exit angle off the end sill which dictated the downstream mobile bed behavior for the Bluestone and Keystone Stilling Basins.

6.9.2 Rigid Bed Experiments

The local scour for the current research was evaluated semi-quantitatively for the High Fr_1 experiments utilizing the Turbulence Intensity Index; which was developed to provide a means of relative comparison of the scour potential immediately downstream of the various stilling basin configurations, with a length scale of observation roughly equal to the d_2. The high exiting turbulence intensity and aeration provided high quality observation of the flow field and turbulent structures for the High Fr_1 experiments. The Low Fr_1 experiments exhibited lower aeration exiting the basin and generally lower frequency and magnitude of macro-scale turbulent structures. In addition, the view downstream of the end sill was obstructed by a vertical support beam that shortened the field of vision to less than the d_2. For these reasons, the turbulence intensity index was not used to describe the scour potential downstream of the Low Fr_1 configurations.

Table 39 demonstrates the general trends of turbulence intensity for the High Fr_1 configurations evaluated. In general, the turbulence intensity increased with increasing $\frac{q_x}{q_d}$ and decreasing $\frac{d'_2}{d_2}$. This trend was not true for both 3c and 4c; both exhibiting a toe curve. It is not clear if the toe curve is attributed to the more erratic trend in downstream turbulence; but it is consistent with the finding related to the influence the toe curve has related to the transition region and the boil height.

Table 39. Summary Table for Near-Bed Turbulence Severity Index for High Froude Configurations

$\frac{q}{q_D}$	TW ID	$\frac{d'}{d_2}$	Configuration / Observed Turbulence Index Value							
			1a	2a	3a	3c	4a	4c	6c	7c
0.6	A	0.97	Low-Mod	Low	Low	Mod-High	Mod	Mod	Low	Low
	B	0.87	Mod	Low	Low-Mod	Mod-High	Mod	Mod	Low-Mod	Low
	C	0.82	Mod	Low	Mod	High	Mod	Mod-High	Mod	Low
	D	0.77	Mod	Low-Mod	Mod	High	Mod	Mod-High	Mod	Low
	E	0.72	Mod-High	Mod	*Jump Lost*	*Jump Lost*	Mod	Mod-High	*Jump Lost*	Low
0.8	A	0.97	Mod	Low	Mod-High	High-Sev	High	Mod-High	Mod-High	Low
	B	0.87	Mod	Low-Mod	Mod-High	High-Sev	High	Mod-High	Mod-High	Low
	C	0.82	Mod	Low-Mod	High	High-Sev	High	Mod-High	High	Low
	D	0.77	Mod-High	Mod	High	High-Sev	High	High	High	Low
	E	0.73	Mod-High	Mod	*Jump Lost*	*Jump Lost*	*Jump Lost*	*Jump Lost*	*Jump Lost*	Low
1	A	0.97	High	Low	Mod-High	High	High	Mod-High	Mod-High	Low
	B	0.87	High	Low-Mod	Mod-High	High	High	High	Mode-High	Low
	C	0.82	High	Mod	High	High-Sev	High	Mod-High	High	Low
	D	0.77	High	Mod -High	High	High	High	High	High	Low-Mod
	E	0.73	*Lost*	*Jump Lost*	*Jump Lost*	*Jump Lost*	*Jump Lost*	*Jump Lost*	*Jump Lost*	Low-Mod
1.2	A	0.97	High-Sev	Mod-High	High	High	High	High	High	Low-Mod
	B	0.87	High-Sev	High	High	High-Sev	High	High	High	Mod
	C	0.82	High-Sev	High	High-Sev	High-Sev	High	Mod-High	High	Mod
	D	0.77	High-Sev	High	*Jump Lost*	*Jump Lost*	High-Sev	High	*Jump Lost*	Mod-High
	E	0.97	*Jump Lost*	*Jump Lost*	*Jump Lost*	*Jump Lost*	*Jump Lost*	*Jump Lost*	*Jump Lost*	Mod-High
1.4	A	0.96	Severe	High	High	High-Sev	High	High	High	High
	B	0.87	Severe	High	High-Sev	High-Sev	High	High	High-Sev	High
	C	0.82	*Jump Lost*	High	*Jump Lost*	*Jump Lost*	High-Sev	High-Sev	High-Sev	High
	D	0.77	*Jump Lost*	*Jump Lost*	*Jump Lost*	*Jump Lost*	*Jump Lost*	*Jump Lost*	*Jump Lost*	High
1.6	A	0.97	Severe	High	High	High-Sev	High	High	High-Sev	High
	B	0.87	Severe	High	High-Sev	High-Sev	High-Sev	High-Sev	High-Sev	High
	C	0.82	*Jump Lost*	High	*Jump Lost*	*Jump Lost*	*Jump Lost*	*Jump Lost*	*Jump Lost*	High

It was observed that configuration 1a exhibited the worse downstream turbulence characteristics for the q_D and above. This is likely attributed to the intermittent ramps influence on the high velocity jet exiting the stilling basins. On the other hand, configuration 7c demonstrated the lowest turbulence intensities throughout the range of flow conditions evaluated. This is likely attributed by the increased momentum transferred to the blocks and the behavior of the high velocity jet as it exits the stilling basin.

The information contained herein can be used to make informed decisions related to selection of the basins stilling basin configuration and the potential to adjust the design based on the site conditions. For example, the optimum basin for a highly erodible foundation may be oversizing the basin to ensure that the turbulence intensity is low throughout the full range of anticipated flow conditions. Similarly, if the foundation is virtually non-erodible, the optimum basin may allow for smaller basin dimensions and adjusting so that the IDF is associated with the q_{160}.

6.9.3 Mobile Bed Experiments

There were several major findings related to re-evaluation of published mobile bed models (Section 4.5) and experiments performed for Bluestone and Keystone Dams (Section 4.6).

Although the end sill lifts the high velocity jet into the flow and away from the downstream bed, turbulent eddies are shed and burst and sweep across the bed at a constant angle of less than 15 degrees from horizontal. It was found that the angle of the downstream scour out-slope remains relatively constant for various flow conditions, although the maximum depth increases with increasing unit discharge. The ultimate scour characteristics and out slope were similar for mobile beds comprised of coarse sand, fine gravel and coarse gravel materials when evaluated at the design discharge for Keystone Dam. All experiments exhibited an exit slope ranging from 6- to 15-degrees for various configurations of the Keystone Dam at design discharge and for the case of Bluestone Dam second stage stilling basin, whereas the $\frac{q_x}{q_D}$ was exceeded by more than a factor of 3.

Based on the experiments described in Sections 4.5, it is anticipated that there will be side wall influences, and associated areas of high local scour observed near the wall of a sectional flume. It is believed that these are primarily due to the redirection of the large-scale macro-turbulent structures (e.g. sweeps and bursts) downward by the high-pressure gradient created by the boundary wall, forcing a strong secondary circulation that entrains material and transports it downstream and towards the center of the flume. Therefore this phenomenon should be considered when making observations of mobile bed scour from the sidewall. This phenomenon was also observed for the rigid bed experiments as the macro-scale turbulent structures exited the basin and exhibited vorticity in the cross-stream direction.

The submerged angle of repose is an important consideration when using granular material to represent local scour tendencies of a cohesive soil or rock mass. The scour hole exit geometry can only steepen to the extent that the material will maintain a stable slope. It was found that the submerged angle of repose for initial motion in a tilt flume was 5-degrees higher than that of the deposition observed in the downstream sediment trap. This is likely the controlling angle in which reasonable scour tendencies can be determined from a granular proxy material, considering the significant stationary rework of the material as the turbulent structures entrain and redeposit the proxy materials in a quasi-equilibrium state.

It is worth reiterating that the physical model is not intended to replicate the scour patterns found in cohesive soils and rock masses; but to evaluate the hydraulic attack of the turbulent flows downstream of the hydraulic jump stilling basins. The coupling of the prototype fluid-solid boundaries is only representative of the behavior of the granular proxy materials; thereby making the application to materials that express different scour evolution and ultimate patterns semi-quantitative in nature. Application to prototype conditions must include an understanding of the scouring process of those materials and appropriate judgment and adjustment in applying estimated hydraulic attack index parameters (e.g. velocity, shear stress, and stream power).

6.10 Research Limitations and Future Study

The are a number of topics that have been identified as research limitations and logical follow-on research efforts or generally lacking in literature and therefore recommended for additional study to advance the state-of-the-art for hydraulic jump stilling basins.

There are several cited case histories of cavitation damage found in literature and therefore the baffled hydraulic jump basin has been identified to have limitation on use. Two of the major damage case histories were explored and summarized within the current research and suggest that the damage to the block was not primarily associated with cavitation phenomenon. Although these case histories may not represent the thresholds of concern for cavitation damage, there are likely conditions that would result in significant cavitation damage. Considering the complicated phenomenon and the inability to directly compute the damage potential, a proper survey of hydraulic jump stilling basins with significant flow history would allow for an index approach to cavitation damage similar to that of an erodibility index. The damage, or lack of, would be correlated to the hydraulic index of flow that most represents the prediction of damage (e.g. cavitation index or incoming velocity) and a threshold developed.

Considering the findings associated with the general lack of observed case histories of cavitation damage related to baffle blocks and the case histories of no damage to chute blocks under conditions that have been published to be of concern, it is recommended that a similar damage survey and associated threshold for damage be developed for chute blocks.

Considering numerous examples of significant damage to stilling basins due to entrainment of durable materials (e.g. rock, riprap, and steel), it is recommended that a systematic evaluation of the ability to flush foreign debris is performed. This would include compilation of existing case histories and surveys of damage, evaluation of the conditions resulting in entrainment for various stilling basins, and potential mitigation strategies. For example, the Type III stilling basin with tapered blocks and ramp may reduce the cavitation damage potential; but the ramps may create a wake zone thar entraps material resulting in significant hydro-abrasion.

The current study only evaluated the scour potential with a mobile bed for relatively load Fr_1 stilling basins that were similar to the USACE (1992) configuration. A systematic evaluation of the scour potential utilizing mobile bed experiments would allow for better informed decisions related to evaluation and selection to the appropriate stilling basin given a particular erodibility of foundation or downstream materials.

Increasingly, Computational Fluid Dynamics modeling with Reynolds's Averaged turbulence closures are used to evaluate the scour potential downstream of hydraulic structures. Given the complicated nature of the macro-scale turbulence structures responsible for a large portion of the local scour, additional verification of these numeric approaches is recommended.

7 REFERENCES

American Concrete Institute (ACI, 1999), Compendium of Case Histories on Repair of Erosion-Damaged Concrete in Hydraulic Structures, Reported by ACI Committee 210, ACI 210.1 R-94.

American Concrete Institute (ACI, 2008), Erosion of Concrete in Hydraulic Structures, Reported by ACI Committee 210.

American Society of Civil Engineers (ASCE, 2021) Infrastructure Report Card, https://infrastructurereportcard.org/

Annandale, G. (1995). Erodibility. Journal of Hydraulic Research. Vol. 33, No. 4, pp. 471 – 494.

Annandale, G. (2006a). Quantification on the Erosive Capacity of Water, Proceedings of GeoCongress 2006. American Society of Civil Engineers. Reston, Virginia.

Annandale, G. (2006b). Scour Technology. McGraw-Hill, New York.

Annandale, G. (2011). Bluestone Dam Representation of Massive Orth-Quartzite in 1:25 and 1:36 scale Models, Technical Memorandum. Golder Associates Inc., February 24, 2011. Lakewood, CO.

Bakhmeteff, B.A. and Matzke, A.E. (1936) The Hydraulic Jump in Terms of Dynamic Similarity. Transactions of the American Society of Civil Engineers, Paper No. 1935, ASCE, Reston, VA.

Bal, A.V., Re, F., Lapetina, and Badano, N. Some Historic Aspects on the Hydraulic Design of the Gatun Spillway in the Panama Canal. 8th IAHR ISHS. Santiago, Chile, 2020.

Basco, D.R. (1984). Optimal Design of Stilling Basins for Overflow Spillways. Journal of Hydraulic Engineering, 1984, 110(1): 79-82, American Society of Civil Engineers. Reston, Virginia.

Bayon, A., Valero, D., Garcia-Bartual, R., Valles-Moran, F., and Lopez-Jimenez, P. (2016). Performance assessment of OpenFOAM and FLOW-3d in the numeric modeling of a low Reynolds number hydraulic jump. Environmental Modelling & Software 80(2016) 322-335, http://dx.doi.org/10.1016/j.envsoft.2016.02.018

Bellin, A. and Fiorotto, V. (1995) Direct Dynamic Force Measurements on Slabs in Spillway Stilling Basins. Journal of Hydraulic Engineering, Vol. 121. No. 10, Paper No. 8222. American Society of Civil Engineers. Reston, Virginia.

Berryhill, R.H. (1957). Stilling Basin Experiences of the Corps of Engineers, Journal of the Hydraulics Division of the American Society of Civil Engineers, Vol. 83, No. HY3, June 1957.

Blaisdell, F.W. (1942) The use of Sand Beds for Comparing Relative Stilling Basin Performance. 33rd Annual Meeting of the Geophysical Union. Washington, DC.

Blaisdell, F.W. (1948) Development and Hydraulic Design, Saint Anthony Falls Stilling Basin, Transactions of the American Society of Civil Engineers, Vol. 113 Issues 1 – January 1948, ASCE, Reston, VA.

Bollaert, E.F.R. (2004). A comprehensive model to evaluate scour formation in plunge pools, Int. J Hydropower & Dams, 2004 (1), pp 94-101.

Bowers, C.E. and Toso, J.W. Karnafuli Project, Model Studies of Spillway Damage. Journal of Hydraulic Engineering, Vol. 114, No. 5, Paper No. 22458.

Buffington, J.M. and Montgomery, D.R. (1997) A Systematic Analysis of Eight Decades of Incipient Motion Studies, with Special Reference to Gravel-Bedded Rivers. Water Resources Research, 33, 1993-2029, http://dx.doi.org/10.1029/96WR03190

Carvalho, R.F., Lemos, C.M., Ramos, C.M. (2008) Numerical computation of the flow in hydraulic jump stilling basins, Journal of Hydraulic Research, 46:6, 739-752, https://doi.org/10.1080/00221686.2008.9521919

Chanson, H. (1996) Prediction of the transition nappe/skimming flow on a stepped channel. Journal of Hydraulic Research. Vol. 34, 1996, No 3. International Association of Hydraulic Engineering and Research.

Chanson, H., Gualtieri, C. (2008) Similitude and scale effects of air entrainment in hydraulic jumps. Journal of Hydraulic Research. International Association of Hydraulic Engineering and Research.

Chanson, H. (2009), Development of the Belanger Equation and Backwater Equation by Jean-Baptiste Belanger (1828). J. Hydraulic Eng, 2009, 135(3): 159-163.

Chanson, H. (2015), Energy Dissipation in Hydraulic Structures, CRC Press, London, UK

Chen, Q., Dai, G., Liu, H. (2002) Volume of Fluid Model for Turbulence Numerical Simulation of Stepped Spillway Overflow. J. Hydraul. Eng., 2002, 128(7): 683-688. https://doi.org/10.1061/(ASCE)0733-9429(2002)128:7(683)

Chesterton, O.J., Ucuncu, M., and Borman, D. (2019) CFD Modeling for dams and reservoirs – best practices workflows, specification and review. Dams and reservoirs 29(4): 148-157, https://doi.org/10.1680/jdare.19.00032

Chinnarasri, C., Kositgittiwong, D., Julien, P.Y. (2012) Model of flow over spillways by computational fluid dynamics. Proceedings of the Institution of Civil Engineers. http://dx.doi.org/10.1680/wama.12.00034

Chow, V.T. (1959). Open-Channel Hydraulics. McGraw-Hill Book Company, New York, NY.

Costa, J.E. (1985) Floods from Dam Failure. Open-file Report 85-560, US Geological Survey, Denver CO.

Gedney, R.H. (1961) Stilling Basin Damage at Chief Joseph Dam. Journal of the Hydraulics Division, 1961, 87(2): pg 97-120. American Society of Civil Engineers. Reston, Virginia.

Elevatrorski, E. A. (1957). Hydraulic Energy Dissipators. Engineering Societies Monographs. McGraw-Hill Book Company, Inc,. New York, New York.

Ettema, R., Arndt, R., Roberts, P, Wahl, T. (ASCE, 2000) *Hydraulic Modeling, Concepts and Practice.* ASCE Manuals and Reports on Engineering Practice No. 97. American Society of Civil Engineers. Reston, Virginia.

Ettema, R., Marian, M. (2004) Scale Effects in Flume Experiments on Flow around a Spur Dike in Flatbed Channel, Journal of Hydraulic Engineering, American Society of Civil Engineers, Reston, VA.

Ettema, R., Gokhan, K. Marian, M. (2006) Similitude of Large-Scale Turbulence in Experiments on Local Scour at Cylinders, Journal of Hydraulic Engineering, American Society of Civil Engineers, Reston, VA.

Ettema, R., Thornton, C., Hogan, T., Biethman, B. (2019) Gross Dam Reservoir Expansion: Hydraulic Model Study of Stepped Spillway Design, CSU-HYD Report No. 2019-2, Hydraulics Laboratory, Fort Collins, CO.

Farabee, T.M. and Casarella, M.J. (1991) Spectral Features of Wall Pressure Fluctuations Beneath Turbulent Boundary Layers. Phsy. Fluids 3, 2410-2420, https://doi.org/10.1063/1.858179

Federal Emergency Management Agency (FEMA, 2013), Selecting and Accommodating Inflow Design Floods for Dams, FEMA P-94, August 2013.

Federal Emergency Management Agency (FEMA, 2014), Technical Manual: Overtopping Protection for Dams, FEMA P-1015, May 2014.

Federal Energy Regulatory Commission (FERC, 2001), Engineering Guidelines for the Evaluation of Hydropower Projects, Chapter 8 Determination of Probable Maximum Flood. https://www.ferc.gov/sites/default/files/2020-04/chap8.pdf

Fiorotto, V. and Rinaldo, A (1992) Fluctuating Uplift and Lining Design in Spillway Stilling Basins. Journal of Hydraulic Engineering, Vol 118, No. 4, Paper No 614.

Freeman, J. R. (1929), Hydraulic Laboratory Practice, The American Society of Mechanical Engineers, New York.

George, M.F. and Annandale, G.W. (2010), Bluestone Dam Rock Scour, International Conference on Scour and Erosion 2010, American Society of Civil Engineers, Reston, Virginia.

Gessler, J. Beginning and ceasing of sediment motion. In River Mechanics; Shen, H.W., Ed.; Water Resources Publications: Littleton, CO, USA, 1971; Chapter 7.

Hager, W.H., Schleiss, A.J., Boes, R.M, Pfister, M., (2021) Hydraulic Engineering of Dams, CRC Press, London, UK.

Heller, V (2011) Scale effects in physical hydraulic engineering models, Journal of Hydraulic Research, 49:3, 293-306, DOI: 10.1080/00221686.2011.578914

Henderson, F.M. (1966) Open Channel Flow. Prentice Hall, Upper Saddle River, NJ.

Ho, D.K. and Riddette, K.M. (2010) Application of computational fluid dynamics to evaluate hydraulic performance of spillways in australia, Australian Journal of Civil Engineering, 6:1, 81-104, DOI: 10.1080/14488353.2010.11463946

Humphries, R.P. and Annandale, G.W. (2015) Scour Assessment in Bedrock – Bluestone Dam Penstock Basin. Golder Associates Inc., Redmond, WA.

Inozemtsev, P.Y. (1969) Cavitation Destruction of Concrete and Protective Facings Under Natural Conditions. Translated from Gidrotekhnicheskoe Stroitel'stvo, No. 1, pp. 24-29, January 1969.

International Commission on Large Dams. (1987). Spillways for Dams, Bulletin 58, Paris, France.

International Commission on Large Dams. (2015). Technical Advancements in Spillway Design – Progress and Innovations from 1985 to 2015, Bulletin 172, Technical Committee on Hydraulic Structures.

International Energy Agency (2020) Hydropower Special Market Report, Analysis and forecast 2030. International Energy Agency. www.iea.org

Islam, M.D., Raid, T., El-Daly, M. (2007) Turbulence Structure Downstream of a Forced Hydraulic Jump. Term Project Report submitted to Dr. N. Rajaratnam, University of Alberta, Edmonton, Canada.

Julien, P.Y. (2010) *Erosion and Sedimentation* (2nd Edition). Cambridge University Press

Julien, P.Y. (2018) *River Mechanics (*2nd Edition). Cambridge University Press

Khatsuria, R.M. (2005). Hydraulic Design of Spillways and Energy Dissipators. Marcel Dekker, New York.

Kirsten, H.A.D. (1982). A Classification System for Excavation in Natural Soils. *The Civil Engineer in South Africa. p*p. 292-308

Launder, B.E, Spaulding, D.B. (1973) The Numerical Computation of Turbulent Flows. Imperial College of Science and Technology. London, UK.

Lesleighter, E.J., Bollaert, E.F.R., McPherson, B.L., and Scrivener, D.C. (2016) Spillway Rock Scour Analysis – Composite of Physical & Numerical Modelling, Paradise Dam, Australia. In B. Crookston & B. Tull is (Eds.), Hydraulic Structures and Water Systems Management. 6th International Symposium on Hydraulic Structures, Portland, OR, 27-30 June. Doi:10.15142/T300628160716 (ISBN 978-1-884575-75-4).

Macian-Perez, J.F., Bayon, A., Garcia-Bartual, R., Lopez-Jimenez, P., Valles-Moran, F. (2020). Charecterization of Structural Properties in High Reynolds Hydraulic Jump Based on CFD and Physical Modeling Approaches. J. Hydraul. Eng.,. 146(12): 04020079. https://ascelibrary.org/doi/10.1061/%28ASCE%29HY.1943-7900.0001820

May, R.P.W. (1987). Cavitation in Hydraulic Structures, Occurrence and Prevention, Report No SR 79, Hydraulics Research Wallingford, Oxfordshire, UK. \

Moses, D.M., Koutsunis, N.A., Halestead, K., Margo, D.A. (2015) Lessons Learned from the Bluestone Dam Inflow Design Flood Update, Proceedings of the U.S. Society on Dams, Louisville, KY.

Moses, D.W. (2016) Memorandum For Record Advisory Meeting, Bluestone Dam Spillway and Stilling Basin. Dam Safety Modification Center, Huntington, WV.

Moses, D.W., and Koutsunis, N.A., (2018) Phased Approach to Modeling for Bluestone Dam Spillway Modification, U.S. Society on Dams, Aurora, CO.

Moses, D.W., and Koutsunis, N.A., (2019). Innovative Approach to Hydraulic Design and Analysis for Bluestone Dam Primary Spillway Stilling Basin, International Commission on Dams, 87th Annual Conference Proceedings, Ottawa, Canada.

Moses, D.W., Crookston, B.M., Thornton, C.I. (2021) Evaluation of Step Edge Geometry of Energy Dissipation of Stepped Chutes: An Informative Comparison, Association of State Dam Safety Officials, Inc, proceedings of the 2021 Annual Conference, Nashville, TN.

Moses, D.W., Thornton, C., Sharp, J.A.; (2022) Historic Perspective and Current Knowledge Gaps in Hydraulic Jump Stilling Basin Design, US Society on Dams, Proceedings of the 2022 Annual Conference, San Diego, CA.

Moses, D.W., and Margo, D.A ; (2023) Decision Framework for Dam Safety Modifications Under Flood Hazard Uncertainty, US Society on Dams, Proceedings of the 2023 Annual Conference, Charleston, SC.

Pells, S.E. (2016). Erosion of Rock in Spillways. Thesis in full fulfilment of Doctor of Philosophy Degree, School of Civil and Environmental Engineering, University of New South Wales.

National Academies of Sciences, Engineering, and Medicine, (2024). Modernizing Probable Maximum Precipitation Estimation. Washington, DC. The National Academies Press. https://doi.org/10.17226/27400

Novak, P., Guinot, V., Jeffrey, A., Reeve, D. 2010. Hydraulic Modelling – an Introduction. Principles, methods, and applications. Spon Press. London, UK.

Nakato, T. 2000. Model Test of Hydraulic Performance of Pit 6 Dam Stilling Basin. Journal of Hydraulic Engineering, 126(9): 638-652, American Society of Civil Engineers, Reston, Virginia.

National Energy Agency (2015). *Best Practice Guidelines for the Use of CFD in Nuclear Reactor Safety Applications.* NEA/CSNI/R(2014)11, Committee on the Safety of Nuclear Installations, National Energy Agency.

National Cooperative Highway Research Program (2019). Relationship Between Erodibility and Properties of Soil. Washington, DC. The National Academies Press.

Natural Resources Conservation Service (1997). Chapter 51 – Earth Spillway Erosion Model. Part 628 Dams, National Engineering Handbook. United States Department of Agriculture.

Nikuradse, J. (1933) Law of Flow in Rough Pipes. VDI-Forschungsheft: Germany) 361. (in German) (Translated in NACA Tech. Memo. No. 1292, 1050).

United States Nuclear Regulatory Commission (USNRC) (2013) Cmputational Fluid Dynamics Best Practices Guidelines for Dry Cask Applications – Final Report. Office of Nuclear Regulatory Research, Office of Nuclear Material Safety and Safeguards. Rockville, MD.

Parker, G. 2004. ID Sediment Transport Morphodynamics with applications to Rivers and Turbidity Currents. St. Anthony Falls Laboratory. University of Minnesota. Minneapolis, Minnesota.

Pereira, G.M. 2020. Spillway Design – Step by Step.CRC Press/Balkema, The Netherlands.

Regan, P. (2009) An Examination of Dam Failures vs Age. US Society on Dams, 2009 Annual Conference, Nashville, TN.

Ripken, J.F. and Dahlin, W.Q. (1972), Hydraulic Model Studies for the Guri Hydroelectric Project – Report on Spillway Cavitation Damage. University of Minnesota, St. Anthony Fall Hydraulic Laboratory, Minneapolis, MN.

Rice, C.E., Kadavy, K.C. (1993). Protection Against Scour at SAF Stilling Basins. J. Hydr. Eng. 119(1): 133-139.

Riegel, R. M., and Beebe, J.C. (1917), The Hydraulic Jump as a Means of Dissipating Energy, Technical Reports, Part III, Dayton, Ohio

Rozanov, N.P., Lysenko, P.E., Bedev, V.D., Kaveshnikov, A.T., and Chepaikin, G.A. (1973), Use of Supercavitating Elements of Spillway Hydraulic Structures, translated from Gidrotekhnicheskoe Stroietstvo, No 8, pp.24-27, August, 1971.

Rozanov, N.P., Kaveshnikov, A.T. (1973), Investigation of Cavitation Damage to Baffle Piers and Flow Splitters, translated from Gidrotekhnicheskoe Stroietstvo, pp.29-32, January, 1973

Schlichting, H., Gersten, K. (2017) Boundary-Layer Theory, Ninth Edition Springer-Verlag Berlin Heidelberg. DOI 10.1007/978-3-662-52919-5

Schoklitsch, A. (1937), Hydraulic Structures – A Text and Handbook, The American Society of Mechanical Engineers, New York, NY.

Shields, A. (1936) Application of Similarity Principles, and Turbulence Research to Bed Load Movement. California Institute of Technology, Pasadena, California

Stanley, C.M., 1934. Study of Stilling Basin Design. Transactions of the American Society of Civil Engineers, 1934199(1): 490-512

Stein, O.R., Julien, P.Y. (1993), Sediment Concentration Below Free Overfall. J. Hyd. Eng., ASCE, 120(9), 1043-59

Suarez, V.L.M., Suarez, B.D (2016), In *Lecciones Aprendidas de los Incidentes y Fallas en las Presas de Venezuela.* Caracas, Venezuela. 27.1-27.34.

Toso, J.W. and Bowers, C.E. (1988) Extreme Pressures in Hydraulic Jump Stilling Basins. Journal of Hydraulic Engineering, Vol. 114, No. 8, Paper No 22657.

US Army Corps of Engineers (USACE) (1935-1937) Construction Photographs of Bonneville Dam, Columbia River, Oregon.

US Army Corps of Engineers (USACE) (1939) Final Report – Laboratory Tests on Hydraulic Models of Bluestone Dam, New River. Huntington, WV. Waterways Experiment Station, Vicksburg, MS.

US Army Corps of Engineers (USACE) (1943) Concrete Abrasion Study, Bonneville Spillway Dam, Bonneville, Oregon. Report No 15-1, Bonneville Hydraulic Laboratory, Bonneville, Oregon.

US Army Corps of Engineers (USACE) (1946) Model Study of Sluice Outlet for Bluestone Dam, New River, West Virginia, Technical Memorandum No. 2-227. Waterways Experiment Station, Vicksburg, MS.

US Army Corps of Engineers (USACE) (1948) A Laboratory Development of Cavitation-Free Baffle Piers, Bluestone Dam, New River, West Virginia, Technical Memorandum No. 2-243. Waterways Experiment Station, Vicksburg, MS.

US Army Corps of Engineers (USACE) (1955) Report on Damage to Baffle Deck and Baffles at Bonneville Dam, Columbia River, Oregon-Washington. Office of the District Engineer, Portland Oregon.

US Army Corps of Engineers (USACE) (1957) Stone Stability, Velocity vs Stone Diameter. Hydraulic Design Criteria, Waterways Experiment Station, Vicksburg, MS.

US Army Corps of Engineers (USACE) (1960) Spillway, Stilling Basin, and Flood-Control Conduits Keystone Dam, Arkansas River – Hydraulic Model Investigation. Technical Report No. 2-555, Waterways Experiment Station, Vicksburg, MS.

US Army Corps of Engineers (USACE) (1964) Spillway for Amistad Dam, Rio Grande, Mexico and United States, Hydraulic Model Investigation. Technical Report No. 2-653, Waterways Experiment Station, Vicksburg, MS.

US Army Corps of Engineers (USACE) (1965) Engineering Manual 1110-2-1603 - Hydraulic Design of Spillways, 1st Print, Headquarters, Department of the Army, Washington, DC.

US Army Corps of Engineers (USACE) (1969) Trends in Baffled, Hydraulic Jump Stilling Basin Designs of the Corps of Engineers Since 1947 – Miscellaneous Paper H-69-1, Waterways Experiment Station, Vicksburg, MS.

US Army Corps of Engineers (USACE) (1970) An experimental Study of Drag Forces and Other Performance Criteria of Baffle Blocks in Hydraulic Jumps, Miscellaneous Paper H-70-4, Waterways Experiment Station, Vicksburg, MS.

US Army Corps of Engineers (USACE) (1972) Pertinent Data on Spillway Tainter Gates for Corps of Engineers Project, Miscellaneous Paper H-72-7, Waterways Experiment Station, Vicksburg, MS.

US Army Corps of Engineers (USACE) (1978) Guidelines for the Design, Adjustment and Operation of Models for the Study of River Sedimentation Problems, Instruction Report H-78-1, Waterways Experiment Station, Vicksburg, MS.

US Army Corps of Engineers (USACE) (1979) Stilling Basins for Outlet Works, Miscellaneous Paper HL-79-8, Waterways Experiment Station, Vicksburg, MS.

US Army Corps of Engineers (USACE) (1980) Engineering Manual 1110-2-1602 – Hydraulic Design of Reservoir Outlet Works, Headquarters, Department of the Army, Washington, DC.

US Army Corps of Engineers (USACE) (1981) Abrasion-Erosion Resistance of Fiber-Reinforced Concrete, Miscellaneous Paper SL-81-32, Waterways Experiment Station, Vicksburg, MS.

US Army Corps of Engineers (USACE) (1987) Engineering Manual 1110-2-1605 – Hydraulic Design of Navigation Dams. Headquarters, Department of the Army, Washington, DC.

US Army Corps of Engineers (USACE) (1988) Dynamic Loading on Sidewall Monoliths of Spillway Stilling Basin, Technical Report HL-88-10, Waterways Experiment Station, Vicksburg, MS

US Army Corps of Engineers (USACE) (1991) Engineering Regulation 1110-8-2 - Inflow Design Flood for Dams and Reservoirs. Headquarters, Department of the Army, Washington, DC.

US Army Corps of Engineers (USACE) (1992) Engineering Manual 1110-2-1603 - Hydraulic Design of Spillways, Headquarters, Department of the Army, Washington, DC.

US Army Corps of Engineers (USACE) (1994a) Water Control Manual for Bluestone Lake -New River, Huntington District, Huntington, WV.

US Army Corps of Engineers (USACE) (1994b) Engineering Manual 1110-2-2908 – Rock Foundations, Headquarters, Department of the Army, Washington, DC.

US Army Corps of Engineers (USACE) (1999) Low-Head Navigation Dam Stilling Basin Design, Technical Report CHL-99-4, Waterways Experiment Station, Vicksburg, MS.

US Army Corps of Engineers (USACE) (2003) Bluestone Lake Dam, Basin Forces and Tailrace Scour, Coastal and Hydraulics Laboratory, Vicksburg, MS.

US Army Corps of Engineers (USACE) (2005) Engineering Manual 1110-2-2100 – Stability Analysis of Concrete Structures, Headquarters, Department of the Army, Washington, DC.

US Army Corps of Engineers (USACE) (2012) Periodic Inspection Report #15, Chief Joseph Dam, Columbia River Washington, US Army Corps of Engineers, Seatle District, Seatle, WA.

US Army Corps of Engineers (USACE) (2012) Keystone Lake Arkansas River, Oklahoma. Water Control Manual. Tulsa District, Tulsa OK.

US Army Corps of Engineers (USACE) (2018) Bluestone Dam, Phase B Physical Hydraulic Model Study, Dam Safety Modification Mandatory Center of Expertise, Huntington, WV.

US Army Corps of Engineers (USACE) (2022) DLS-104 - Best Practices in Dam and Levee Safety Risk Analysis Workshop. https://publibrary.planusace.us/#/series/Best%20Practices-Manual

US Bureau of Reclamation (USBR) (1939), Spillways and Energy Dissipators. Bureau of Reclamation, Hydraulic Laboratory, Denver, CO.

US Bureau of Reclamation (USBR) (1948), Similitude in Hydraulic Model Testing, Hydraulic Laboratory Report No. Hyd-246. Bureau of Reclamation, Research and Geology Division of Design and Construction Branch, Denver, CO.

US Bureau of Reclamation (USBR) (1955) Progress Report Research Study on Stilling Basins, Energy Dissipators, and Associated Appurtenances, Laboratory Report Hydr-399, Engineering Laboratories Branch, Denver, CO.

US Bureau of Reclamation (USBR) (1955) Progress Report Research Study on Stilling Basins and Bucket Dissipators, Laboratory Report Hydr-380, Engineering Laboratories Branch, Denver, CO.

US Bureau of Reclamation (USBR) (1978) Low Froude Number Stilling Basins Design, REC-ERC-78-8, Engineering and Research Center, Denver, CO.

US Bureau of Reclamation (USBR) (1979) Research on Abrasive Materials in Stilling Basins, Hydraulic Report 572, Engineering and Research Center, Denver, CO.

US Bureau of Reclamation (USBR) (1980) Hydraulic Laboratory Techniques. US. Department of the Interior. Bureau of Reclamation. Denver, CO.

US Bureau of Reclamation (USBR) (1984) Hydraulic Design of Stilling Basins and Energy Dissipators - A water Resources Technical Publication, 8th Edition, Denver, CO.

US Bureau of Reclamation (USBR) (1987) Design of Small Dams – A water Resources Technical Publication, 3rd Edition, Denver, CO.

US Bureau of Reclamation (USBR) (2001) Water Measurement Manual – A water Resources Technical Publication, 3rd Edition, Washington, DC.

US Bureau of Reclamation (USBR) (2009) Cavitation Potential of the Folsom Auxiliary Spillway Stilling Basin Baffle Blocks, Technical Services Center, Denver, CO.

US Bureau of Reclamation (USBR) (2012) Hydraulic Laboratory Report HL-2012-02 – Performance of Type III Stilling Basins – Stepped Spillway Studies, Technical Services Center, Denver, CO.

US Bureau of Reclamation (USBR) (2019) Flow Deflectors to Reduce Abrasion Damage in Stilling Basins – 40 Year Progress Report, HL-2019-02, Research and Development Office, Denver, CO.

US Department of Agriculture (USDA) (1959) The SAF Stilling Basin – A structure to Dissipate the Destructive Energy in High-Velocity Flow from Spillways, Agricultural Handbook No 156.

US Nuclear Regulatory Commission (USNRC) (2013) Computational Fluid Dynamics Best Practices Guidelines for Dry Cask Applications – Final Report, NUREG-2152, Office of Nuclear Regulatory Research, Washington, D.C.

US Weather Bureau (1952) Maximum 24-Hour Precipitation in the United States, Hydrometeorological Section, Hydrological Services Division, Washington, D.C.

Weather Bureau (1952), Maximum 24-Hour Precipitation in the United States. Hydrometeorlogical Section, Hydrological Services Division. Washington, D.C.

Willey, J., Ewing, T., Lesleigher, E., Dymke, J. (2010) Numerical and physical modelling for a complex stepped spillway. Hydropower & Dams, Issue Three, 2010.

Willey, J., Ewing, T., Wark, B., Lesleigher, E. (2012) Complementary Use of Physical and Numerical Modelling Techniques in Spillway Design Refinement. Commission Internationale Des Grands Barrages, Kyoto, Juin 2012.

World Meteorological Organization (2009), Manual on Estimation of Probable Maximum Precipitation (PMP), WMO-No. 1045, Geneva, Switzerland.

Yalin, M.S., Karakan, E. (1979) Inception of Sediment Transport. Journal of the Hydraulics Division, 1979, 105(11): 1433-1443, American Society of Civil Engineers. https://doi.org/10.1061/JYCEAJ.0005306

Yager, E.M., Vendittie, J.G., Smith, H.J, and Schmeedckle, M.W. (2018) The trouble with shear stress. Geomorphology 323 (2018) 41-50. https://doi.org/10.1016/j.geomorph.2018.09.008

Zhang, A. T.; Johannes, U., Wolfram, S. (2018). Power of the River: Introducing the Global Dam Tracker (GDAT). Columbia, Center on Global Energy Policy.

LIST OF ACRONYMS

ASCE	American Society of Civil Engineers
cfs	Cubic Feet Per Second (ft^3/s)
CHL	Coastal and Hydraulics Laboratory (Engineering Research and Development Center)
ERDC	Engineering Research and Development Center (United States Army Corps of Engineers)
FEMA	Federal Emergency Management Agency
NAS	National Academies of Sciences, Engineering, and Medicine
NCHRP	National Cooperative Highway Research Program
RMS	Root Mean Square
SAF	Saint Anthony Falls (Hydraulic Laboratory)
USACE	United States Army Corps of Engineers
USBR	United States Bureau of Reclamation
USD	United States Dollar